# INVESTIGATING THE EFFECTS OF ENVIRONMENTAL CONDITIONS ON *PIM1* DNA STRUCTURES AND THE DOXORUBICIN BINDING

A THESIS SUBMITTED TO
THE GRADUATE SCHOOL OF NATURAL AND APPLIED SCIENCES
OF
MIDDLE EAST TECHNICAL UNIVERSITY

BY

SABA OROUJI

IN PARTIAL FULFILLMENT OF THE REQUIREMENTS
FOR
THE DEGREE OF MASTER OF SCIENCE
IN
BIOCHEMISTRY

JUNE 2024

Approval of the thesis:

**INVESTIGATING THE EFFECTS OF ENVIRONMENTAL CONDITIONS ON *PIM1* DNA STRUCTURES AND THE DOXORUBICIN BINDING**

submitted by **SABA OROUJI** in partial fulfillment of the requirements for the degree of **Master of Science** i**n Biochemistry, Middle East Technical University** by,

Prof. Dr. Naci Emre Altun
Dean, **Graduate School of Natural and Applied Sciences** _____

Assoc. Prof. Dr. Özgül Persil Çetinkol
Head of the Department, Biochemistry _____

Assoc. Prof. Dr. Özgül Persil Çetinkol
Supervisor, Biochemistry, METU _____

Prof.Dr. Ayşe Elif Erson Bensan
Co-Supervisor, Biological Sciences, METU _____

**Examining Committee Members:**

Prof. Dr. Mesut Muyan
Biological Sciences, METU _____

Assoc. Prof. Dr. Özgül Persil Çetinkol
Biochemistry, METU _____

Prof. Dr. Birsen Can Demirdöğen
Biomedical Engineering, TOBB University _____

Prof. Dr. Ayşe Elif Erson Bensan
Biological Sciences, METU _____

Assoc. Prof. Dr. Serhan Türkyılmaz
Chemistry, METU _____

Date: 07.06.2024

**I hereby declare that all information in this document has been obtained and presented in accordance with academic rules and ethical conduct. I also declare that, as required by these rules and conduct, I have fully cited and referenced all material and results that are not original to this work.**

Name Last name : Saba Orouji

Signature :

# ABSTRACT

## INVESTIGATING THE EFFECTS OF ENVIRONMENTAL CONDITIONS ON *PIM1* DNA STRUCTURES AND THE DOXORUBICIN BINDING

Orouji, Saba
Master of Science, Biochemistry
Supervisor: Assoc. Prof. Dr. Özgül Persil Çetinkol
Co-Supervisor: Prof. Dr. Ayşe Elif Erson Bensan

June 2024, 180 pages

Triple negative breast cancer (TNBC), which lacks the ER (estrogen receptor), PR (progesterone receptor), and HER-2 (Erb-B2 receptor tyrosine kinase 2) expressions are accounted for the 25% of all breast cancer related deaths in 2019. *PIM1* oncogenes were recently found to be overexpressed in TNBC type breast cancer tumors and *PIM1* sequences were found to adopt unique G-quadruplex-duplex hybrid type secondary structures.

Within the scope of this thesis, first the effect of pH (pH 7.0 or 5.5) and ions ($K^+$ or $Na^+$) on the possible secondary structures (G4, i-motif and dsDNA) of the three *PIM1* gene sequences was investigated using UV-Vis and CD spectroscopy. All three sequences were found to be stable under the conditions investigated, and plausibly coexist together. The lower pH was found to be stabilizing the i-motif structure, while destabilizing the dsDNA. The effect of pH on the G4 structure was almost negligible. Since the secondary structures of the *PIM1* gene could be plausible targets in TNBC, the interactions between the anti-cancer agent Doxorubicin (Dox) and these secondary structures were investigated via UV-Vis absorption, Circular Dichroism (CD) and Fluorescence spectroscopy experiments in the second part of

this thesis. The affinity of Dox towards different nucleic acid structures was also investigated via competition dialysis experiments.

Our investigations revealed that Dox exhibited significant yet almost equal affinity for all *PIM1* gene secondary structures. We believe our studies will shed light on and contribute to ongoing research on the potential of *PIM1* to be a target for TNBC type breast cancer treatment.

Keywords: Breast cancer, *PIM1*, G-quadruplex, i-motif, Doxorubicin

# ÖZ

## ÇEVRESEL KOŞULLARIN *PIM1* DNA YAPILARI VE DOKSORUBİSİN BAĞLANMASI ÜZERİNDEKİ ETKİLERİNİN ARAŞTIRILMASI

Orouji, Saba
Yüksek Lisans, Biyokimya
Tez Yöneticisi: Doç. Dr. Özgül Persil Çetinkol
Ortak Tez Yöneticisi: Prof. Dr. Ayşe Elif Erson Bensan

Haziran 2024, 180 sayfa

ER, PR ve HER-2 ekspresyonundan yoksun olan üçlü negatif meme kanseri (TNBC), 2019'daki tüm meme kanserine bağlı ölümlerin %25'ini oluşturan meme kanseri türüdür. Yakın zamanda, *PIM1* onkojenlerinin TNBC tipi meme kanseri tümörlerinde aşırı eksprese edildiği ve de *PIM1* genlerinin G-quadruplex-duplex hibrit tipi ikincil yapılarını oluşturduğu gösterilmiştir.

Bu tez kapsamında, öncelikli olarak, farklı pH (7.0 veya 5.5), tampon çözelti tipi ve iyon çeşidinin ($K^+$ veya $Na^+$) *PIM1* gen dizilerinin olası ikincil yapıları (G4, i-motif ve dsDNA) üzerindeki etkisi araştırılmıştır. Her üç dizinin de araştırılan koşullar altında stabil olduğu ve birlikte aynı ortamda oluşabilecekleri belirlenmiştir. Daha düşük pH'ın dsDNA'yı daha kararsız hale getirirken, i-motif yapısını stabilize ettiği belirlenmiştir. pH'ın G4 yapısı üzerinde ise nerdeyse hiç bir etkisinin olmadığı gözlemlenmiştir. $K^+$ veya $Na^+$ katyonlarının varlığında dsDNA ve i-motif yapılarının karalığında bir değişiklik gözlemlenmezken, $K^+$'un $Na^+$'ya göre daha kararlı hale getirdiği gözlemlenmiştir.

Bu tezin ikinci bölümde ise, anti-kanser ajanı Doksorubisin (Dox) ile *PIM1* geninin oluşturduğu farklı ikincil yapılar arasındaki etkileşimler UV-Vis absorpsiyonu,

Circular Dichroism (CD) ve Floresans spektroskopisi yöntemleri ile incelenmiştir. Son olarak, Dox'un farklı nükleik asit yapılarına olan ilgisi ise rekabetçi diyaliz deneyleriyle belirlenmiştir.

Araştırmalarımız Dox'un tüm *PIM1* geni ikincil yapılarına yaklaşık olarak aynı afinite ile bağlandığını ortaya çıkarmıştır. Elde edilen bu sonuçların Dox'un etki mekanizmalarına yeni bir yaklaşım kazandırabileceği ve de *PIM1*'in TNBC tipi meme kanseri tedavisi için bir hedef olma potansiyeli ile ilgili devam eden araştırmalara katkıda bulunabileceği düşünülmektedir.

Anahtar Kelimeler: Meme kanseri, *PIM1*, G-dörtlü, i-motif, Doksorubisin

To my lovely family

## ACKNOWLEDGMENTS

The author wishes to express his deepest gratitude to her supervisor Prof. Dr. Özgül Persil Çetinkol and co-supervisor Prof. Dr. Ayşe Elif Erson Bensan for their guidance, advice, criticism, encouragements, and insight throughout the research.

This study was supported by Scientific and Technological Research Council of Turkey (TUBITAK) under the grant number 221Z018. The author thanks to TUBITAK for their supports.

## TABLE OF CONTENTS

ABSTRACT ..... v

ÖZ ..... vii

ACKNOWLEDGMENTS ..... x

TABLE OF CONTENTS ..... xi

LIST OF TABLES ..... xvi

LIST OF FIGURES ..... xviii

LIST OF ABBREVIATIONS ..... xxvii

CHAPTERS

1 INTRODUCTION ..... 1

1.1 Deoxyribonucleic Acid (DNA) ..... 1

1.2 DNA Structures and Properties ..... 2

1.2.1 G-quadruplex Structures ..... 7

1.2.2 i-motif ..... 10

1.3 Duplex-Quadruplex Equilibria in Guanine- and Cytosine-rich DNA ..... 12

1.4 DNA and Cancer Therapies ..... 14

1.4.1 DNA Interactions with Drugs ..... 16

1.5 Doxorubicin Interactions with Genomic DNA ..... 18

1.5.1 Dox Interaction with G4 Structures ..... 20

1.5.2 Dox Interactions with i-motifs ..... 21

1.6 G-quadruplex Structures in *PIM1* Gene ..... 21

1.7 Scope of the Thesis ..... 23

2 Materials and Methods ..... 27

2.1 Investigating Effect of Environmental Conditions on *PIM1* Gene Structures ..... 27

2.1.1 Sample Preparation ..... 27

2.1.2 UV-Vis and CD Experiments ..... 28

2.1.3 UV-Vis Thermal Denaturation Experiments ..... 28

2.2 Examining the Interaction Between *PIM1* DNA Structures and Doxorubicin ..... 29

2.2.1 Sample Preparation ..... 29

2.2.2 UV-Vis, CD and Thermal Denaturation Experiments ..... 29

2.2.3 Fluorescence Experiments and Determination of Association Constants ..... 30

2.2.4 Competition Dialysis Assay ..... 31

3 RESULTS AND DISCUSSION ..... 33

3.1 Investigating the Effect of pH on *PIM1* G4 Structures ..... 33

3.1.1 Characterization of G4 Structures in K-phosphate Buffer via Circular Dichroism Spectroscopy ..... 33

3.1.2 Characterization of G4 Structures in K-phosphate Buffer via UV-Vis Thermal Denaturation Experiments ..... 35

3.2 Investigating the Effects of Salt on *PIM1* G4 Structures ..... 38

3.2.1 Characterization of G4 Structures in Na-phosphate Buffer via Circular Dichroism Spectroscopy ..... 38

3.2.2 Characterization of G4 Structures in Na-phosphate Buffer via UV-Vis Thermal Denaturation Experiments ..... 42

3.3 Investigating i-motif Formation in C-rich sequences of *PIM1* and the Effect of pH on Those Structures ..... 46

3.3.1 Characterization of i-motif Structure in K-phosphate Buffer via Circular Dichroism Spectroscopy .....46

3.3.2 Characterization of i-motif Structures in K-phosphate Buffer via UV-Vis Thermal Denaturation Experiments .....49

3.4 Investigating Effects of salt on I4 structures of *PIM1* .....53

3.4.1 Characterization of i-motif Structures in Na-phosphate Buffer via Circular Dichroism Spectroscopy .....53

3.4.2 Characterization of i-motif Structures in Na-phosphate Buffer via UV-Vis Thermal Denaturation Experiments .....55

3.5 Investigating DNA Duplex Formation in *PIM1* Sequences .....59

3.5.1 Characterization of Double Helical DNA in K-phosphate Buffer via Circular Dichroism Spectroscopy .....59

3.5.2 Characterization of Double Helical DNA in *PIM1* Sequences in K-phosphate Buffer via UV-Vis Thermal Denaturation Experiments.....62

3.6 Investigating Effects of Salt on DNA Duplex *PIM1* Structures .....64

3.6.1 Characterization of Double Helical DNA in Na-phosphate Buffer via Circular Dichroism Spectroscopy .....64

3.6.2 Characterization of the Double Helical DNA in Na-phosphate Buffer via UV-Vis Thermal Denaturation Experiments .....68

3.7 Examining the Interactions Between G4 Structures of *PIM1* and Doxorubicin .....71

3.7.1 Characterization of Dox Binding to G4 structures via CD Spectroscopy71

3.7.2 Characterization of Dox Binding to G4 structures via UV–Vis Absorption Spectroscopy .....76

3.7.3 Characterization of Dox Binding and the Stability of the G4-Dox Complexes via Thermal Denaturation Experiments .....79

3.7.4 Characterization of Dox binding to G4 structures via Fluorescence Spectroscopy ..... 84

3.8 Examining the Interactions Between i-motif Structures of *PIM1* and Doxorubicin ..... 89

3.8.1 Characterization of Dox Binding to i-motif Structures via CD Spectroscopy ..... 89

3.8.2 Characterization of Dox Binding to i-motif Structures via UV–Vis Absorption Spectroscopy ..... 93

3.8.3 Characterization of Dox Binding and the Stability of the i-motif-Dox Complexes via Thermal Denaturation Experiments ..... 96

3.8.4 Characterization of Dox Binding to i-motif Structures via Fluorescence Spectroscopy ..... 104

3.9 Examining the Interaction Between Duplex Structures of *PIM1* and Doxorubicin ..... 109

3.9.1 Characterization of Dox Binding to Duplex Structures via CD Spectroscopy ..... 109

3.9.2 Characterization of Dox Binding to Duplex Structures via UV–Vis Absorption Spectroscopy ..... 114

3.9.3 Characterization of Dox Binding and the Stability of the DNA-Dox Complexes via Thermal Denaturation Experiments ..... 117

3.9.4 Characterization of Dox Binding to Duplex Structures via Fluorescence Spectroscopy ..... 124

3.10 Competition Dialysis ..... 129

4 THESIS CONCLUSION ..... 135

4.1 Investigating the Effects of Environmental Conditions on the *PIM1* DNA Structures ..... 135

4.2 Examining the Interaction Between Doxorubicin and *PIM1* DNA Structures .....137

REFERENCES .....139

APPENDICES

A. Preparation of Buffer and Stock Solutions .....153

B. List of Nucleic Acid Sequences Used in This Study .....156

C. UV-Vis Thermal Denaturation Experiments and Melt Curves.....157

D. Association Constant Experiments .....176

E. Competition Dialysis .....179

## LIST OF TABLES

TABLES

Table 1. Comparison of the Tm values of 3.0 μM DNA solution of G1, G2, G3 obtained by monitoring the absorbance change at 295 nm, under two different pHs in K-phosphate or Na-phosphate buffer. ..... 46
Table 2. Comparison of the Tm values of 3.0 μM DNA solution of I1, I2, I3 obtained by monitoring the absorbance change at 265 nm, under two different pHs in K-phosphate or Na-phosphate buffer. ..... 59
Table 3. Comparison of the Tm values of 3.0 μM DNA solution of D1, D2, D3 obtained by monitoring the absorbance change at 260 nm, under two different pHs in K-phosphate or Na-phosphate buffer. ..... 71
Table 4. Comparison of the Tm values of 3.0 μM DNA solutions in the absence and presence of 3.0, 6.0 and 30 μM of Dox at pH 7.0 and pH 5.5 in K-phosphate buffer. ..... 84
Table 5. Association constants determined by Fluorescence titration experiments of Dox-DNA ..... 89
Table 6. Comparison of the Tm values of 3.0 μM DNA solutions in the absence and presence of 3.0, 6.0 and 30 μM of Dox at pH 7.0 and pH 5.5 in K-phosphate buffer. ..... 104
Table 7. Association constants determined by Fluorescence titration experiments of Dox-DNA ..... 109
Table 8. Comparison of the Tm values of 3.0 μM DNA solutions in the absence and presence of 3.0, 6.0 and 30 μM of Dox at pH 7.0 and pH 5.5 in K-phosphate buffer. ..... 124
Table 9. Association constants determined by Fluorescence titration experiments of Dox-DNA ..... 129
Table 10. Competition Dialysis results of Dox. ..... 132
Table 11. List of nucleic acid sequences used in this study. ..... 156

Table 12. List of nucleic acid structures used in the competition dialysis assay and their extinction coefficient values for concentration adjustments. ..... 179

## LIST OF FIGURES

FIGURES

Figure 1. Watson-Crick base pairing and the antiparallel double helix structure of DNA. The arrows represent 5′→3′ directionality. Adenine (A) pairs with thymine (T) and guanine (G) pairs with cytosine (C). ..... 2
Figure 2. Configurations of DNA double helix A) A-DNA B) B-DNA C) Z-DNA [17]. ..... 6
Figure 3. Helical representation of (A) intramolecular and (B) intermolecular DNA triplex [18]. ..... 6
Figure 4. (A) G-quartet with Hoogsteen hydrogen bonded guanine and schematic drawing of a G4 structure and (B) hemi-protonated C–$C^+$ base pairs and schematic representation of an *i*-motif structure [48]. ..... 12
Figure 5. Structure of Doxorubicin ..... 18
Figure 6. Schematic diagrams of *PIM1* Form 1 and Form 2 QDHs are shown in (A) and (B), respectively [99]. ..... 23
Figure 7. CD spectra of 3.0 μM DNA solution A) G1 B) G2 C) G3 at pH 7.0 and 5.5 in 20 mM K-phosphate with 20 mM KCl buffer at 15 °C. ..... 34
Figure 8. UV-Vis thermal denaturation profiles of 3.0 μM DNA solution, A) G1 B) G2 C) G3, obtained by monitoring the absorbance change at 295 nm, at pH 7.0 and 5.5 in K-phosphate buffer. ..... 37
Figure 9. Comparison of the CD spectra of 3.0 μM DNA solution A) G1 B) G2 C) G3 in K-phosphate or Na-phosphate buffer at pH 7.0. ..... 40
Figure 10. Comparison of the CD spectra of 3.0 μM DNA solution A) G1 B) G2 C) G3 at pH 7.0 and 5.5 in 20 mM Na-phosphate with 20 mM NaCl buffer at 15 °C. ..... 41
Figure 11. Comparison of the UV-Vis thermal denaturation profiles of 3.0 μM A) G1 B) G2 C) G3, in K-phosphate or Na-phosphate buffer at pH 7.0, obtained by monitoring the absorbance change at 295 nm. ..... 44

Figure 12. Comparison of the UV-Vis thermal denaturation profiles of 3.0 μM DNA solution A) G1 B) G2 C) G3, obtained by monitoring the absorbance change at 295 nm, at pH 7.0 and 5.5 in Na-phosphate buffer. ..... 45
Figure 13. CD spectra of 3.0 μM DNA solution, A) I1 B) I2 C) I3, at pH 7.0 and 5.5 in 20 mM K-phosphate with 20 mM KCl buffer at 15 °C. ..... 48
Figure 14. UV-Vis thermal melting profiles of 3.0 μM DNA solution, A) I1 B) I2 C) I3, at pH 7.0 in K-phosphate buffer obtained by monitoring the absorbance change at 265 nm and 295 nm. ..... 51
Figure 15. UV-Vis thermal melting profiles of 3.0 μM DNA solution, A) I1 B) I2 C) I3, at pH 5.5 in K-phosphate buffer obtained by monitoring the absorbance change at 265 nm and 295 nm. ..... 52
Figure 16. CD spectra of 3.0 μM DNA solution, A) I1 B) I2 C) I3, at pH 7.0 and 5.5 in 20 mM Na-phosphate with 20 mM NaCl buffer at 15 °C. ..... 54
Figure 17. UV-Vis thermal melting profiles of 3.0 μM DNA solution, A) I1 B) I2 C) I3, at pH 7.0 in Na-phosphate buffer obtained by monitoring the absorbance change at 265 nm and 295 nm. ..... 57
Figure 18. UV-Vis thermal melting profiles of 3.0 μM DNA solution, A) I1 B) I2 C) I3, at pH 5.5 in Na-phosphate buffer obtained by monitoring the absorbance change at 265 nm and 295 nm. ..... 58
Figure 19. CD spectra of 3.0 μM DNA solution, A) D1 B) D2 C) D3, at pH 7.0 and 5.5 in 20 mM K-phosphate with 20 mM KCl buffer at 15 °C. ..... 61
Figure 20. UV-Vis thermal denaturation profiles of 3.0 μM DNA solution, A) D1 B) D2 C) D3, obtained by monitoring the absorbance change at 260 nm, at pH 7.0 and 5.5, in K-phosphate buffer..... 63
Figure 21. Comparison of the CD spectra of 3.0 μM DNA solution A) D1 B) D2 C) D3 in K-phosphate or Na-phosphate buffer at pH 7.0. ..... 65
Figure 22. Comparison of the CD spectra of 3.0 μM DNA solution A) D1 B) D2 C) D3 in K-phosphate or Na-phosphate buffer at pH 5.5. ..... 66
Figure 23. CD spectra of 3.0 μM DNA solution, A) D1 B) D2 C) D3, at pH 7.0 and 5.5 in 20 mM Na-phosphate with 20 mM NaCl buffer at 15 °C. ..... 67

Figure 24. UV-Vis thermal denaturation profiles of 3.0 μM DNA solution, A) D1 B) D2 C) D3, obtained by monitoring the absorbance change at 260 nm, at pH 7.0 and 5.5 in Na-phosphate buffer. ..... 70
Figure 25. Comparison of the CD spectra of 3.0 μM of A) G1 B) G2 C) G3, in the absence and presence of 3.0, 6.0 and 30 μM Dox with the 3.0, 6.0 and 30 μM Dox spectra at pH 7.0. ..... 74
Figure 26. Comparison of the CD spectra of 3.0 μM of A) G1 B) G2 C) G3, in the absence and presence of 3.0, 6.0 and 30 μM Dox with the 3.0, 6.0 and 30 μM Dox spectra at pH 5.5. ..... 75
Figure 27. UV–Vis absorption spectra of 3.0 μM A) G1 B) G2 C) G3 in the absence and presence of 30 μM Dox at pH 7.0 in K-phosphate buffer. Red lines represent Dox alone, grey lines show oligonucleotide alone and blank lines denote the DNA:Dox sample. ..... 77
Figure 28. UV–Vis absorption spectra of 3.0 μM A) G1 B) G2 C) G3 in the absence and presence of 30 μM Dox at pH 5.5 in K-phosphate buffer. Red lines represent Dox alone, grey lines show oligonucleotide alone and blank lines denote the DNA:Dox sample. ..... 78
Figure 29. Comparison of the UV-Vis thermal melting profiles of 3.0 μM A) G1 B) G2 C) G3, in K-phosphate buffer at pH 7.0 in the absence and presence of 3.0 μM Dox by monitoring absorbance at 295 nm. ..... 80
Figure 30. Comparison of the UV-Vis thermal melting profiles of 3.0 μM A) G2 B) G3, in K-phosphate buffer at pH 7.0 in the absence and presence of 6.0 μM Dox by monitoring absorbance at 295 nm. ..... 81
Figure 31. Comparison of the UV-Vis thermal melting profiles of 3.0 μM A) G1 B) G2 and C) G3, in K-phosphate buffer at pH 5.5 in the absence and presence of 3.0 μM Dox by monitoring absorbance at 295 nm. ..... 82
Figure 32. Comparison of the UV-Vis thermal melting profiles of 3.0 μM A) G1 B) G2 and C) G3, in K-phosphate buffer at pH 5.5 in the absence and presence of 6.0 μM Dox by monitoring absorbance at 295 nm. ..... 83

Figure 33. Changes in fluorescence intensity of A) 3.0 μM (1:1) B) 6.0 μM (1:2) C) 30 μM (1:10) free Dox (black line) upon binding to 3.0 μM *PIM1* G-quadruplex structures at pH 7.0. ..... 86
Figure 34. Changes in fluorescence intensity of A) 3.0 μM (1:1) B) 6.0 μM (1:2) C) 30 μM (1:10) free Dox (black line) upon binding to 3.0 μM *PIM1* G-quadruplex structures at pH 5.5. ..... 87
Figure 35. Fluorescence intensity measurements for 1.0 μM solutions of Dox in the presence of increasing concentrations of A) G1 B) G2 C) G3 at pH 7.0 and Fraction bound vs Concentration of DNA (M in strand) obtained from the titration results (1st replicate). ..... 88
Figure 36. Comparison of the CD spectra of 3.0 μM of A) I1 B) I2 C) I3, in the absence and presence of 3.0, 6.0 and 30 μM Dox with the 3.0, 6.0 and 30 μM Dox spectra at pH 7.0. ..... 91
Figure 37. Comparison of the CD spectra of 3.0 μM of A) I1 B) I2 C) I3, in the absence and presence of 3.0, 6.0 and 30 μM Dox with the 3.0, 6.0 and 30 μM Dox spectra at pH 5.5. ..... 92
Figure 38. UV–Vis absorption spectra of 3.0 μM A) I1 B) I2 C) I3 in the absence and presence of 30 μM Dox at pH 7.0 in K-phosphate buffer. Red lines represent Dox alone, grey lines show oligonucleotide alone and blank lines denote the interaction between Dox and DNA. ..... 94
Figure 39. UV–Vis absorption spectra of 3.0 μM A) I1 B) I2 C) I3 in the absence and presence of 30 μM Dox at pH 5.5 in K-phosphate buffer. Red lines represent Dox alone, grey lines show oligonucleotide alone and blank lines denote the interaction between Dox and DNA. ..... 95
Figure 40. Comparison of the UV-Vis thermal melting profiles of 3.0 μM A) I1 B) I2 C) I3 in K-phosphate buffer at pH 7.0 in the absence and presence of 3.0 μM Dox by monitoring absorbance at 265 nm. ..... 98
Figure 41. Comparison of the UV-Vis thermal melting profiles of 3.0 μM A) I1 B) I2 C) I3 in K-phosphate buffer at pH 7.0 in the absence and presence of 6.0 μM Dox by monitoring absorbance at 265 nm. ..... 99

Figure 42. Comparison of the UV-Vis thermal melting profiles of 3.0 μM A) 11 B) I2 C) I3 in K-phosphate buffer at pH 7.0 in the absence and presence of 30 μM Dox by monitoring absorbance at 265 nm. ..... 100
Figure 43. Comparison of the UV-Vis thermal melting profiles of 3.0 μM A) I1 B) I2 C) I3 in K-phosphate buffer at pH 5.5 in the absence and presence of 3.0 μM Dox by monitoring absorbance at 265 nm. ..... 101
Figure 44. Comparison of the UV-Vis thermal melting profiles of 3.0 μM A) I1 B) I2 C) I3 in K-phosphate buffer at pH 5.5 in the absence and presence of 6.0 μM Dox by monitoring absorbance at 265 nm. ..... 102
Figure 45. Comparison of the UV-Vis thermal melting profiles of 3.0 μM A) I1 B) I2 C) I3 in K-phosphate buffer at pH 5.5 in the absence and presence of 30 μM Dox by monitoring absorbance at 265 nm. ..... 103
Figure 46. Changes in fluorescence intensity of A) 3.0 μM (1:1) B) 6.0 μM (1:2) C) 30 μM (1:10) free Dox (black line) upon binding to 3.0 μM *PIM1* i-motif structures at pH 7.0. ..... 106
Figure 47. Changes in fluorescence intensity of A) 3.0 μM (1:1) B) 6.0 μM (1:2) C) 30 μM (1:10) free Dox (black line) upon binding to 3.0 μM *PIM1* i-motif structures at pH 5.5. ..... 107
Figure 48. Fluorescence intensity measurements for 1.0 μM solutions of Dox in the presence of increasing concentrations of A) I1 B) I2 C) I3 at pH 7.0 and Fraction bound vs Concentration of DNA (M in strand) obtained from the titration results (1st replicate). ..... 108
Figure 49. Comparison of the CD spectra of 3.0 μM of A) D1 B) D2 C) D3, in the absence and presence of 3.0, 6.0 and 30 μM Dox with the 3.0, 6.0 and 30 μM Dox spectra at pH 7.0. ..... 112
Figure 50. Comparison of the CD spectra of 3.0 μM of A) D1 B) D2 C) D3, in the absence and presence of 3.0, 6.0 and 30 μM Dox with the 3.0, 6.0 and 30 μM Dox spectra at pH 5.5. ..... 113
Figure 51. UV–Vis absorption spectra of 3 μM A) D1 B) D2 C) D3 in the absence and presence of 30 μM Dox at pH 7.0 in K-phosphate buffer. Red lines represent

Dox alone, grey lines show oligonucleotide alone and blank lines denote the interaction between Dox and DNA. ..... 115
Figure 52. UV–Vis absorption spectra of 3.0 μM A) D1 B) D2 C) D3 in the absence and presence of 30 μM Dox at pH 5.5 in K-phosphate buffer. Red lines represent Dox alone, grey lines show oligonucleotide alone and blank lines denote DNA:Dox samples. ..... 116
Figure 53. Comparison of the UV-Vis thermal melting profiles of 3.0 μM A) D1 B) D2 C) D3, in K-phosphate buffer at pH 7.0 in the absence and presence of 3.0 μM Dox by monitoring absorbance at 260 nm. ..... 118
Figure 54. Comparison of the UV-Vis thermal melting profiles of 3.0 μM A) D1 B) D2 C) D3, in K-phosphate buffer at pH 7.0 in the absence and presence of 6.0 μM Dox by monitoring absorbance at 260 nm. ..... 119
Figure 55. Comparison of the UV-Vis thermal melting profiles of 3.0 μM A) D1 B) D2 C) D3, in K-phosphate buffer at pH 7.0 in the absence and presence of 30 μM Dox by monitoring absorbance at 260 nm. ..... 120
Figure 56. Comparison of the UV-Vis thermal melting profiles of 3.0 μM A) D1 B) D2 C) D3, in K-phosphate buffer at pH 5.5 in the absence and presence of 3.0 μM Dox by monitoring absorbance at 260 nm. ..... 121
Figure 57. Comparison of the UV-Vis thermal melting profiles of 3.0 μM A) D1 B) D2 C) D3, in K-phosphate buffer at pH 5.5 in the absence and presence of 6.0 μM Dox by monitoring absorbance at 260 nm. ..... 122
Figure 58. Comparison of the UV-Vis thermal melting profiles of 3.0 μM A) D1 B) D2 C) D3, in K-phosphate buffer at pH 5.5 in the absence and presence of 30 μM Dox by monitoring absorbance at 260 nm. ..... 123
Figure 59. Changes in fluorescence intensity of A) 3.0 μM (1:1) B) 6.0 μM (1:2) C) 30 μM (1:10) free Dox (black line) upon binding to 3.0 μM *PIM1* duplex structures at pH 7.0. ..... 126
Figure 60. Changes in fluorescence intensity of A) 3.0 μM (1:1) B) 6.0 μM (1:2) C) 30 μM (1:10) free Dox (black line) upon binding to 3.0 μM *PIM1* duplex structures at pH 5.5. ..... 127

Figure 61. Fluorescence intensity measurements for 1.0 μM solutions of Dox in the presence of increasing concentrations of A) D1 B) D2 C) D3 at pH 7.0 and Fraction bound vs Concentration of DNA (M in strand) obtained from the titration results (1st replicate). ..... 128
Figure 62. Fluorescence Intensity vs Wavelength (nm) spectra of the samples obtained from the competition dialysis cassettes containing 16 different nucleic acid structures at the end of 48 hours (1st replicate). ..... 131
Figure 63. Fluorescence Intensity vs Wavelength (nm) spectra of the samples obtained from the competition dialysis cassettes containing 16 different nucleic acid structures at the end of 48 hours (2nd replicate). ..... 131
Figure 64. Average $C_b/C_f$ values obtained from the Competition Dialysis experiment. ..... 133
Figure 65. UV-Vis absorption spectra of 3.0 μM A) G1 B) G2 C) G3 in K-phosphate buffer at pH 7.0 and D) G1 E) G2 F) G3 at pH 5.5 obtained during thermal denaturation experiments. ..... 157
Figure 66. UV-Vis absorption spectra of 3.0 μM A) I1 B) I2 C) I3 in K-phosphate buffer at pH 7.0 and D) I1 E) I2 F) I3 at pH 5.5 obtained during thermal denaturation experiments..... 158
Figure 67. UV-Vis absorption spectra of 3.0 μM A) D1 B) D2 C) D3 in K-phosphate buffer at pH 7.0 and D) D1 E) D2 F) D3 at pH 5.5 obtained during thermal denaturation experiments. ..... 159
Figure 68. UV-Vis absorption spectra of 3.0 μM A) G1 B) G2 C) G3 in Na-phosphate buffer at pH 7.0 and D) G1 E) G2 F) G3 at pH 5.5 obtained during thermal denaturation experiments ..... 160
Figure 69. UV-Vis absorption spectra of 3.0 μM A) I1 B) I2 C) I3 in Na-phosphate buffer at pH 7.0 and D) I1 E) I2 F) I3 at pH 5.5 obtained during thermal denaturation experiments..... 161
Figure 70. UV-Vis absorption spectra of 3.0 μM A) D1 B) D2 C) D3 in Na-phosphate buffer at pH 7.0 and D) D1 E) D2 F) D3 at pH 5.5 obtained during thermal denaturation experiments. ..... 162

Figure 71. UV-Vis absorption spectra of A) 1:1 B) 1:2 C) 1:10 G1:Dox at pH 7.0 and D) 1:1 E) 1:2 F) 1:10 G2:Dox at pH 5.5 in K-phosphate buffer obtained during thermal denaturation experiments ..... 163
Figure 72. UV-Vis absorption spectra of A) 1:1 B) 1:2 C) 1:10 G2:Dox at pH 7.0 and D) 1:1 E) 1:2 F) 1:10 G2:Dox at pH 5.5 in K-phosphate buffer obtained during thermal denaturation experiments ..... 164
Figure 73. UV-Vis absorption spectra of A) 1:1 B) 1:2 C) 1:10 G3:Dox at pH 7.0 and D) 1:1 E) 1:2 F) 1:10 G3:Dox at pH 5.5 in K-phosphate buffer obtained during thermal denaturation experiments ..... 165
Figure 74. UV-Vis absorption spectra of A) 1:1 B) 1:2 C) 1:10; I1:Dox at pH 7.0 and D) 1:1 E) 1:2 F) 1:10: I1:Dox at pH 5.5 in K-phosphate buffer obtained during thermal denaturation experiments ..... 166
Figure 75. UV-Vis absorption spectra of A) 1:1 B) 1:2 C) 1:10; I2:Dox at pH 7.0 and D) 1:1 E) 1:2 F) 1:10: I2:Dox at pH 5.5 in K-phosphate buffer obtained during thermal denaturation experiments ..... 167
Figure 76. UV-Vis absorption spectra of A) 1:1 B) 1:2 C) 1:10; I3:Dox at pH 7.0 and D) 1:1 E) 1:2 F) 1:10: I3:Dox at pH 5.5 in K-phosphate buffer obtained during thermal denaturation experiments ..... 168
Figure 77. UV-Vis absorption spectra of A) 1:1 B) 1:2 C) 1:10; D1:Dox at pH 7.0 and D) 1:1 E) 1:2 F) 1:10: D1:Dox at pH 5.5 in K-phosphate buffer obtained during thermal denaturation experiments ..... 169
Figure 78. UV-Vis absorption spectra of A) 1:1 B) 1:2 C) 1:10; D2:Dox at pH 7.0 and D) 1:1 E) 1:2 F) 1:10: D2:Dox at pH 5.5 in K-phosphate buffer obtained during thermal denaturation experiments ..... 170
Figure 79. UV-Vis absorption spectra of A) 1:1 B) 1:2 C) 1:10; D3:Dox at pH 7.0 and D) 1:1 E) 1:2 F) 1:10; D3:Dox at pH 5.5 in K-phosphate buffer obtained during thermal denaturation experiments ..... 171
Figure 80. UV-Vis thermal melting profiles of 3.0 μM G1 in K-phosphate buffer at pH 7.0 in the presence of 6.0 μM Dox by monitoring absorbance at 295 nm. ..... 172

Figure 81. UV-Vis thermal melting profiles of 3.0 μM G1 in K-phosphate buffer at pH 7.0 in the presence of 30 μM Dox by monitoring absorbance at 295 nm.....172
Figure 82. UV-Vis thermal melting profiles of 3.0 μM G2 in K-phosphate buffer at pH 7.0 in the presence of 30 μM Dox by monitoring absorbance at 295 nm.....173
Figure 83. UV-Vis thermal melting profiles of 3.0 μM G3 in K-phosphate buffer at pH 7.0 in the presence of 30 μM Dox by monitoring absorbance at 295 nm.....173
Figure 84. UV-Vis thermal melting profiles of 3.0 μM G1 in K-phosphate buffer at pH 5.5 in the presence of 30 μM Dox by monitoring absorbance at 295 nm.....174
Figure 85. UV-Vis thermal melting profiles of 3.0 μM G2 in K-phosphate buffer at pH 5.5 in the presence of 30 μM Dox by monitoring absorbance at 295 nm.....174
Figure 86. UV-Vis thermal melting profiles of 3.0 μM G3 in K-phosphate buffer at pH 5.5 in the presence of 30 μM Dox by monitoring absorbance at 295 nm.....175
Figure 87. Fluorescence intensity measurements for 1.0 μM solutions of Dox in the presence of increasing concentrations of A) G1 B) G2 C) G3 at pH 7.0 and Fraction bound vs Concentration of DNA (M in strand) obtained from the titration results (2nd replicate).....176
Figure 88. Fluorescence intensity measurements for 1.0 μM solutions of Dox in the presence of increasing concentrations of A) G1 B) G2 C) G3 at pH 7.0 and Fraction bound vs Concentration of DNA (M in strand) obtained from the titration results (2nd replicate).....177
Figure 89. Fluorescence intensity measurements for 1.0 μM solutions of Dox in the presence of increasing concentrations of A) D1 B) D2 C) D3 at pH 7.0 and Fraction bound vs Concentration of DNA (M in strand) obtained from the titration results (2nd replicate).....178
Figure 90. Dox calibration curve constructed for the competition dialysis assay (two replicates). .....180

## LIST OF ABBREVIATIONS

ABBREVIATIONS

| | |
|---|---|
| $K_a$ | Association constant |
| CD | Circular Dichroism |
| DNA | Deoxyribonucleic Acid |
| RNA | Ribonucleic Acid |
| NMR | Nuclear Magnetic Resonance |
| UV-Vis | Ultraviolet-Visible |
| Tm | Melting Temperature |
| TNBC | Triple Negative Breast Cancer |
| Dox | Doxorubicin |
| dsDNA | Double Strand DNA |
| G4 | G-quadruplex |
| I4 | i-motif |

# CHAPTER 1

# INTRODUCTION

## 1.1 Deoxyribonucleic Acid (DNA)

Deoxyribonucleic acid (DNA), which is one of the most important macromolecules in life, is composed of monomers called nucleotides. The main components of a nucleotide are an aromatic base (purine or pyrimidine ring), deoxyribose sugar and phosphate group (Figure 1) [1], [2]. Each polynucleotide chain composed of nucleotides has two distinct ends (5′and 3′) that give directionality to it. Typically, 5′ end has a free phosphate group and 3′ end has a free hydroxyl group. Bases are attached to each sugar by a glycosidic bond. Nucleotides in DNA are connected by phosphodiester bonds between the sugar of one nucleotide and the phosphate group of the other one. In double helical genomic DNA, the two strands running anti-parallel to each other are held together by stacking interactions and hydrogen bonding between pairs of bases. Purine bases are adenine (A) and guanine (G), and two pyrimidine bases found in DNA are thymine (T) and cytosine (C). Uracil (U) is also a pyrimidine base similar to thymine while it is a component of Ribonucleic acid (RNA). Each nitrogen base has a distinct structure enabling the formation of specific hydrogen bonding patterns through the presence of electron-accepting and donating sites. In genomic DNA, A prefers to hydrogen bond with T and G prefers to hydrogen bonds with C, and consequently, in a given genomic DNA sample, the quantity of A equals that of T, and G equals that of C. The spatial arrangement of base pairs results in the creation of major and minor grooves in the double helical genomic DNA. The bases are informational molecules of the cell, and the different placement of hydrogen bond donor and accepter groups give them the unique identity to serve as the genetic information. DNA's unique structure enables it to carry, retain and express heredity information in a cell where mutations and unusual

rearrangement of DNA can influence the gene expression. Damage to the DNA structure and replication errors has a significant role in the initiation of different diseases. Therefore, investigating the DNA structure is crucial to gain more information about the regulation of gene expression, transmission of the genetic information as well as the cell viability [1], [2].

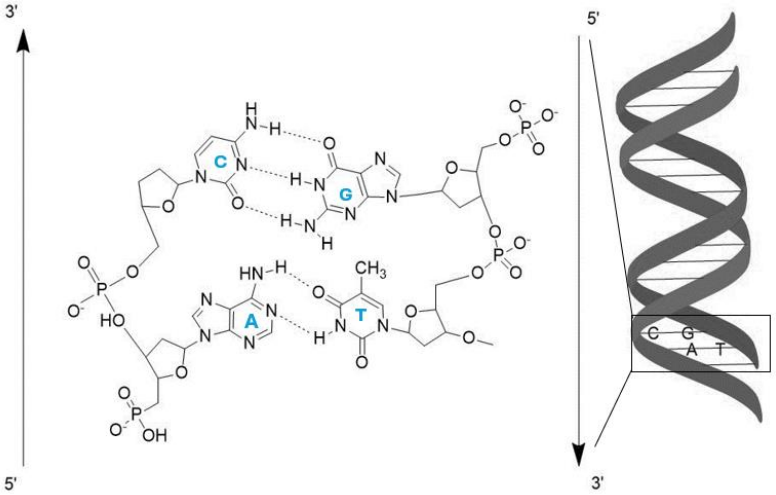


Figure 1. Watson-Crick base pairing and the antiparallel double helix structure of DNA. The arrows represent 5′→3′ directionality. Adenine (A) pairs with thymine (T) and guanine (G) pairs with cytosine (C).

## 1.2 DNA Structures and Properties

For many years after the revelation of the classical structure of the DNA double helix by Watson and Crick in 1953 [3] (Figure 1), most scientists accepted the idea that DNA was structurally a very uniform molecule [1]. According to this model, DNA is a right-handed double helix formed by two individual DNA strands aligned in an antiparallel fashion. These strands are held together by hydrogen bonds between bases and further stabilized by π-stacking between adjacent bases. This common form is named as the B-form DNA. However today we know that DNA is structurally a flexible molecule and can form a variety of secondary structures depending on the sequence and the environment. A-DNA and Z-DNA are examples of other double helical secondary structures formed by the coiling of two DNA strands (Figure 2).

In A-DNA model, the bases are tilted significantly with respect to the helical axis. The grooves are not as deep as in B-DNA and the bases are more located towards the outside of the double helix. The structural differences of Z-DNA model as a left-handed helix with right-handed forms include rotations about the glycoside bonds and orientations of base pairs within the helix [1].

DNA double helical secondary structure and its stability is strongly influenced by pH, temperature, ionic strength, and molecular crowding conditions along with the sequence [4].

A recent systematic experimental study explored the influence of buffer type and concentration on the stability of double helix DNA [5]. The study analyzed the thermal stability of calf thymus DNA using UV–Vis spectroscopy at different buffer concentrations ranging from 1 to 250 mM at pH 7.4. The findings revealed that the buffers (at the same ionic strength) affect DNA thermal stability in the order: Tris > cacodylate > phosphate > citrate. They also suggest that the Tm values rise as the buffer concentration increases mainly due to the reduced repulsion forces between DNA strands when the buffer concentration is high [5]. By the way, measuring the melting temperature (Tm) that shows the temperature at which half of the base pairs are open in a DNA chain is one of the simplest ways of measuring the stability of different DNA structures. At high temperatures, DNA experiences denaturation by strand separation. A-T base pairs, with only two hydrogen bonds, are less resistant to heat-induced denaturation compared to G-C base pairs, which have three hydrogen bonds [6]. A higher Tm indicates greater thermodynamic stability of the DNA structure [7]. In another study, Schildkraut and Lifson investigated the influence of salt concentration on DNA stability and its secondary structure by measuring the melting temperature (Tm) of bacterial DNA. In that study, DNA Tm values increased from 78.6 ºC in 0.01 M KCl to 98.7 ºC in 0.60 M KCl [8].

The pH can significantly affect DNA structure and stability. Around the neutral pH, from pH 5 to 9, common nucleic acid duplexes exhibit significant stability. Below

pH 5 and above pH 9, standard duplexes are destabilized due to the changes in ionization state of functional groups (such as amino and carboxyl groups) which can disrupt hydrogen bonding and stacking between base pairs [9].

Due to the flexibility of DNA, transitions from one helix form to another may occur under certain conditions [10]. The free energies associated with transitions from A-to-Z and B-to-Z conformations depend significantly on the sequence context of a given nucleic acid and environmental conditions. Among purines, guanine bases contribute to a higher stability of the Z conformation due to water-mediated hydrogen bonding networks facilitated by the exocyclic N2 group of guanosine residues. Consequently, GC-rich sequences exhibit the highest ability to adopt the Z conformation [10].

Additionally, salts and ions play a crucial role in stabilizing the Z conformation. Trivalent salts are more effective than divalent salts, which in turn are more effective than monovalent salts in promoting the Z conformation. Ions in the direct Hofmeister series are known to facilitate transitions from A- and B-DNA to the Z-DNA conformation. Increasing concentrations of Hofmeister ions can therefore stabilize the more hydrophobic Z conformation and facilitate the B-to-Z transition. Besides, the relative stability of the Z-DNA conformation generally decreases upon raising the temperature [11]. Sugiyama et al. reported proportions of Z, B and single-strand conformations of d(CGCGCG) as a function of temperature in 2.6 M NaCl, 5 mM Na-cacodylate buffer at pH 7.0 by using a combination of UV and CD spectroscopy [12]. At 2 ºC, there was a 1:1 mixture of B and Z conformations, with the proportion of B increasing as the temperature rises. By approximately 35 ºC, the proportion of the Z conformation was nearly zero [12].

A-DNA which is strongly implicated as a necessary structure in several polymerase reactions has been demonstrated to have increased stability in response to UV radiation and chemical toxicity. Besides, it has been identified as the most biologically active non-B-DNA conformation [13].

While B-DNA is stable under a broad variety of conditions, A-DNA has been observed under conditions of reduced water content, low hydration condition, high salt concentrations and moderately high ionic-strength environments [13], [14]. Whelan et al. investigated B-DNA shift to A-DNA in live cells upon dehydration (drying under nitrogen) using FTIR spectroscopy. They also demonstrated a return to B-DNA by subsequent rehydration of cells upon introducing ultrapure water directly beside the beam path. They report characteristic changes in FT-IR bands for B-conformation (fully hydrated DNA) to A-conformation transition which is a shift in the phosphate antisymmetric stretching vibration from 1225 $cm^{-1}$ to1238 $cm^{-1}$ [13]. They believe that the spectroscopic evidence for the reversible B- to A-DNA transition in eukaryotic cells and A-DNA resistance to various kinds of damage, highlights the potential biological significance of the genome-wide B- to A-DNA transition [13].

In addition to double helix structure, DNA can adopt various non-canonical conformations based on its sequence, which are especially stable in the crowded intracellular environment. Triplex DNA (Figure 3) is one of the examples of DNA secondary structures which is formed when a third strand is base paired to a duplex DNA and form a three stranded assembly [15]. Additionally, guanine-rich, and cytosine-rich sequences in complementary strands of DNA have the capacity to create unique tetra-stranded DNA structures, namely G-quadruplexes (G4s) and i-motifs (I4s) (Figure 4). The sequences which can form those tetraplex arrangements are found to be usually located in functionally important regions of DNA such as telomeric or centromeric sequences and promoter regions of genes. The fact that they are present *in vivo* indicates that four-stranded structures are involved in regulating genomic processes. All these different DNA structures have been shown to participate in various processes such as replication, transcription, and translation. And, investigating the connections between the formation and the functional implications of these noncanonical DNA structures represents a contemporary scientific endeavor [16].

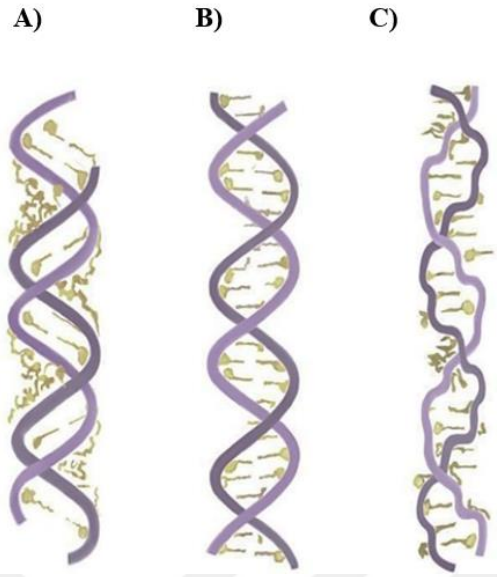


Figure 2. Configurations of DNA double helix A) A-DNA B) B-DNA C) Z-DNA [17]. *

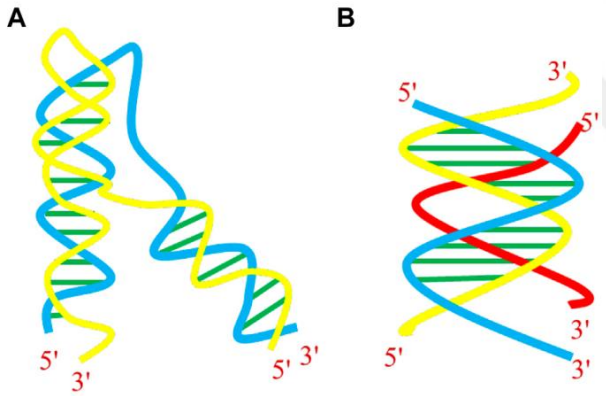


Figure 3. Helical representation of (A) intramolecular and (B) intermolecular DNA triplex [18].†

* The open access journal allows usage of content without permission.
† The open access journal allows usage of content without permission.

### 1.2.1 G-quadruplex Structures

Four guanine bases can base pair with each other using both the Watson-Crick and the Hoogsteen hydrogen bonding and can form planar structures knowns as G-quartets. Stacks of two or more G-quartets form noncanonical secondary structures called G-quadruplexes (G4s) (Figure 4A). DNA G-quadruplexes are notably found at telomeres and oncogene promoters, influencing crucial cellular processes such as replication, gene expression and regulation, telomere maintenance, and transcription [16]. This quadruple helical structure is stabilized by cations centrally coordinated to O6 of the guanines [20]. G-quadruplexes can be unimolecular (one DNA strand) or intermolecular (two or four DNA strand). Besides, according to the combinations of strand directions G4s can adopt wide diversity of topologies [21]. Parallel, antiparallel and hybrid structures are three mainly accepted forms of G4s. G-quadruplex conformations vary depending on environmental factors such as cations, pH, crowding, and temperature which means the same sequence can adopt different topologies. This polymorphism makes G4s versatile building blocks for nanomolecular devices and sensors [22].

For instance, to investigate G4s role in various cellular processes and functions, characterization of vital G4 forming oncogenes such as *C-MYC* were performed [23], [24]. The evidence for G-quadruplex formation at the *C-MYC* promoter is provided by an investigation by Siddiqui-Jain et al. [23], proposing two topologies, called “chair” and “basket”. Following that, another study [23] reported propeller-type parallel-stranded G-quadruplexes instead of chair and basket. Consequently, new mechanisms have been used to target G4s and control *MYC* expression [25]. The formation of a G-quadruplex on the G-rich strand and an i-motif on the C-rich strand was shown to suppress *MYC* expression, with nucleolin protein identified as the specific protein responsible from the folding of the strand into the G-quadruplex structure [26].

Moreover, the sequences located between the G-quartets form loops. Loop length and sequences also found to have a significant impact on the folding (topology) and

stability of G-quadruplexes [27]. In an investigation by Hazel et al. [27], loop length effect on G-quadruplex folding was studied for different sequences based upon the human telomeric repeat d[$AG_3(T_2AG_3)_3$]. According to their results, structures with single T1 or T2 and three T2 loops favor the formation of both parallel and anti-parallel G4s while three T1 loops favor only the formation of the parallel structure. Besides, it has been shown that there is substantial decrease in melting points as loop lengths increase [27].

Another crucial factor that affects G4 formation and stability is the type of monovalent cation in the environment. Among the most extensively characterized monovalent cations, the preference for G-quadruplex formation is in the order of $K^+$ > $Na^+$ > $Li^+$ [20]. Concerning this issue, Hud et al. [28] studied competition between $K^+$ and $Na^+$ ions for coordination in [d($G_3T_4G_3$)]$_2$. They found out that, upon addition of KCl, two $K^+$ selectively replace the bound $Na^+$ in [d($G_3T_4G_3$)]$_2$ with a net free energy change (ΔG°) of -1.7 kcal/mol at 25 °C. They believe that this preferential binding of $K^+$ is by the preferential hydration of $Na^+$ compared to $K^+$ [28]. In another investigation by Mergny et al. [29] eight different sequences susceptible of forming an intramolecular G-quartet have been tested in NaCl or KCl. The Tm values were independent of pH, while they were higher in KCl than in NaCl, which is a well-known property of G-quadruplexes. This was a result of more negative (more favorable) enthalpies of G-quartet formation in the presence of $K^+$ ion. The changes in Tm values were between +7 and +30 ºC higher depending on the oligonucleotide [29].

The stability of G-quadruplexes is not always reported to be independent of pH. In an intriguing study, Hardin et al. demonstrated the presence of C.$C^+$ base pairs in G-rich sequences for the first time [30]. In this study Tm values were plotted as a function of pH ranging from 6 to 9 and the resulted curves showed a dramatic destabilization at pH 6.5 and 8.5. Their experiments revealed the $pK_a$ in the 9-9.5 range due to the deprotonation of the deoxyguanosine imino proton. Additionally, there was another $pK_a$ value at 6.8. Considering the increase in $pK_a$ values for Cytidines from 4.2 to 7.0 due to the protonation of N3 atom, they concluded that the

other $pK_a$ value at 6.8 for $d(CGCG3GCG)_4$ G-quadruplex structure indicates formation of $C.C^+$ base pairs [30].

In another study, Benabou et al. observed similar results for the SMARCA4 gene, which is associated with ovarian cancer [31]. Acid-base titrations monitored by CD and molecular absorption showed pH-dependent transition with $pH_{1/2}$ value equal to 7.1 ± 0.2. A dramatic change in CD spectra was observed. The results revealed that the presence of cytosine bases at the first and third loops produces a strong stabilization of the G-quadruplex structure at near neutral pH values because of the formation of an additional $C{\cdot}C^+$ base pair. The absence of the acid-base transition with $pH_{1/2}$ value equal to 7.1 in mutated sequences, where the hypothesized $C{\cdot}C^+$ base pair cannot be formed, was taken as the evidence for vital role of this base pair in the pH-dependent folding of the DNA sequence. CD-monitored melting experiments revealed an increase in Tm values from 36.0 °C at pH 7.4 to 60.0 °C at pH 4.9 using 150 mM KCl [31].

In the study conducted by Yan et al. [32] the effect of pH on different natural G-quadruplex forming sequences was investigated. Intermolecular G-quadruplexes without loop were less stable at pH 4.5 in comparison to neutral pH (pH 7.0). While for intramolecular G-quadruplexes, an increase of Tms were observed comparing with that at neutral pH. Additionally, they found that G-quadruplexes with selected loops could undergo quick conformational transformations upon pH change. They believe this can be used to design pH-driven nanodevices such as a nanoswitch.

The fact that G-quadruplex structures excessively exist in telomeres and oncogene promoters, underscores their importance as promising therapeutic targets. This potential has fueled interest in utilizing specific ligands to inhibit cancer cell growth, emphasizing their relevance in cancer therapy [33], [34]. For instance, one of the G4s ligand MM41 was reported to cause an 80 % decrease in growth of tumor in *in vivo* model for pancreatic cancer [35].

Moreover, the multifaceted roles of G4s in genomic processes and their therapeutic potential emphasize the importance of comprehensively understanding their

conformational dynamics in various environmental conditions. The impact of environmental factors on G4 conformational changes is crucial for designing effective G4-forming sequences and therapeutic agents targeting these sequences in addition to unraveling their *in vivo* functions [34].

### 1.2.2 i-motif

i-motif (I4) is another four stranded DNA structure (two parallel stranded duplexes) formed by cytosine-rich sequences in which the bases are held together by hemi-protonated cytosine-cytosine$^+$ (C:C$^+$) base pairs (Figure 4B). In fact, this is the only known nucleic acid structure that involves base intercalation. This structure is often present in functionally important parts of the genome such as telomeres and promoter regions. i-motifs formation in proto-oncogene regions such as *Bcl$_2$* and *HRAS* is shown to interfere with DNA replication, suggesting them as potential targets for the diagnosis of cancer risk and therapeutic interventions [36], [37]. DNA i-motif structure was initially characterized by Gehring et al. studying d(TCCCCC) sequence [38]. Subsequently, several i-motif structures have been determined using crystallography and NMR. It is well known that the i-motif structure is formed in solutions with low pH values due to the hemi protonation of cytosine. The highest stability of the i-motif structures occurs at pH values near the pK$_a$ of cytosine, approximately 4.6. At higher pH levels, cytosine bases deprotonate, leading to the unfolding of the structure into a single-stranded form. Conversely, at excessively low pH values (below approximately 3), all cytosine bases become protonated, preventing the formation of the hydrogen bond pattern required for the C:C$^+$ base pairing [39]. However, some studies report the formation of this structure in neutral or alkaline pH environments. Zhou et al. have demonstrated that the i-motif structure can be formed at pH 7.0–7.5 at 4 °C [40]. There are also other reports revealing that the molecular crowding could induce the formation of a stable i-motif at physiological pHs [41].

There are only a few reports with inconsistent conclusions on the ion and buffer effects on i-motif formation and stability. Mergny et al. reported destabilization of i-motif structure upon increasing the $Na^+$ concentration from 0 to 100 mM [39]. In contrast Kim et al. found that $Na^+$ cations stabilize i-motif formation while $Li^+$ cations promote unfolding of i-motif [42]. Recently, it was discovered by Gao and Hou that $K^+$ has opposite effects on the thermal stability of i-motif structures in different buffer systems. In their study $K^+$ was found to stabilize i-motif structures in phosphate, saline sodium citrate, and sodium cacodylate buffer while disrupting i-motif formation in MES and Bis-Tris buffers [43].

i-motifs potential role in various important biological processes like replication, regulation of oncogene expression, and telomere functions make this non-canonical structure an emerging area of research in medicinal and nucleic acid chemistry. These studies investigate its potential as a target for both anticancer drug design and gene regulation processes. In the past few years, i-motif structure has got several applications especially in the field of nanotechnology and analytical chemistry due to its pH driven conformational changes. Conformational changes of the i-motif structure have been modulated for applications such as molecular switches, biosensors and nanomachines [44], [45], [46]. The latest application of DNA i-motif structure to design intelligent drug delivery systems has gained considerable interest for the treatment of cancer. This system relies on the pH-responsive behavior of i-motif DNA, taking advantage of the higher acidity of tumor centers compared to healthy tissues. As a result, it can efficiently deliver drug payloads to specific target sites [47]. Overall, both i-motifs and G4 structures are increasingly utilized also in nanotechnology as responsive structural components sensitive to cations and pH [48].

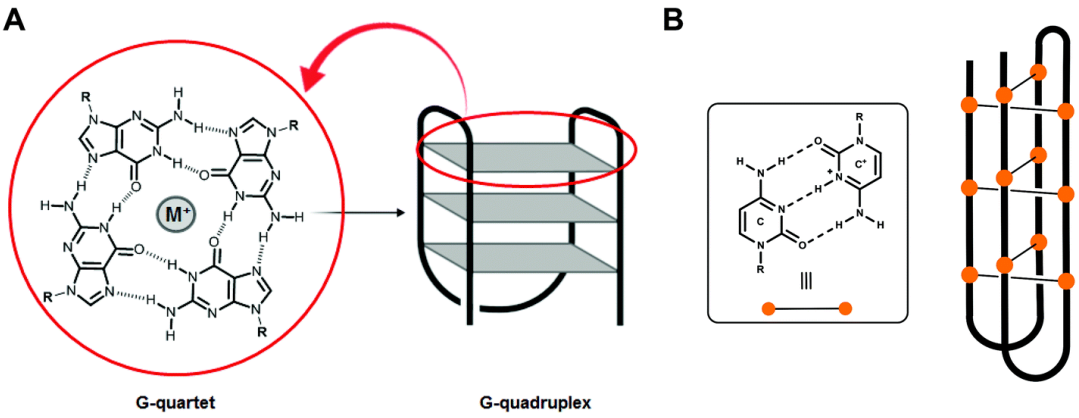


Figure 4. (A) G-quartet with Hoogsteen hydrogen bonded guanine and schematic drawing of a G4 structure and (B) hemi-protonated C–C$^+$ base pairs and schematic representation of an *i*-motif structure [48]. ‡

## 1.3 Duplex-Quadruplex Equilibria in Guanine- and Cytosine-rich DNA

In a DNA duplex with a guanine-rich strand, the complementary strand is necessarily a cytosine-rich sequence. A disruption in the original Watson-Crick duplex is the first requirement for the formation of a G-quadruplex or i-motif in a double-stranded DNA. Due to the role of secondary structures in the regulation of genomic processes, especially inhibiting DNA replication and transcription in the promoter regions of many oncogenes, duplex-tetraplex competition has gained a great interest recently [48]. Direct competition between duplex DNA and noncanonical secondary structures, including G-quadruplex and i-motif, may be a common mechanism of tetraplex formation within the genome. As an alternative to direct duplex-tetraplex competition, quadruplex structures may form in the genome, following the accumulation of negative supercoiling after transcription and replication, which can decrease stability of the duplex [49]. At equilibrium *in vitro*, the preference for a particular conformation is determined by the difference in the change in free energy

‡: The open access journal allows usage of content without permission.

(ΔG°) during the formation of a duplex from single strands and the combined free energies involved in forming noncanonical structures from those same single strands. Thermodynamic stabilities of the duplex and tetraplex structures result in the duplex tetraplex competition. Number of quartets, stacking and electrostatic interactions, length and sequence of loops and environmental conditions (especially the counterion nature and pH) are the factors that affect the prevalence of noncanonical secondary structures [50].

Abou Assi et al. [51] have studied several human telomeric sequences to investigate whether the temporary formation of i-motif structures in the C-rich strand would free up the G-rich strand for inhibition of telomerase. They concluded that the G-quadruplex, *i*-motif, and duplex conformations in the human telomeric DNA were coexisting at neutral pH. In another effort, Liu et al. characterized the conformational preferences of DNA in an equimolar mixture of complementary G-rich and C-rich strands from the promoter region of the *c-MYC* oncogene. The results revealed that, at acidic pH, elevated potassium, and room temperature the G-quadruplex and *i*-motif structures prevail over the duplex state however, at neutral pH, i-motif is not formed, and duplex structure coexists with G4s [52]. Additionally, Khan et al. investigated the pH influence on promoter region of the B-cell lymphoma (*BCL-2*) gene [53]. At pH 7.1 in the presence of 150 mM KCl, equimolar amounts of the two C-rich and the complementary G-rich strand, were found to form a duplex. As the pH decreases to 5.0, the conformational distribution was observed to shift towards the G-quadruplex and i-motif structures. This result is in great accordance with promoter region of *c-KIT* [54] and *n-MYC* oncogenes [55]. Not all DNA oligonucleotides containing complementary G-rich and C-rich strands tend to separate at acidic pH and create tetraplex structures. This means that, for some sequences, a decrease in pH is not sufficient for the induction of the duplex-tetraplex transition [49].

In an investigation to determine the ability of a specific sequence to undergo a pH-induced duplex-to-tetraplex transition, human telomeric DNA was studied [56]. The results revealed that, at room temperature and in the presence of 100 mM NaCl, an

equimolar mixture of d($T_2AG_3T_2AG_3T_2AG_3T_2AG_3$) and d($C_3TA_2C_3TA_2C_3TA_2C_3TA_2$) overwhelmingly adopts the duplex structure both at pH 7.4 and pH 5.0. At acidic pH just about 5 % of the population may assume the G-quadruplex and i-motif structures. Additionally, Konig et al. have studied destabilization effect of sequences that are susceptible to form G-quadruplexes and i-motifs on duplex stretches [57]. They believe that either a G-quadruplex or an i-motif is able to form, but the formation of both motifs adjacent to duplex DNA appears to be energetically unfavorable, particularly at lower pH values. Additionally, they showed that both G-quadruplexes and i-motifs are capable of destabilizing directly proximal duplex DNA [57].

Overall, the stabilities of the G-quadruplex formed by the G-rich strand and the i-motif formed by the C-rich strand significantly influence the competition between duplex and tetraplex structures. Intercellular influences such as chromatin structure, duplex supercoiling and the presence of specific proteins (such as chromatin structure) could also shift the equilibrium to favor quadruplex formation over duplex formation. Furthermore, drugs that identify and selectively bind to G4s and i-motifs with an affinity surpassing their binding to B-DNA, possess the potential to shift the duplex-tetraplex equilibrium towards the quadruplex formation [58].

## 1.4 DNA and Cancer Therapies

Cell growth is normally controlled by the actions of certain genes inside each cell. Cancer begins when cells in the body become abnormal and start to grow out of control [59]. Different types of mutations and damage to DNA within cellular nuclei can influence gene expression and other biochemical processes that affect cell growth. When a proto-oncogene which normally helps cells to grow and divide undergoes a mutation, it transforms into an oncogene, causing uncontrolled cell growth and division. Oncogenes have the potential to transform normal cells into diseased cells, possibly leading to the development of cancer [60].

The choice of treatments for cancer varies depending on the condition and stage of the disease. Options include surgery, radiotherapy, chemotherapy, and immunotherapy. Chemotherapy involves the use of chemicals to halt specific cellular functions. One of the chemotherapy targets is DNA, with the goal of eliminating tumor cells by preventing cell growth and division. The damage to DNA, resulting in the loss of genomic DNA will result in senescence or cell death if not repaired. Platinum complexes such as cisplatin and some nitrogen mustards including mustine, chlorambucil and melphalan are well-known classical anticancer drugs targeting the DNA. The cytotoxic impact of nitrogen mustards has been observed through the alkylation of DNA cross-links, thereby influencing the integrity of the double-stranded DNA. These alkylators disrupt the normal DNA replication machinery over a time span ranging from a short duration to several days [59], [61].

Unfortunately, the lack of selectivity in drugs, coupled with the heterogeneous nature of cancers, poses a significant challenge for clinical treatments. Additionally, more effective, and selective drugs are needed to overcome drug resistance problems. Therefore, cancer research has dramatically shifted to the discovery of new methods which are also able to recognize specific DNA sequences. Using small molecule DNA binders has been in the limelight of drug-discovery programs due to their ability to control gene expression and demonstrate therapeutic development [62]. In this context, the diversity of DNA topologies and structures such as G4 and i-motifs, underscores the challenges associated with the programmed DNA recognition [63].

Elevated G4 formation in tumor tissues compared with normal tissues shows this noncanonical DNA structure role as an accelerator of cancer genome evolution [64]. For instance, Wolfe and co-workers [65] have shown that eIF4A, a translation initiation factor with G4 helicase activity, facilitates the development of T-cell acute lymphoblastic leukemia.

Moreover, Chen et al. demonstrated that single-walled carbon nanotubes selectively stabilize human telomeric i-motif DNA, thereby inhibiting telomerase activity in living cells. Their research revealed that the stabilization of the i-motif structure and

the concurrent formation of G-quadruplexes result in the uncapping of telomeres and displacement of telomere-binding proteins. This process triggers a DNA-damage response at the telomeric level, leading to the cessation of tumor cell growth [66].

The interaction between DNA structures and small molecules occurs through different mechanisms which alters the normal activity of DNA and control the development of tumor cells with consequent cytotoxic effect and cell death [67].

### 1.4.1 DNA Interactions with Drugs

As mentioned above, targeting DNA is a promising field of study due to its importance in regulation of gene expression and cell growth. Many antitumor compounds can interact strongly and specifically with DNA that could be mediated also through water molecules and counterions. There are two main modes of interaction between the DNA and the small molecule drugs: covalent and non-covalent. Mitomycin, anthramycin and bleomycin $A_2$ are examples of covalent binders which cause enduring harm to DNA and its functions [68]. Mitomycin in this category, does not react directly with DNA. Activation of mitomycin, which results in covalent cross-linking of DNA duplex structure, occurs by reduction of quinone and then cascade of spontaneous transformations to open aziridine ring and produce a structure with high alkylating activity. This structure alkylates 2-amino group of guanines in the minor groove of DNA. Crosslinking of this drug is for CG.CG sequence of the duplex DNA. Mitomycin has a variety of biological effects such as inhibition of DNA synthesis, mutagenesis, simulation of genetic recombination and chromosome breakage, and induction of DNA repair response (SOS) [69].

Groove binding and intercalation are the main non-covalent modes of the binding. Groove binding ligands are also among potential chemotherapeutic agents. Bulky molecules can easily interact through major groove which has multiple sites of interaction. The minor groove is smaller and has fewer binding sites. However, it

usually has free sites and thus more available for small molecules to attack. Most of the potential therapeutic agents are minor groove binders and there is a selectivity toward A and T rich regions [70], [71]. NMR and crystallographic studies have been used to investigate the binding nature of minor groove binders [70]. Netropsin, is a non-covalent minor-groove binder with antiviral and antitumor activity. The detailed experimental information regarding the interactions between this drug and A/T base pairs were provided by determination of crystal structure of netropsin bound to the d(CGCGAATTCGCG) duplex sequence [71]. The roughly planar structure of netropsin, fits into the narrow minor groove in the A-A-T-T center of the structure positioning pyrrole and amide groups of it close to the walls of the groove. It slightly widens the groove without causing unwinding or elongation of the double helix. Netropsin interaction with DNA and RNA prevents their synthesis by inhibition of the corresponding polymerase reaction. Many modifications to the natural structures have been made to cover and recognize extended blocks of A/T base pairs [71].

In intercalation, the aromatic portion of the drug is inserted between two base pairs of the double helix. It results in distortion and unwinding of the double helix [72], [73]. Anthracyclines are a vital group of intercalators which can be used in the treatment of different kinds of cancers [74]. The interactions of Doxorubicin (Dox) (Figure 5), which is an anthracycline, is given in detail below, since the interactions of Dox with *PIM1* sequences are investigated within this thesis.

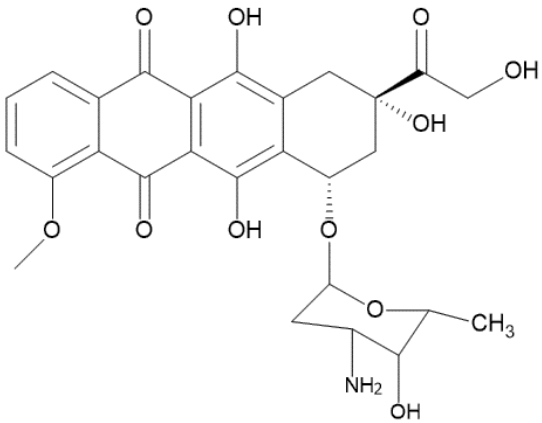


Figure 5. Structure of Doxorubicin

## 1.5 Doxorubicin Interactions with Genomic DNA

Doxorubicin (Dox) and daunorubicin, are examples of anthracyclines which can act as very effective antitumor agents. Anthracyclines are planar, aromatic molecules, able to bind DNA by intercalating between DNA base pairs. Over the past 50 years, they have been used as a key in treatment of leukemia, malignant lymphoma, and breast cancers [75]. The structure of the anthracycline derivative Dox is shown in Figure 5. Although the kinetics and mechanisms of action of Dox have been studied extensively over the past decades, its precise modes of action remain complex and still relatively unknown [76].

DNA damage is one of the most important effects of Dox that result in anti-tumor activity [77]. Generally, anthracycline drugs interact with B-DNA. The mechanism involves intercalation of anthraquinone part at GC sequences and there is an interaction with sugar part of drug with minor groove. Both Dox and daunorubicin have an amino group which can be protonated and involved in charge-charge interactions with the negatively charged phosphate backbone of DNA. These interactions resulting in slight changes in DNA topology inhibit DNA replication and transcription. For instance, it is known that, *in vivo* the binding of Dox to DNA and the formation of DNA-Dox complex results in the inhibition of DNA

topoisomerase II which is one of the essential enzymes in DNA replication [78], [79].

Senescence induction in cancer cells is another well-known mechanism of Dox action. This was established as the primary mechanism of therapeutic activity of Dox in the FU-SY-1 synovial sarcoma cell line [80]. Growth arrest, induction of DSBs (double-strand breaks), up-regulation of P21, and ATM (ataxia-telangiectasia mutated protein kinase) activation was shown following drug treatment [80]. Typically, senescent cells display characteristic features like cell-cycle arrest, expression of senescence-associated β-galactosidase, telomere shortening and secretion of multiple factors including inflammatory factors such as Matrix metalloproteinases (MMPs) [80].

In addition to induction of DNA damage by intercalation or topoisomerase II inhibition, Dox also induces apoptosis through the production of reactive oxygen species (ROS). ROS which normally function as cellular messengers in redox signaling events at relatively low concentrations, can lead to DNA damage when present in excessive amounts, through the action of radicals on DNA bases and the sugar–phosphate backbone [81].

On the other hand, along with its potent anticancer properties, it has a potential to cause dose-dependent cardiotoxicity via generation of reactive oxygen species (ROS), which can limit its clinical utility [81]. Mechanisms of the cardio toxic effect of Dox have also been under investigation and several molecules were proposed to prevent the toxicity of Dox [82], [83]. Dose-dependent cardiotoxicity of Dox underscores the importance of developing targeted delivery systems for this agent [84].

Even though all the action mechanisms of Dox *in vivo* are not known, it is known that Dox not only interacts with B form DNA but also displays high affinity towards the G-quadruplex structure of human telomere [85], [86], *VEGF* promoter [87] and

*c- MYC* [88].

### 1.5.1 Dox Interaction with G4 Structures

Since G4 structures could result in transcriptional silencing, the drugs that stabilize G4s can suppress gene expression. Binding of drugs to G4 structure can downregulate gene overexpression and alter the prognosis of several cancers [88]. Human telomeric sequence interaction with Dox in the presence of $K^+$ is studied by Manet et al. [86]. Association constant of Dox with 5′-d[GGG(TTAGGG)$_3$]-3′ obtained from titration experiments was reported as: $K_1 = (1.49 \pm 0.21) \times 10^5$ $M^{-1}$ which is slightly lower than its affinity to duplex DNA, which was $0.54 \times 10^6$ $M^{-1}$. The fluorescence quenching technique was used to confirm complexation, and Circular Dichroism (CD) spectra of the complexes revealed that the drug binding influences the equilibrium between quadruplex conformations. The binding of the drug influences the population of quadruplex conformations, showing a preference for antiparallel conformers. Binding of Doxorubicin to the G4 was found to increase the Tm values of the DNA structure from 62 ºC to 67 ºC [88]. Recently, another study by our research group has proven the stabilization of G-quadruplex forming *VEGF* $Pu_{22}$ promoter sequence by Dox [87]. Association constant was determined by titration experiments using Fluorescence spectroscopy yielded the value of $K_a = 7.50 \times 10^6$. Dox interaction with the wild type *c- MYC* G4 forming sequence [88], revealed external binding of the compound with partial stacking at the end quartets via fluorescence displacement assay technique using ThT and $H_2$DAC. An increase in the Tm values of the G-quadruplex structure was observed but the nature of the structure was intact upon Dox binding. The binding constants were of the order of $10^6$ $M^{-1}$ which is comparable with other G4 binding ligands [88]. Nevertheless, only a few reports exist examining Dox interactions with G4s and evaluating its mechanism of action through G4 structures which are thought plausibly to provide insight into its mechanism of action and to the dose-dependent cardiotoxic effects [89].

### 1.5.2 Dox Interactions with i-motifs

i-motif structure is believed to be a highly dynamic structure that exists in equilibrium with flexible hairpin species which could be attractive targets for small molecule control of gene expression [90]. According to a pioneering study reporting a pH-controlled cytosine-rich drug-release device, Dox is released from the duplex stem of a hairpin structure by the formation of i-motifs at acidic pH [91]. This study reports a significant increase in the Tm values of hairpin structure of C-rich DNA upon Dox interaction at neutral pH, while there is not an increase for i-motif DNA stability at acidic pH. They believe that a reduction in fluorescence intensity at neutral pH which increases again when pH changes from 7.0 to 5.0, proves the release of Dox following i-motif formation at acidic pH. After this study, different investigations have reported the design of i-motif based biological systems such as i-motif-coated exosomes, to deliver Dox to cancer cells efficiently [92], [93]. The utilization of a pH-driven C-rich DNA drug release device relies on the principle that Dox can bind to the hairpin species or double stranded DNA at neutral pH, while no interactions are observed at the acidic pH found in tumor cells, where the i-motif structure is formed. However, there is no direct study reported in the literature investigating the interactions of i-motif structure with the Dox. On the other hand, the interactions of i-motif structures with widely used G-quadruplex ligands, such as BRACO-19, Berberine and Mitoxantrone, were investigated previously and these ligands were found to be destabilizing the i-motif structures [94], [95].

## 1.6 G-quadruplex Structures in *PIM1* Gene

Proviral insertion site in Moloney murine leukemia virus (PIM) genes were initially recognized as oncogenes in mouse models during the 1980s and were subsequently discovered to encode serine/threonine kinases with a broad range of cellular targets [96]. They composed of three different isoforms as *PIM1*, *PIM2*, and *PIM3* which are single-copy genes located on three different chromosomes. PIM family proteins

play a vital role in apoptosis, cell cycle regulation and cell proliferation. PIM kinases are potent oncogenes and they have shown to be involved in tumorigenesis. They are able to enhance tumor growth and induce chemo-resistance, which makes them attractive therapeutic targets for cancer therapy. Since PIM kinases lack a regulatory domain, they exhibit constitutive activity after expression. Therefore, their activity seems to be controlled at the transcriptional, translational, and proteasomal degradation levels [96]. They are overexpressed in a range of hematopoietic malignancies and solid cancers. *PIM1*, the first member to be discovered, was identified through cloning of the retroviral integration sites in lymphomas (cancer of the lymphatic system) induced by the MMLV or Moloney murine leukemia virus. This group of PIM kinases is predominantly expressed in hematopoietic cells. Moreover, oncogenic collaboration of *PIM1* with *c- MYC* have been demonstrated in prostatic cancer and lymphomagenesis [97].

Overexpression of *PIM1* oncogene has also been implicated in triple-negative breast cancer (known as TNBC) which lacks targeted therapies and exhibits poor prognosis. *PIM1* is thought to create a protection from spontaneous and chemotherapy induced apoptosis and promote cell cycle in TNBCs [98], [99]. Brasó-Maristany et al. reported *PIM1* relationships with *MYC* activation and identified a potential application for *PIM1* inhibitors in overcoming the high resistance of TNBC to chemotherapy-induced cell death through apoptosis [100]. They demonstrated that the pan-PIM kinase inhibitor AZD1208 [101] influences cancer cell growth suppression and reduces the resistance of TNBC cell lines to apoptosis. In addition, Nuclear Magnetic Resonance (NMR) studies by Tan et al. [99], revealed that *PIM1* oncogene has a G-quadruplex duplex hybrid (QDH) structure. Three different DNA sequences of *PIM1* gene, *PIM1-SLQS08, PIM1-SLQS07* and *PIM1-SLQS02* were examined in their study. The results have suggested that two different quadruplex duplex hybrid structures for *PIM1* gene can coexist within the natural sequence context (Figure 6). Form 1 has a (3+1) G-tetrad core with a coaxially oriented duplex stem and form 2 consists of a chair-type G-tetrad core and an adjoining G•C•G•C tetrad, with a hairpin stem-loop. *PIM1-SLQS07* adopts Form 1, *PIM1-SLQS02* exists

in Form 2 and *PIM1-SLQS08* comprises a mixture of both Form 1 and Form 2. They proposed that the quadruplex–duplex junction present in *PIM1* gene, could provide a unique interface for ligand targeting. And the design and development of inhibitors that target these QDH structures could be an attractive approach for the regulation of the *PIM1* gene expression and treatment of TNBC [99].

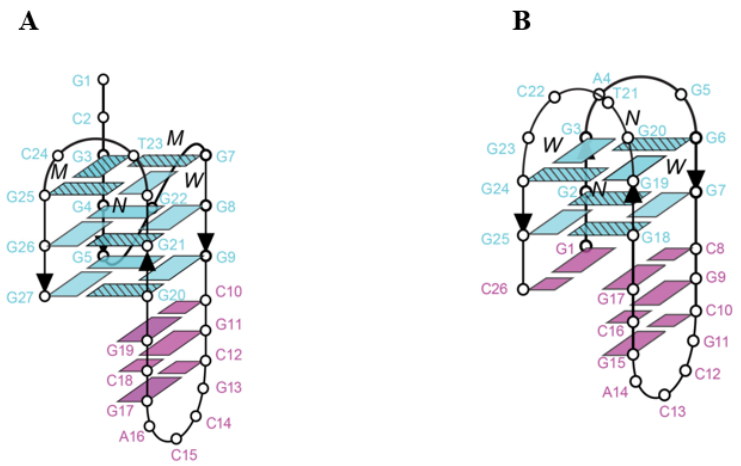


Figure 6. Schematic diagrams of *PIM1* Form 1 and Form 2 QDHs are shown in (A) and (B), respectively [99].[§]

## 1.7 Scope of the Thesis

Triple-negative breast cancer (TNBC) is an aggressive subtype of breast cancer where tumors lack ER (estrogen receptor), PR (progesterone receptor) and HER-2 (Erb-B2 receptor tyrosine kinase 2) expressions. TNBCs have a poor prognosis and generally lack targeted therapies [102], [99]. *PIM1* (proviral insertion site in Moloney murine leukemia virus) is one of the overexpressed oncogenes in TNBCs [103]. Interestingly, *PIM1* promoter sequences were found to adopt unique G-quadruplex-duplex hybrid-type secondary structures at pH 7.0 [99].

---

[§]: The open access journal allows usage of content without permission.

Since, the G-quadruplex-duplex hybrid structures of *PIM1* genes represent attractive targets for drug binding towards the downregulation of the *PIM1* gene for anticancer treatment instead of direct small-molecule binding of oncogenic proteins for inhibition [99], the effect of the environmental conditions such as pH, buffer type and the cation type on the secondary structures (G4, I4 and dsDNA) of the *PIM1* gene sequences are investigated in the first part of this thesis. The *PIM1*-SLQS08 (named as G1 in this work), *PIM1*-SLQS07 (named as G2) and *PIM1*-SLQS02 (named as G3) DNAs used by Tan et al. [99] and their complementary strands named as I1, I2 and I3 were used in our investigation. It has been known that depending on the solution conditions such as buffer medium, pH and the nature of stabilizing cation, G4s can adopt different topologies and structures [104]. Accordingly, it was hypothesized that the environmental conditions might have altered the prevalence of a certain secondary structure over the others, which might possibly affect the gene expression. The changes in UV-Vis and CD spectra of *PIM1* duplex, G4 and i-motif DNAs due to the differences in environmental conditions are used to detect structural changes. UV-Vis thermal denaturation experiments are conducted to reveal the stability changes in the structures by depicting the increase/decrease in thermal denaturation temperatures depending on various environmental conditions.

To the best of our knowledge, the formation of the duplex and i-motif structures in the *PIM1* gene sequences have never been investigated before. The effects of environmental conditions on the *PIM1* G4 sequences have also never been investigated.

In the second part of this thesis, the affinity and relative selectivity of Dox as an anti-cancer agent for dsDNA, G4 and i-motifs are investigated by UV-Vis, CD and Fluorescence experiments. Competitive dialysis was performed to determine the selectivity of Dox to all possible secondary structures of the selected *PIM1* gene sequences and the titration experiments were performed in order to assess the binding affinity of Dox to these secondary structures. While Dox proves effective as a model anti-cancer drug, there is a necessity for further explanations on its mechanism of action and to resolve dose-dependent challenges. So far, no studies questioned the

plausible binding of Dox to the *PIM1* gene, and the role of such binding on decreased *PIM1* gene expression. Besides, there are no reports on Dox's interactions with different types of DNA structures and its possible effects on modulations within structures when G-quadruplexes, i-motifs, and duplex DNA are all plausibly present together in the same environment.

Overall, we believe our studies will shed light on and contribute to ongoing research on the potential of understanding the secondary structures that can possibly form on the *PIM1* gene and *PIM1* gene to be a target for TNBC type breast cancer treatment.

# CHAPTER 2

# Materials and Methods

## 2.1 Investigating Effect of Environmental Conditions on *PIM1* Gene Structures

### 2.1.1 Sample Preparation

The *PIM1*-SLQS08 (named as G1 in this work), *PIM1*-SLQS07 (named as G2) and *PIM1*-SLQS02 (named as G3) DNAs and complementary strands to them named as I1, I2 and I3 respectively, used in the experiments were purchased from Integrated DNA Technologies (IDT) (Leuven, Belgium). The concentrations of the oligonucleotides were calculated with UV-Vis absorption spectroscopy by using the molar extinction coefficients *PIM1*-SLQS08; ε260=261900 $M^{-1}cm^{-1}$, *PIM1*-SLQS07; ε260=255800 $M^{-1}cm^{-1}$, *PIM1*-SLQS02; ε260=245200 $M^{-1}cm^{-1}$, *PIM1*-SLQS08-comp; ε260=228900 $M^{-1}cm^{-1}$, *PIM1*-SLQS07-comp; ε260=218700 $M^{-1}cm^{-1}$, *PIM1*-SLQS02-comp; ε260=212200 $M^{-1}cm^{-1}$. 3.0 μM DNA solutions were prepared in 20 mM K-phosphate buffer with 20 mM KCl or in 20 mM Na-phosphate buffer with 20 mM NaCl unless otherwise mentioned. The pH of the buffer was adjusted to either 7.0 or 5.5. The preparation of the buffer and salt solutions was described in Appendix A.

Duplex DNAs were prepared as described below:

Duplex D1 sample was prepared by mixing 1:1 equimolar ratio of *PIM1-SLQS08* (named as G1) and *PIM1-SLQS08*-comp (named as I1) using 1.5 μM of each DNA sequence.

Duplex D2 sample was prepared by mixing 1:1 equimolar ratio of *PIM1-SLQS07* (named as G2) and *PIM1-SLQS07*-comp (named as I2) using 1.5 µM of each DNA sequence.

Duplex D3 sample was prepared by mixing 1:1 equimolar ratio of *PIM1-SLQS02* (named as G3) and *PIM1-SLQS02*-comp (named as I3) using 1.5 µM of each DNA sequence.

The DNA solutions were annealed by heating at 92-93 ºC for 5 minutes in water bath and left overnight for cooling down to ensure the formation of proper G4, I4 or dsDNA structures.

### 2.1.2 UV-Vis and CD Experiments

UV-Vis and CD absorption experiments were performed via UV-Vis absorption spectroscopy (Agilent Technologies Cary 8454) and CD spectroscopy (JASCO J-1500 spectropolarimeter) with CTU-100 Circulating Thermostat Unit. All the UV spectra were collected between 190-1100 nm in a quartz cuvette from Agilent Technologies with an optical path of 10 mm. Previously prepared samples for UV-Vis thermal denaturation studies were used in CD studies. All the CD spectra were collected between 200-550 nm at 15 $^{o}$C at 100 nm/min scanning speed with 1.00 nm bandwidth.

### 2.1.3 UV-Vis Thermal Denaturation Experiments

The UV–Vis thermal denaturation experiments were performed via UV-Vis absorption spectroscopy (Agilent Technologies Cary 8454) by varying the temperature between 15 °C and 95 °C with 2 °C/min increments. All the UV spectra were collected between 190-1100 nm in a quartz cuvette from Agilent Technologies with an optical path of 10 mm. Before recording the spectrum, the background signal was recorded in the relevant buffer. It was subtracted by the spectrophotometer in an

automatic mode. We also subtracted the melt curve at 330 nm from melt curves at 295 nm or 260 nm or 265 nm manually to adjust for the background shifts. We used normalized melting curves to find Tm values at 295 nm, 260 nm and 265 nm. The temperature at which normalized absorbance is 0.5 a.u. (where 50 % of the secondary structure has unfolded) corresponds to Tm [105]. Thermal denaturation experiments were performed for all the samples whose descriptions were given in section 2.1.1. Igor Pro software was used for data analysis.

## 2.2 Examining the Interaction Between *PIM1* DNA Structures and Doxorubicin

### 2.2.1 Sample Preparation

Varying concentrations of Dox were added to the annealed oligonucleotide solutions mentioned in 2.1 for the preparation of 0:1, 1:0, 1:1, 1:2 and 1:10 (DNA: Dox) equimolar ratio samples. The samples were mixed and centrifuged to ensure complete interaction between Dox and DNA. Doxorubicin (Dox) was a gift from Deva pharmaceuticals (obtained from Zhejiang Hisun Pharmaceutical CO., LTD (Zhejiang, China)).

### 2.2.2 UV-Vis, CD and Thermal Denaturation Experiments

In order to assess the binding of Dox to the different secondary structures of *PIM1* UV-Vis, CD experiments (as described in 2.1.2) were performed also for DNA:Dox samples. In addition, the stability of the secondary structures in the presence of Dox were determined using Thermal denaturation studies (Section 2.1.3).

### 2.2.3 Fluorescence Experiments and Determination of Association Constants

Fluorescence spectroscopy is also used to assess the binding of Dox to the *PIM1* gene sequences. The fluorescence emission spectra of Dox were compared to the fluorescence spectra of Dox in the presence of varying concentrations of DNA. The parameters for the fluorescence measurements were: Emission spectra collected from 500 to 700 nm, excitation wavelength 485 nm, excitation and emission slits: 5.0 nm and 10 nm, operation 700 V, scan rate 600 nm/min. Binding (association) constants ($K_a$) were determined by fluorometric titration experiments using Cary Eclipse Fluorescence spectrophotometer. The DNA solutions were prepared prior to experiments, by the same annealing procedure and buffer conditions described in the previous section. Briefly, 2.5 mL of 1.0 μM Dox solution was titrated with 50.0 μM oligonucleotide + 1.0 μM Dox solution with 0.25-0.5 μM concentration increments.

Binding constants were determined by plotting the fraction bound against DNA concentration and calculating association constant as:

$$\frac{1}{[\mathrm{DNA}]} \quad (\mathrm{M}^{-1})$$

where [DNA] is the DNA concentration that yields half binding [106].

The fluorescence spectra were recorded by monitoring the decrease in the fluorescence intensity as the Dox solution was titrated with DNA-Dox solution using a simple two state model.

The Fraction bound was calculated as:

$$\text{Fraction bound} = \frac{F_{max} - \mathrm{F}_i}{F_{max} - F_{min}}$$

Where: $F_i$ is the relative fluorescence intensity at a given DNA concentration ([DNA]).

$F_{min}$ is the fluorescence intensity of Dox in the presence of DNA at relatively high concentration.

$F_{max}$ is fluorescence intensity of Dox in the absence of DNA.

Igor Pro software (Wavemetrics Inc, USA) was used in all the data analysis. Binding constants were obtained as an average of two replicates for each DNA:Dox titration and reported with standard deviations.

### 2.2.4 Competition Dialysis Assay

Competition dialysis experiments were accomplished according to the previously reported procedure by Chaires et. al. [107]. Preparation of the buffer solutions used in this experiment were described in Appendix A, the sequences of the nucleic acids were listed in Table 11, Appendix B and the oligonucleotides included in the experimental set up were listed in Table 12, Appendix E. Construction of the calibration curve was also given in Appendix E. The nucleic acid structures were prepared according to the procedure described by Chaires et. al. [108]. Oligonucleotides including $Tel_{24}$, $TC_4T$, $TG_4T$, $C_4T_4C_4$, $G_4T_4G_4$, $dA_{32}$ and $dT_{32}$ were purchased from Integrated DNA Technologies (IDT) (Leuven, Belgium).

The concentrations of the oligonucleotides used in this assay were calculated using the extinction coefficient values listed in Table 12, Appendix E that are obtained from IDT.

All the prepared oligonucleotides were annealed according to previously described procedure, in Na-phosphate buffer. For each competition dialysis experiment 0.6 mL of 3.0 μM of oligonucleotide, in monomeric units (nucleotide, base pair, triplet and quartet) were put into Pierce (Thermofischer Scientific, USA) 7000 Da molecular cutoff dialysis cassettes. Then, the cassettes were dialyzed against 750 mL of 1.0 μM Doxorubicin solution for 48 hours. After the dialysis period, oligonucleotide solutions were taken out from the dialysis cassettes and 10 %(w/v) SDS was added to release the bound Dox from the nucleic acids to ensure the Dox molecules were free in solution for measurement purposes. Following that, the Dox concentration in each cassette was determined by Fluorescence spectroscopy. The parameters for the

fluorescence measurements were the same as the parameters described in the previous section. The calibration curve for the Dox molecule was constructed using the same instrument and parameters prior to the competition dialysis experiments. Using the linear equation supplied by the calibration curve, the amount of the bound ligand to each oligonucleotide was determined. Corrections were made by considering the dilution effect caused by buffer in each cassette. Two independent dialysis assays were performed for Dox. The ratio of bound ligand ($C_b$) to free ligand (Cf) was determined by the equation: $C_b/ C_f = (C_t/ C_f)-1$ where $C_t$ is the total Doxorubicin concentration in each dialysis cassette after the dialysis period, $C_f$ is the Doxorubicin concentration in the positive control dialysis cassette (which only included buffer) [107].

# CHAPTER 3

# RESULTS AND DISCUSSION

## 3.1 Investigating the Effect of pH on *PIM1* G4 Structures

### 3.1.1 Characterization of G4 Structures in K-phosphate Buffer via Circular Dichroism Spectroscopy

CD spectroscopy is a commonly used technique for the characterization of G-quadruplexes [109]. Thus, to characterize G4 structures of *PIM1* gene and investigate the effect of pH on those structures, first the CD spectra were collected for all three G-quadruplex forming sequences of *PIM1* in K-phosphate buffer at pH 7.0 and pH 5.5 (Figure 7). The CD spectrum for *PIM1*-SLQS07 (named as G2 in this work) at pH 7.0 has a positive peak at 266 nm with a shoulder around 290 nm and a negative peak at 245 nm (Figure 7B, black line). These characteristic peaks are indicative of a 3+1 hybrid G-quadruplex structure [110], confirming perfect agreement with the previous report on *PIM1*-SLQS07 topology at pH 7.0 [99]. As shown with the red line, changing the pH value from 7.0 to 5.5 resulted in a decrease in the intensity of the peaks at 266 nm and 290 nm, however, the 3+1 hybrid nature of this structure is preserved [110]. *PIM1*-SLQS02 sequence (named as G3 in this work) is observed to have a positive peak at 292 nm and a negative peak at 258 nm showing an antiparallel nature at pH 7.0 (Figure 7C, black line) [110]. The intensity of peaks in the CD spectrum of G3 also decreased at pH 5.5 compared to the intensity of the peaks obtained at pH 7.0, but the prevalence of the antiparallel structure remained unchanged (Figure 7C, red line). The other *PIM1* sequence, *PIM1*-SLQS08 (named as G1 in this work) exhibits a positive peak at 289 nm accompanied by a

shoulder around 270 nm which indicates the existence of both structures at pH 7.0 (Figure 7A, black line) [110]. When the pH of the solution was altered to 5.5, the shoulder peak disappeared, indicating a shift to a completely antiparallel structure (Figure 7A, red line) [110].

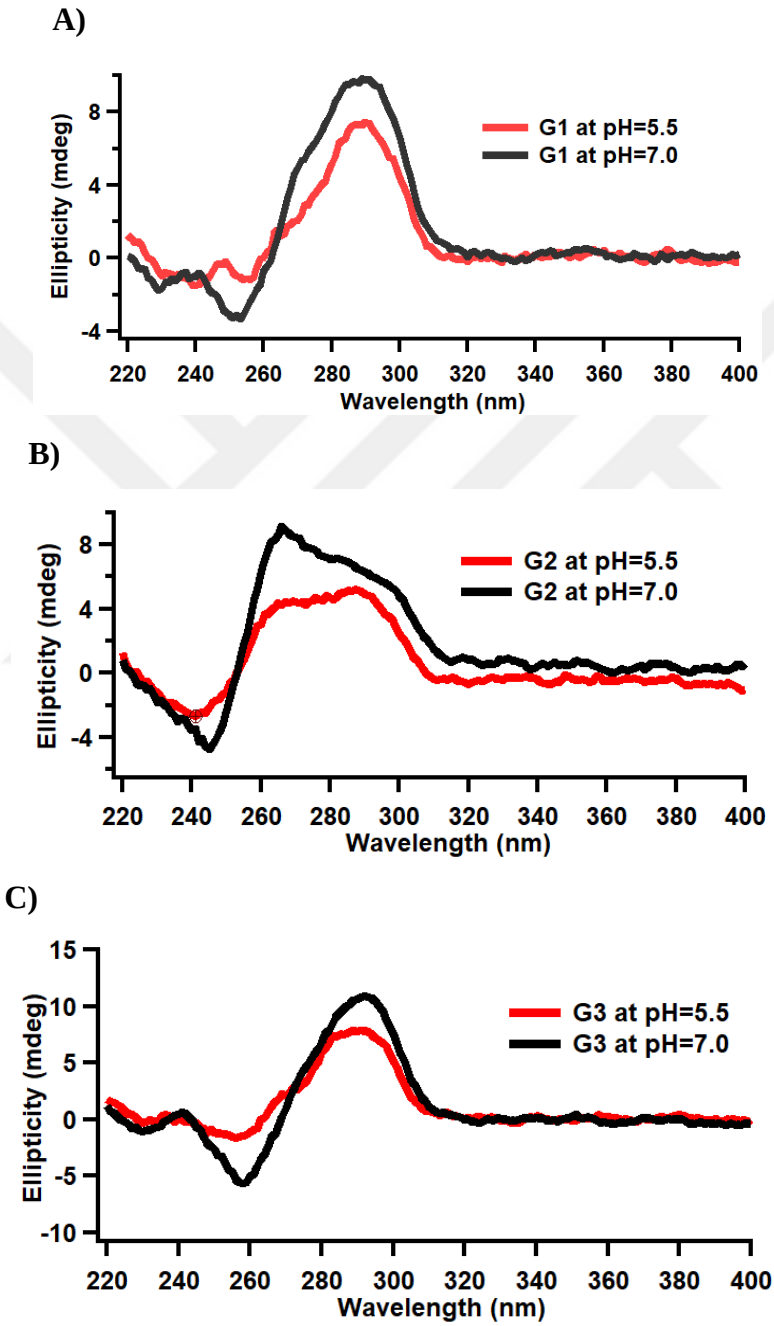


Figure 7. CD spectra of 3.0 µM DNA solution A) G1 B) G2 C) G3 at pH 7.0 and 5.5 in 20 mM K-phosphate with 20 mM KCl buffer at 15 °C.

Overall, the effect of pH is observed to be dependent on the sequence and the structure. Consequently, structures with a particular loop composition display notable alterations, while others exhibit little to no change [32], [111], [31]. Here we observed that while there were not substantial transitions for G2 and G3 G-quadruplex structures, antiparallel structure was found to be favored in G1 sequence upon pH change. This observation demonstrates the importance of how minor sequence changes could lead to a change in the structure [30]. Additionally, Yan et al. [32] demonstrated that reducing the pH from 7.0 to 4.5 decreased the peak intensity at 290 nm in the human telomeric G-quadruplex structure in a $K^+$ containing environment while gradually changing its conformation from hybrid to antiparallel. G-quadruplex structure was disrupted when the pH dropped below 4.0 [32]. A decrease in the intensity of peaks was also noted in our studied G-quadruplex samples when the pH was changed from 7.0 to 5.5.

### 3.1.2 Characterization of G4 Structures in K-phosphate Buffer via UV-Vis Thermal Denaturation Experiments

Following the confirmation of G-quadruplex structure formation, UV-Visible thermal denaturation experiments were conducted to reveal the stabilities of *PIM1* with respect to pH. The corresponding UV-Vis absorption spectra for the thermal denaturation experiments are given in Appendix C, Figures 65-79. In Figure 8, solid lines represent the thermal denaturation profiles at pH 7.0 and the lines with markers represent pH 5.5 obtained by monitoring the absorbance change at 295 nm with respect to temperature for G1, G2 and G3. Tan et.al. previously reported thermal denaturation temperature values for G2 and G3 at pH 7.0 as 65 ºC and 67 ºC respectively [99]. As shown in Table 1, the Tm values obtained here are found to be in accordance with their reported values. We also determined the Tm value of G1 as 65 ºC at pH 7.0, indicating that all *PIM1* sequences appear to have similar stability at neutral pH overall. At pH 5.5, the Tm values obtained for G1, G2 and G3 were 67

ºC, 64 ºC, and 66 ºC, respectively. Slightly lower Tm values for G2 and G3 indicate a minor destabilization of *PIM1* G4s at pH 5.5. Yet, one should keep in mind that the difference in Tm might also be in our experimental error range. By the way, relatively large hysteresis was observed between denaturation and annealing (Figure 8) at lower pH 5.5 where the Tm obtained from the denaturation was always higher than that obtained from the annealing curve as also reported previously. The presence of hysteresis between the denaturation and annealing profiles of a G-quadruplex was attributed to the absence of thermodynamic equilibrium due to the slow folding and/or unfolding processes [112]. On the other hand, no hysteresis was observed at pH 7.0 under these conditions, which indicates the establishment of the equilibrium at a faster rate at pH 7.0.

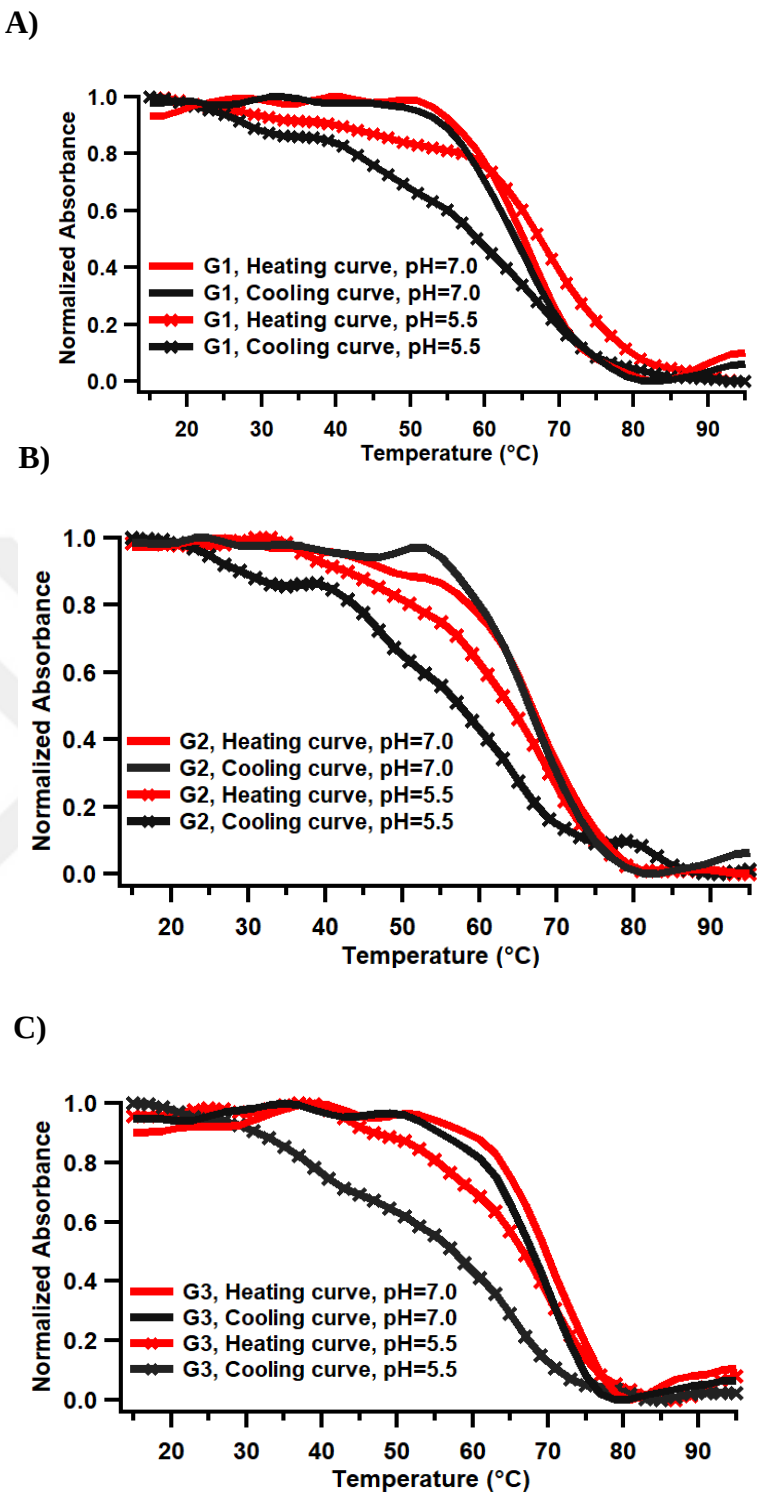


Figure 8. UV-Vis thermal denaturation profiles of 3.0 µM DNA solution, A) G1 B) G2 C) G3, obtained by monitoring the absorbance change at 295 nm, at pH 7.0 and 5.5 in K-phosphate buffer.

## 3.2 Investigating the Effects of Salt on *PIM1* G4 Structures

To further study the influence of environmental conditions on the formation of *PIM1* gene secondary structures, we investigated the secondary structures and thermal stabilities of G4s by reperforming experiments in Na-phosphate buffer with NaCl instead of K-phosphate with KCl.

### 3.2.1 Characterization of G4 Structures in Na-phosphate Buffer via Circular Dichroism Spectroscopy

Figure 9A shows the changes in the CD spectra of G1 in the presence of $Na^+$. As we discussed in 3.1 section, G1 adopts both 3+1 hybrid and antiparallel structures. In the presence of $Na^+$, the maximum ellipticity at 289 nm shifts slightly to a lower wavelength of around 282 nm while there is a shoulder at 290 nm. These changes observed in the CD spectra of G1 indicate that $Na^+$ induces some changes in the relative abundance of two structures, promoting the prevalence of the hybrid structure. Similarly, the CD spectra of G2 (Figure 9B) also exhibits a positive peak at 288 nm with a negative peak centered around 255 nm in the presence of $Na^+$. These findings strongly suggest the transformation of 3+1 hybrid structure of G2 in the presence of $K^+$ into an antiparallel G-quadruplex structure in the presence of $Na^+$. In contrast to the other sequences, G3, which adopts an antiparallel structure in the potassium phosphate buffer, demonstrates no significant change in the nature of the G4 structure in the presence of $Na^+$ (Figure 9C). It is well-known that G4s can undergo conformation changes upon exchange of $Na^+/K^+$ [113], [114] and, the transformation of G4 parallel structures into antiparallel structures in the presence of $Na^+$ are present in the literature for G4 sequences [115]. $Na^+$ seemed to promote the formation of antiparallel structures also in *PIM1* G4 sequences. Yet, it is still interesting to see how those small differences in *PIM1* sequences result in structural differences and that these different structures behave differently in $Na^+/K^+$

environments. This behavior reflects also the importance of the ion type in regulation of the G4 structures *in vivo*.

*PIM1* G4 structures were also investigated at pH 5.5 in Na-phosphate buffer with NaCl. The CD spectra displayed in Figure 10, reveals that the intensity of peaks has decreased considerably for all sequences, especially for G1 upon decreasing pH to 5.5. As mentioned before, a decrease in the intensity of peaks at 290 nm was observed previously for human telomeric G-quadruplex structure which was entirely disrupted under pH 4.0 [32].

For G2 (Figure 10B), the 3+1 hybrid structure, which was transformed into an antiparallel structure in Na-phosphate solution, is induced again at this acidic pH. On the other hand, the antiparallel nature of G3 has not really changed at pH 5.5 in comparison to pH 7.0, once again revealing the importance of the sequence in the transitions of secondary structures.

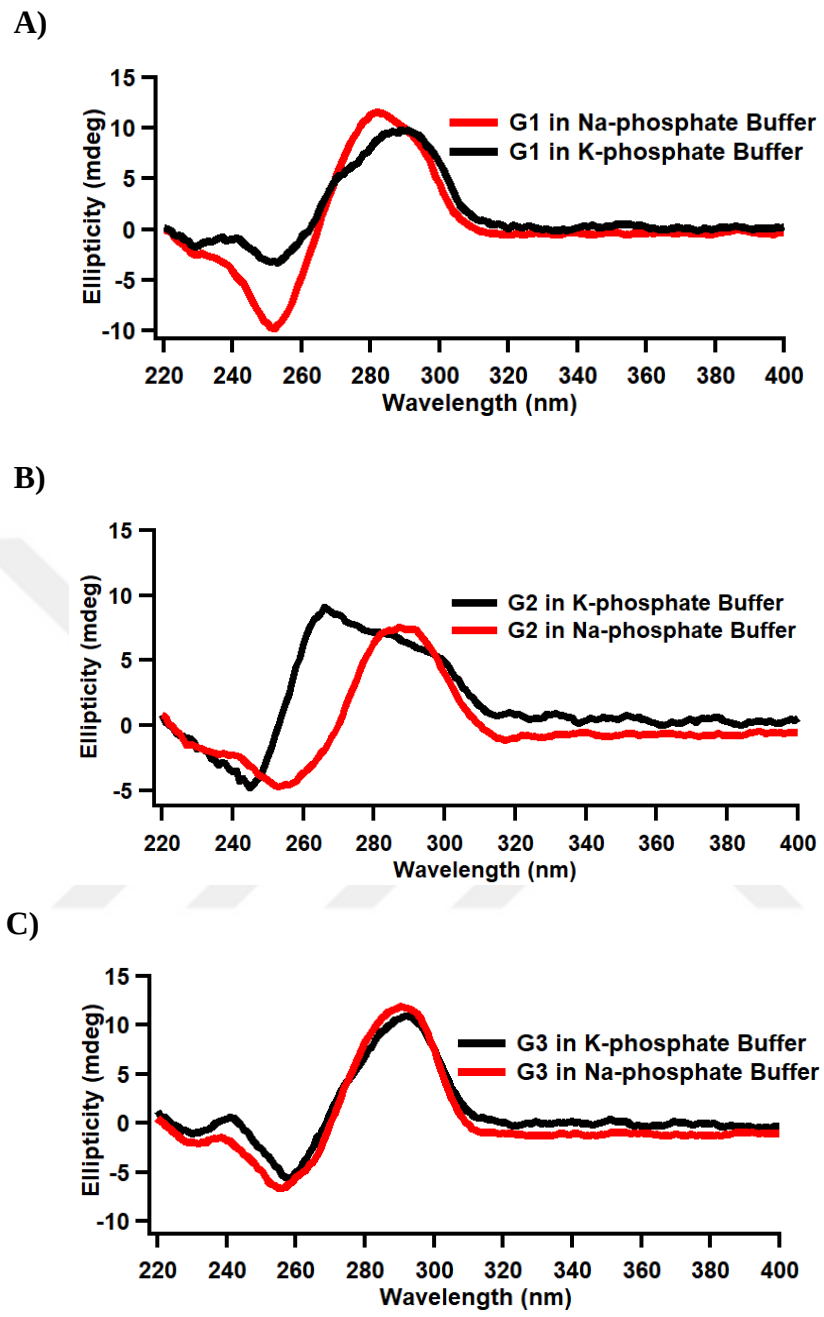


Figure 9. Comparison of the CD spectra of 3.0 µM DNA solution A) G1 B) G2 C) G3 in K-phosphate or Na-phosphate buffer at pH 7.0.

**A)**

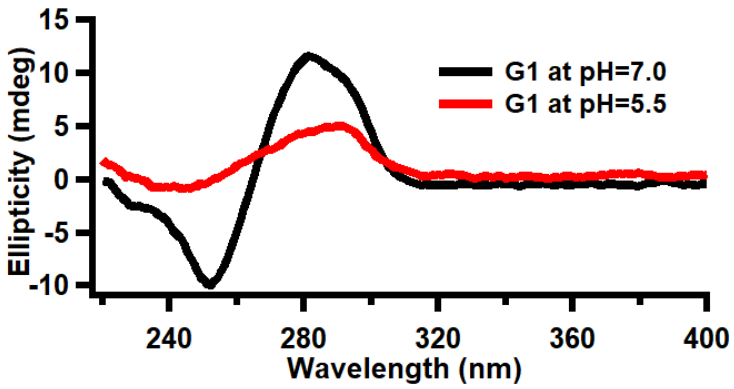


**B)**

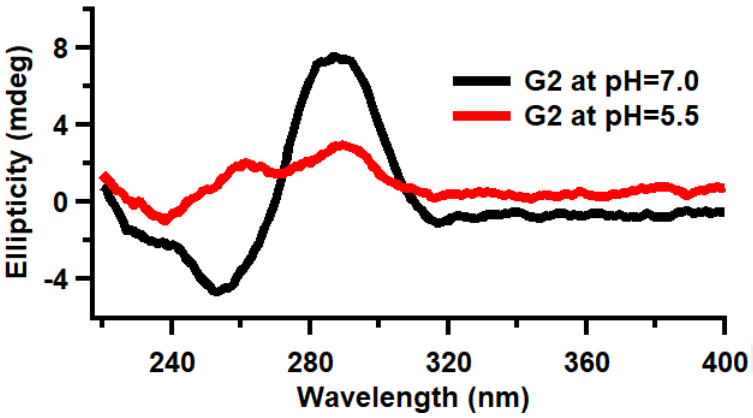


**C)**

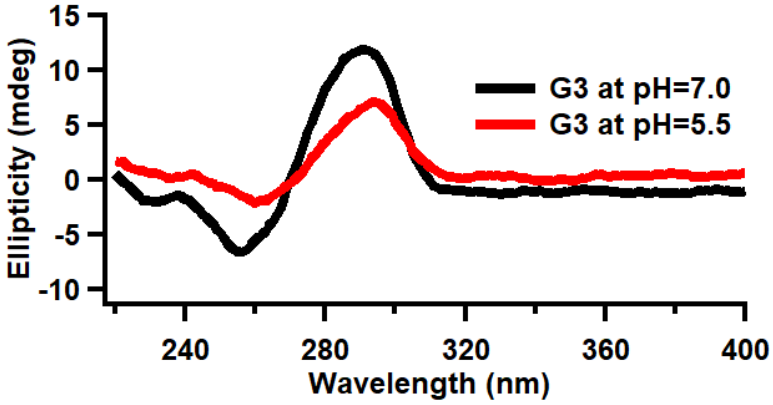


Figure 10. Comparison of the CD spectra of 3.0 µM DNA solution A) G1 B) G2 C) G3 at pH 7.0 and 5.5 in 20 mM Na-phosphate with 20 mM NaCl buffer at 15 °C.

### 3.2.2 Characterization of G4 Structures in Na-phosphate Buffer via UV-Vis Thermal Denaturation Experiments

As discussed in 1.2.1, cation in the solution can significantly impact the stability of G-quadruplex structures by associating with formation and stacking of G-tetrads [28].

The exact effect of $K^+$ substitution with $Na^+$ on the stability of G-quadruplexes is strongly dependent on the sequences of oligonucleotides as shown by Mergny et al. [29]. They represented an increase in ΔTm values between +7 and +30 ºC for eight different G-rich sequences.

Figure 11 reveals the changes in thermal denaturation profiles of G4s after the buffer change. Solid lines represent the samples in K-phosphate buffer and lines with markers represent the samples in Na-phosphate buffer. As compared in Table 1 and Figure 11, the Tm values for G1, G2, and G3 decrease about 10 ºC, 16 ºC, and 19 ºC respectively, upon exchange of $K^+$ with $Na^+$. Results confirm lower stability of these structures in NaCl instead of KCl which is a well-known characteristic of G-quadruplexes [111], [31]. There are several studies reporting strong preference for G4 formation in the presence of $K^+$ among other alkali cations [113], [28], [114]. Hud et al, reported a net free energy change ($\Delta G°$) of $-1.7 \pm 0.15$ kcal/mol for G-quadruplex structure of d($G_3T_4G_3$) when NaCl is replaced with KCl [28]. The main explanation for the cation-dependent stability differences is the bulkiness of them. On the other hand, free energy of hydration of cations can explain the stability difference observed between $Na^+$ and $K^+$ solutions. The process of cation binding to G-quadruplexes involves both a positive free energy of dehydration and a negative free energy of coordination. $Na^+$ exhibits favorable coordination energy while its binding is penalized by its stronger hydration as compared to $K^+$. Typically, the hydration energy of alkali

cations inversely correlates with their ionic radii. $K^+$ consistently presents the best compromise and stabilizes G4s more effectively than $Na^+$ and $Rb^+$ [29].

Overall, it was interesting to see that the highest destabilization was observed in G3 structure, which was already in antiparallel form in $K^+$ solution such that the structure changed very slightly in the presence of $Na^+$ solution.

Next, the effect of pH on G4 structures in the presence of $Na^+$ was investigated via monitoring changes in absorbance at 295 nm with respect to temperature at pH 5.5. As discussed in 1.2.1, G-quadruplex stability is not dependent on pH for the G- rich strands of human telomeric DNA between 7.0 and 4.0 [114]. On the other hand, there could be some stabilization at acidic pH values due to the formation of $C{\cdot}C^+$ base pairs on the complementary sequences [30], [31].

Since the CD spectra revealed relatively significant changes, we expected to observe different Tm values at pH 5.5 compared to Tm values obtained at pH 7.0. However, as displayed in Figure 12, Tm values did not exhibit a trend upon change of pH from 7.0 to 5.5. While G2 showed a minor decrease in its stability, G1 exhibited slight stabilization. This stabilization at acidic pH was also observed in K-phosphate buffer. No change was detected in the stability of G3, which was consistent with the CD spectra that no structural change was observed in the CD spectra of G3 upon pH change. Similar to the results at K-phosphate buffer, hysteresis was observed between the denaturation and annealing profiles of a G-quadruplex at pH 5.5 which attributed to the absence of thermodynamic equilibrium due to the slow folding and/or unfolding processes. The corresponding UV-Vis absorption spectra for the thermal denaturation experiments are given in Appendix C, Figures 65-79.

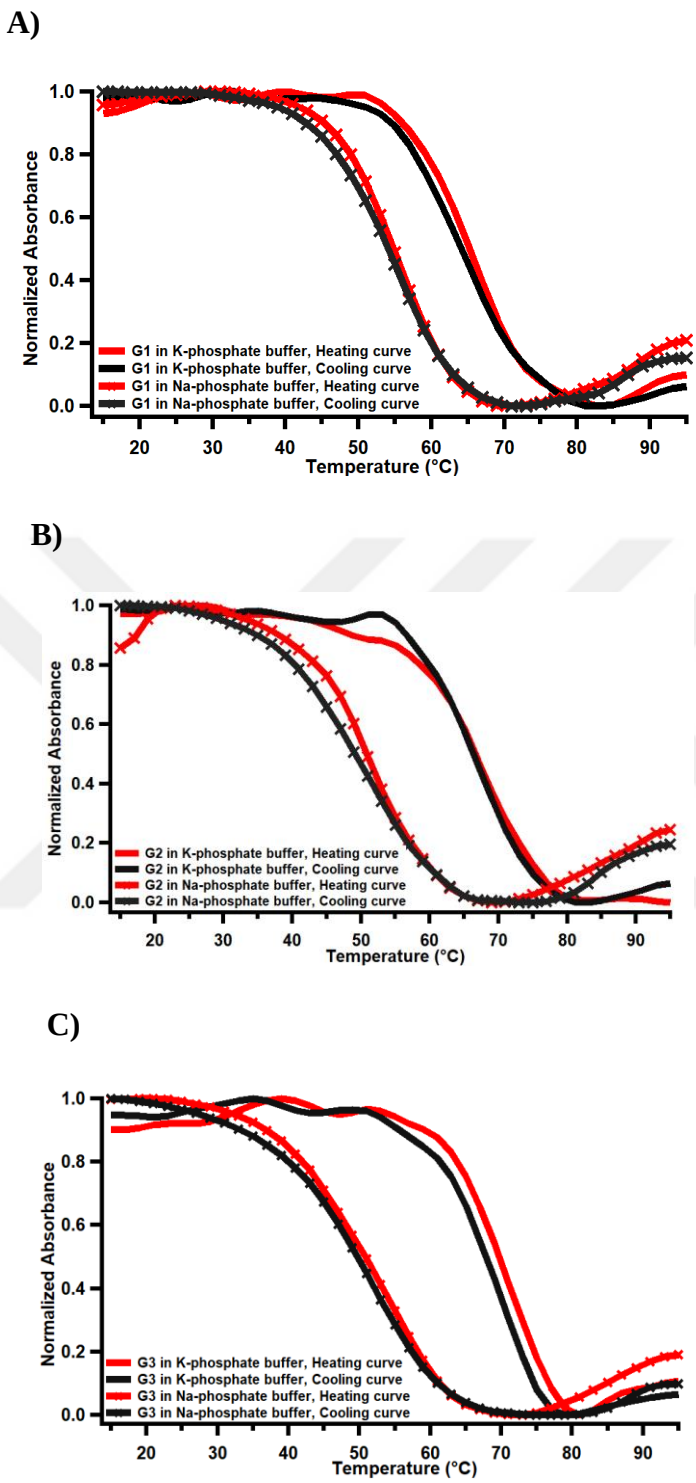


Figure 11. Comparison of the UV-Vis thermal denaturation profiles of 3.0 μM A) G1 B) G2 C) G3, in K-phosphate or Na-phosphate buffer at pH 7.0, obtained by monitoring the absorbance change at 295 nm.

A)

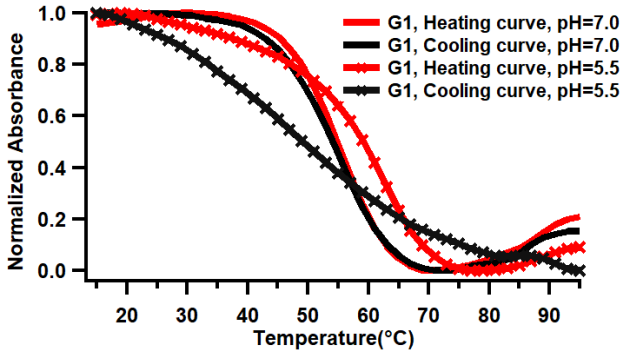


B)

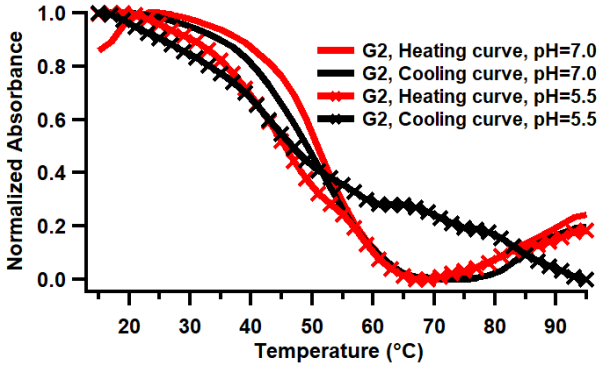


C)

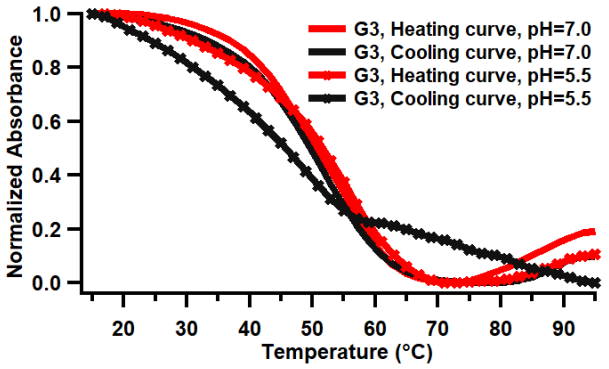


Figure 12. Comparison of the UV-Vis thermal denaturation profiles of 3.0 µM DNA solution A) G1 B) G2 C) G3, obtained by monitoring the absorbance change at 295 nm, at pH 7.0 and 5.5 in Na-phosphate buffer.

Table 1. Comparison of the Tm values of 3.0 μM DNA solution of G1, G2, G3 obtained by monitoring the absorbance change at 295 nm, under two different pHs in K-phosphate or Na-phosphate buffer.

| **DNAs** | **Tm** | | | |
|---|---|---|---|---|
| | **K-phosphate** | | **Na-phosphate** | |
| | **pH= 7.0** | **pH= 5.5** | **pH= 7.0** | **pH= 5.5** |
| **G1** | 65 ºC | 67 ºC | 55 ºC | 59 ºC |
| **G2** | 67 ºC | 64 ºC | 51 ºC | 45 ºC |
| **G3** | 70 ºC | 66 ºC | 51 ºC | 51 ºC |

## 3.3 Investigating i-motif Formation in C-rich sequences of *PIM1* and the Effect of pH on Those Structures

### 3.3.1 Characterization of i-motif Structure in K-phosphate Buffer via Circular Dichroism Spectroscopy

After confirming the formation of the G-quadruplex structures in the selected *PIM1* sequences, the plausibility of the formation of the i-motif structure in the complementary C-rich sequences was investigated first via CD spectroscopy. Contrary to G-quadruplexes which can adopt several distinct structures, single folding topology of i-motifs results in a single type of CD spectra [16]. This characteristic CD spectrum is reported to have a positive peak with a maximum at around 287 nm and a negative peak at around 265 nm [16]. CD spectroscopy analyses of complementary strands of G1 *(PIM1-SLQS08)*, G2 *(PIM1-SLQS07)*, G3 (*PIM1-SLQS02)* (named as I1, I2 and I3 respectively in this work) at two different pHs in 20 mM K-phosphate buffer with 20 mM KCl are shown in Figure 13. In Figure 13, the red lines and the black lines represent pH 5.5 and pH 7.0, respectively. The comparison of the spectra at pH 5.5 and pH 7.0, reveals a noticeable increase in the intensity of the positive peak at around 287 nm, which also shifts towards the red, while concurrently, the negative peak at 260 nm deepens. These changes prove

the formation of an ordered i-motif structure with $C{\cdot}C^+$ pairing at acidic pH as it was shown for *$(CnT_3)_3Cn$* sequences by Školáková et. al. [16]. Furthermore, CD analyses by Singh and Kukreti [117] revealed that C-rich DNA oligonucleotide sequences of *MYH7* gene (HM34C) forms the i-motif structure at acidic pH (5.2) in the presence of 0.1 M NaCl but remains unstructured at physiological pH. They propose that the highest CD amplitude at pH 5.7 corresponds to the formation of a maximum number of i-motif species (involving $C{\cdot}C^+$ pairing) compared to their population at physiological pH (7.4), a trend also observed in our samples, particularly in I1. Additionally, they observed a shift in the positive peak from 286 nm to 280 nm which could be due to the decreased cytosine protonation at neutral pH in comparison to acidic pH. In our samples, I1 displays the most significant shift, transitioning from 288 nm to 284 nm (Figure 13A). On the other hand, they indicated that the positive peak at 280 nm with a negative band at 244 nm at 4 ºC for RM34C gene, could also indicate the $C–C^+$ base pairing and thus i-motif structure formation at neutral pH of 7.4 [117]. As displayed in Figure 13, I1, I2 and I3 samples display positive and negative peaks at 284 nm, 249 nm; 286 nm, 255nm and 287 nm, 247 nm respectively at pH 7.0 which apparently suggests the formation of i-motifs even at neutral pH. Although, the population of ordered structures may be lower compared to acidic pH of 5.5.

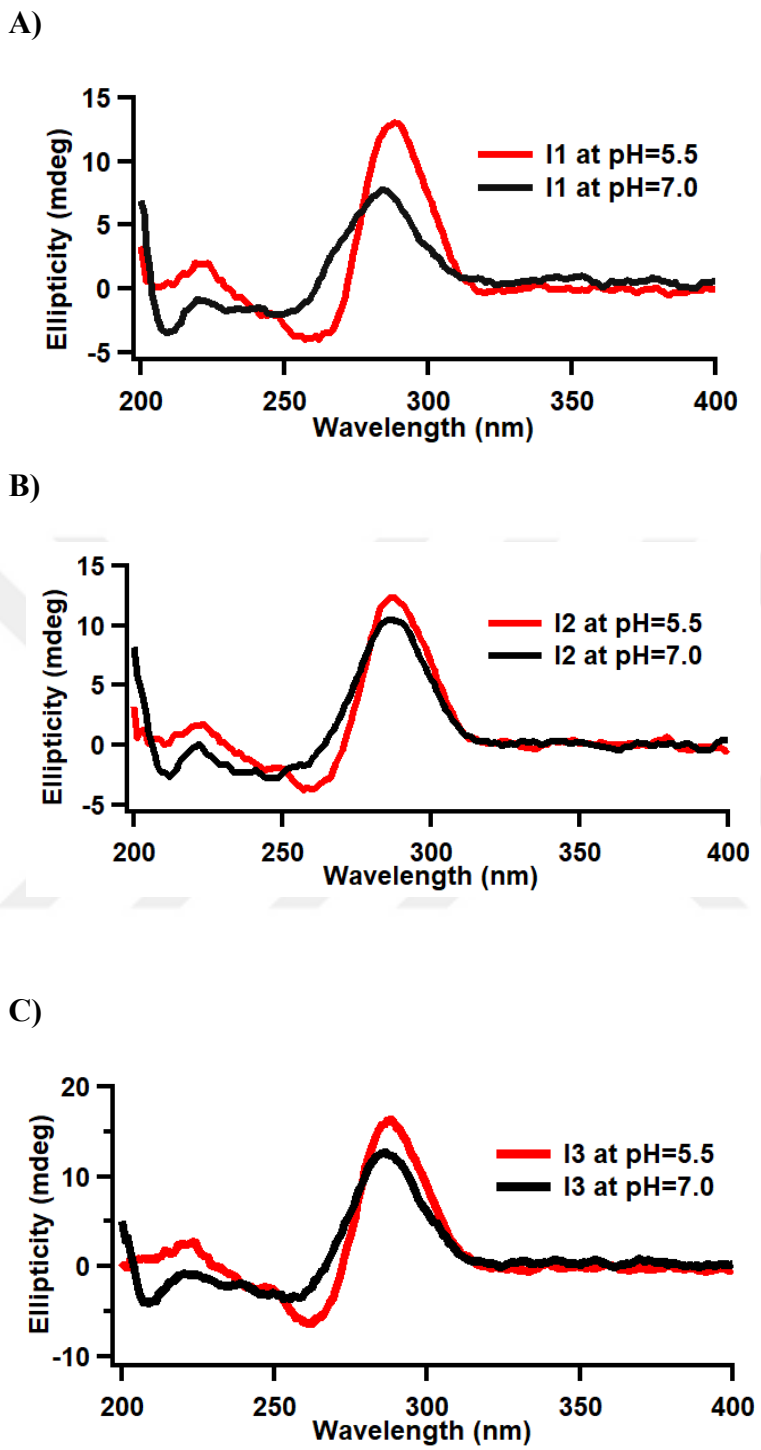


Figure 13. CD spectra of 3.0 µM DNA solution, A) I1 B) I2 C) I3, at pH 7.0 and 5.5 in 20 mM K-phosphate with 20 mM KCl buffer at 15 °C.

### 3.3.2 Characterization of i-motif Structures in K-phosphate Buffer via UV-Vis Thermal Denaturation Experiments

After examining the structural properties by Circular Dichroism spectroscopy, the thermal stability of the samples was investigated at pH 7.0 and 5.5 by UV-Vis thermal denaturation experiments. The corresponding UV-Vis absorption spectra for the thermal denaturation experiments are given in Appendix C, Figures 65-79. Thermal denaturation profiles given in Figures 14 and 15 are obtained by monitoring the absorbance changes at 265 nm or 295 nm with respect to temperature for each sample. Generally, a sharp sigmoidal hyperchromic effect at 265 nm and an inverted sigmoidal hypochromism at 295 nm are accepted as the diagnostic characteristics for i-motif structures [39]. In Figure 14 and Figure 15, solid lines represent the thermal denaturation profiles at 265 nm, while lines with markers represent the profiles at 295 nm. These profiles clearly exhibit characteristics for i-motif structures formation both at pH 7.0 and 5.5. As discussed in the previous section, Singh et al. demonstrated the formation of i-motifs at neutral pH for C-rich sequences of *MYH7β* promoter (RM34C) in 20 mM sodium cacodylate buffer [117]. This sequence exhibited characteristic thermal denaturation profiles similar to ours, while, HM34C sequence did not yield any melting curve, indicating an unstructured single strand at pH 7.4 [117].

In addition, a good cross-over between the thermal denaturation profiles obtained at 265 and 295 nm was identified for the I1, I2 and I3 samples prepared in K-phospahte with a pH of 5.5 (Figure 15) which was reported also as a sign of the presence of stable i-motif structures in the *MYH7β* promoter [117]. On the other hand, no cross-over was observed in the thermal denaturation profiles at neutral pH possibly due to the low stability of the i-motif structures at that pH (Figure 14).

According to previous studies, the Tm values of i-motifs is determined from melting profiles at 265 nm [51], [118]. Table 2 displays the calculated Tm values for the C-rich strands of *PIM1*.

Recently, Chaudhary et al. explored i-motif formation in the promoter region of *GRIN1* gene. In this study, the Tm values of C-rich secondary structure formed by GRIN1c sequence decreases from 46 °C to 30 °C as the pH is increased from 3.6 to 8.1, indicating the destabilization of i-motif structure with an increase in pH [119]. In our samples, we observed a decrease of about 12 °C, 20 °C, and 18 °C in Tm values when pH is changed from 5.5 to 7.0 in K-phosphate buffer. This finding suggests the higher stability at acidic pH compared to neutral pH, consistent with expectations for i-motifs.

Overall, our findings via CD and UV-Visible experiments are in great accordance with previous studies confirming the formation of stable and ordered i-motif structure at pH 5.5. In addition, our results suggest the formation of a less structured, less stable i-motif structure at pH 7.0.

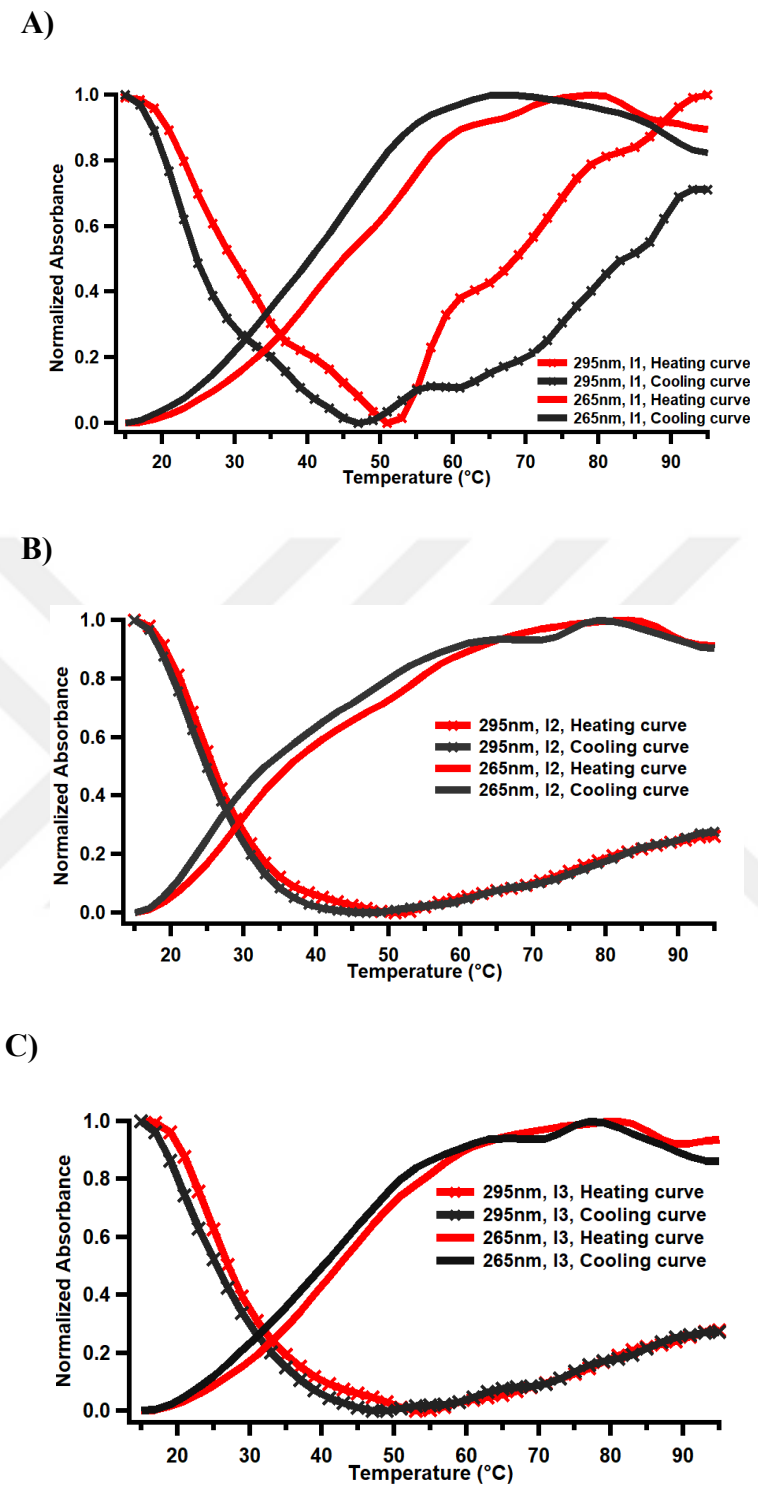


Figure 14. UV-Vis thermal melting profiles of 3.0 µM DNA solution, A) I1 B) I2 C) I3, at pH 7.0 in K-phosphate buffer obtained by monitoring the absorbance change at 265 nm and 295 nm.

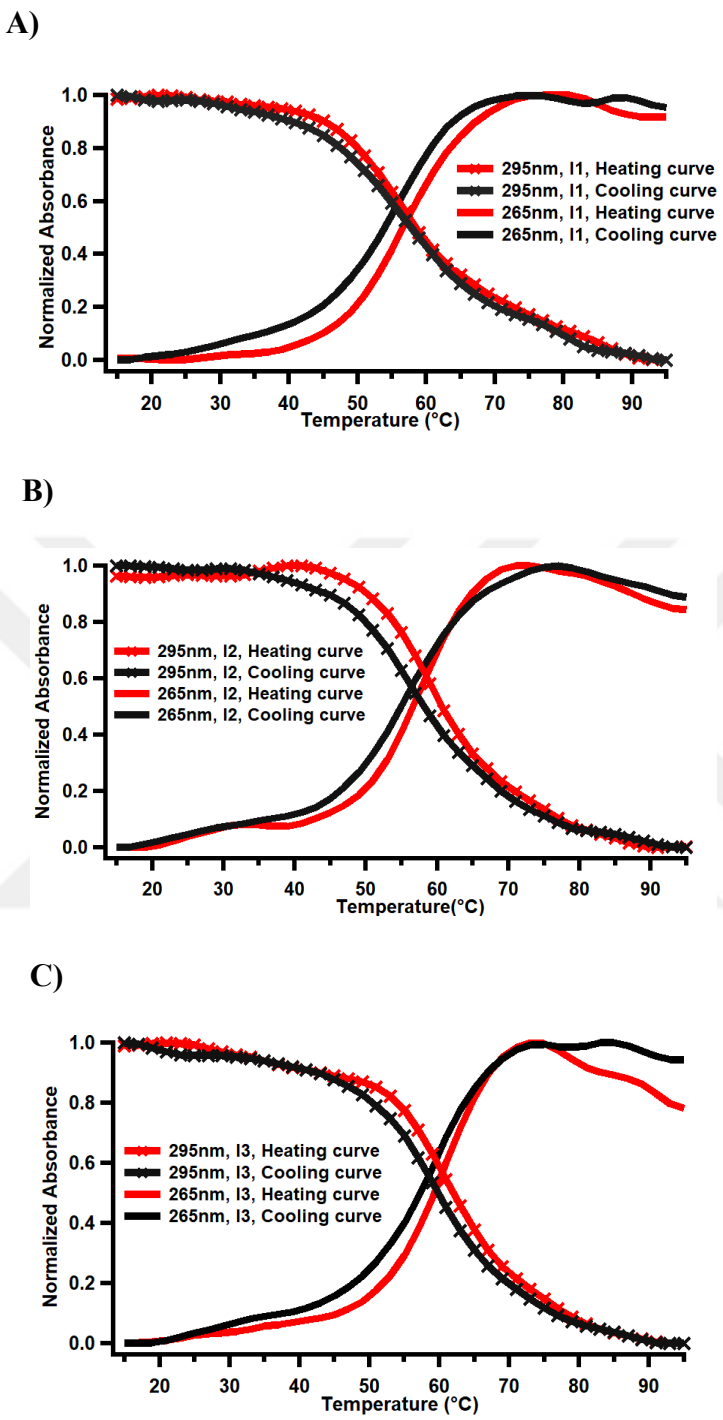


Figure 15. UV-Vis thermal melting profiles of 3.0 µM DNA solution, A) I1 B) I2 C) I3, at pH 5.5 in K-phosphate buffer obtained by monitoring the absorbance change at 265 nm and 295 nm.

## 3.4 Investigating Effects of salt on I4 structures of *PIM1*

### 3.4.1 Characterization of i-motif Structures in Na-phosphate Buffer via Circular Dichroism Spectroscopy

To study the structural changes resulting from the use of $Na^+$ ions instead of $K^+$ in the C-rich strands of the *PIM1* gene, Circular Dichroism experiments were conducted. Figure 16 displays the CD spectra of I1, I2 and I3 in 20 mM Na-phosphate buffer with 20 mM NaCl at pH 7.0 and pH 5.5. As mentioned above, the maximum peak around 288 nm and minimum peak around 265 nm are taken as the characteristic peaks for i-motifs [16]. The comparison of the spectra obtained in Na-phosphate buffer at pH 5.5 and pH 7.0, reveals also noticeable increase in the intensity of the positive peak, which also shifts towards the red, while the negative peak at 260 nm deepens. These changes observed are very similar to the changes observed in the K-phosphate buffer and prove the formation of an ordered i-motif structure with $C{\cdot}C^+$ pairing at acidic pH [16]. Similar to K-phosphate buffer, the significant amplitude of the peaks at around 280 nm and the presence of a minimum at around 250 nm at pH 7.0 reflects the presence of i-motif structures also at neutral pH which might be less structured in comparison to i-motif structure obtained at acidic pH [117]. Overall, these results clearly prove the formation of ordered i-motif structures at pH 5.5 in Na-phosphate buffer.

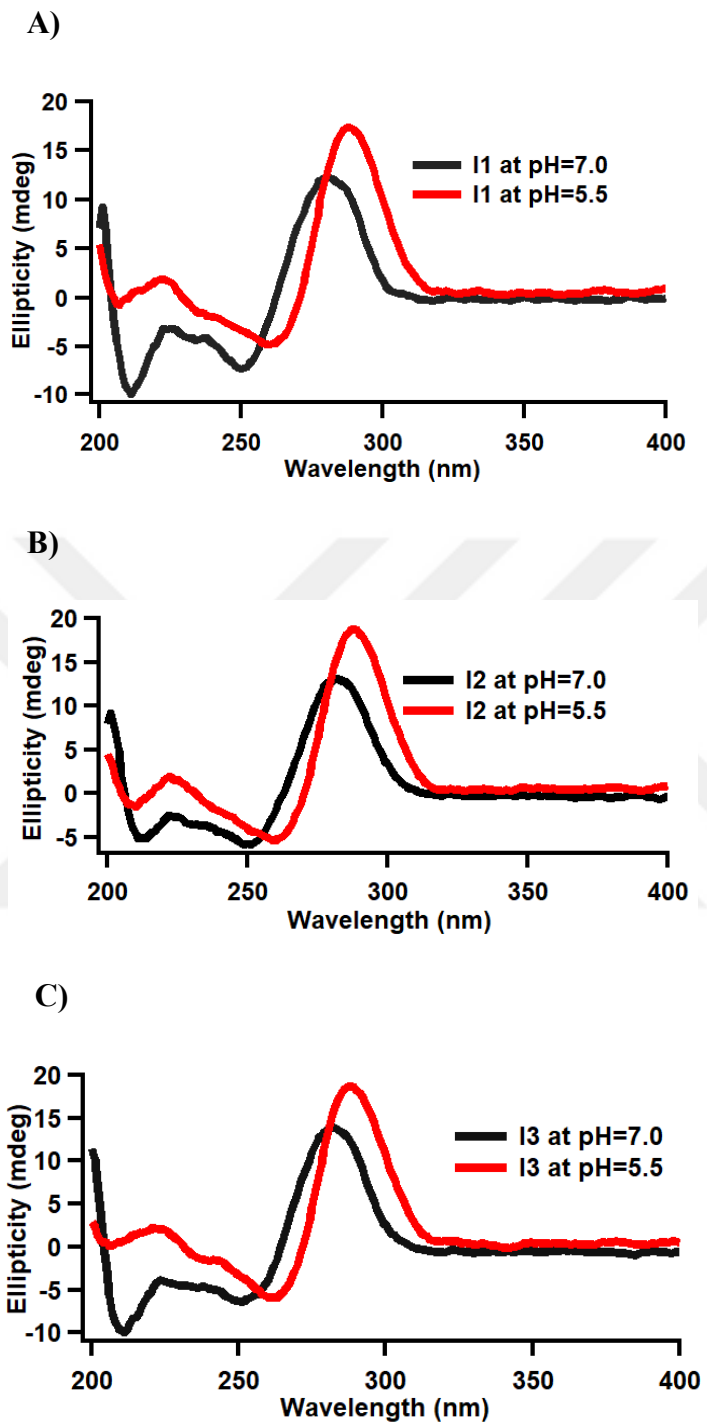


Figure 16. CD spectra of 3.0 µM DNA solution, A) I1 B) I2 C) I3, at pH 7.0 and 5.5 in 20 mM Na-phosphate with 20 mM NaCl buffer at 15 °C.

### 3.4.2 Characterization of i-motif Structures in Na-phosphate Buffer via UV-Vis Thermal Denaturation Experiments

As it was shown in the previous section, a sharp sigmoidal hyperchromic effect at 265 nm and an inverted sigmoidal hypochromism at 295 nm are accepted as diagnostic characteristics for the formation of the i-motif structure [39]. In Figure 17 and Figure 18, the solid lines represent the thermal denaturation profiles at 265 nm, while lines with markers represent the thermal denaturation profiles at 295 nm. These profiles clearly exhibit characteristics for i-motif structures formation at pH 5.5 (Figure 18). On the other hand, the thermal denaturation profiles obtained by monitoring the absorbance changes at 295 nm of all three sequences, especially for I1 sequence, at pH 7.0 do not display perfect sigmoidal hypochromism (Figure 17). As mentioned in the previous section, a good cross-over (at 265 and 295 nm) is also accepted as an indication of the presence of stable i-motif structures. This characteristic is evident in the Tm profiles of all three sequences at pH 5.5 in Na-phosphate buffer (Figure 18). On the other hand, no cross-over was observed in the thermal denaturation profiles at neutral pH possibly due to the low stability of the structures (Figure 17). Table 2 displays the calculated Tm values for the C-rich strands of *PIM1*. The findings provide evidence for the formation of secondary structures with significantly higher stability at acidic pH compared to neutral pH, consistent with expectations for i-motifs [119]. UV-Visible experiments align with CD analyses, clearly prove the formation of ordered i-motif structures at pH 5.5 in Na-phosphate buffer.

Table 2 also displays changes in Tm values upon changing the buffer. the Tm values reflect that the effect of $K^+/Na^+$ ion change in the i-motif structures differ from what is observed for G-quadruplex structures of *PIM1* gene, aligning with the belief that salt has moderate impact on the stability of i-motifs in comparison to G-quadruplex structures [120]. In a recent study conducted by Kim and Hong, i-motif structures in human telomere sequences are reported to exhibit almost identical Tm values in the presence of $Li^+$, $Na^+$ or $K^+$ ions at a salt concentration of 100 mM [120]. Additionally,

they confirmed the destabilization of i-motifs with the increasing concentration of monovalent cations (> 200 mM).

In our samples, the stabilities of the i-motifs were almost the same in the presence of $K^+$ and $Na^+$ cations at pH 5.5 with only 1 ºC and 2 ºC increase in Tm values for I1 and I2 respectively (Table 2). No change was observed in the Tm value of I3 in NaCl and KCl at pH 5.5 (Table 2). The Tm values obtained for the samples prepared at pH 7.0 in the presence of $K^+$ or $Na^+$ were also close to each other. As displayed in Table 2, the stability of the i-motif structures decreased slightly when the cation was exchanged to $Na^+$. While the Tm values of I1 and I3 decreased by 4 ºC, the Tm of I2 decreased by only 2 ºC. (Table 2). Overall, it is evident that under identical conditions, $Na^+$ ions induce significant destabilization in comparison to $K^+$ ions in G-quadruplex structures of the *PIM1* gene (8-19 ºC), whereas they exhibit almost no or little destabilizing effect on i-motif structures of the complementary strands.

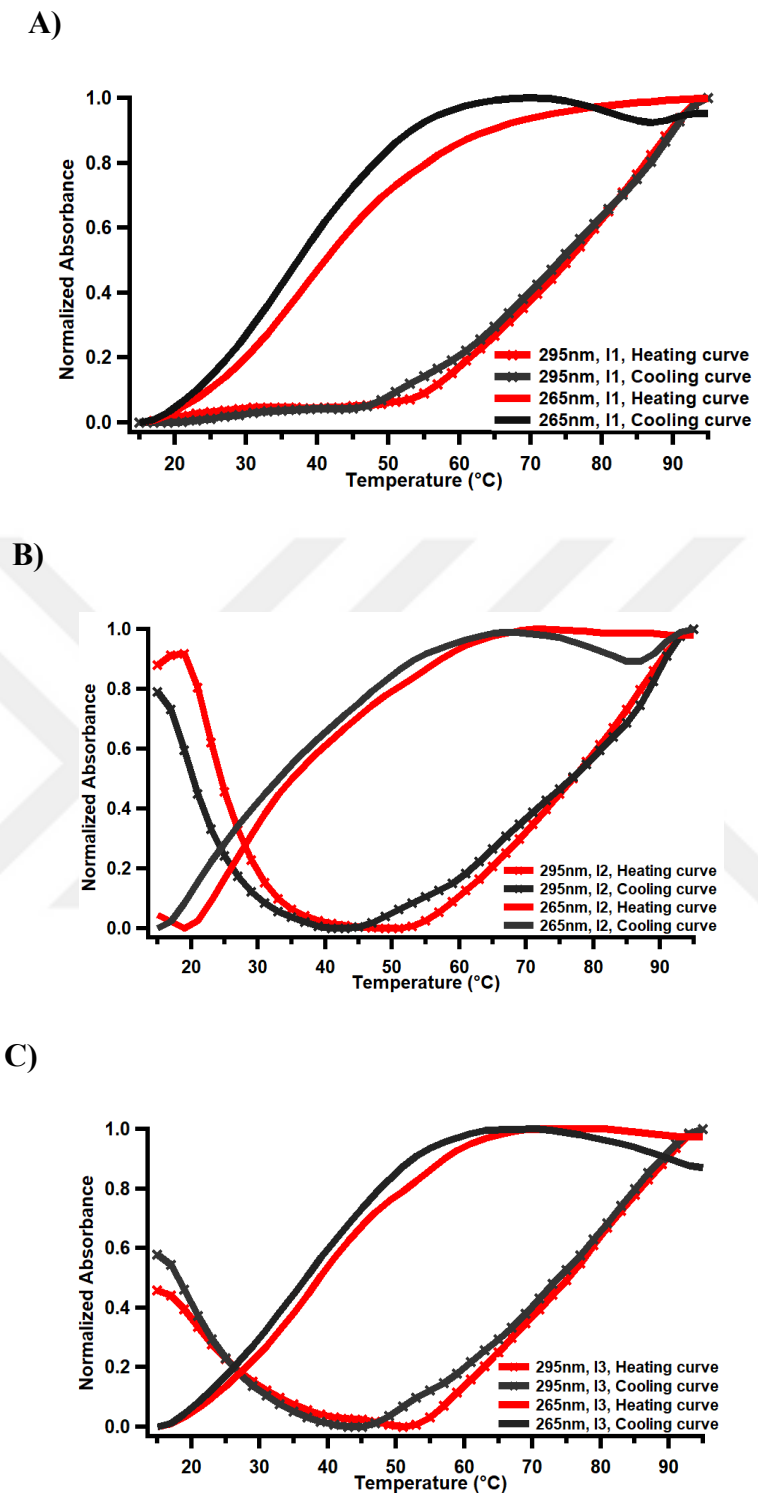


Figure 17. UV-Vis thermal melting profiles of 3.0 µM DNA solution, A) I1 B) I2 C) I3, at pH 7.0 in Na-phosphate buffer obtained by monitoring the absorbance change at 265 nm and 295 nm.

A)

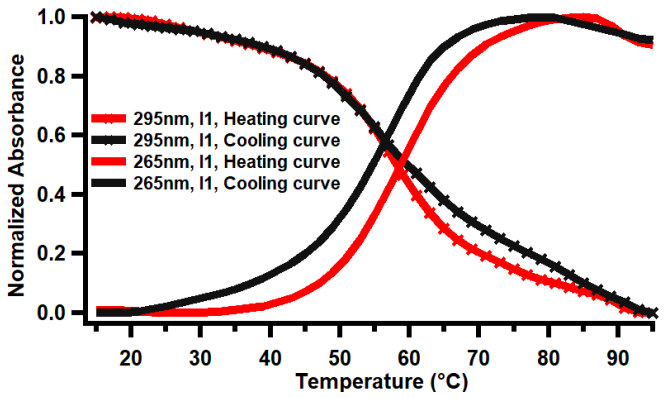


B)

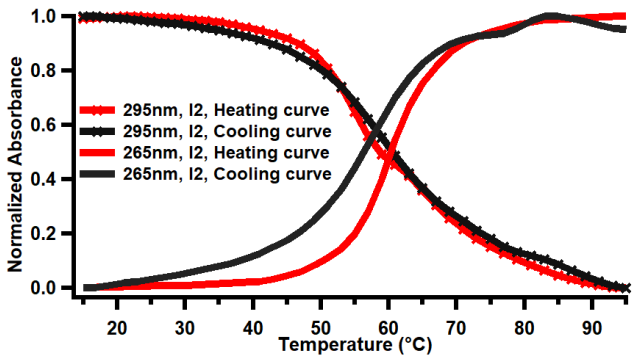


C)

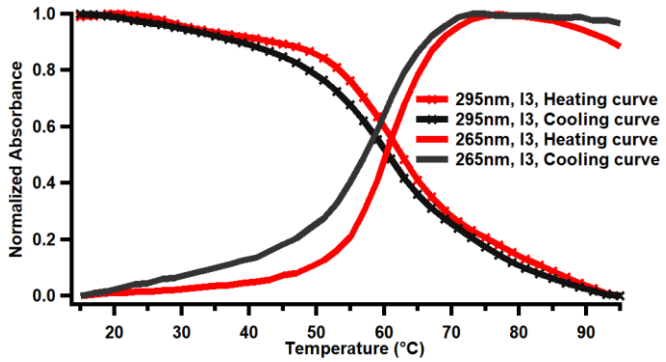


Figure 18. UV-Vis thermal melting profiles of 3.0 µM DNA solution, A) I1 B) I2 C) I3, at pH 5.5 in Na-phosphate buffer obtained by monitoring the absorbance change at 265 nm and 295 nm.

Table 2. Comparison of the Tm values of 3.0 μM DNA solution of I1, I2, I3 obtained by monitoring the absorbance change at 265 nm, under two different pHs in K-phosphate or Na-phosphate buffer.

| **DNAs** | **Tm** | | | |
|---|---|---|---|---|
| | **K-phosphate** | | **Na-phosphate** | |
| | **pH= 7.0** | **pH= 5.5** | **pH= 7.0** | **pH= 5.5** |
| **I1** | 45 ºC | 57 ºC | 41 ºC | 58 ºC |
| **I2** | 37 ºC | 57 ºC | 35 ºC | 59 ºC |
| **I3** | 43 ºC | 61 ºC | 39 ºC | 61 ºC |

## 3.5 Investigating DNA Duplex Formation in *PIM1* Sequences

After confirming the formation of G-quadruplex and i-motif structures in *PIM1* gene, we hypothesized that duplex DNA structures might still be the dominant structure when the two complementary G-rich and C-rich strands of *PIM1* gene exist in the sample.

### 3.5.1 Characterization of Double Helical DNA in K-phosphate Buffer via Circular Dichroism Spectroscopy

At first step, Circular Dichroism analyses were performed for samples containing 1.5 μM of each complementary strand in 20 mM K-phosphate buffer with 20 mM KCl at pH 7.0 and pH 5.5 (Figure 19). B-form DNA are known to have characteristic positive peaks between 250 and 280 nm and two negative peaks at 210 and 240 nm. A-form duplex is characterized by a positive peak at 260 nm and negative peak at 210 [109]. The first sample named as D1 in this work (containing G1 and I1), exhibits a positive peak at 269 nm with a shoulder at 286 nm and negative peaks at around 240 and 210 nm at pH 7.0 (Figure 19A), which confirms the formation of B-form DNA duplex [121]. When the pH was decreased to 5.5 the intensity at 286 nm was

increased. This could reflect a change in the stability of the double helical DNA or the presence of other structures (G-quadruplex and i-motif) according to the previous studies [49], [56]. Similar characteristic CD spectra were also observed for D2 sample (containing G2 and I2) and D3 sample (containing G3 and I3) at pH 7.0, shown in Figure 19B and C. For all three samples, the shoulder at around 285 nm becomes the dominant peak at pH 5.5. The most significant change at pH 5.5 is observed for D3, where the peak at 269 nm has completely disappeared. In a study conducted by Li et al. [41], a rise in the CD positive peak at 287 nm and the negative peak at 263 nm was observed as the pH decreased from 7.4 to 5.8 in a sample containing both G-rich and C-rich sequences of the *C-myb* proto-oncogene in PBS buffer (20 mM $NaH_2PO_4$-$Na_2HPO_4$) with 100 mM KCl This observation is taken as the conversion of a portion of the double strand to an i-motif structure [41]. Additionally, Abou Assi et al. [51] reported the formation of i-motifs in Human telomeric DNA by decreasing the pH gradually from 7.4 to 5.8 in 20 mM K-phosphate and 70 mM KCl buffer. Other reports also indicated that a decrease in pH promotes the formation of other secondary structures such as i-motifs and G-quadruplexes [54], [55]. Collectively, the results confirm the presence of i-motif or G-quadruplex structures, with the duplex being the predominant conformation at pH 7.0. Conversely, at pH 5.5, i-motifs and G-quadruplexes become the prevailing conformations.

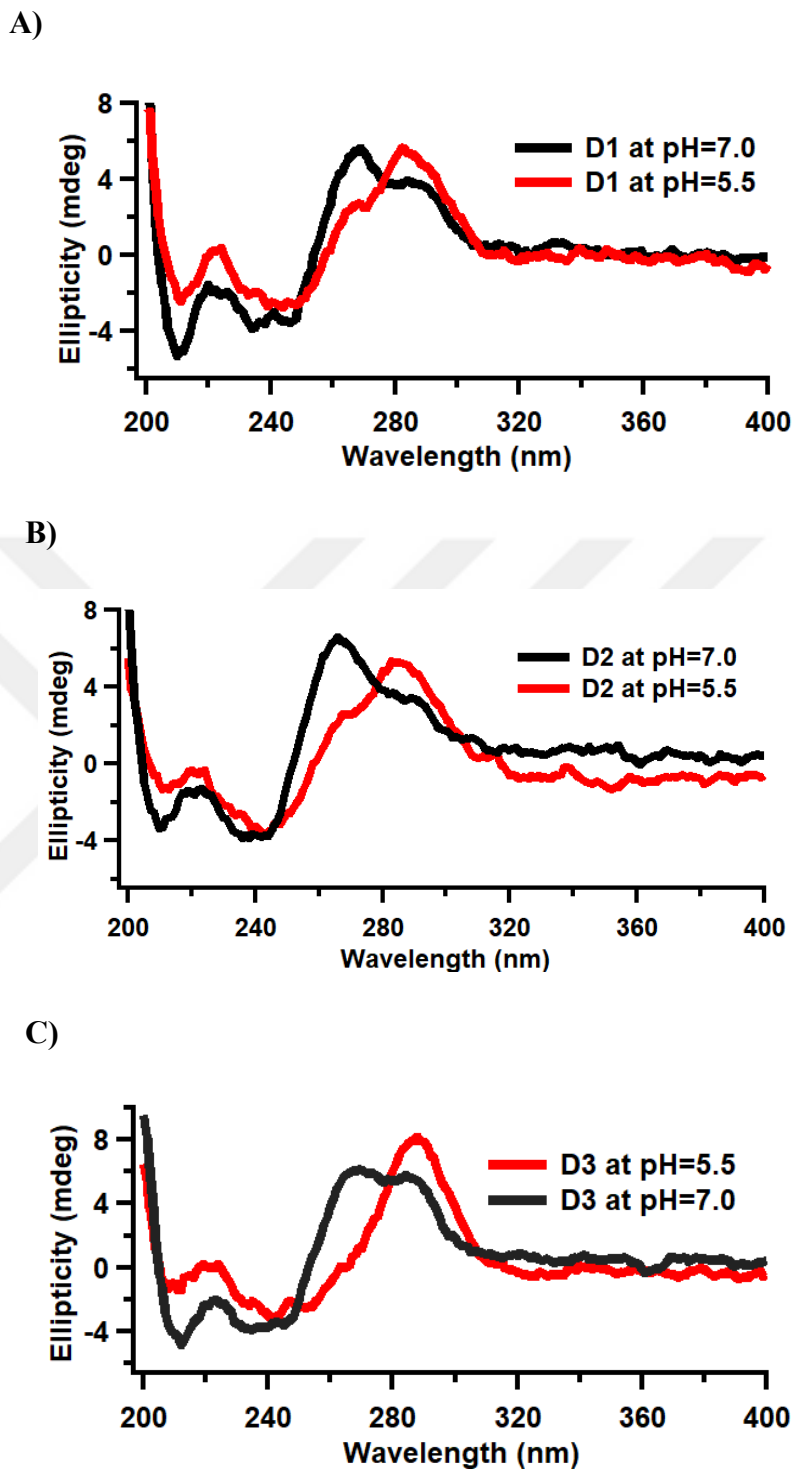


Figure 19. CD spectra of 3.0 µM DNA solution, A) D1 B) D2 C) D3, at pH 7.0 and 5.5 in 20 mM K-phosphate with 20 mM KCl buffer at 15 °C.

### 3.5.2 Characterization of Double Helical DNA in *PIM1* Sequences in K-phosphate Buffer via UV-Vis Thermal Denaturation Experiments

In the next step, thermal denaturation analyses were conducted to study the stabilities of the duplex structures at pH 7.0 and 5.5 (Figure 20). At pH 7.0, the melting profiles are found to be biphasic whereas at pH 5.5 only a single transition is observed for all three samples. For D1 the first transition is not as clear as D2 and D3. Table 3 represents Tm values for D1, D2 and D3 at two pHs. Alterations in pH values lead to a decrease in Tm values for all three samples (Table 3) which reveals higher stabilities at pH 7.0. As discussed in 1.2 section, DNA duplexes are more stable at neutral pHs [10]. Previously, Serrano-Chacón et al. reported three-dimensional structure of an i-motif/duplex junction which has a biphasic thermal denaturation profiles as ours [122]. They believe that the lower Tm at pH 7.0 (26.9 °C) corresponds to the denaturation of the i-motif moiety, and the higher Tm (62.6 °C) to the denaturation of the B-DNA part. This observation is consistent with their CD results exhibiting a maximum at 284 nm at low temperatures that blue shifts upon heating, and a minimum at 250 nm that red shifts at temperatures more than 35 °C [122]. Accordingly, the presence of the biphasic nature of our thermal denaturation profiles obtained might be reflecting the formation of local G4s and i-motifs in DNA duplex structure at pH 7.0.

A hysteresis between the denaturation and annealing profiles is also observed for these samples at pH 5.5 which is attributed to the absence of thermodynamic equilibrium due to the slow folding and/or unfolding processes as mentioned previously [112]. The corresponding UV-Vis absorption spectra for the thermal denaturation experiments are given in Appendix C, Figures 65-79.

A)

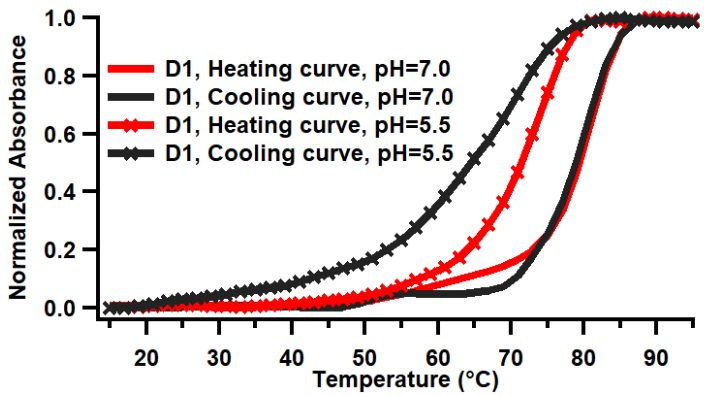


B)

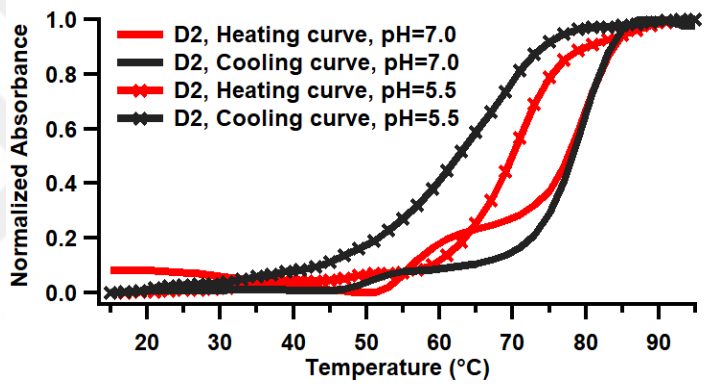


C)

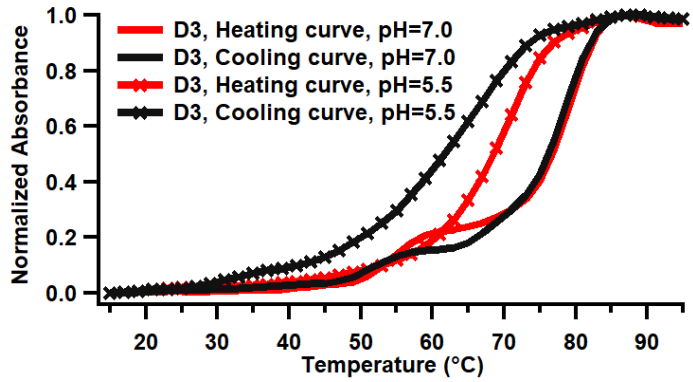


Figure 20. UV-Vis thermal denaturation profiles of 3.0 µM DNA solution, A) D1 B) D2 C) D3, obtained by monitoring the absorbance change at 260 nm, at pH 7.0 and 5.5, in K-phosphate buffer.

## 3.6 Investigating Effects of Salt on DNA Duplex *PIM1* Structures

### 3.6.1 Characterization of Double Helical DNA in Na-phosphate Buffer via Circular Dichroism Spectroscopy

In Figures 21 and 22, the Circular Dichroism spectra of D1, D2 and D3 in 20 mM Na-phosphate buffer with 20 mM NaCl are compared to the spectra obtained in K-phosphate and KCl system which was discussed earlier at two different pHs. The results suggest that, despite an increase in the intensity of peaks, the nature of structures has not changed in Na-phosphate buffer at pH 7.0. According to previous studies, due to the higher stability of i-motifs at acidic pH there could be a rise in the CD positive peak at around 285 nm as the pH decreases [41]. According to CD spectra obtained at pH 5.5 (Figure 22), the positive peak at around 285 nm increases while the small shoulder at 267 nm is completely lost in the spectra of D1 and D2. The observed changes might be an indication of a change in duplex-tetraplex equilibria in these samples. Similar to the results obtained in K-phosphate buffer, comparing the spectra of samples at pH 7.0 and 5.5 (Figure 23) revealed an increase in the positive peaks at around 285 nm which supports the conversion of a portion of the double stranded helix to an i-motif structure at acidic pH [41]. Overall, the results suggest the presence of i-motif or G-quadruplex structures, with the duplex conformation at pH 7.0 and pH 5.5, while i-motifs and G-quadruplexes might be the prevailing conformations at acidic pH. This observation is in an agreement with reports indicating that a decrease in pH promotes the formation of other secondary structures such as i-motifs and G-quadruplexes as mentioned above [54], [55].

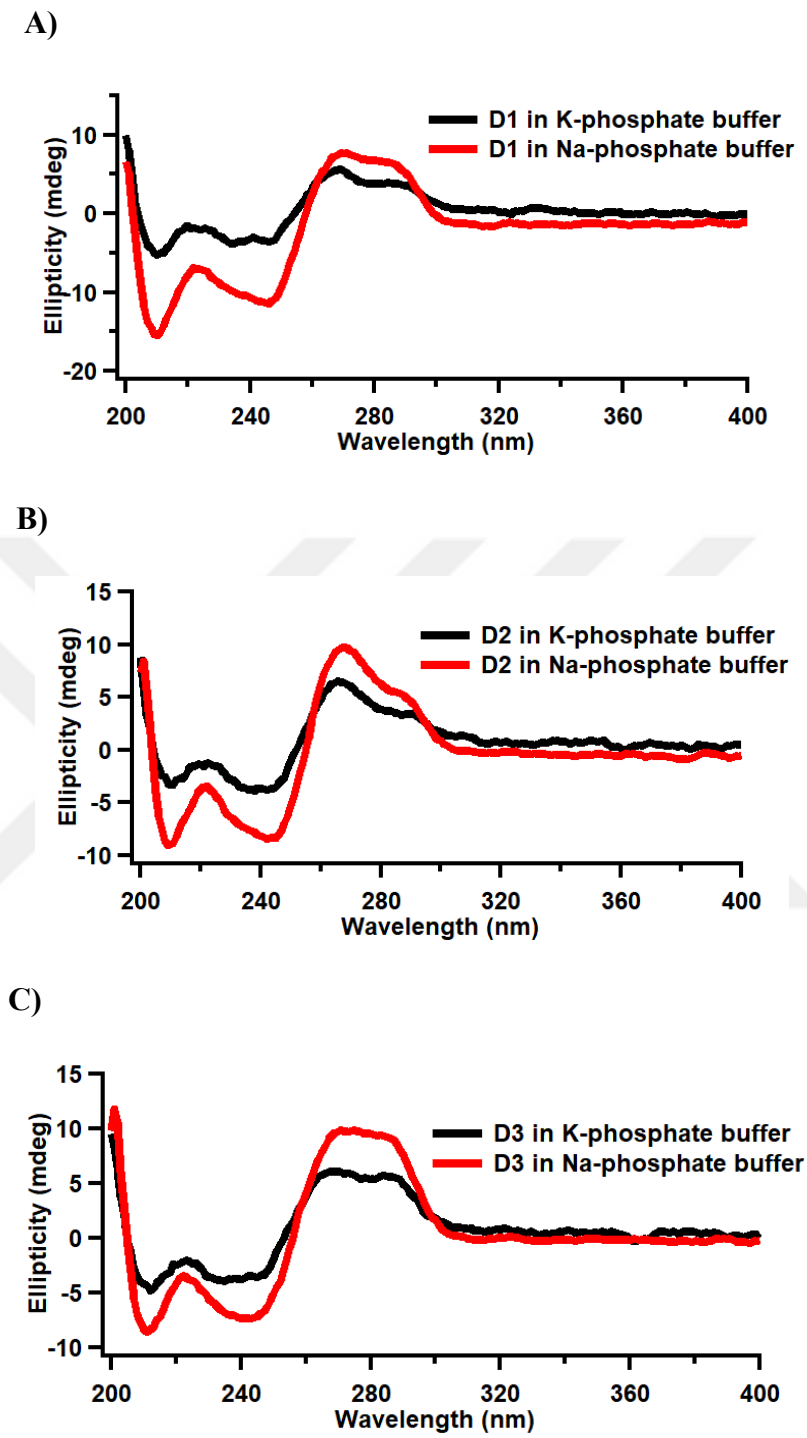


Figure 21. Comparison of the CD spectra of 3.0 µM DNA solution A) D1 B) D2 C) D3 in K-phosphate or Na-phosphate buffer at pH 7.0.

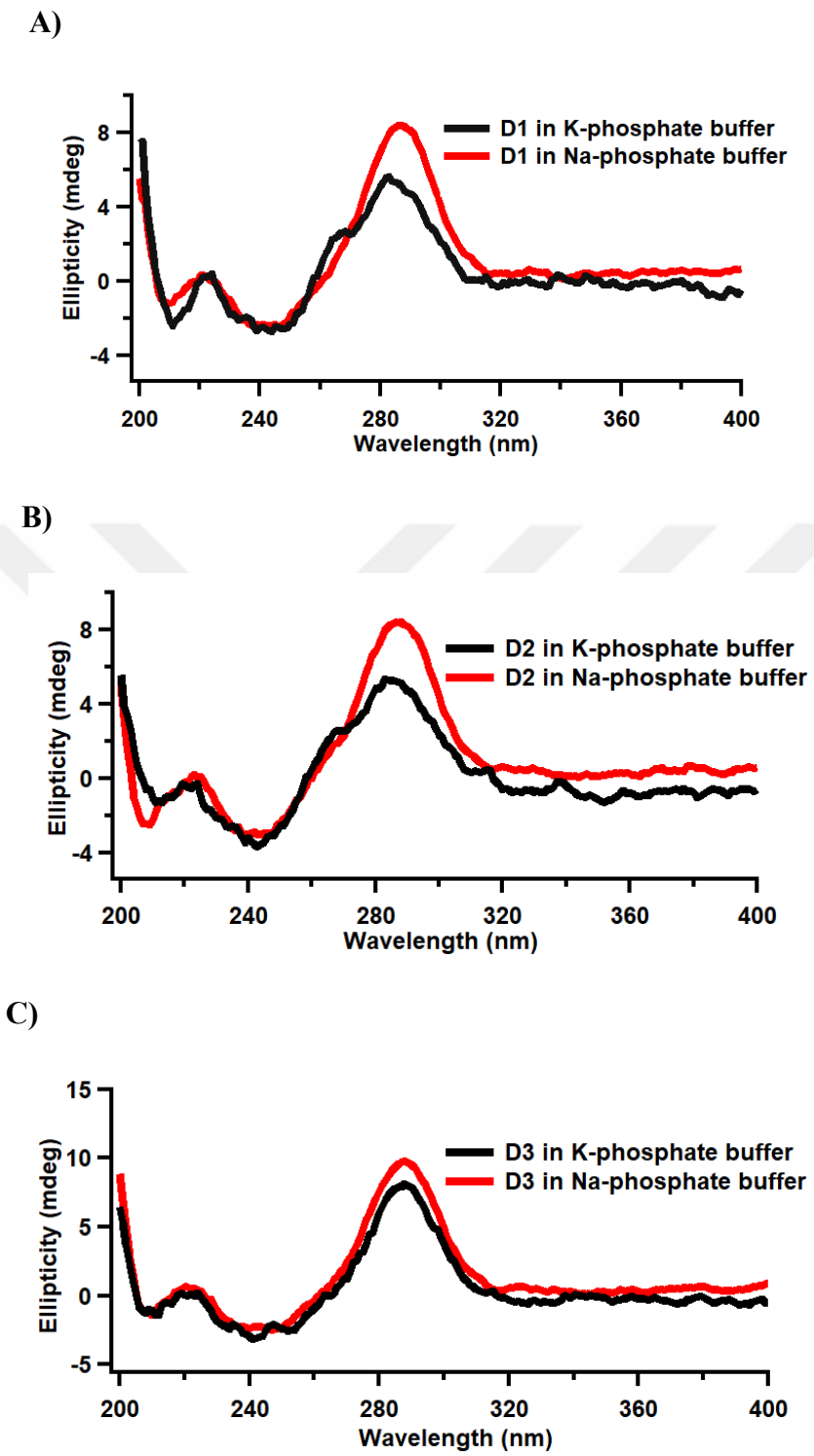


Figure 22. Comparison of the CD spectra of 3.0 µM DNA solution A) D1 B) D2 C) D3 in K-phosphate or Na-phosphate buffer at pH 5.5.

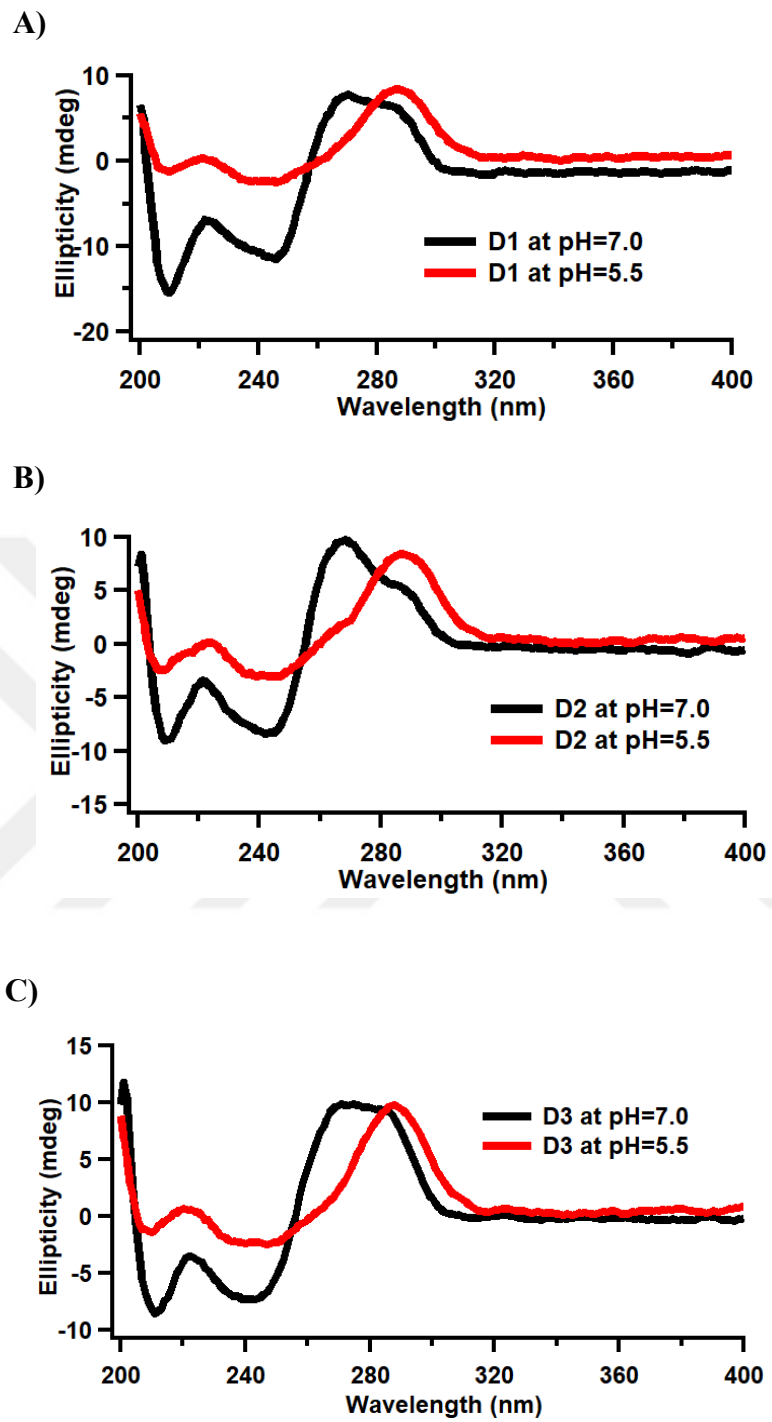


Figure 23. CD spectra of 3.0 µM DNA solution, A) D1 B) D2 C) D3, at pH 7.0 and 5.5 in 20 mM Na-phosphate with 20 mM NaCl buffer at 15 °C.

### 3.6.2 Characterization of the Double Helical DNA in Na-phosphate Buffer via UV-Vis Thermal Denaturation Experiments

The stabilization of the duplex state of DNA by the cations is a very well-known fact. The stability enhancement of the Double Helical DNA is known to go up to counter ion concentrations of approximately 1 M. Higher concentrations of cations are known to lead to the destabilization of the duplex form [123]. Additionally, Nakano et al. reported identical effect of $Na^+$ and $K^+$ ions on thermal stability of d(GCCAGTTAA)/d(TT-AACTGGC) duplex structure [124]. In another investigation by Owczarzy et al. [125] $Tris^+$, $Na^+$ and $K^+$ ions are found to stabilize DNA duplexes to a similar degree. While $Mg^{2+}$ ions stabilize DNA duplexes significantly more than the same concentrations of monovalent ions.

Consistent with these findings, the Tm values of D1, D2, and D3 presented in Table 3 suggest no variations in the stabilities of the duplex structure formed in NaCl compared to KCl at pH 7.0. However, small differences in Tm values of D1 and D2 were observed at pH 5.5 (Table 3), aligning with their CD analysis, which has shown some changes between the CD profiles of the samples prepared in the presence of $K^+$ or $Na^+$ (Figure 24).

Since the CD analyses in the previous part (Figure 21) illustrated no substantial change in the structure between being in the Na-phosphate and K-phosphate buffer at pH 7.0, we expected to observe thermal denaturation profiles for the samples in the Na-phosphate similar to the ones observed in K-phosphate buffer. However, thermal analysis depicted in Figure 24, exhibits monophasic profiles, contrary to the biphasic profiles obtained in K-phosphate, which reflects the occurrence of changes in the duplex-quadruplex equilibrium. This observation could be the result of the changes in stabilities of other secondary structures that exist in the sample, especially G-quadruplexes which are more stable in solutions containing $K^+$ compared to $Na^+$ [49].

As discussed in Section 1.2, the DNA duplex structure is stable within the pH range of 5 to 9, and destabilization occurs at pH levels below 5 and above 9. Hence, we expected similar stability for pH 5.5 and 7.0. However, similar to the results obtained in K-phosphate buffer, alterations in pH values lead to a decrease in Tm values by 20 ºC, 8 ºC and 10 ºC for D1, D2 and D3, respectively (Table 3) which reveals higher stabilities of samples at neutral pH. In this regard, Konig et al. reported lower stability of a DNA duplex structure at pH 4.0 (Tm=39 ºC) in comparison to pH 7.4 (pH=54 ºC), using 10 mM Britton-Robinson buffer and 80 mM KCl [57]. Additionally, they investigated the effect of quadruplex structures formation on the stability of adjacent duplex DNA. They concluded that both G-quadruplexes and i-motifs are capable of destabilizing directly proximal duplex DNA. Tm values decreased about 4.4 and 4.1 ºC upon formation of G4 structure at pH 7.4 or I4 structures at pH 4.0, respectively.

In another study conducted by Cristofari et al. [126] i-motif formation was investigated in C-rich strand of *EGFR* promoter. The Tm value of equimolar mixtures of G- and C-rich strands of EGFR-272 at pH 7.0 corresponds to 82 ºC and there are two Tm values at pH 5.0 which are 46.1 ºC and 77.7 ºC in 100 mM KCl. Additionally, in the absence of KCl Tm decreases from 68.9 ºC at pH 7.0 to 52.4 ºC at pH 5.0. Their fluorescence melting analyses were in agreement with CD experiments revealing that the formation of i-motif structures impair duplex formation, and it efficiently competes with the canonical double helix structure.

Overall, the decrease in Tm values of *PIM1* dsDNA in both K- and Na-phosphate buffers may be due to the destabilization of double helix DNA upon formation of four-stranded structures.

Hysteresis was again observed between the denaturation and annealing profiles of samples at pH 5.5 which is attributed to the absence of thermodynamic equilibrium due to the slow folding and/or unfolding processes [112]. The corresponding UV-Vis absorption spectra for the thermal denaturation experiments are given in Appendix C, Figures 65-79.

A)

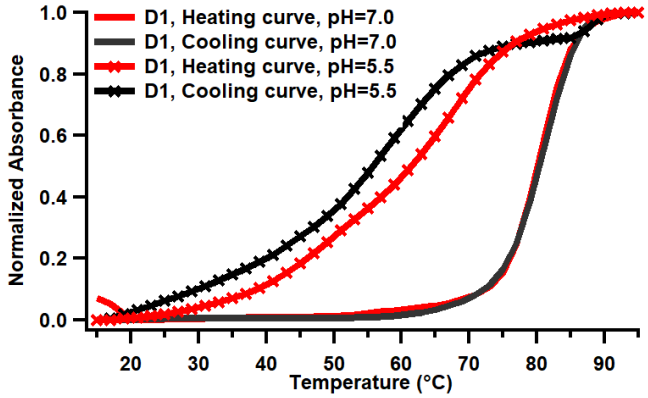


B)

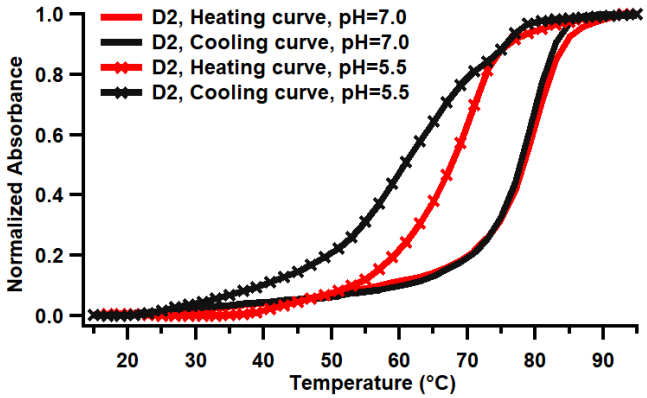


C)

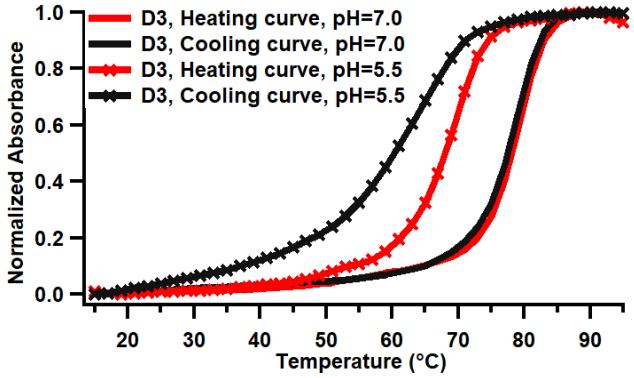


Figure 24. UV-Vis thermal denaturation profiles of 3.0 µM DNA solution, A) D1 B) D2 C) D3, obtained by monitoring the absorbance change at 260 nm, at pH 7.0 and 5.5 in Na-phosphate buffer.

Table 3. Comparison of the Tm values of 3.0 μM DNA solution of D1, D2, D3 obtained by monitoring the absorbance change at 260 nm, under two different pHs in K-phosphate or Na-phosphate buffer.

| **DNAs** | **Tm** | | | |
|---|---|---|---|---|
| | **K-phosphate** | | **Na-phosphate** | |
| | **pH= 7.0** | **pH=5.5** | **pH=7.0** | **pH= 5.5** |
| **D1** | 59 & 81 ºC | 72 ºC | 81 ºC | 63 ºC |
| **D2** | 55 & 79°C | 70 ºC | 79 ºC | 68 ºC |
| **D3** | 55 & 79°C | 69 ºC | 79 ºC | 68 ºC |

## 3.7 Examining the Interactions Between G4 Structures of *PIM1* and Doxorubicin

### 3.7.1 Characterization of Dox Binding to G4 structures via CD Spectroscopy

While Dox proves effective in downregulating gene expression and acting as an anti-cancer drug, there are only a few reports examining Dox interactions with G4s and evaluating its mechanism of action through G4 structures. This can provide solutions to the dose-dependent cardiotoxic effects and resolve dose-dependent challenges by providing further explanations on its mechanism of action [81], [82]. Furthermore, considering that there are no studies questioning the plausible binding of Dox to the *PIM1* gene, and the role of such binding on decreased *PIM1* gene expression we directed our efforts to explore Dox interaction with *PIM1* secondary structures.

At first, we performed CD analyses to study structural changes upon Doxorubicin (Dox) binding to *PIM1* G-quadruplex structures. In Figure 25 and 26, dashed lines indicate the spectra of the oligonucleotide only samples and the colored lines represent the 3.0, 6.0 and 30 μM Dox or Dox with 3.0 μM DNA at pH 7.0 and pH 5.5, respectively.

As discussed in 3.1.1, G2 has a positive peak at 266 nm with a shoulder around 290 nm and a negative peak at 245 nm at pH 7.0 (Figure 7B). These characteristic peaks

are indicative of a 3+1 hybrid G-quadruplex structure. The 3+1 hybrid nature of this structure is preserved at pH 5.5. G3 displays a positive peak at 292 nm and a negative peak at 258 nm showing an antiparallel nature at pH 7.0 (Figure 7C). The intensity of peaks in the CD spectrum of G3 decreased at pH 5.5 but the prevalence of the antiparallel structure remained unchanged. G1, exhibited a positive peak at 289 nm accompanied by a shoulder around 270 nm which indicates the existence of both structures at pH 7.0. When the pH of the solution was altered to 5.5, the shoulder peak disappeared, indicating a shift to a completely antiparallel structure.

On the other hand, the sample containing 30 μM Dox (solid black line) displayed broad positive bands around 350 nm, a negative band around 290 nm, and another positive band at 234 nm with a shoulder at 250 nm in the CD spectra. The relative intensity of the bands, especially at 234 nm and 250 nm differed from each other based on the pH of the environment. The band at 234 nm was sharper and more intense at pH 7.0. Our findings align with those of Airoldi et al. [127] where 23 μM Dox exhibited a broad positive band around 350 nm, another positive peak at around 230 nm with a shoulder at 250 nm, and a minimum at 289 nm.

In a recent study conducted by Tariq and Barthwal Daunomycin's affinity towards telomeric G-quadruplex DNA was examined. Reductions in band intensity were observed at 290, 265, and 240 nm in the CD spectrum of telomeric G4. These changes are believed to reflect the alterations in the relative populations of G-quadruplex conformations [128]. On the other hand, in a study by Airoldi et al. [127], titration of polyGC with doxorubicin exhibits gradual increase in the intensity of maximum peak at around 280 nm.

In our samples, addition of Dox onto the DNA resulted in different changes in the spectra of the G4s depending on the Dox concentration (Figure 25 and 26). In 1:1 and 1:2 (DNA:Dox) samples at pH 7.0 (Figure 25), Dox binding resulted in moderate shifts in the position of positive and negative peaks to lower wavelengths and a decrease in the intensity of the G4 characteristic bands especially for G1 and G3. However, no major structural transition is observed as assessed by the position of

the peaks for G2 and G3. But G1 sequence, which adopts both antiparallel and 3+1 hybrid structures at pH 7.0, was found to favor the prevalence of 3+1 hybrid structure in 1:10 solutions at both pHs.

At pH 5.5, in contrast to neutral pH, there is an increase in intensity of peaks upon Dox addition except for G1 and G3 1:10 solution (Figure 26). However, similar to our previous results at pH 7.0, there is no substantial change in the nature of the G-quadruplex structures.

Significant shifts of the positive peaks at around 280 nm to lower wavelengths were observed at high Dox concentration at both pH 7.0 and 5.5 (1:10 solutions exhibited as green lines in Figure 25 and Figure 26).

Accordingly, if there was no interaction between DNAs and Dox, one should expect a spectrum that is equal to the mathematical sum of 1:0 DNA:Dox and 0:10 DNA:Dox spectra for 1:10 DNA:Dox spectrum. However, as it is obvious, the spectra of DNA:Dox is different from the DNA+Dox spectrum especially at 290 nm. Moreover, emergence of a positive peak around 230 nm for DNA:Dox 1:10 solutions could be the effect of high Dox concentration. In addition, the disappearance of the broad positive band at 350 nm suggests that a different type of chirality is probably induced in Dox structure upon its interaction with G4s. The appearance of a minimum at 308 nm which is observed for all samples at both pHs, could also be attributed to the formation of the Dox-DNA complexes [127].

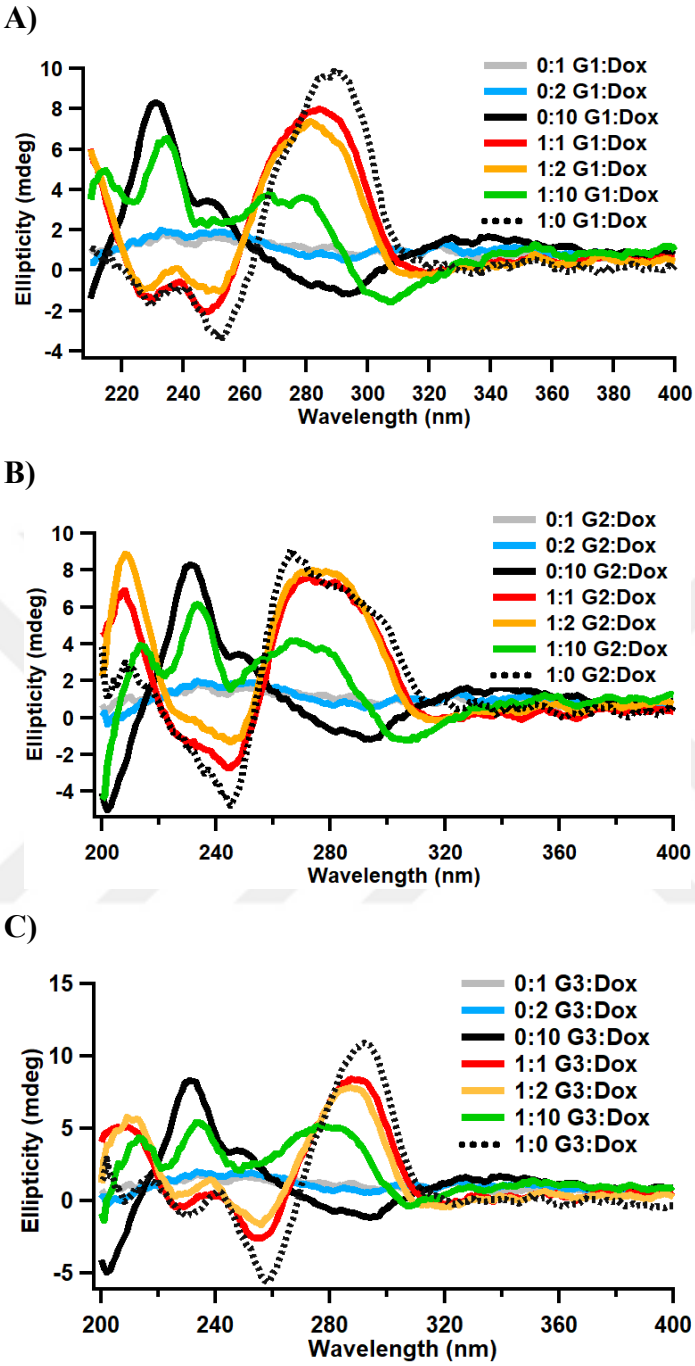


Figure 25. Comparison of the CD spectra of 3.0 µM of A) G1 B) G2 C) G3, in the absence and presence of 3.0, 6.0 and 30 µM Dox with the 3.0, 6.0 and 30 µM Dox spectra at pH 7.0.

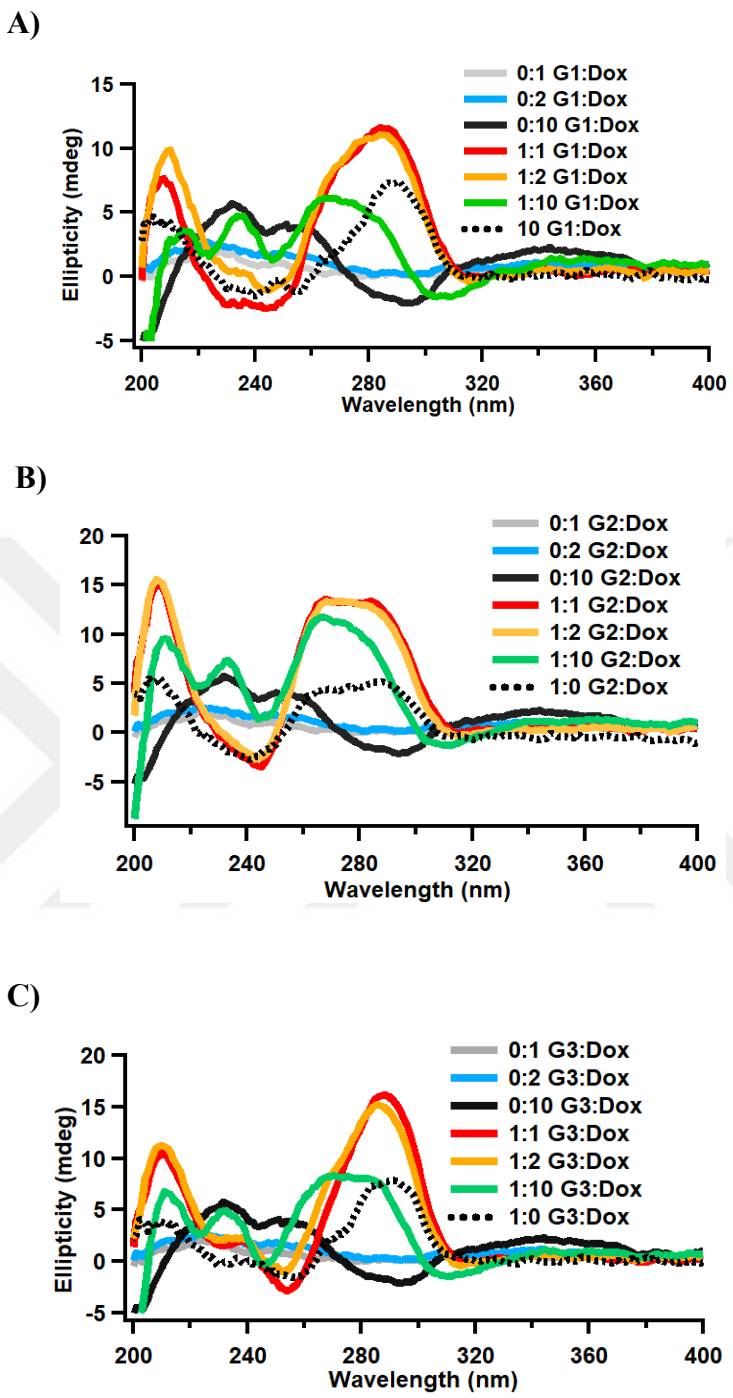


Figure 26. Comparison of the CD spectra of 3.0 µM of A) G1 B) G2 C) G3, in the absence and presence of 3.0, 6.0 and 30 µM Dox with the 3.0, 6.0 and 30 µM Dox spectra at pH 5.5.

### 3.7.2 Characterization of Dox Binding to G4 structures via UV–Vis Absorption Spectroscopy

To verify the binding between Dox and the *PIM1* G-quadruplex structures at pH 7.0 and 5.5, further investigations were conducted using UV–Vis spectroscopy at relatively high Dox concentrations since the major changes were observed at high Dox concentration during our investigations via CD. Comparing the UV–Vis absorption spectra of 3.0 μM samples in the absence and presence of Dox (DNA:Dox 1:10) with free Dox as given in Figure 27 and 28, confirms the binding of Dox to these G4s at pH 7.0 and 5.5, respectively. A significant hypochromic effect was observed in the absorption maxima of Dox at 480 nm upon its binding to all G4 structures of *PIM1* gene. Dox intercalation to double helical DNA leads to a reduction in intensity at 480 nm and induces a red shift in the absorbance region of Dox. The hypochromic effect and the red shift are generally observed due to the stacking of the aromatic moiety of the chromophore in between the DNA base pairs [129]. Although a red shift was not observed in our samples, a notable hypochromic effect was evident in the absorption maxima of Dox at 480 nm in the presence of 3.0 μM DNA. This confirms the binding of Dox to all G4 structures of the *PIM1* gene at both pH 7.0 and 5.5.

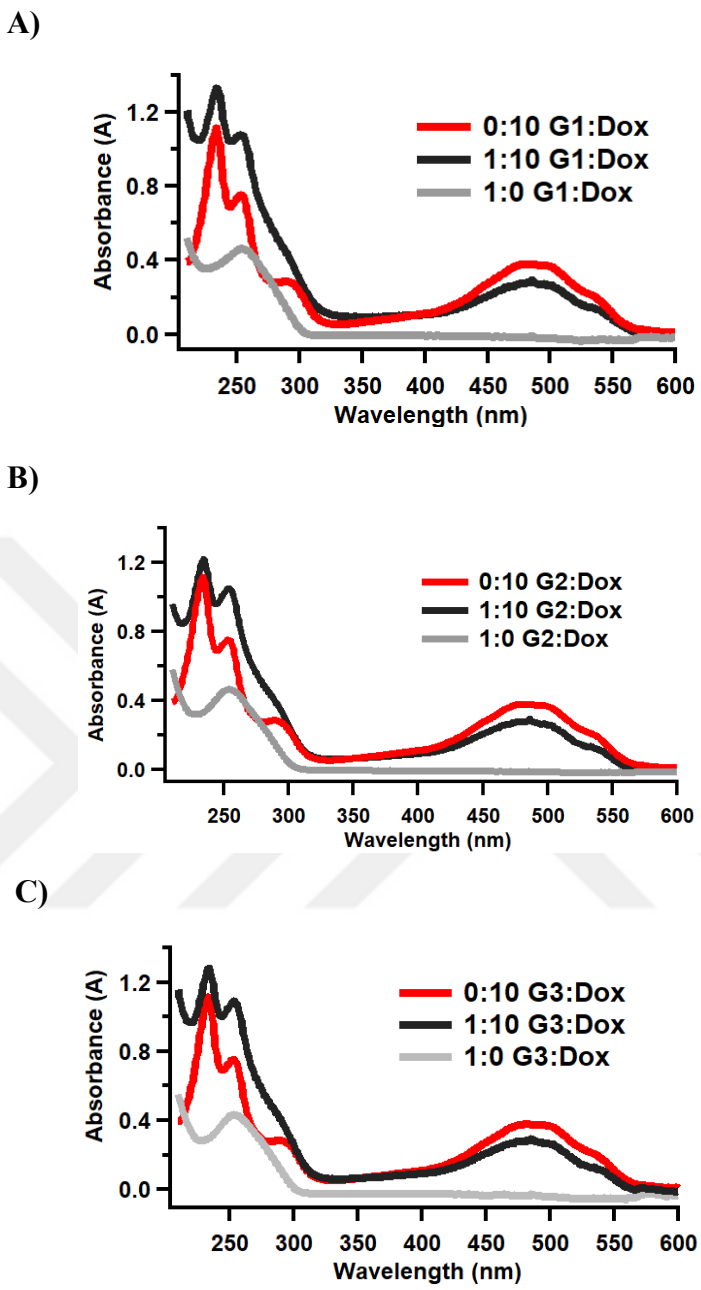


Figure 27. UV–Vis absorption spectra of 3.0 µM A) G1 B) G2 C) G3 in the absence and presence of 30 µM Dox at pH 7.0 in K-phosphate buffer. Red lines represent Dox alone, grey lines show oligonucleotide alone and blank lines denote the DNA:Dox sample.

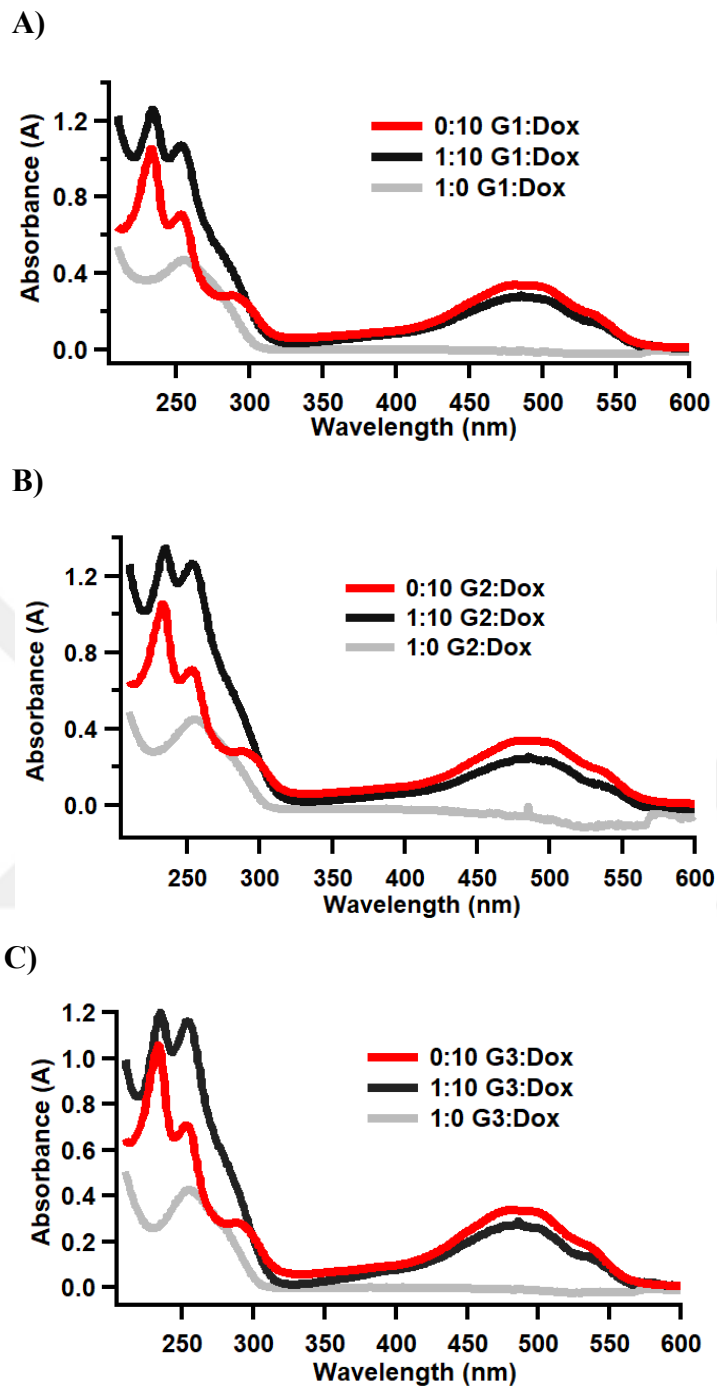


Figure 28. UV–Vis absorption spectra of 3.0 µM A) G1 B) G2 C) G3 in the absence and presence of 30 µM Dox at pH 5.5 in K-phosphate buffer. Red lines represent Dox alone, grey lines show oligonucleotide alone and blank lines denote the DNA:Dox sample.

### 3.7.3 Characterization of Dox Binding and the Stability of the G4-Dox Complexes via Thermal Denaturation Experiments

Thermal denaturation experiments were performed to observe the changes in the stability of nucleic acid structures upon their interactions with Dox [129]. An increase in Tm value means that the small molecule inserts a stabilizing effect on the nucleic acid structure and causes it to unfold at higher temperatures. For instance, Manet et al. reported an increase from 62 ºC to 67 ºC upon Dox binding to human telomeric sequence in the presence of $K^+$ [85].

In this study, thermal denaturation temperatures of samples containing 1:0, 1:1, 1:2, 1:10 and 0:10 equimolar ratios of DNA (3.0 μM):Dox were measured via UV-Vis absorption spectroscopy between 15ºC and 95ºC (Table 4). The corresponding UV-Vis absorption spectra for the thermal denaturation experiments were given in Appendix C, Figures 65-79. The increase in temperature from 15ºC to 95ºC resulted in unfolding of the G4 structures. In Figures 29-32 lines with markers represent the thermal denaturation profiles of DNA-Dox samples while solid lines represent the profiles of DNA structures alone. These Figures clearly display higher stability of the G4 structures in the presence of Dox as a result of Dox binding to G-quadruplex structures at both pH 7.0 and pH 5.5. The corresponding Tm values are represented in Table 4. Typically, a decreasing trend in the UV-Vis absorbance at 295 is expected as the temperature increases due to the denaturation of G4s [130]. However, such a trend was not observed in the thermal denaturation profiles of DNA:Dox 1:10 samples at both pHs, and G1: Dox 1:2 at pH 7.0, as given in Appendix C Figures 80-86 probably due to the interference from the Dox absorption. Thus, Tm values are not calculated for these samples. The stabilization ability of Dox is observed to be relatively identical on all *PIM1* G4 structures, with a 5 ºC, 2 ºC and 3 ºC increase in Tm values for DNA:Dox 1:1 solutions of G1, G2 and G3 respectively at pH 7.0. The increment in Tm values for 1:2 solutions is slightly higher, with a 4 °C increase for G2 and a 5 °C increase for G3 at pH 7.0. At pH 5.5, the Tm values for 1:1 solutions are notably identical at 71 ºC with G2 demonstrating the highest change as 7 °C. G2

also exhibits highest shifts among 1:2 solutions with 10 °C increase in its Tm value, stating the relatively better stabilization of DNA-Dox complexes at pH 5.5 compared to pH 7.0.

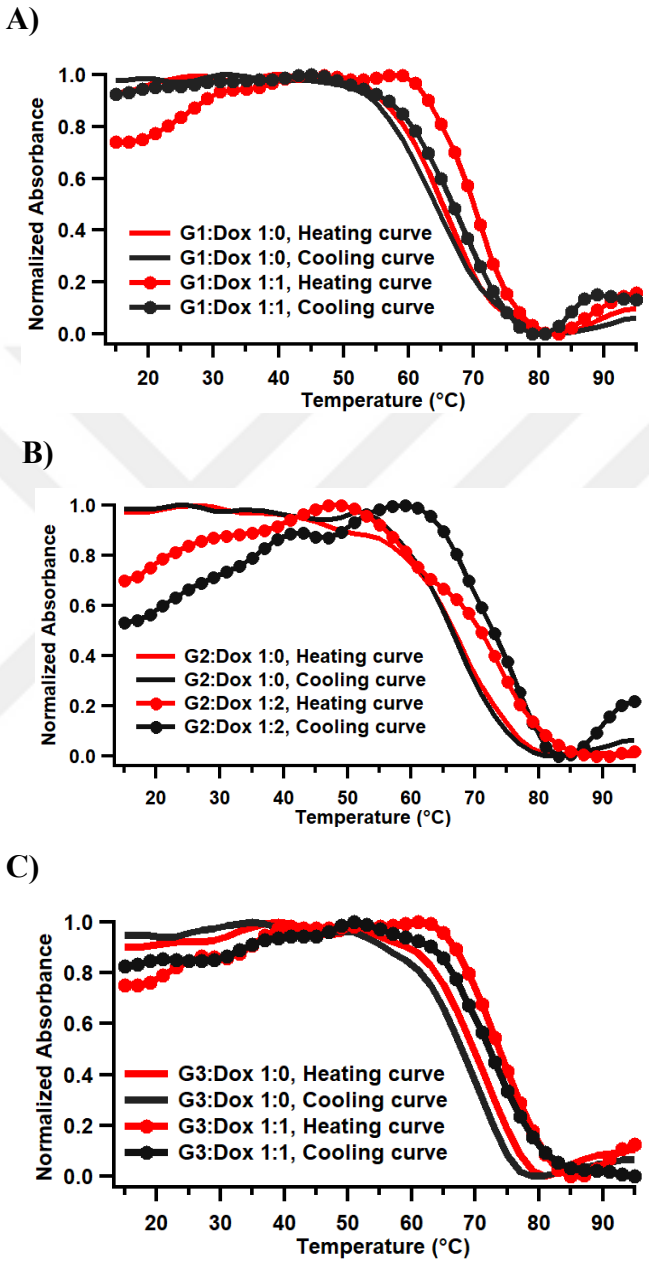


Figure 29. Comparison of the UV-Vis thermal melting profiles of 3.0 μM A) G1 B) G2 C) G3, in K-phosphate buffer at pH 7.0 in the absence and presence of 3.0 μM Dox by monitoring absorbance at 295 nm.

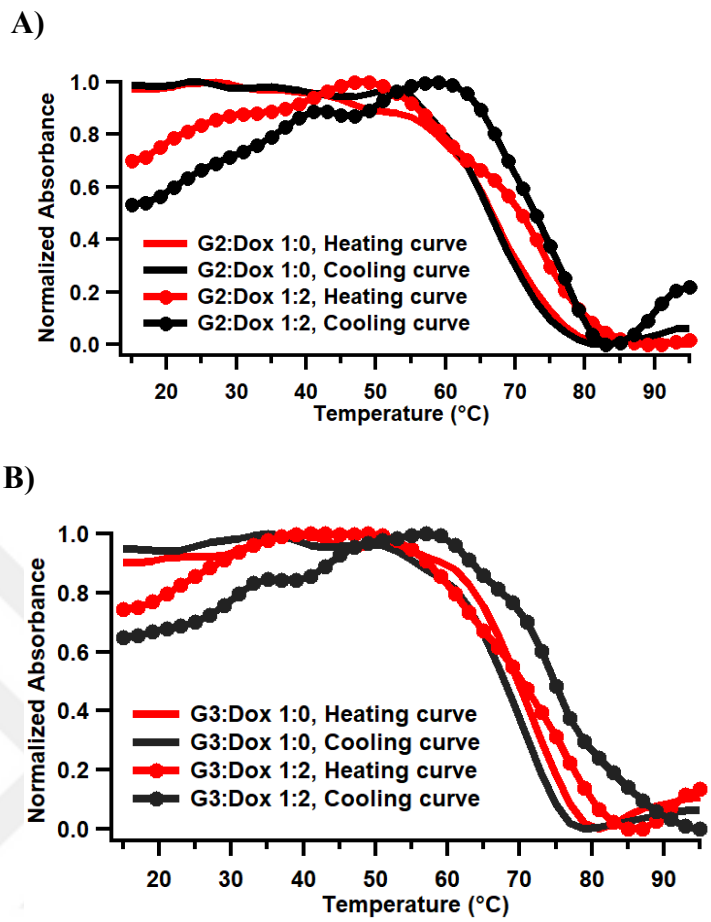


Figure 30. Comparison of the UV-Vis thermal melting profiles of 3.0 µM A) G2 B) G3, in K-phosphate buffer at pH 7.0 in the absence and presence of 6.0 µM Dox by monitoring absorbance at 295 nm.

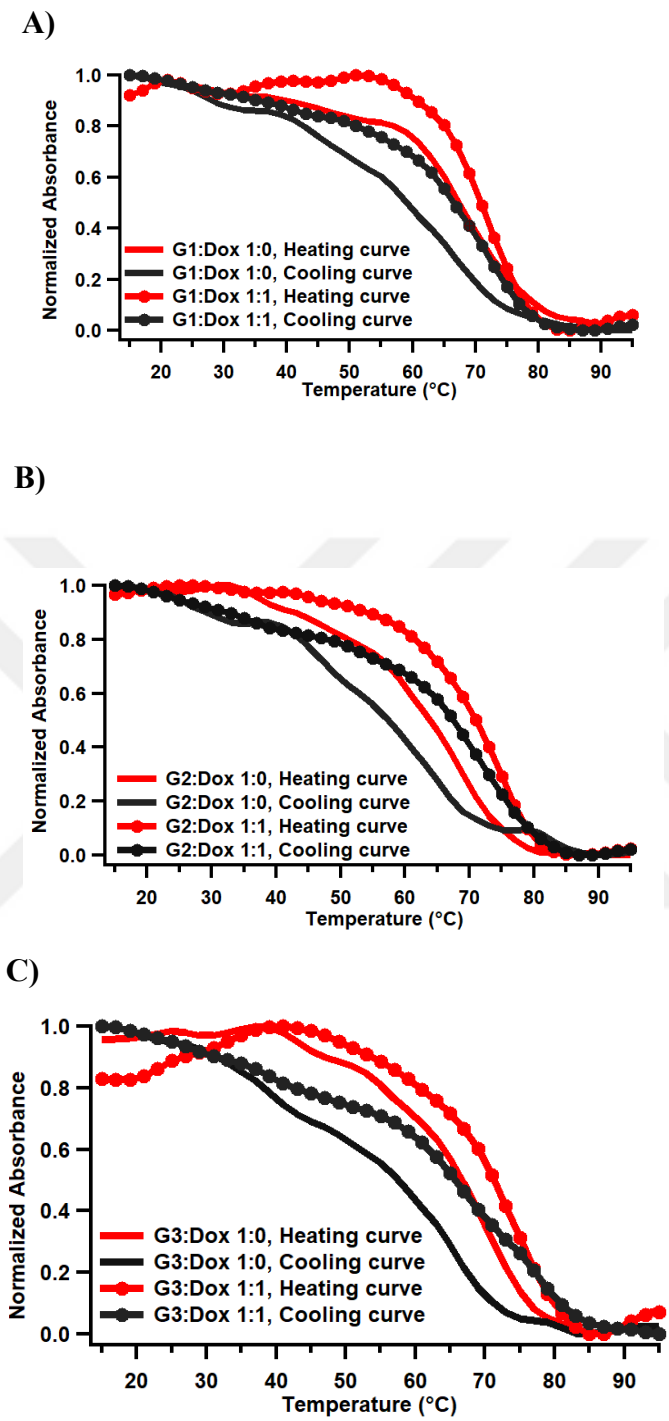


Figure 31. Comparison of the UV-Vis thermal melting profiles of 3.0 µM A) G1 B) G2 and C) G3, in K-phosphate buffer at pH 5.5 in the absence and presence of 3.0 µM Dox by monitoring absorbance at 295 nm.

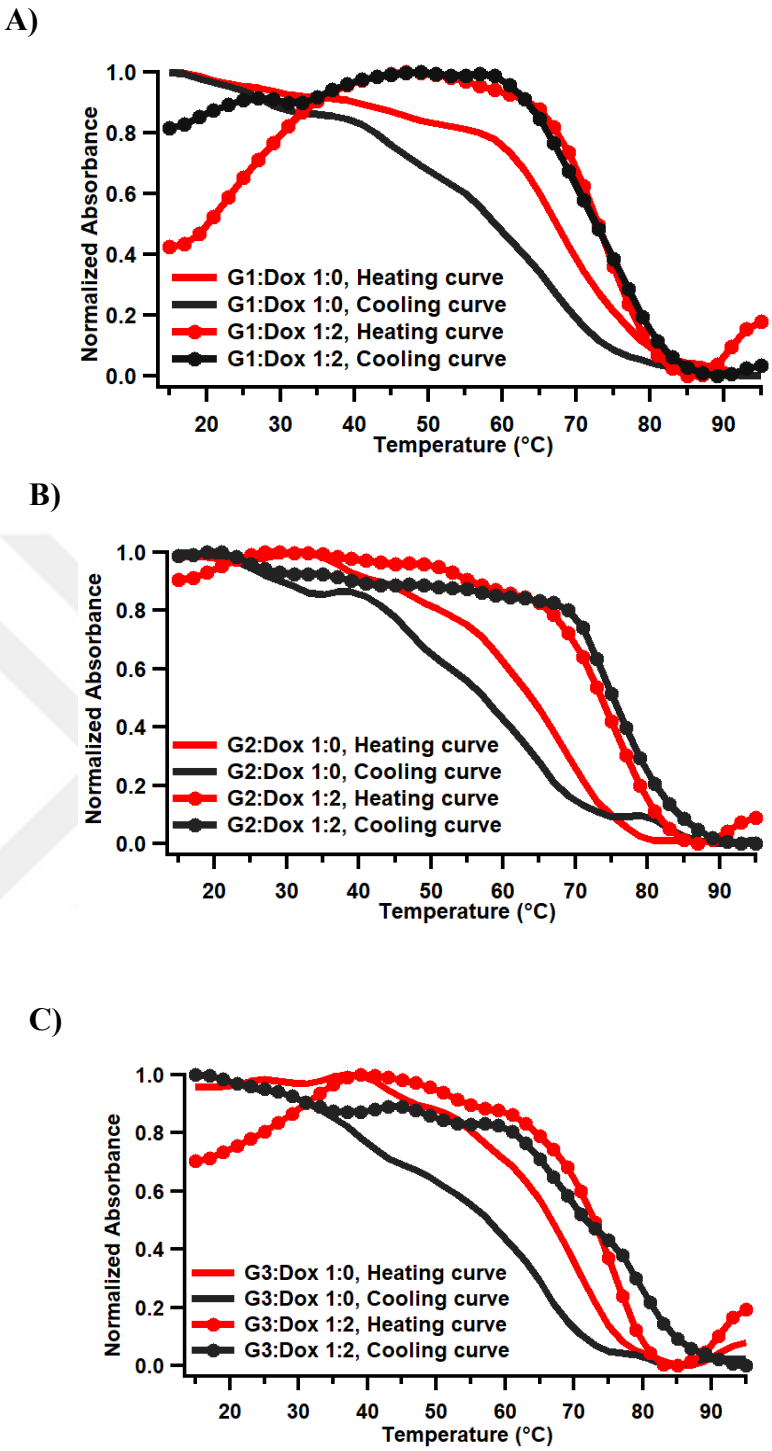


Figure 32. Comparison of the UV-Vis thermal melting profiles of 3.0 µM A) G1 B) G2 and C) G3, in K-phosphate buffer at pH 5.5 in the absence and presence of 6.0 µM Dox by monitoring absorbance at 295 nm.

Table 4. Comparison of the Tm values of 3.0 μM DNA solutions in the absence and presence of 3.0, 6.0 and 30 μM of Dox at pH 7.0 and pH 5.5 in K-phosphate buffer.

| **DNAs** | **Tm** | |
|---|---|---|
| | **pH= 7.0** | **pH= 5.5** |
| **G1: Dox 1:0** | 65 ºC | 67 ºC |
| **G1: Dox 1:1** | 70 ºC | 71 ºC |
| **G1: Dox 1:2** | - | 73 ºC |
| **G1: Dox 1:10** | - | - |
| **G2: Dox 1:0** | 67 ºC | 64 ºC |
| **G2: Dox 1:1** | 69 ºC | 71 ºC |
| **G2: Dox 1:2** | 71 ºC | 74 ºC |
| **G2: Dox 1:10** | - | - |
| **G3: Dox 1:0** | 70 ºC | 66 ºC |
| **G3: Dox 1:1** | 73 ºC | 71 ºC |
| **G3: Dox 1:2** | 75 ºC | 73 ºC |
| **G3: Dox 1:10** | - | - |

### 3.7.4 Characterization of Dox binding to G4 structures via Fluorescence Spectroscopy

Another essential technique to characterize Dox binding is the measurement of Dox fluorescence quenching in the presence of DNA [131]. Figure 25 and Figure 26 clearly indicate the decrease in fluorescence intensity of free Dox in the presence of all G4 structures at pH 7.0 and pH 5.5, respectively. Thus, validating the binding of Dox to *PIM1* gene G4s. The changes are almost similar for different G-quadruplex structures at both pHs with G2 demonstrating highest changes for all ratios at pH 5.5 which has also the highest changes in Tm values.

By taking advantage of decrease in fluorescence intensity, the association constants ($K_a$) of Dox with *PIM1* G4s were determined via titration experiments [132], [106]. Spectra were recorded by monitoring the decrease in the fluorescence intensity as the Dox solution was titrated with DNA-Dox solution. The representative titrations are shown in Figure 35. The experiments were done in duplicates for the $K_a$

calculations and the second replicates are given in Appendix E, Figures 73-80. The obtained $K_a$ values were $(2.47 \pm 0.12)\times10^6$, $(1.64 \pm 0.04)\times10^6$ and $(1.98 \pm 0.00)\times10^6$ for the binding between G1, G2 and G3 with Dox, respectively (Table 5). These $K_a$ values are lower than the previously reported Ka value for Dox complex with G-quadruplex structure of VEGF $Pu_{22}T_{12}T_{13}$ $(1.36 \pm 0.29)\times10^7$ [87], and with $Pu_{22}$ G4-Dox complex $(7.50 \pm 0.74)\times10^6$ [87].

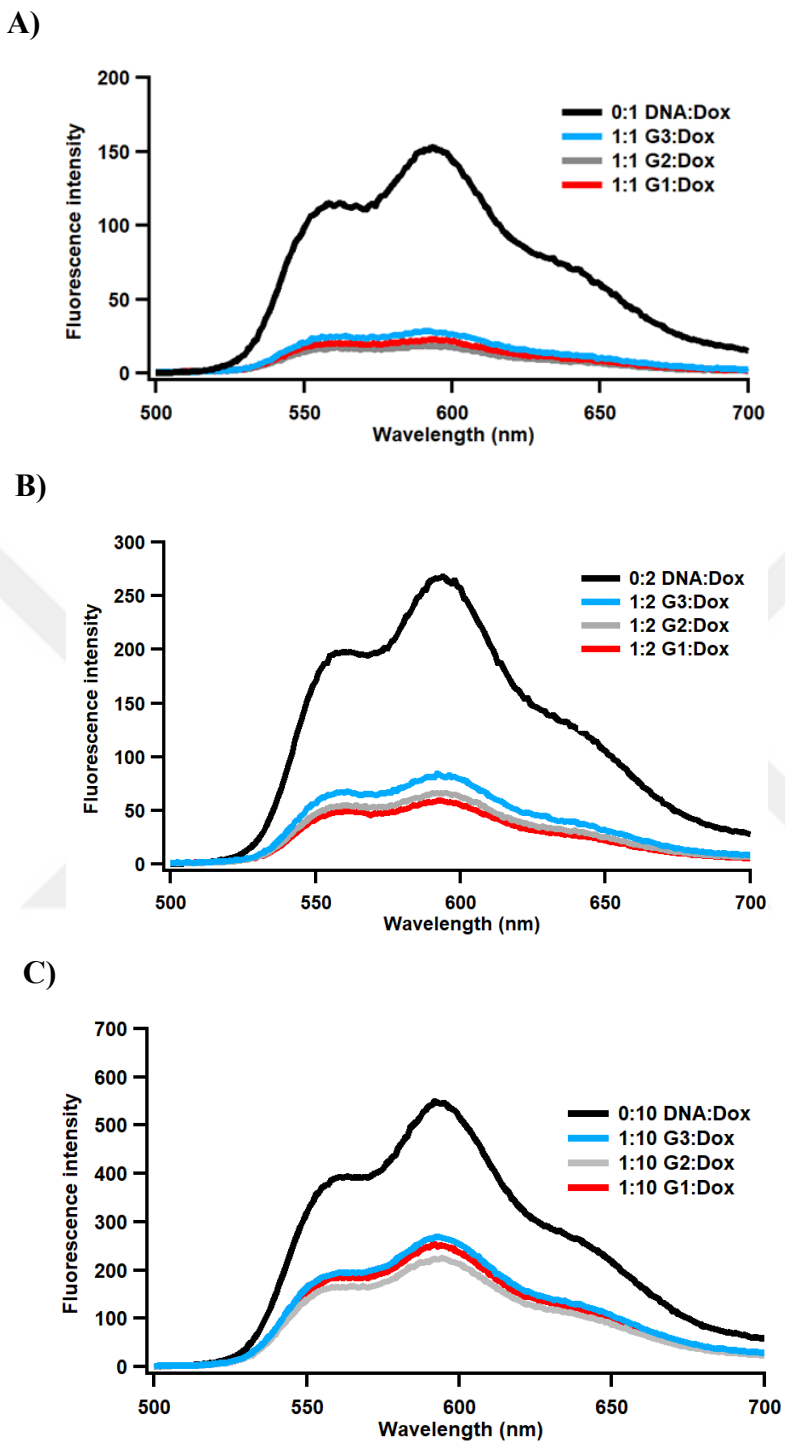


Figure 33. Changes in fluorescence intensity of A) 3.0 µM (1:1) B) 6.0 µM (1:2) C) 30 µM (1:10) free Dox (black line) upon binding to 3.0 µM *PIM1* G-quadruplex structures at pH 7.0.

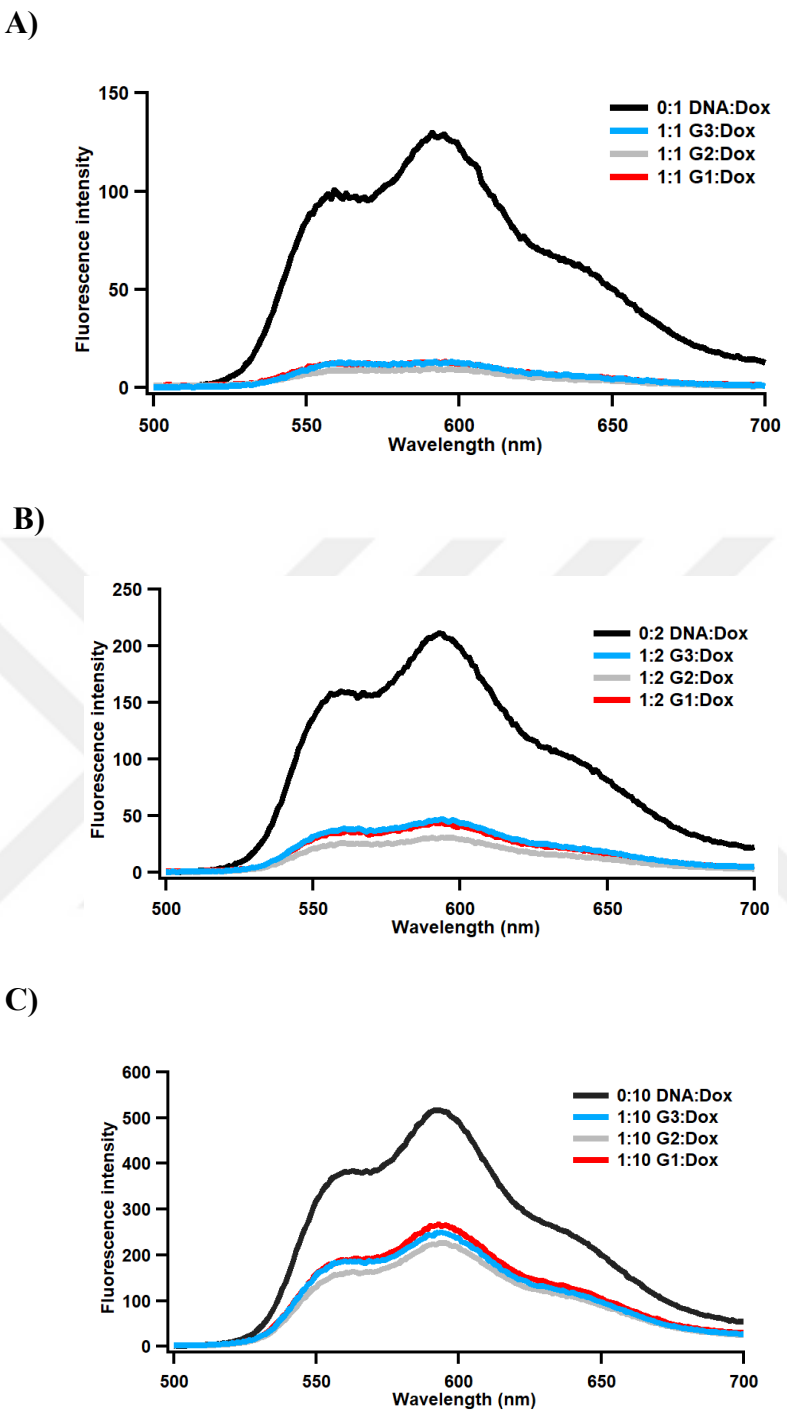


Figure 34. Changes in fluorescence intensity of A) 3.0 µM (1:1) B) 6.0 µM (1:2) C) 30 µM (1:10) free Dox (black line) upon binding to 3.0 µM *PIM1* G-quadruplex structures at pH 5.5.

**A)**

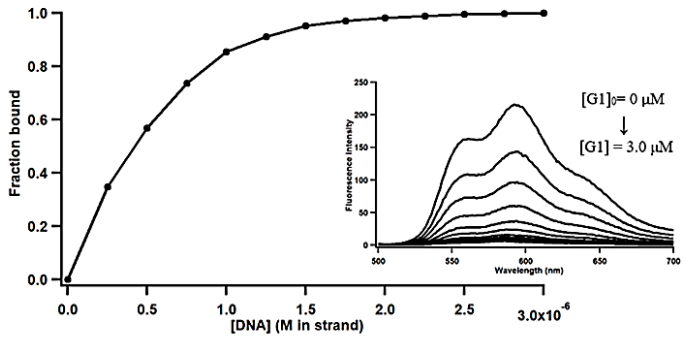


**B)**

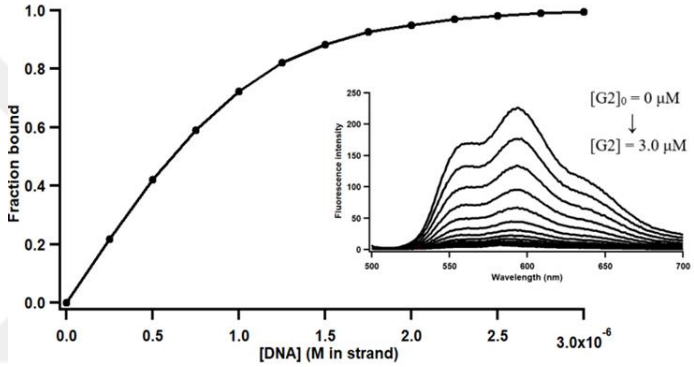


**C)**

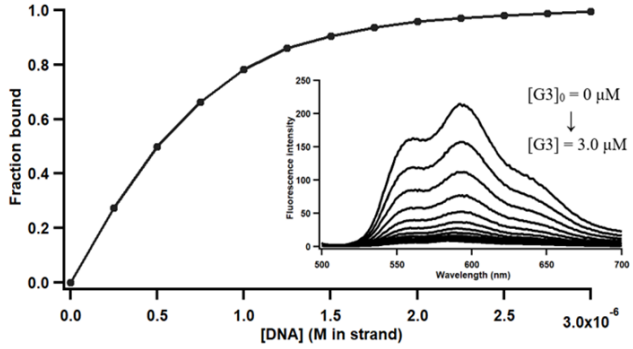


Figure 35. Fluorescence intensity measurements for 1.0 µM solutions of Dox in the presence of increasing concentrations of A) G1 B) G2 C) G3 at pH 7.0 and Fraction bound vs Concentration of DNA (M in strand) obtained from the titration results (1st replicate).

Table 5. Association constants determined by Fluorescence titration experiments of Dox-DNA

| **DNA-Dox** | **1st replicate x-half** | **$K_a$** | **2nd replicate x-half** | **$K_a$** | **$K_a$ Average** |
|---|---|---|---|---|---|
| **G1-Dox** | $4.22\times10^{-7}$ | $2.38\times10^{6}$ | $3.91\times10^{-7}$ | $2.56\times10^{6}$ | $(2.47 \pm 0.12)\times10^{6}$ |
| **G2-Dox** | $6.20\times10^{-7}$ | $1.61\times10^{6}$ | $6.01\times10^{-7}$ | $1.67\times10^{6}$ | $(1.64 \pm 0.04)\times10^{6}$ |
| **G3-Dox** | $5.06\times10^{-7}$ | $1.98\times10^{6}$ | $5.06\times10^{-7}$ | $1.98\times10^{6}$ | $(1.98 \pm 0.00)\times10^{6}$ |

## 3.8 Examining the Interactions Between i-motif Structures of *PIM1* and Doxorubicin

### 3.8.1 Characterization of Dox Binding to i-motif Structures via CD Spectroscopy

In addition to G-quadruplex structures, i-motifs also play a role in the transcription control of several cancer-related genes. Therefore, investigating compounds that bind to i-motifs is also crucial for cancer diagnosis and therapeutics [133]. Furthermore, considering a study conducted by Abdelhamid et al. [94] which revealed interactions of G-quadruplex ligands with i-motif structures, it is essential to examine both the G-quadruplex and the i-motif when reporting on a molecule that appears to bind specifically to a given DNA secondary structure which may have stabilizing or destabilizing effect on i-motifs.

Accordingly, after confirming the interactions between Dox and G4 structures of *PIM1* gene, the interactions between Dox and i-motif structures in the complementary strands were also investigated. Initially Circular Dichroism analyses were conducted to study structural changes upon Doxorubicin binding to *PIM1* i-motif structures. In Figure 36 and 37, dashed lines indicate the spectra of the only i-

motif structures, and the colored lines represent the 3.0, 6.0 and 30 μM Dox or Dox with 3.0 μM DNA at pH 7.0 and pH 5.5. As discussed previously, a high maximum around 285 nm and a negative peak at 265 nm are taken as the indication of the formation of an i-motif structure [16].

As in Figure 36 and Figure 37, the sample containing 30 μM Dox (solid black line) displayed a very broad positive band around 350 nm, a negative band around 290 nm, and another positive band at 234 nm with a shoulder at 250 nm in the CD spectra. The relative intensity of the bands, especially at 234 nm and 250 nm differed from each other based on the pH of the environment. The band at 234 nm was sharper and more intense at pH 7.0. Our findings align with those of Airoldi et al. [127] where 23 μM Dox exhibited a broad positive band around 350 nm, another positive peak at around 230 nm with a shoulder at 250 nm, and a minimum at 289 nm. When the i-motif structures and Dox were together, moderate shifts in the position of positive and negative peaks especially at pH 7.0 to lower wavelengths was observed, which can be taken as the evidence for the presence of interactions between i-motif structures and Dox. If there was no interaction between DNAs and Dox, one should expect a spectrum that is equal to the mathematical sum of for instance 1:0 DNA:Dox and 0:10 DNA:Dox spectra for 1:10 DNA:Dox solutions at 290 nm. The lack of additiveness of the spectra clearly demonstrates the interactions between the i-motif structures and the Dox. On the other hand, no major structural transition is observed for 1:1 and 1:2 and 1:10 solutions at both pHs, meaning that the main i-motif structure was mainly preserved even in the presence of Dox. Moreover, the appearance of a minimum at 310 nm may be ascribed to the formation of the Dox-DNA complex [127]. This minimum is evidently detectable for all samples of I1, as well as for the 1:2 and 1:10 samples of I2 and I3 at pH 7.0. The intensity of that peak seemed to be increasing with increasing Dox in pH 7.0 samples. However, at pH 5.5, it is only detectable for the 1:10 samples of I2 and I3. As observed for G-quadruplexes, the disappearance of the broad positive band at 350 nm suggests that a different type of chirality is probably induced in Dox structure upon its interaction with C-rich strands of *PIM1* gene with an exception for I2 and I3 at pH 5.5.

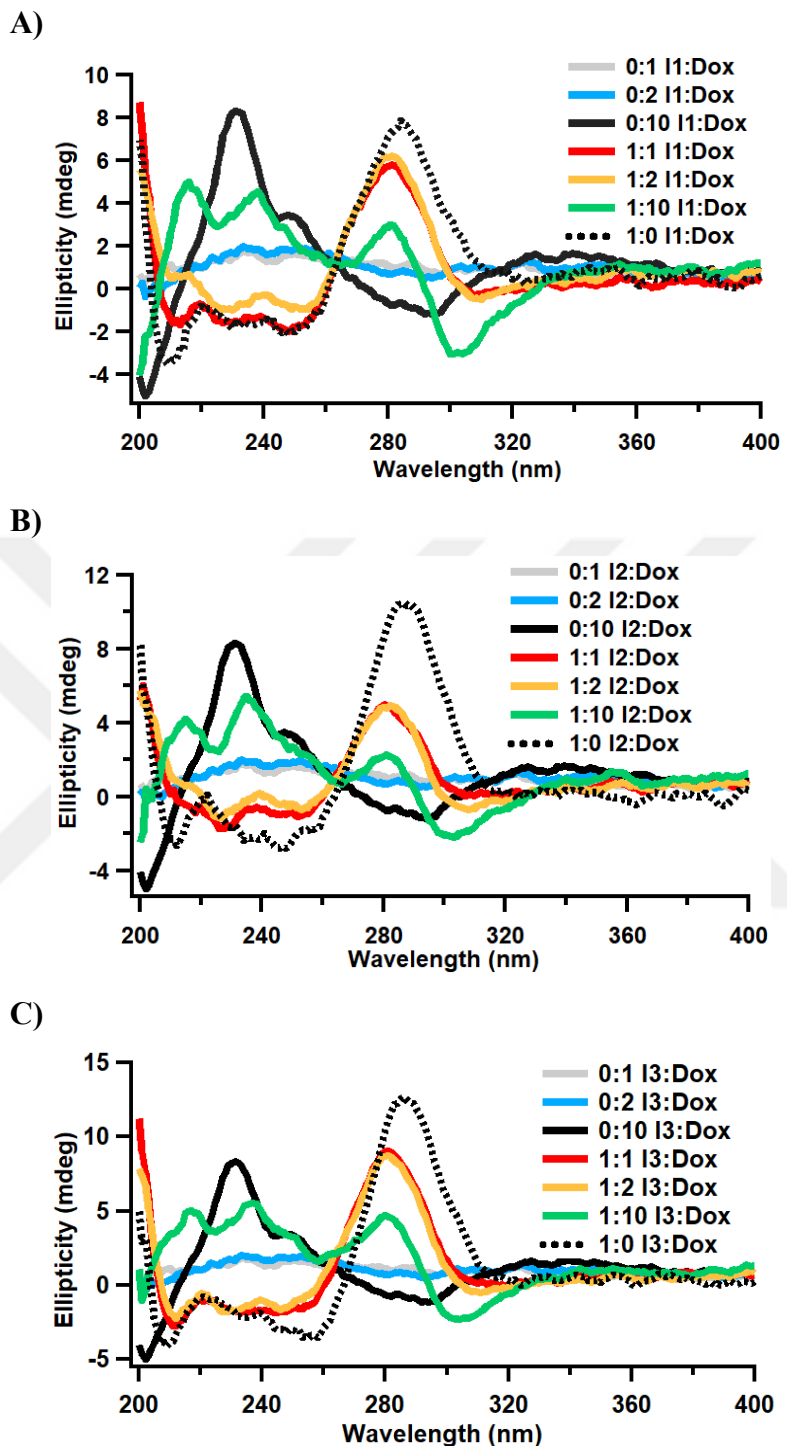


Figure 36. Comparison of the CD spectra of 3.0 µM of A) I1 B) I2 C) I3, in the absence and presence of 3.0, 6.0 and 30 µM Dox with the 3.0, 6.0 and 30 µM Dox spectra at pH 7.0.

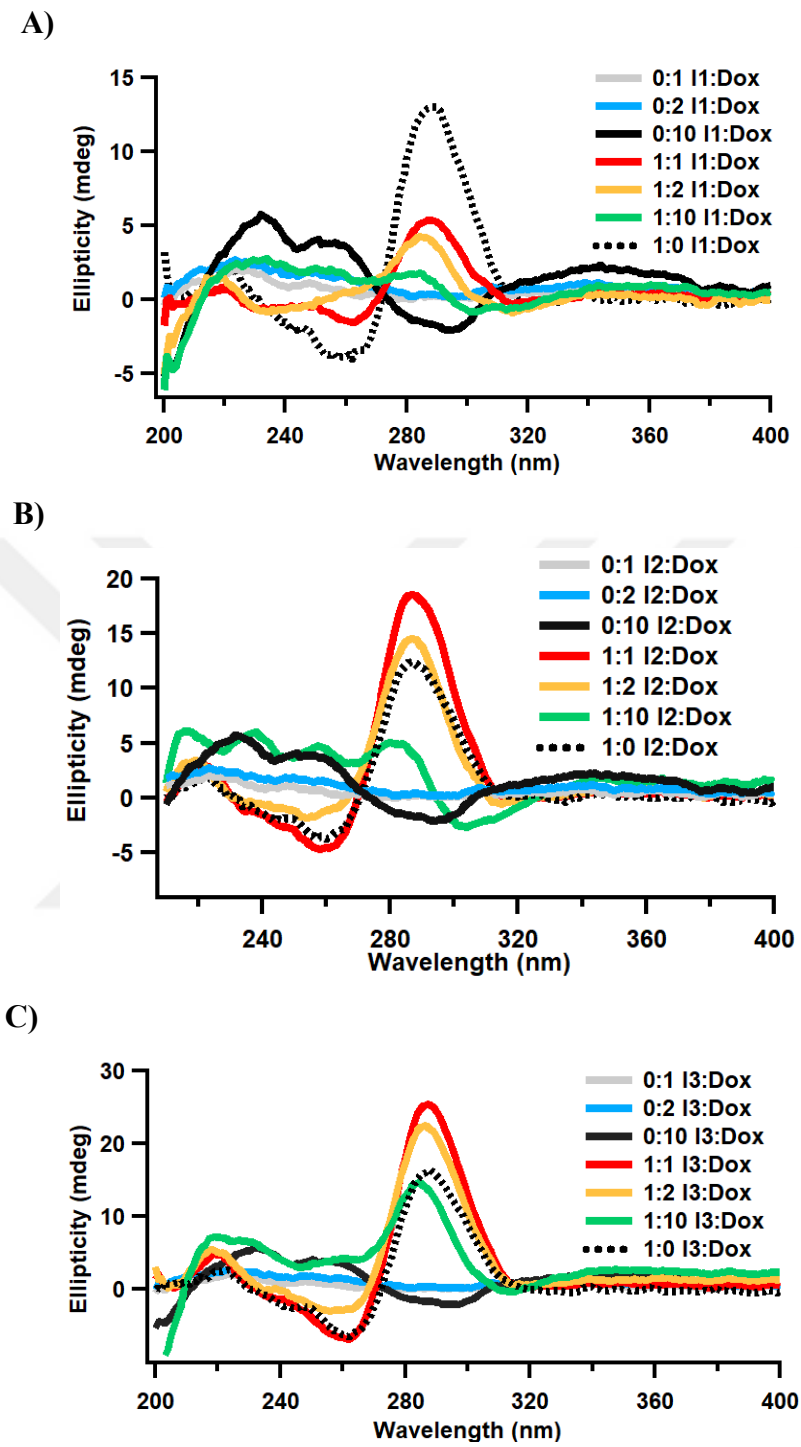


Figure 37. Comparison of the CD spectra of 3.0 µM of A) I1 B) I2 C) I3, in the absence and presence of 3.0, 6.0 and 30 µM Dox with the 3.0, 6.0 and 30 µM Dox spectra at pH 5.5.

### 3.8.2 Characterization of Dox Binding to i-motif Structures via UV–Vis Absorption Spectroscopy

To verify the binding between Dox and the i-motif structures in C-rich strands of *PIM1* gene at pH 7.0 and 5.5, further investigations were conducted using UV–Vis spectroscopy at relatively high Dox concentrations. Comparing the UV–Vis absorption spectra of 3.0 μM samples in the absence and presence of Dox (DNA:Dox 1:10) with free Dox spectrum at pH 7.0 and 5.5 (Figure 38 and 39), confirms the binding of Dox to the i-motif structures both at pH 7.0 and 5.5. A significant hypochromic effect was observed in the absorption maxima of Dox at 480 nm upon its binding to all I4 structures similar to its binding to G4 structures of *PIM1* gene. Again, a red shift was not observed upon binding of Dox to i-motif structures, but the notable hypochromic effect can be taken as an indication of the interaction between the Dox and DNA in all the samples investigated at both pH 7.0 and 5.5.

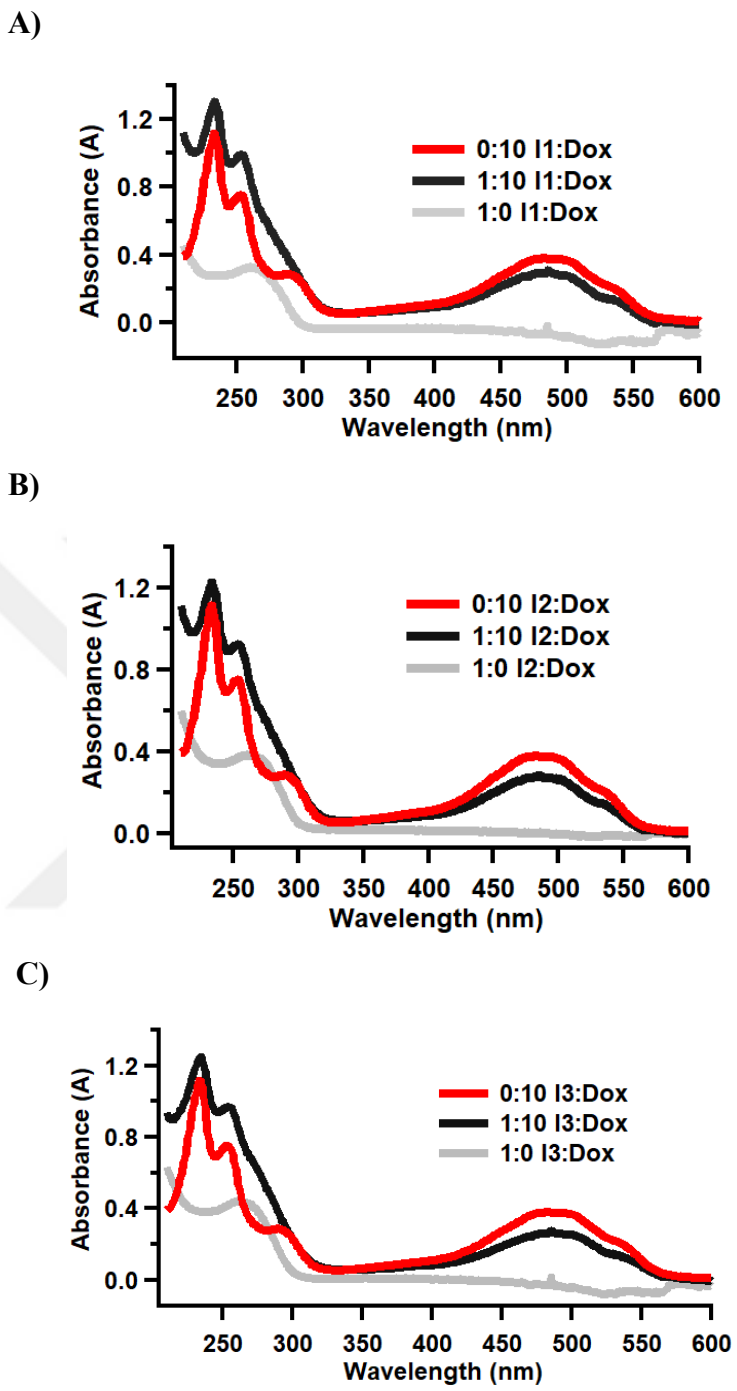


Figure 38. UV–Vis absorption spectra of 3.0 µM A) I1 B) I2 C) I3 in the absence and presence of 30 µM Dox at pH 7.0 in K-phosphate buffer. Red lines represent Dox alone, grey lines show oligonucleotide alone and blank lines denote the interaction between Dox and DNA.

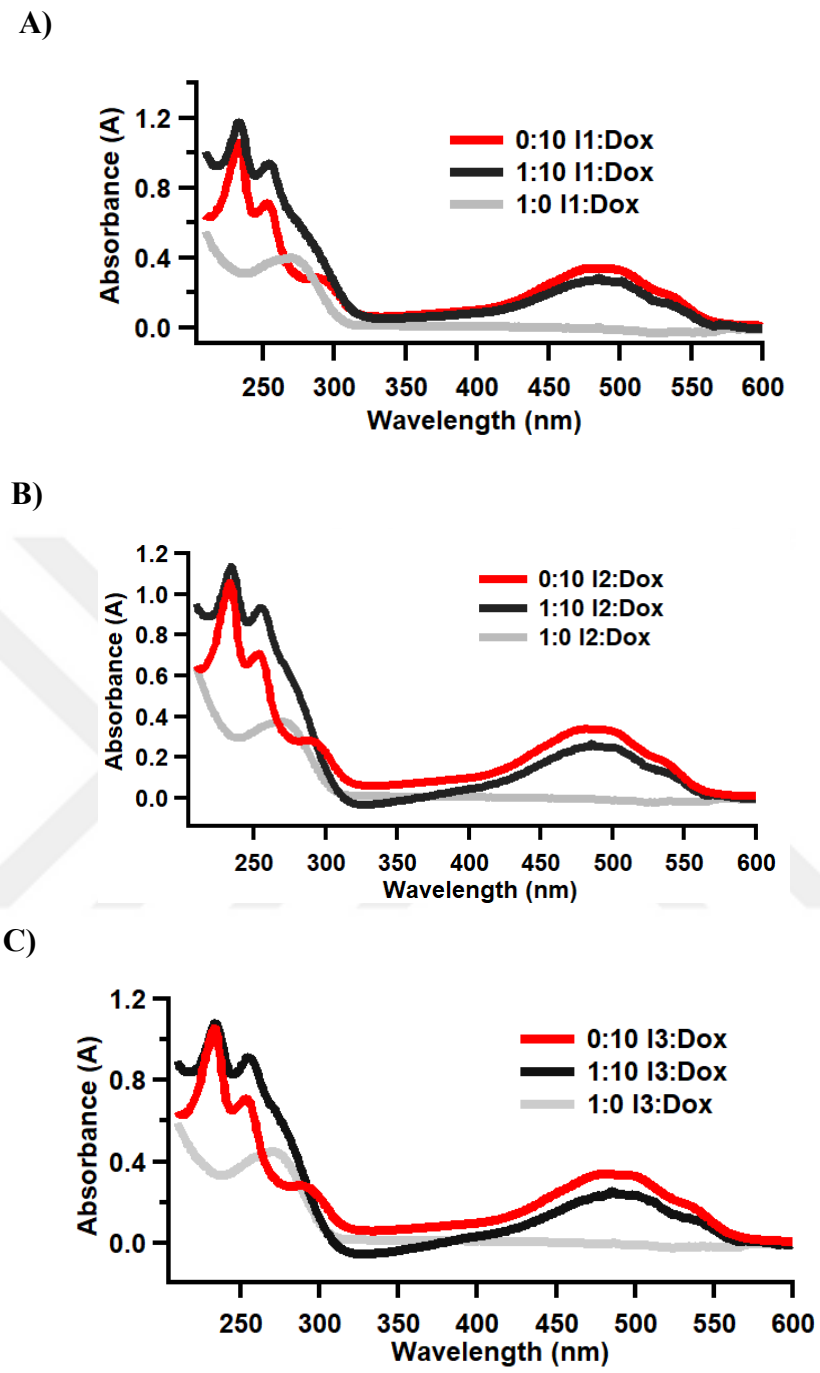


Figure 39. UV–Vis absorption spectra of 3.0 μM A) I1 B) I2 C) I3 in the absence and presence of 30 μM Dox at pH 5.5 in K-phosphate buffer. Red lines represent Dox alone, grey lines show oligonucleotide alone and blank lines denote the interaction between Dox and DNA.

### 3.8.3 Characterization of Dox Binding and the Stability of the i-motif-Dox Complexes via Thermal Denaturation Experiments

As mentioned above, an increase in Tm value means the stabilizing effect of the small molecule on the nucleic acid structure. For instance, in an study conducted by Wang et al, phenanthroline derivatives were found to stabilize the human telomeric i-motif structure, resulting in a 10.1 ºC increase in Tm values for 1:10 solution of DNA:Compound [134]. As we performed for G-quadruplex structures, thermal denaturation profiles of also i-motif samples containing 1:0, 1:1, 1:2, 1:10 and 0:10 equimolar ratios of DNA (3.0 μM):Dox were obtained via UV-Vis absorption spectroscopy between 15ºC and 95ºC by monitoring the absorbance value at 265 nm with respect to temperature. The increase in temperature from 15ºC to 95ºC resulted in unfolding of the i-motif structures. The corresponding UV-Vis absorption spectra for the thermal denaturation experiments were given in Appendix C, Figures 65-79.

In Figures 40-45, lines with markers represent DNA-Dox samples while solid lines represent the only DNA samples. Figures 40-42 represent 1:1, 1:2 and 1:10 DNA:Dox samples respectively at pH 7.0. while Figures 43-45 denote thermal denaturation profiles of 1:1, 1:2 and 1:10 DNA:Dox samples respectively at pH 5.5. The thermal denaturation profiles obtained clearly display the higher stability of the i-motif structures in the presence of Dox as a result of Dox binding to i-motif structures at both pH 7.0 and 5.5. The stabilization ability of Dox is relatively identical for i-motif structures, with a 10, 8 and 10 ºC increase in Tm values for DNA:Dox 1:1 solutions of I1, I2 and I3 respectively at pH 7.0 (Table 6). The increment in Tm values for 1:2 and 1:10 solutions are higher than 1:1 solutions as expected (Table 6). At pH 5.5, the changes in Tm values are significantly less compared to pH 7.0. This observation may be attributed to their inherent higher stability of the i-motif structures at acidic pH levels, such that not much additional stability arises in the presence of Dox. There is also no change in the Tm values for 1:1 solutions of I2 and I3 at this acidic pH. However, the increase in Tm values of all the i-motif structures in 1:2 and 1:10 samples was observed. Yet, the transition

was a bit broad compared to the samples without Dox. According to an investigation conducted by Xu et al. [91] the absence of an increase in Tm values of i-motif DNA upon Dox addition at acidic pH indicates a lack of interaction between them. However, we believe in here the increase in Tm values at pH 5.5 especially for 1:2 and 1:10 DNA:Dox solutions and the change in the thermal denaturation profile in terms of the broadness of the profiles suggests the interaction of Dox with *PIM1* gene i-motif structures under these conditions.

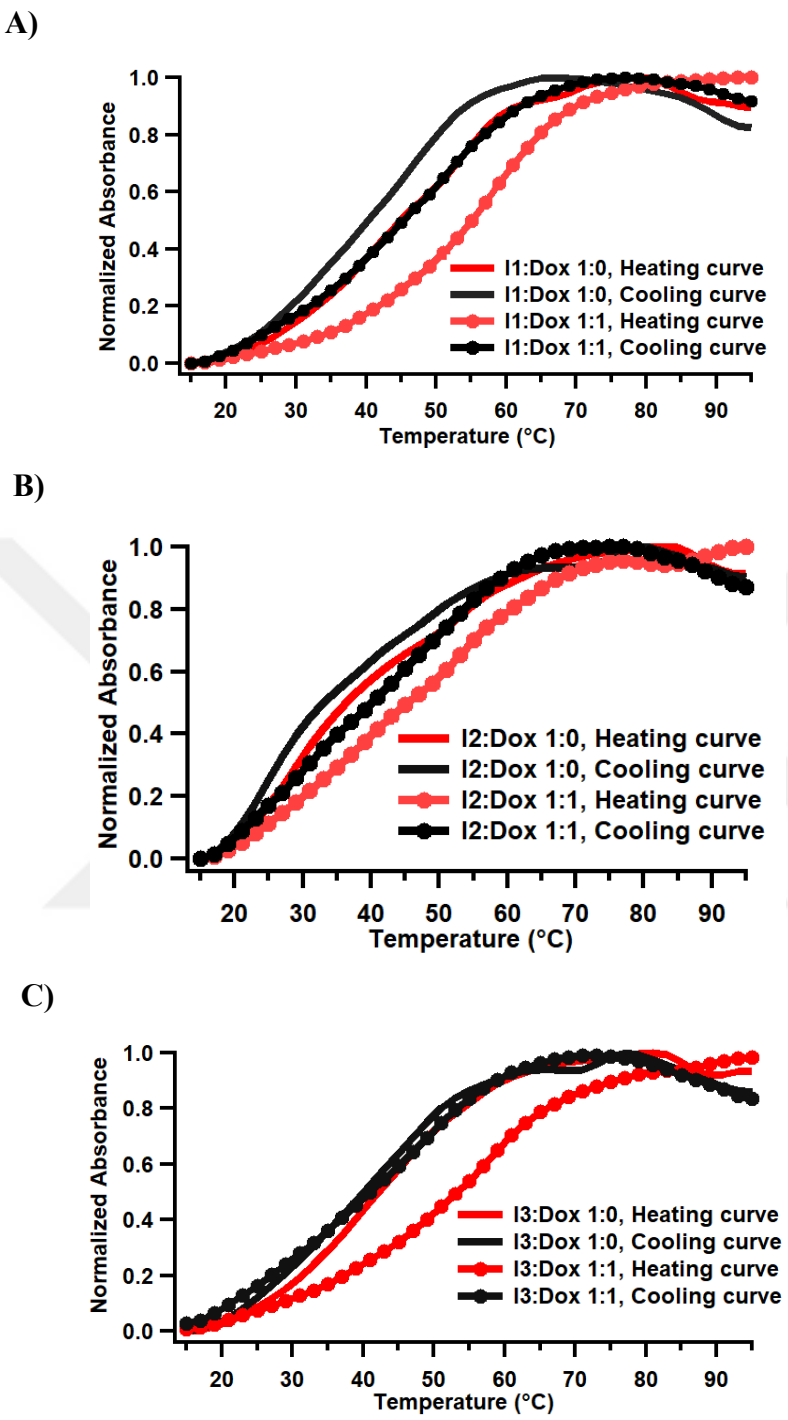


Figure 40. Comparison of the UV-Vis thermal melting profiles of 3.0 µM A) I1 B) I2 C) I3 in K-phosphate buffer at pH 7.0 in the absence and presence of 3.0 µM Dox by monitoring absorbance at 265 nm.

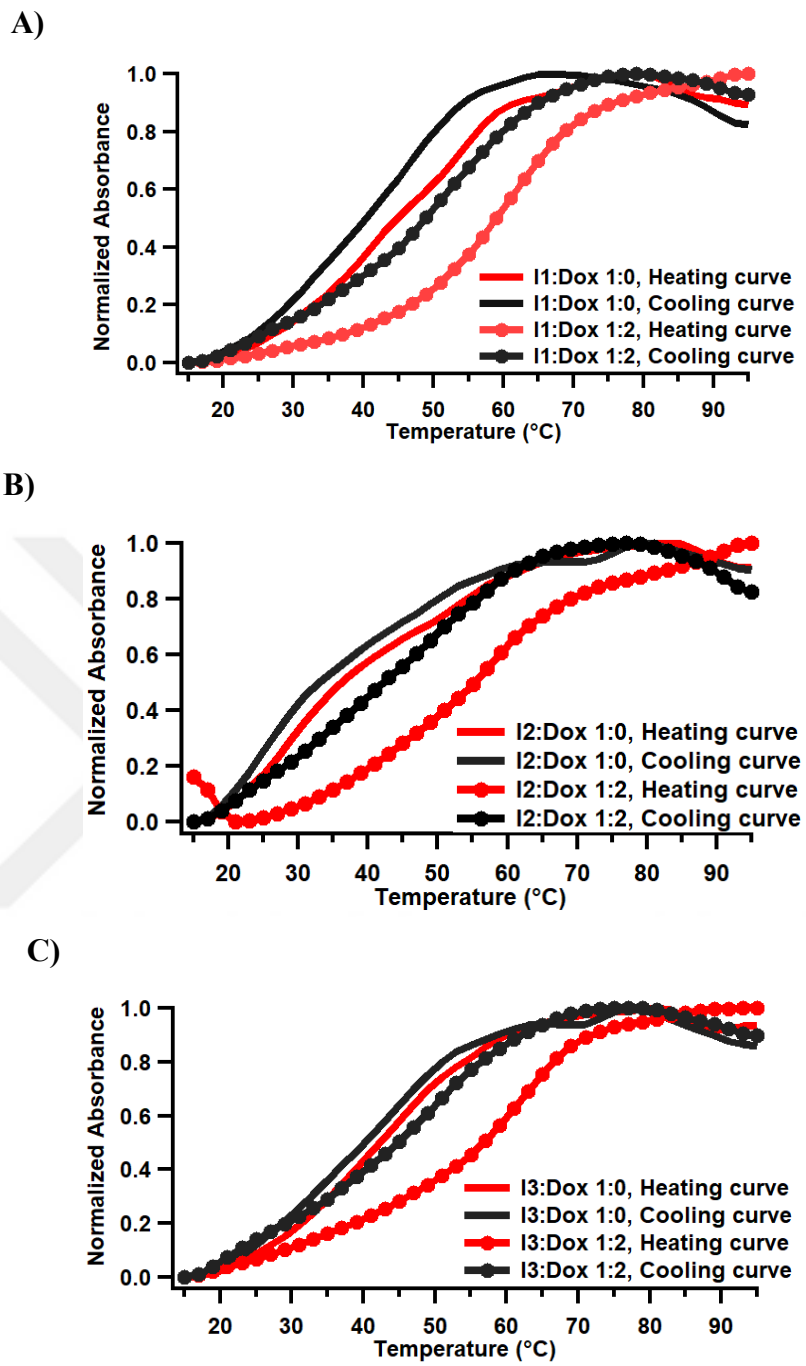


Figure 41. Comparison of the UV-Vis thermal melting profiles of 3.0 µM A) I1 B) I2 C) I3 in K-phosphate buffer at pH 7.0 in the absence and presence of 6.0 µM Dox by monitoring absorbance at 265 nm.

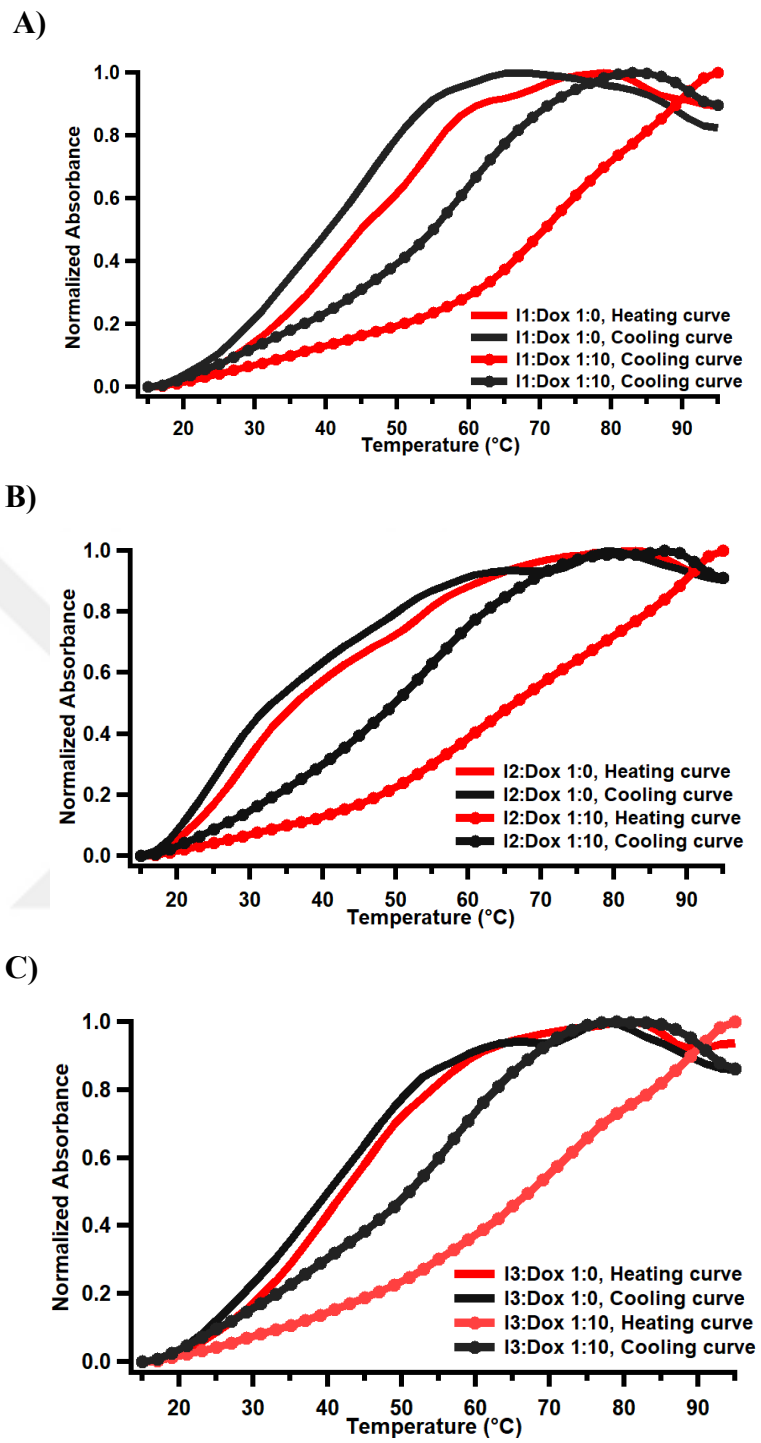


Figure 42. Comparison of the UV-Vis thermal melting profiles of 3.0 µM A) 11 B) I2 C) I3 in K-phosphate buffer at pH 7.0 in the absence and presence of 30 µM Dox by monitoring absorbance at 265 nm.

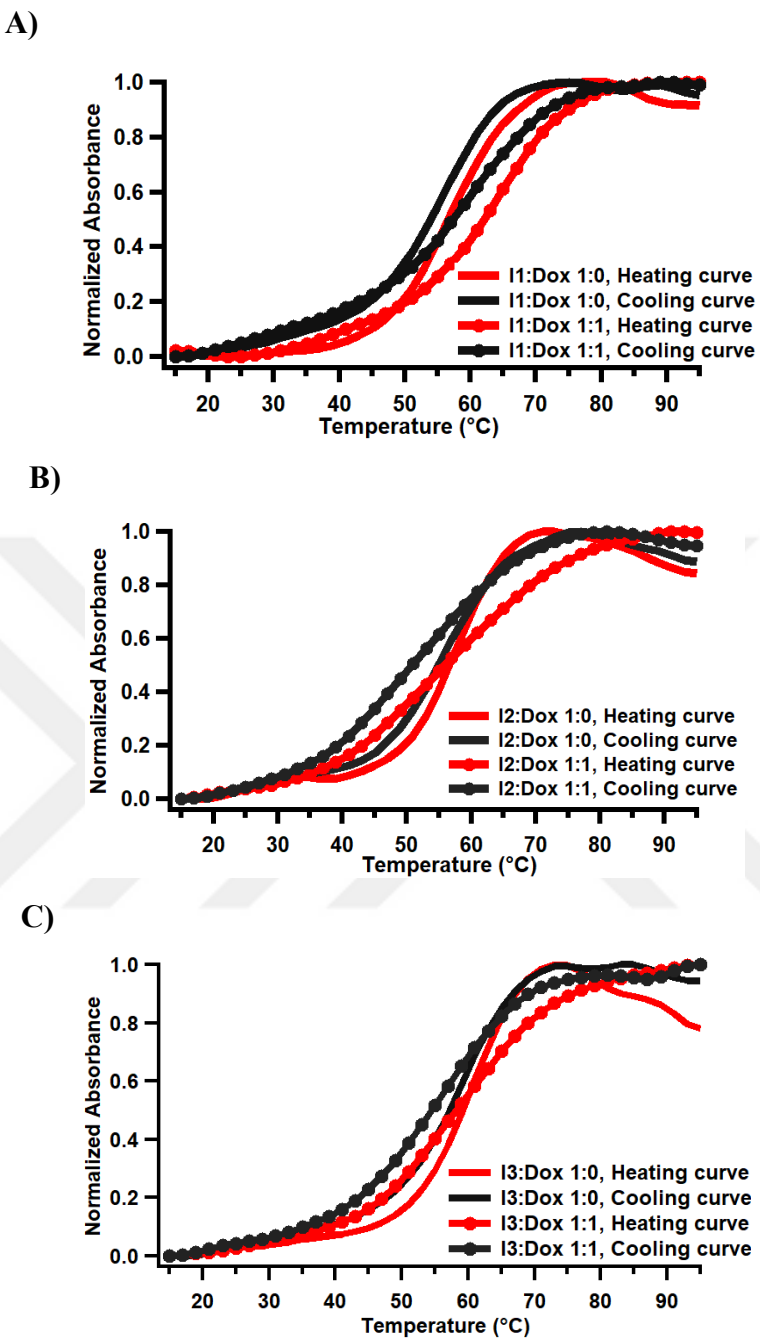


Figure 43. Comparison of the UV-Vis thermal melting profiles of 3.0 µM A) I1 B) I2 C) I3 in K-phosphate buffer at pH 5.5 in the absence and presence of 3.0 µM Dox by monitoring absorbance at 265 nm.

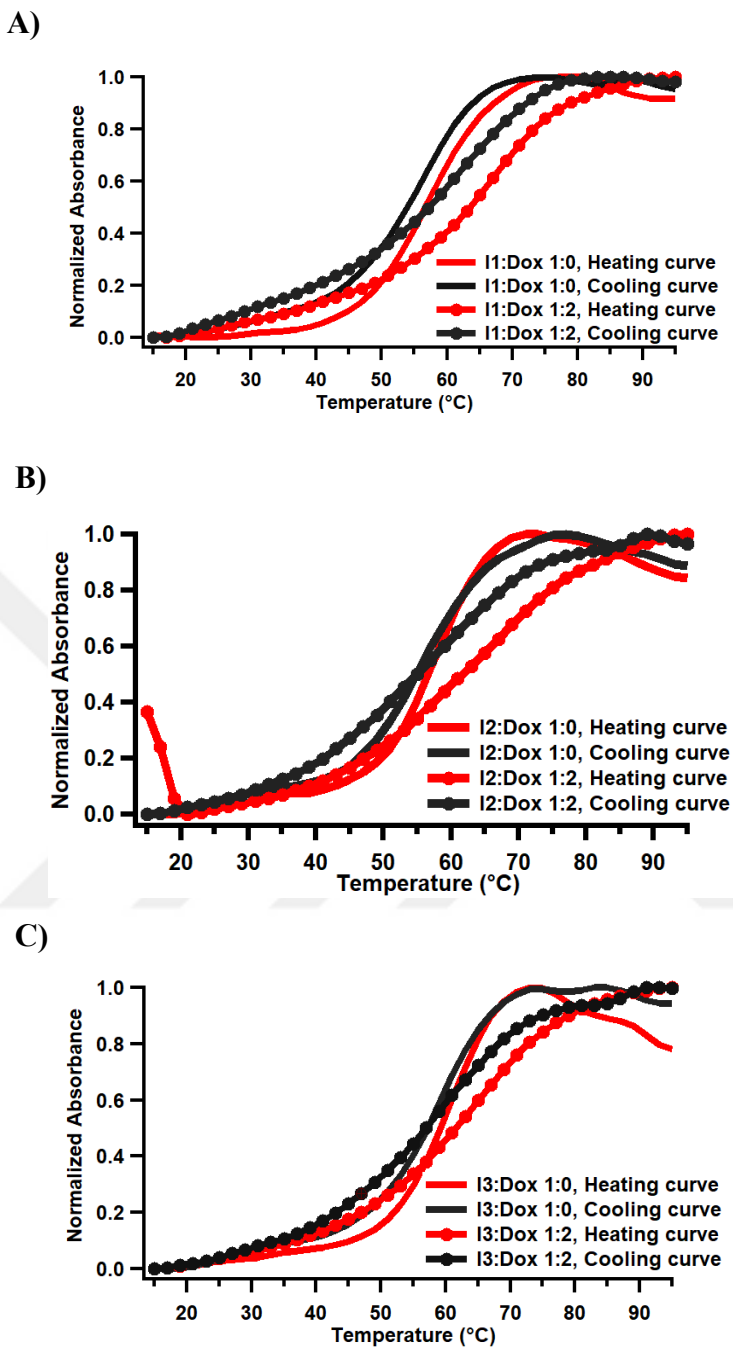


Figure 44. Comparison of the UV-Vis thermal melting profiles of 3.0 µM A) I1 B) I2 C) I3 in K-phosphate buffer at pH 5.5 in the absence and presence of 6.0 µM Dox by monitoring absorbance at 265 nm.

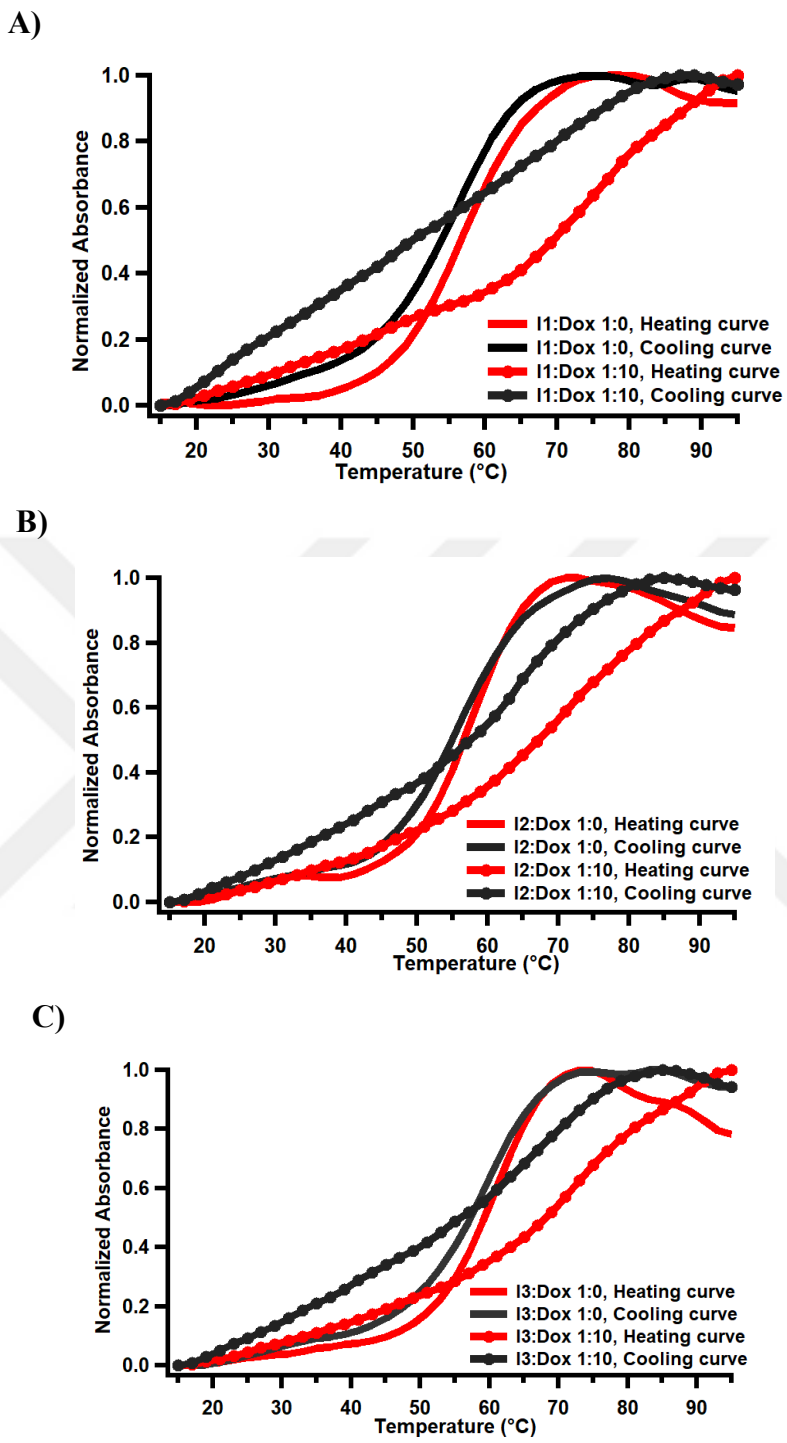


Figure 45. Comparison of the UV-Vis thermal melting profiles of 3.0 µM A) I1 B) I2 C) I3 in K-phosphate buffer at pH 5.5 in the absence and presence of 30 µM Dox by monitoring absorbance at 265 nm.

Table 6. Comparison of the Tm values of 3.0 μM DNA solutions in the absence and presence of 3.0, 6.0 and 30 μM of Dox at pH 7.0 and pH 5.5 in K-phosphate buffer.

| **DNA:Dox** | **Tm** | |
|---|---|---|
| | **pH= 7.0** | **pH= 5.5** |
| **I1: Dox 1:0** | 45 ºC | 57 ºC |
| **I1: Dox 1:1** | 55 ºC | 62 ºC |
| **I1: Dox 1:2** | 59 ºC | 63 ºC |
| **I1: Dox 1:10** | 71 ºC | 70 ºC |
| **I2: Dox 1:0** | 37 ºC | 57 ºC |
| **I2: Dox 1:1** | 45 ºC | 57 ºC |
| **I2: Dox 1:2** | 55 ºC | 62 ºC |
| **I2: Dox 1:10** | 67 ºC | 67 ºC |
| **I3: Dox 1:0** | 43 ºC | 59 ºC |
| **I3: Dox 1:1** | 53 ºC | 59 ºC |
| **I3: Dox 1:2** | 57 ºC | 62 ºC |
| **I3: Dox 1:10** | 67 ºC | 69 ºC |

### 3.8.4 Characterization of Dox Binding to i-motif Structures via Fluorescence Spectroscopy

Dox fluorescence quenching upon DNA binding is an essential technique to characterize Dox binding [127]. Figures 46 and 47 clearly show the decrease in fluorescence intensity of free Dox (black line) in the presence of all i-motif structures of *PIM1* at both pHs, thus validating the binding of Dox to those structures. To the best of our knowledge, this is the first time that fluorescence quenching experiments along with CD and UV analyses have demonstrated the Dox binding to i-motif structures. As discussed in 1.5.2, several studies have documented the release of Dox from the hairpin structure due to the formation of i-motifs at acidic pH levels [91], [92], [93]. Xu et al. believe that a reduction in fluorescence intensity at neutral pH which increases again when pH changes from 7.0 to 5.0, proves the release of Dox following i-motif formation at acidic pH [91]. However, this trend is not observed in our investigation. At pH 7.0, the most significant changes in fluorescence intensity upon Dox addition are observed in I2 sequence (grey line) for both 1:1 and 1:2

solutions, while I3 (blue line) shows the smallest change. However, I2 and I1 exhibit similar changes in fluorescence intensity for 1:10 solutions. Figure 46 illustrates the changes in fluorescence intensity of I1, I2 and I3 (red, grey, and blue lines respectively) in comparison to free Dox (black line) at pH 5.5. All sequences exhibit almost the same changes in fluorescence intensity, with I1 showing the smallest change.

By taking advantage of decrease in fluorescence intensity, the association constants ($K_a$) of Dox with C-rich strands of *PIM1* gene were determined via titration.

The obtained $K_a$ values were $(7.07 \pm 0.35)\times10^6$, $(6.89 \pm 0.71)\times10^6$ and $(5.18 \pm 0.00)\times10^6$ for the binding between I1, I2 and I3 with Dox, respectively at pH 7.0 (Table 7). These $K_a$ values are comparable with association constants of *PIM1* G4 structures calculated previously (Table 5) and much higher than association constants reported for flavonoids interaction with *Bcl-2* i-motif structures which are around $10^4$ $M^{-1}$ [135].

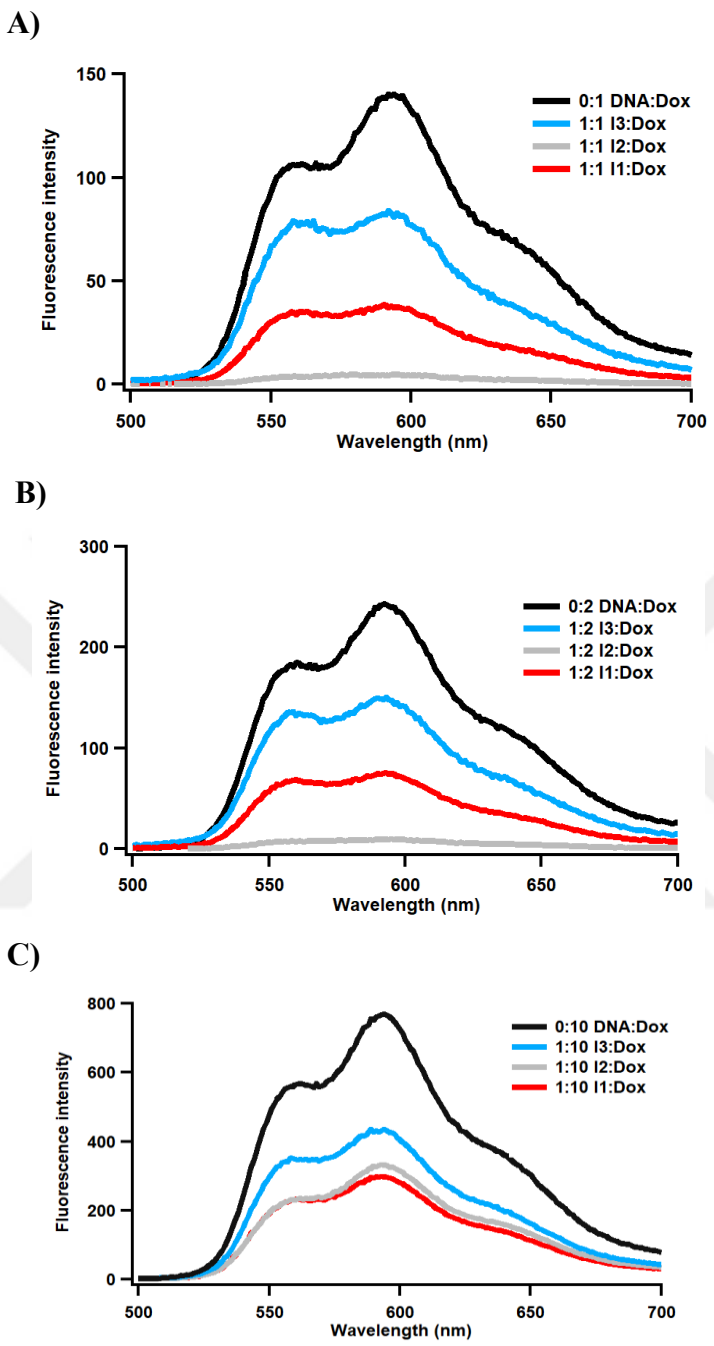


Figure 46. Changes in fluorescence intensity of A) 3.0 µM (1:1) B) 6.0 µM (1:2) C) 30 µM (1:10) free Dox (black line) upon binding to 3.0 µM *PIM1* i-motif structures at pH 7.0.

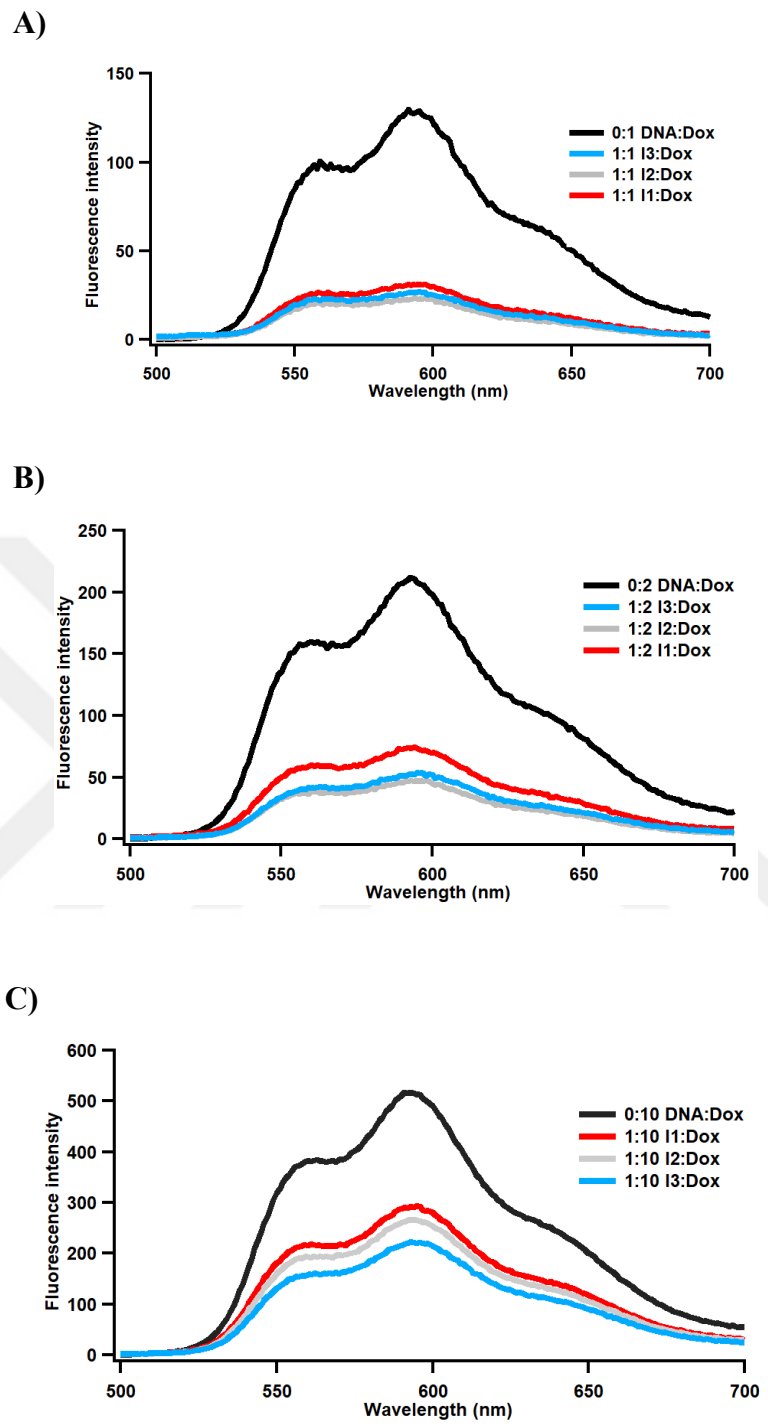


Figure 47. Changes in fluorescence intensity of A) 3.0 µM (1:1) B) 6.0 µM (1:2) C) 30 µM (1:10) free Dox (black line) upon binding to 3.0 µM *PIM1* i-motif structures at pH 5.5.

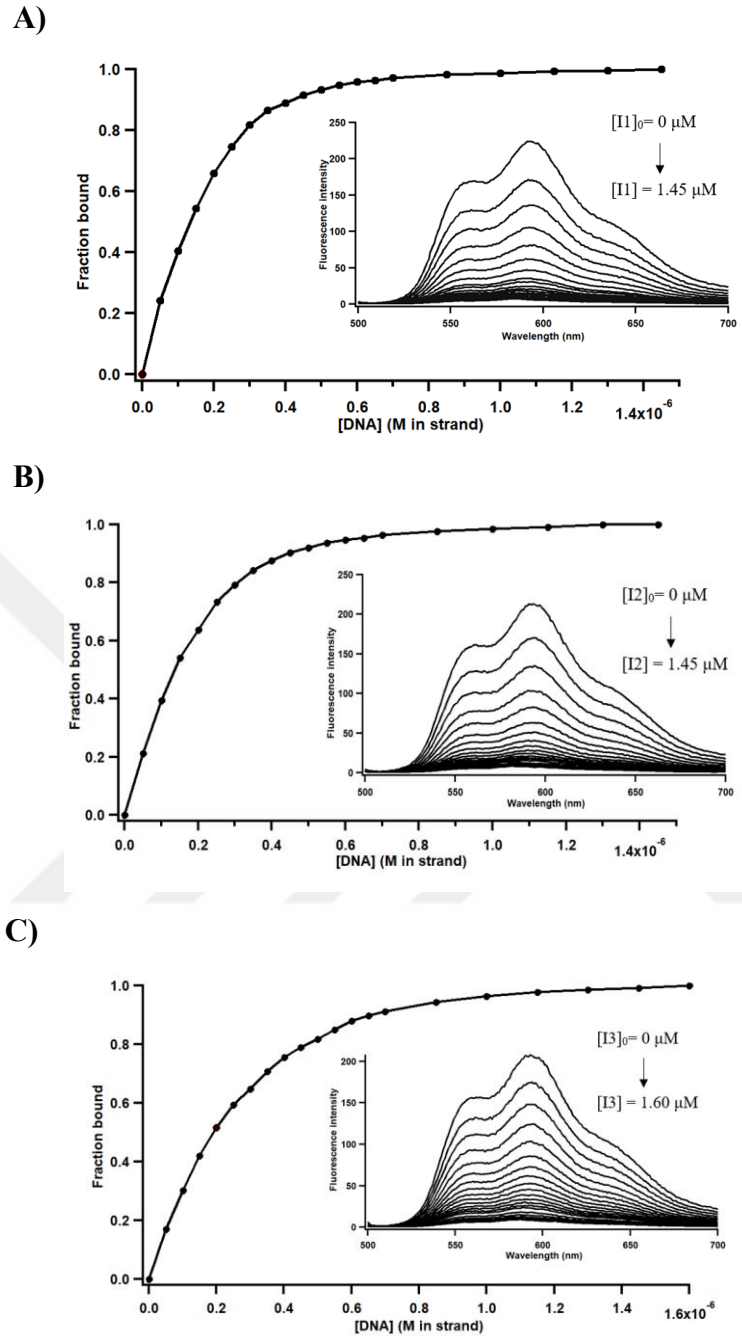


Figure 48. Fluorescence intensity measurements for 1.0 µM solutions of Dox in the presence of increasing concentrations of A) I1 B) I2 C) I3 at pH 7.0 and Fraction bound vs Concentration of DNA (M in strand) obtained from the titration results (1st replicate).

Table 7. Association constants determined by Fluorescence titration experiments of Dox-DNA

| **DNA-Dox** | **1st replicate x-half** | **$K_a$** | **2nd replicate x-half** | **$K_a$** | **$K_a$ Average** |
|---|---|---|---|---|---|
| **I1-Dox** | $1.38\times10^{-7}$ | $7.25\times10^{6}$ | $1.45\times10^{-7}$ | $6.90\times10^{6}$ | $(7.07 \pm 0.35)\times10^{6}$ |
| **I2-Dox** | $1.38\times10^{-7}$ | $7.25\times10^{6}$ | $1.53\times10^{-7}$ | $6.54\times10^{6}$ | $(6.89 \pm 0.71)\times10^{6}$ |
| **I3-Dox** | $1.93\times10^{-7}$ | $5.18\times10^{6}$ | $1.93\times10^{-7}$ | $5.18\times10^{6}$ | $(5.18 \pm 0.00)\times10^{6}$ |

## 3.9 Examining the Interaction Between Duplex Structures of *PIM1* and Doxorubicin

Doxorubicin has been proven to be an effective anti-cancer drug that intercalates to B-form double stranded DNA as discussed previously. It disrupts the function of vital cellular processes such as replication and transcription and ultimately induce apoptosis upon its binding to double helical DNA [83]. In this context, we hypothesized that Dox would exhibit an affinity towards double-stranded *PIM1* DNA structures.

### 3.9.1 Characterization of Dox Binding to Duplex Structures via CD Spectroscopy

In order to demonstrate a comprehensive study on Dox's affinity towards *PIM1* gene structures, we performed CD analysis to study structural changes upon Dox binding to *PIM1* duplex structures. In Figures 49 and 50, dashed lines show oligonucleotides alone and the colored lines represent the 3.0, 6.0 and 30 μM Dox or Dox with 3.0 μM DNA at pH 7.0 and pH 5.5.

As discussed in 3.5.1 section B-form DNA exposes characteristic positive peaks between 250 and 280 nm and two negative peaks at 210 and 240 nm in its CD spectrum [109]. Previously we have concluded the formation of the B-form DNA structure for D1, D2 and D3 along with i-motif or G-quadruplex structures at pH 7.0. We have also demonstrated the presence of those other secondary structures at pH 5.5 along with the duplex.

As mentioned before, the sample containing only 30 μM Dox (solid black line) displayed broad positive bands around 350 nm, a negative band around 290 nm, and another positive band at 234 nm with a shoulder at 250 nm in the CD spectra.

Binding of Dox to D1, D2 and D3 leads to alterations in the intensity of peaks at both pH levels (Figures 49 and 50). For D1, D2 and D3 at pH 7.0 (Figure 49) there is an increase in positive peak at around 260-290 nm and decrease in the negative peaks at around 240 nm and 210 nm for 1:1 and 1:2 solutions which reflect the interactions between the double stranded DNA and Dox [75]. Moreover, 1:10 sample of D1 displays an increase at 280 nm while the peaks around 260 nm and 290 nm are removed in Figure 49 A, B, green lines display elimination of shoulder at around 290 nm and enhancement of peak around 270 nm. In a previous study, Agudelo investigated the Dox binding to calf-thymus DNA at varying concentrations of Dox. He observed major shifting of the bands at 211 to 214 and 246 to 240 nm accompanied by an increase in intensity and the split of the band at 280 to 270 and 258 nm in the spectra of Dox–DNA complexes at high Dox concentration (0.5 M) [75]. They concluded that the spectral shifts observed were due to a partial B to A-DNA transition and the major intensity changes observed were due to the base destacking as Dox intercalation occurs [75]. Our results align almost perfectly with Agudelo's findings. At pH 5.5, D1, D2 and D3 display an increase in positive peak between 260 nm and 290 nm and decrease in negative peak for 1:2 and 1:10 samples (Figure 50). There is a blue shift in the positive peak for all 1:10 samples at pH 5.5 which indicates prevalence of B-DNA at high Dox concentrations.

Additionally, in an investigation by Akhter and Rajeswary [136], the decrease in the intensity of CD negative band at 242 nm and increase in the ellipticity at 270 nm along with an induced negative peak at 305 nm for B-form DNA duplex structure of *hmga1* gene prove binding of Dox to this structure. The changes in the intensity around 270 nm is believed to reflect alterations in the winding angle in a double helical DNA structure indicating unwinding induced by the intercalation of drugs [136], [137]. Consistent with their results, we observed the formation of a negative peak around 305 nm in all samples at pH 7.0 and in the 1:10 samples at pH 5.5. Furthermore, the reduction in the intensity of the negative peak around 245 nm in all samples at pH 7.0, as well as in the 1:2 and 1:10 samples at pH 5.5, reflects the binding of Dox to these structures. There is also an increase in the intensity of positive peak between 270-280 nm of all samples at both pHs.

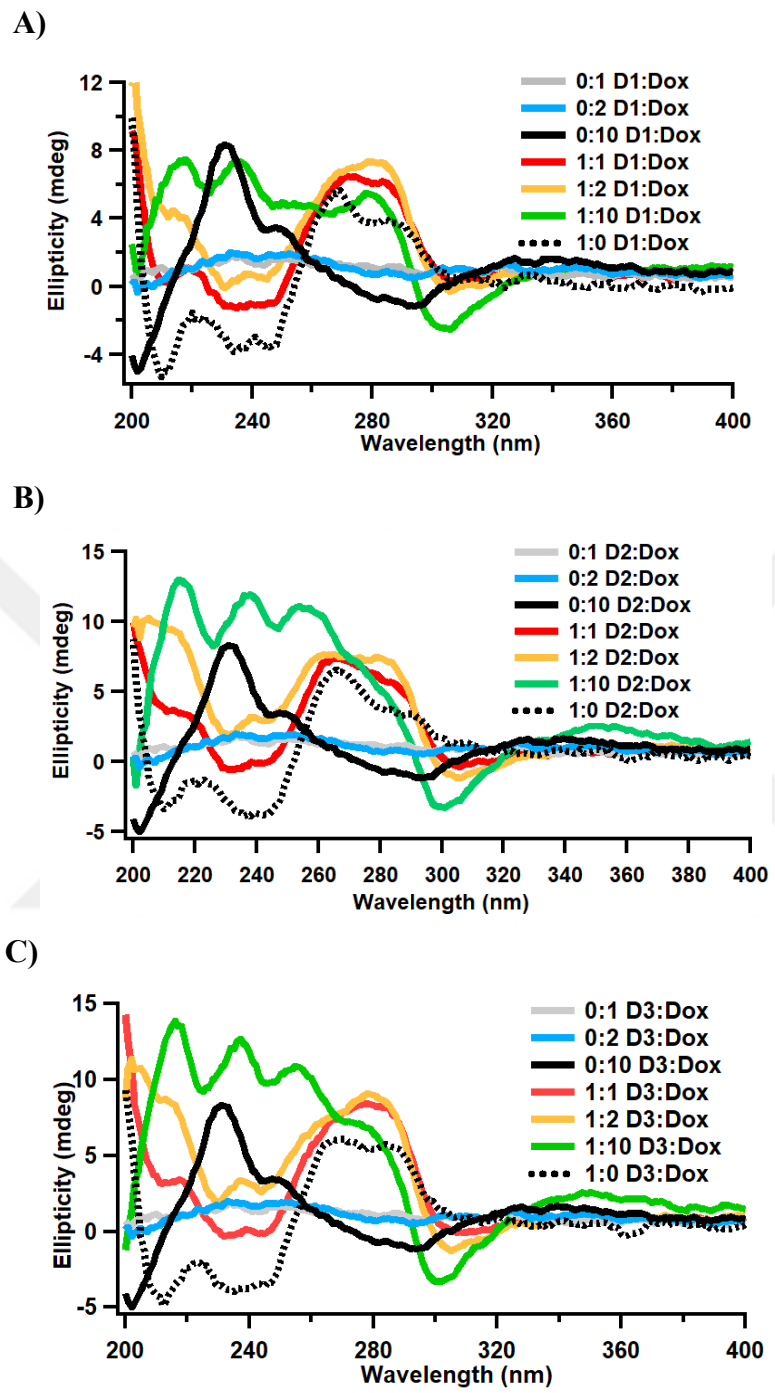


Figure 49. Comparison of the CD spectra of 3.0 µM of A) D1 B) D2 C) D3, in the absence and presence of 3.0, 6.0 and 30 µM Dox with the 3.0, 6.0 and 30 µM Dox spectra at pH 7.0.

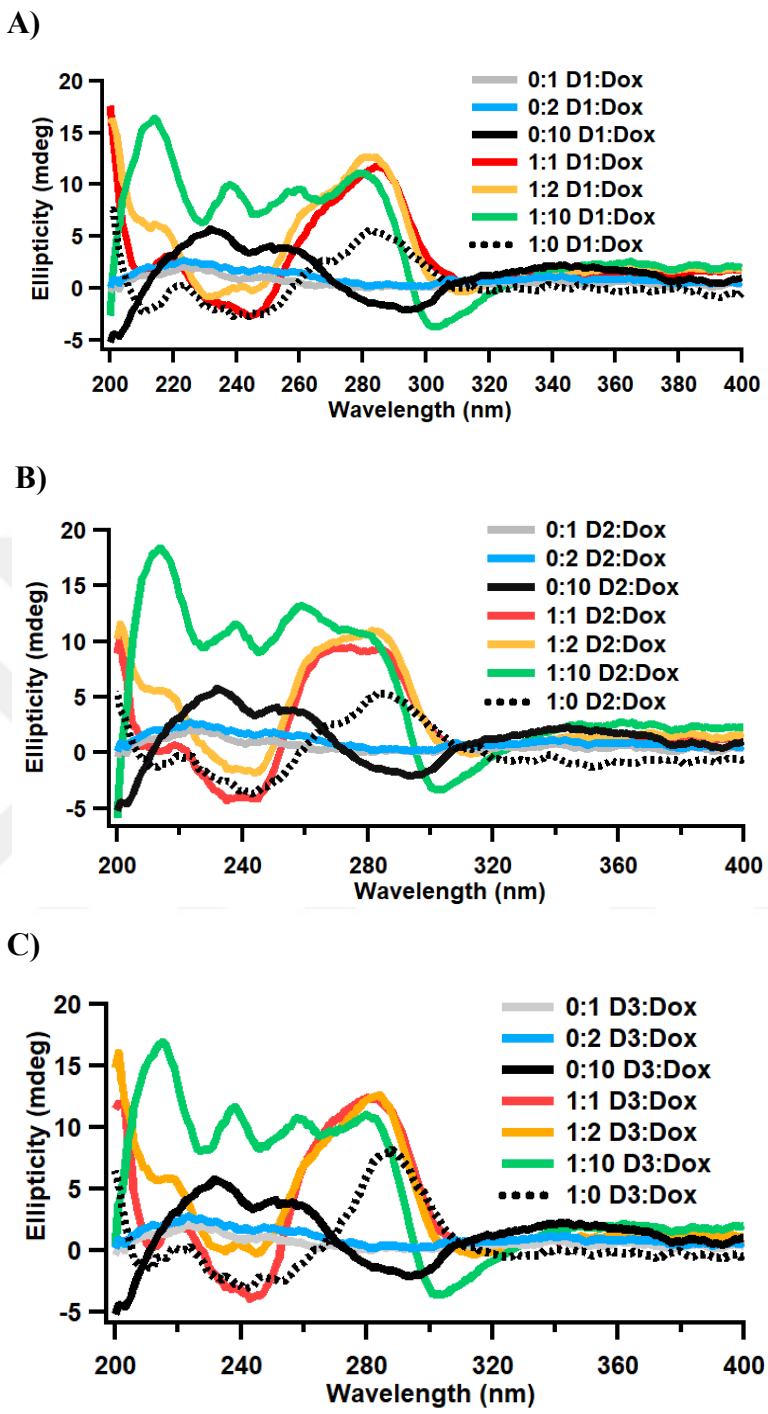


Figure 50. Comparison of the CD spectra of 3.0 µM of A) D1 B) D2 C) D3, in the absence and presence of 3.0, 6.0 and 30 µM Dox with the 3.0, 6.0 and 30 µM Dox spectra at pH 5.5.

### 3.9.2 Characterization of Dox Binding to Duplex Structures via UV–Vis Absorption Spectroscopy

To verify the binding between Dox to the *PIM1* gene duplex structures at pH 7.0 and 5.5, further investigations were conducted using UV–Vis spectroscopy at relatively high Dox concentrations. UV–Vis absorption spectra of 3.0 μM samples in the absence and presence of Dox (DNA:Dox 1:10) with free Dox as given in Figures 51 and 52, confirms the binding of Dox to these duplex structures at pH 7.0 and 5.5, respectively. Dox intercalation leads to a reduction in intensity at 480 nm and induces a red shift in the absorbance region of Dox. The hypochromic effect and the red shift are generally observed due to the stacking of the aromatic moiety of the chromophore in between the DNA base pairs [129]. The hypochromic effect and the red shift were present in the absorption maxima of Dox at 480 nm in the presence of 3.0 μM DNA. There is just an exception for D1 at pH 7.0 which does not show a detectable red shift upon Dox addition while displays a significant decrease in the intensity. This confirms the binding of Dox to all duplex structures of the *PIM1* gene at both pH 7.0 and 5.5.

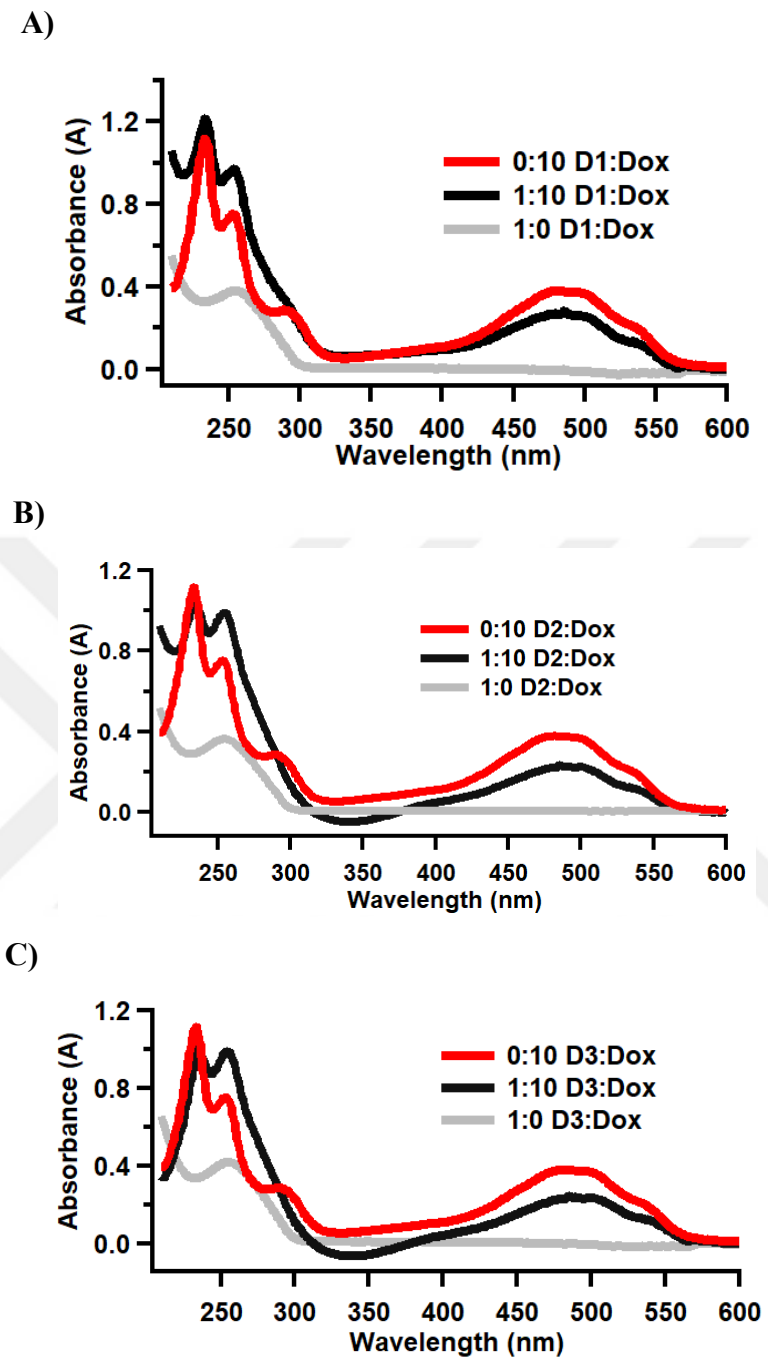


Figure 51. UV–Vis absorption spectra of 3 μM A) D1 B) D2 C) D3 in the absence and presence of 30 μM Dox at pH 7.0 in K-phosphate buffer. Red lines represent Dox alone, grey lines show oligonucleotide alone and blank lines denote the interaction between Dox and DNA.

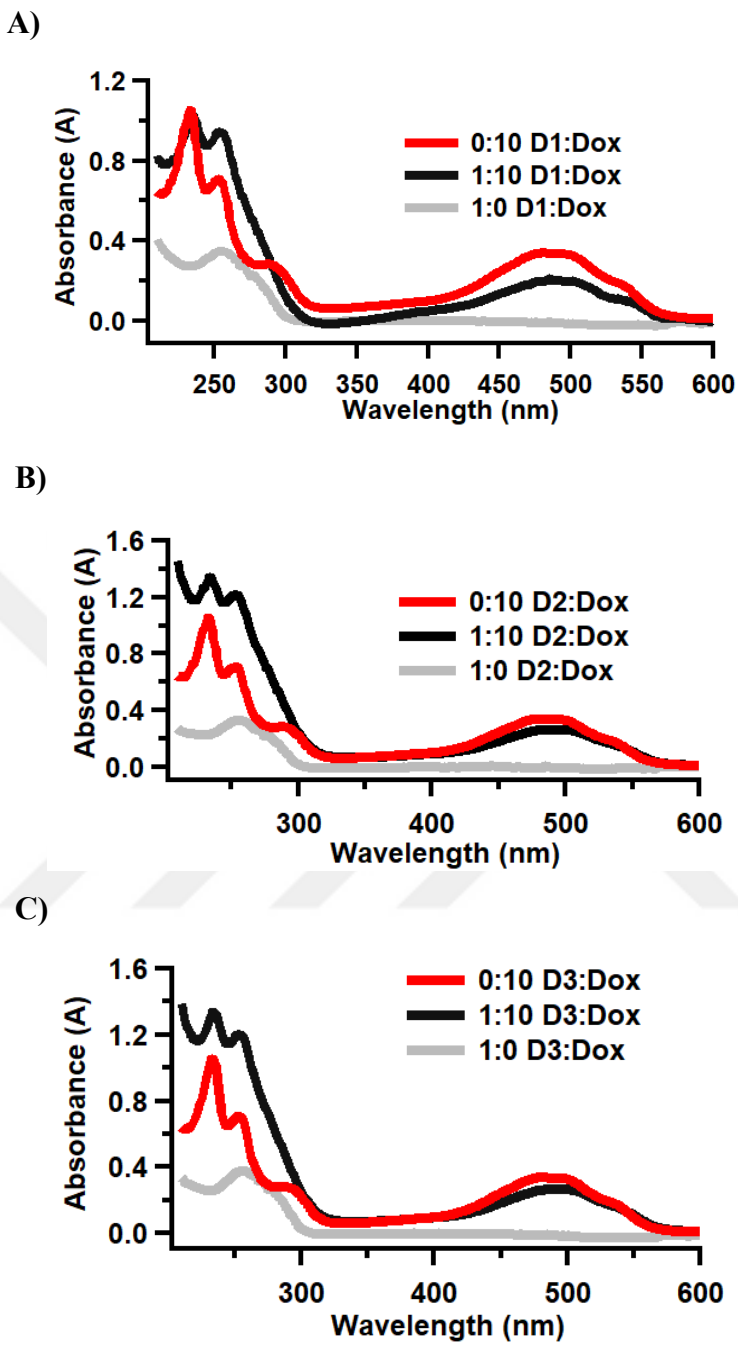


Figure 52. UV–Vis absorption spectra of 3.0 µM A) D1 B) D2 C) D3 in the absence and presence of 30 µM Dox at pH 5.5 in K-phosphate buffer. Red lines represent Dox alone, grey lines show oligonucleotide alone and blank lines denote DNA:Dox samples.

### 3.9.3 Characterization of Dox Binding and the Stability of the DNA-Dox Complexes via Thermal Denaturation Experiments

Thermal denaturation experiments were performed to observe the changes in the stability of nucleic acid structures upon their interactions with Dox [129]. An increase in Tm value means that the small molecule inserts a stabilizing effect on the nucleic acid structure and causes it to unfold at higher temperatures. Similar to the thermal denaturation experiments performed for G-quadruplex and i-motif structures of *PIM1* gene, thermal denaturation temperatures experiments for the samples containing 1:0, 1:1, 1:2, 1:10 and 0:10 equimolar ratios of duplex DNA (3.0 μM):Dox were measured via UV-Vis absorption spectroscopy between 15ºC and 95ºC (the corresponding UV-Vis absorption spectra for the thermal denaturation experiments were given in Appendix C, Figures 65-79). The increase in temperature from 15ºC to 95ºC resulted in unfolding of the duplex DNA structures. Akhter and Rajeswary [136] previously reported +10 °C enhancement in the Tm values of DNA duplex structure of *hmga1* gene when Dox:DNA mole ratio is 0.9, using 10 mM Sodium Cacodylate buffer with 10 mM NaCl, at pH 7.0. Their DNA melting results were in an agreement with UV-spectrophotometric titration, Circular Dichroism and Fluorescence spectroscopy analyses demonstrating a strong complexation between Dox and duplex DNA [136].

Figures 53-58 clearly display higher stability of the D1, D2 and D3 in the presence of Dox as a result of Dox binding to duplex DNA structures at pH 7.0 and 5.5, respectively. The stabilization ability of Dox is identical for all duplex structures, with a 4 ºC and 6 ºC increase in Tm values for DNA:Dox 1:1 and 1:2 solutions, respectively at pH 7.0 (Table 8). The increment in Tm values for 1:10 solutions are higher than 1:1 and 1:2 as we expect. At pH 5.5, the changes in Tm values are slightly higher compared to pH 7.0 (Table 8). There is about 10 ºC, 13 ºC and 12 ºC increment for 1:1 samples of D1, D2 and D3 respectively. 1:2 samples exhibit almost the same stability upon Dox addition with 15 ºC increment for D1 and D2 and a 14 ºC for D3.

1:10 samples at pH 5.5 displayed, the highest changes in Tm values of duplex structures with 19 ºC, 21 ºC, 22 ºC increment for D1, D2 and D3, respectively.

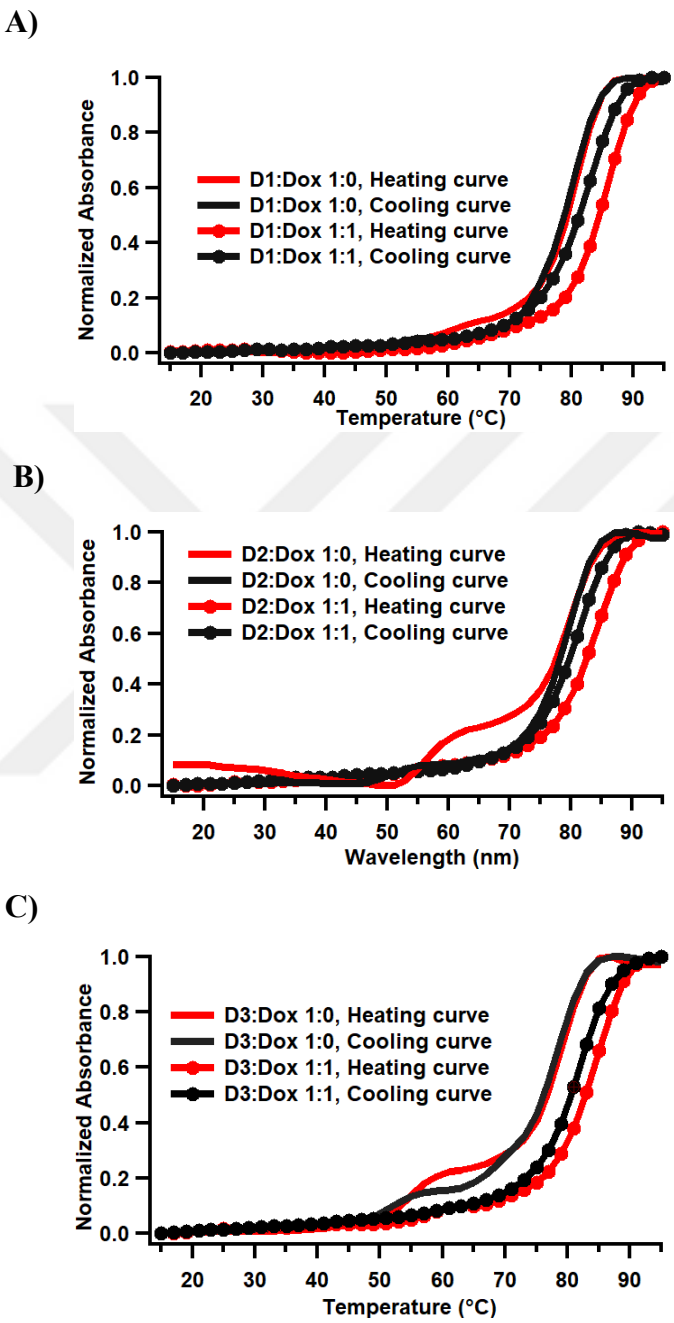


Figure 53. Comparison of the UV-Vis thermal melting profiles of 3.0 µM A) D1 B) D2 C) D3, in K-phosphate buffer at pH 7.0 in the absence and presence of 3.0 µM Dox by monitoring absorbance at 260 nm.

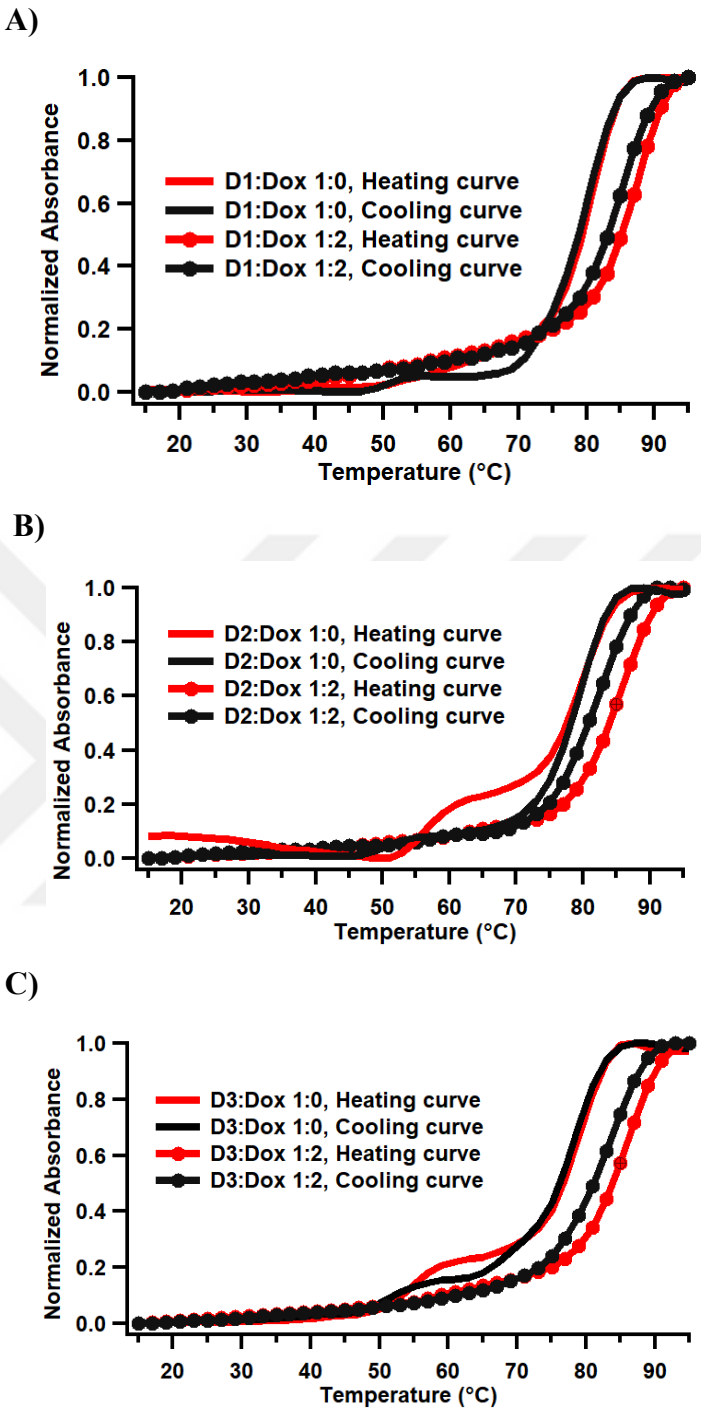


Figure 54. Comparison of the UV-Vis thermal melting profiles of 3.0 µM A) D1 B) D2 C) D3, in K-phosphate buffer at pH 7.0 in the absence and presence of 6.0 µM Dox by monitoring absorbance at 260 nm.

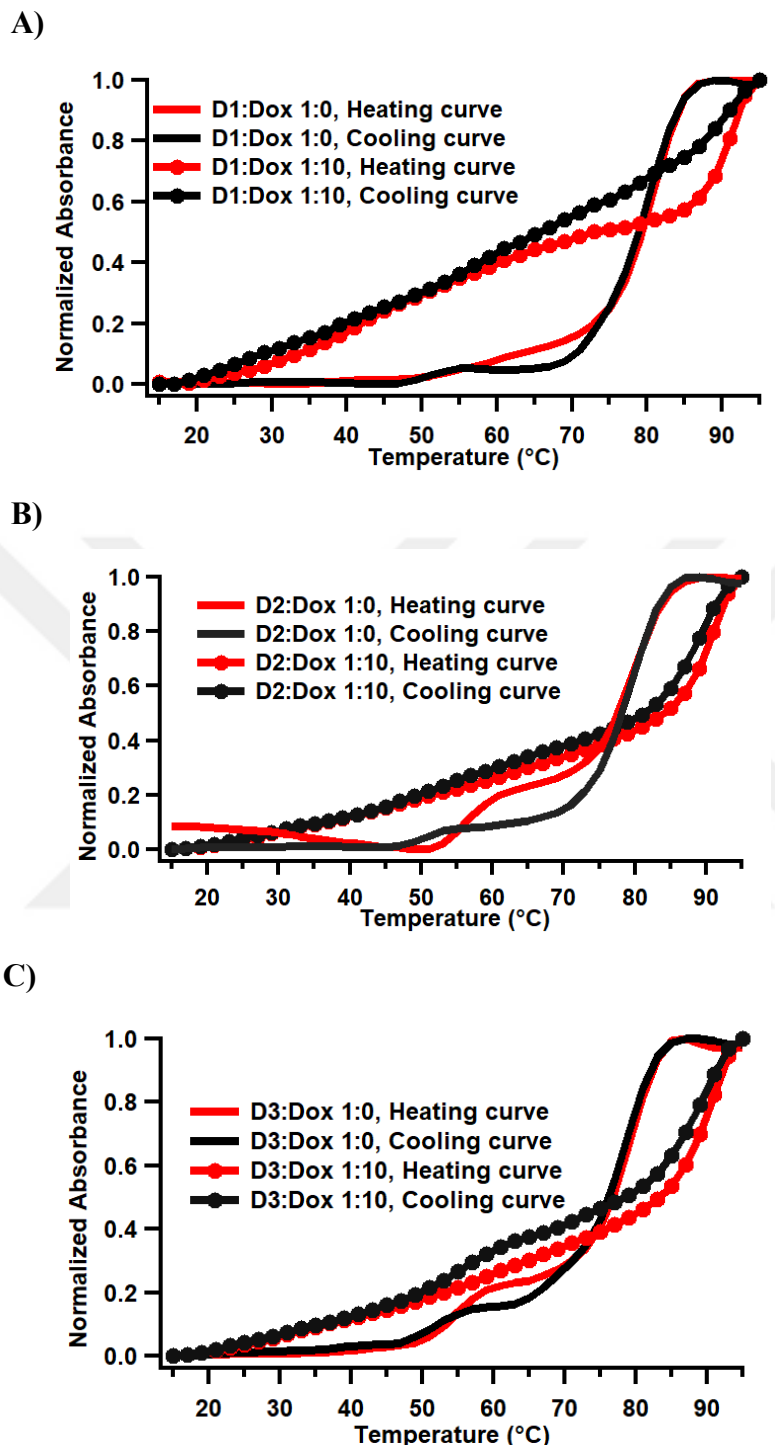


Figure 55. Comparison of the UV-Vis thermal melting profiles of 3.0 µM A) D1 B) D2 C) D3, in K-phosphate buffer at pH 7.0 in the absence and presence of 30 µM Dox by monitoring absorbance at 260 nm.

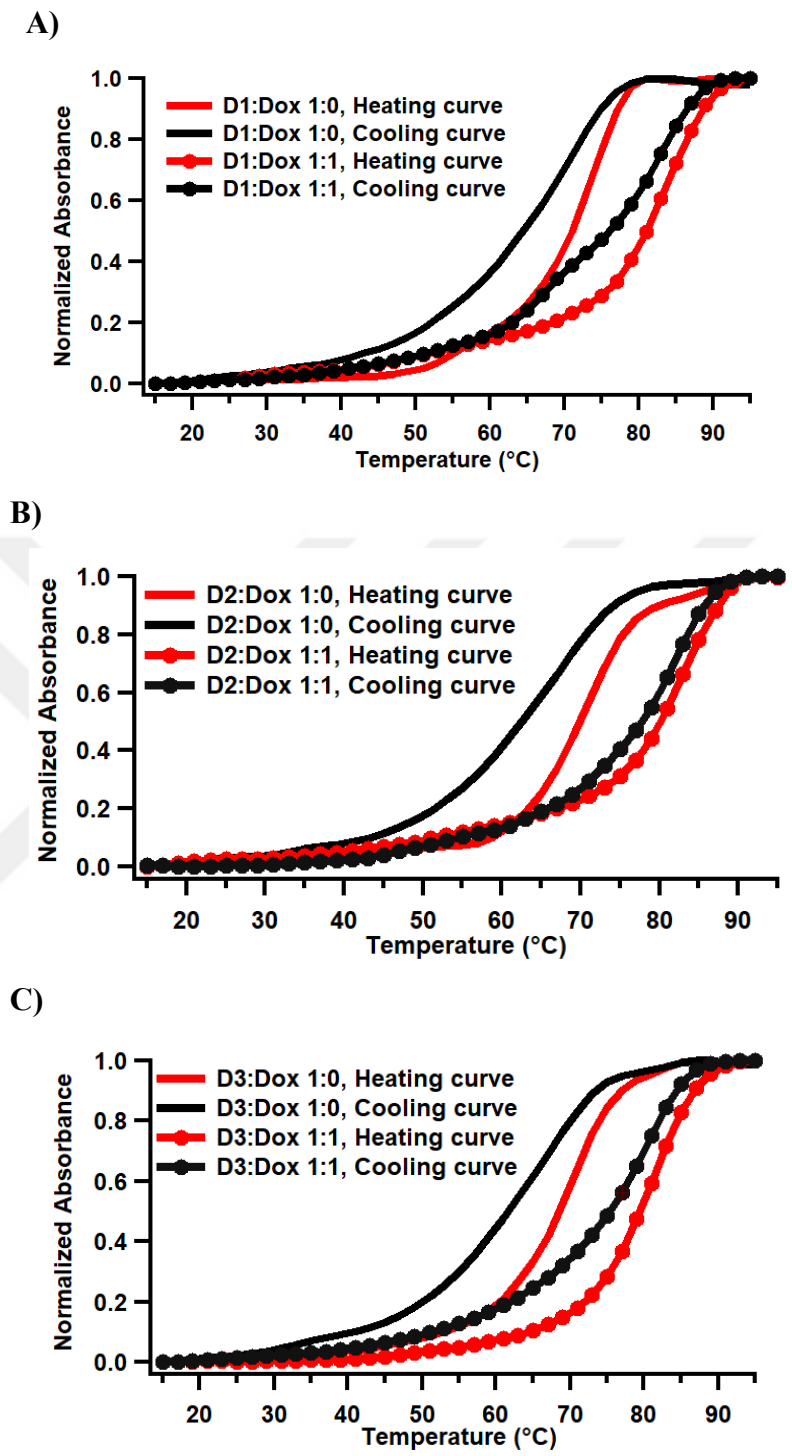


Figure 56. Comparison of the UV-Vis thermal melting profiles of 3.0 µM A) D1 B) D2 C) D3, in K-phosphate buffer at pH 5.5 in the absence and presence of 3.0 µM Dox by monitoring absorbance at 260 nm.

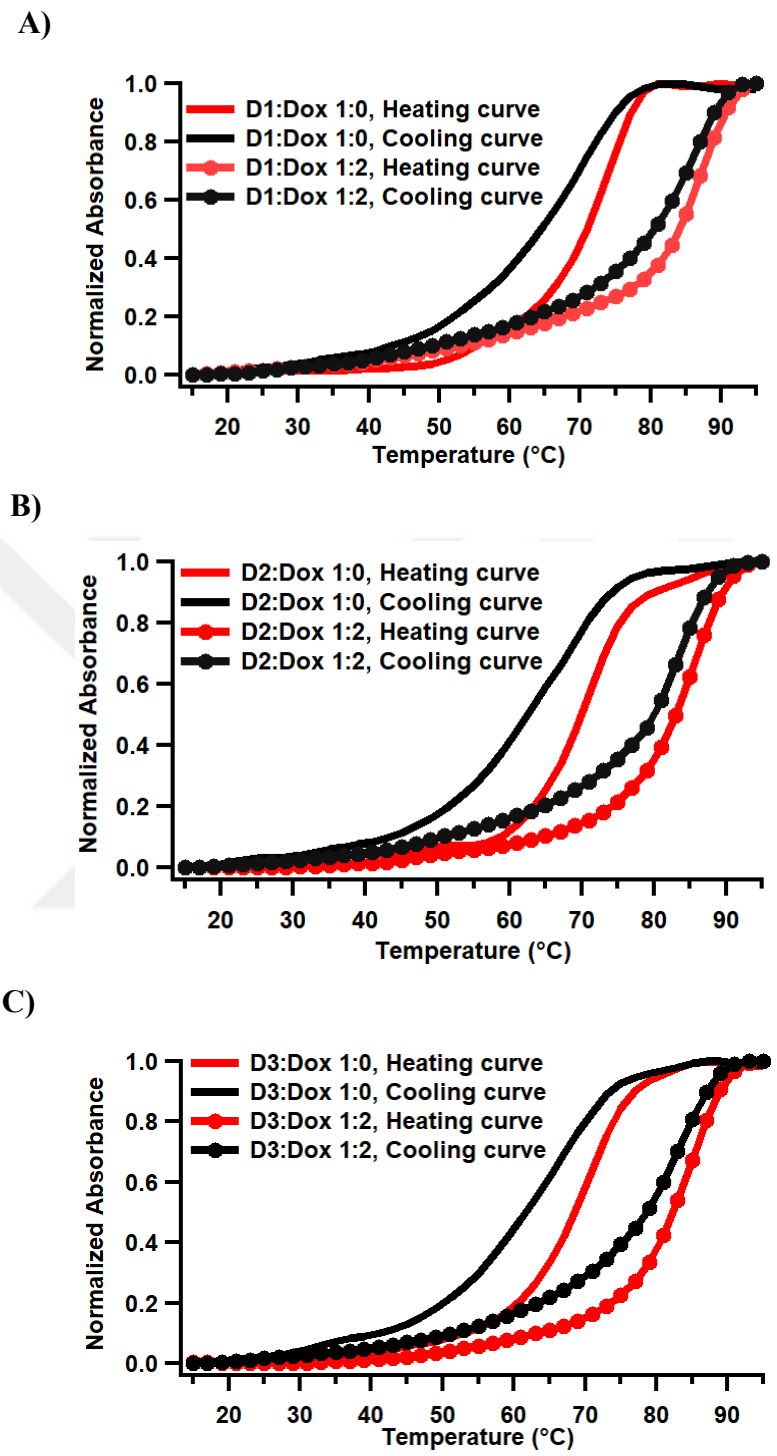


Figure 57. Comparison of the UV-Vis thermal melting profiles of 3.0 µM A) D1 B) D2 C) D3, in K-phosphate buffer at pH 5.5 in the absence and presence of 6.0 µM Dox by monitoring absorbance at 260 nm.

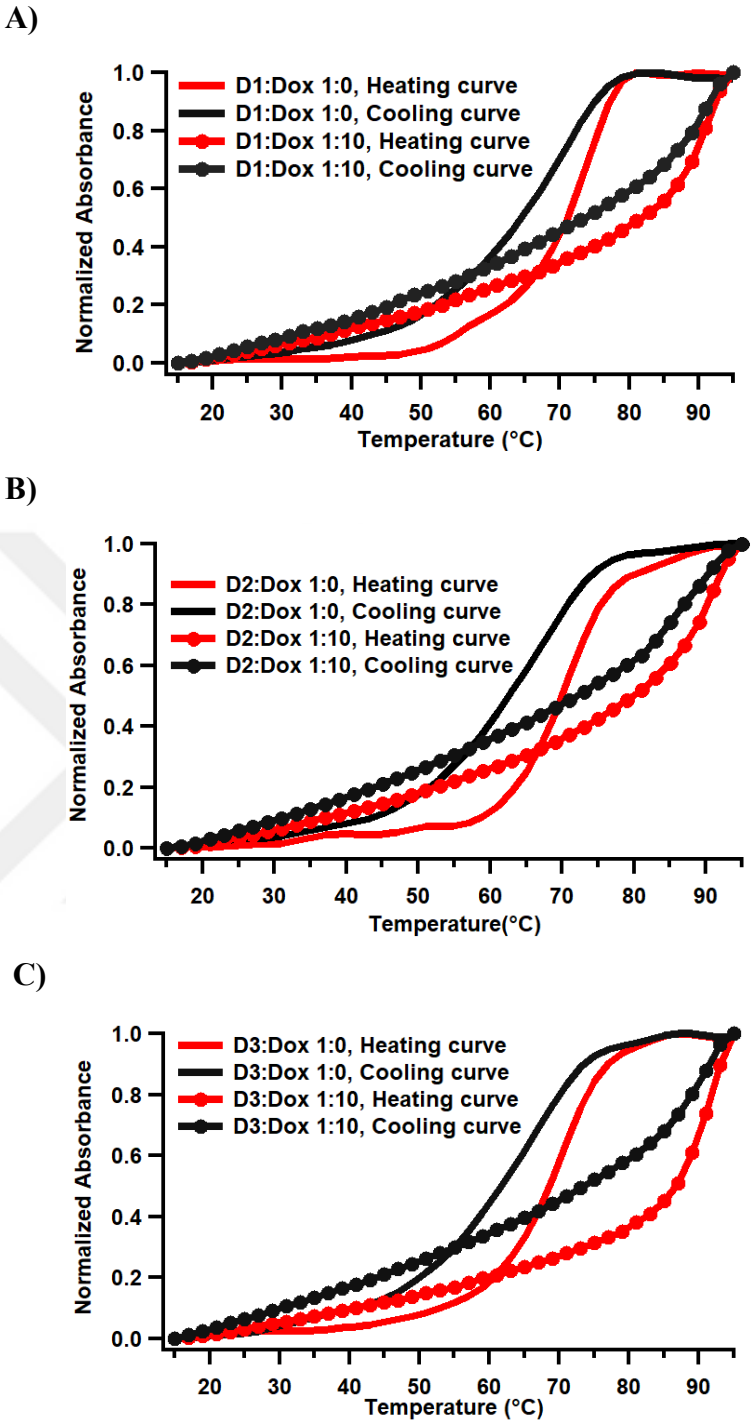


Figure 58. Comparison of the UV-Vis thermal melting profiles of 3.0 µM A) D1 B) D2 C) D3, in K-phosphate buffer at pH 5.5 in the absence and presence of 30 µM Dox by monitoring absorbance at 260 nm.

Table 8. Comparison of the Tm values of 3.0 μM DNA solutions in the absence and presence of 3.0, 6.0 and 30 μM of Dox at pH 7.0 and pH 5.5 in K-phosphate buffer.

| **DNA:Dox** | **Tm** | |
|---|---|---|
| | **pH= 7.0** | **pH= 5.5** |
| **D1: Dox 1:0** | 59 & 81 ºC | 72 ºC |
| **D1: Dox 1:1** | 85 ºC | 82 ºC |
| **D1: Dox 1:2** | 87 ºC | 87 ºC |
| **D1: Dox 1:10** | 91 ºC | 91 ºC |
| **D2: Dox 1:0** | 55 & 79°C | 70 ºC |
| **D2: Dox 1:1** | 83 ºC | 83 ºC |
| **D2: Dox 1:2** | 85 ºC | 85 ºC |
| **D2: Dox 1:10** | 91 ºC | 91 ºC |
| **D3: Dox 1:0** | 55 & 79°C | 69 ºC |
| **D3: Dox 1:1** | 83 ºC | 81 ºC |
| **D3: Dox 1:2** | 85 ºC | 83 ºC |
| **D3: Dox 1:10** | 91 ºC | 91 ºC |

### 3.9.4 Characterization of Dox Binding to Duplex Structures via Fluorescence Spectroscopy

The binding of Dox to double stranded structures was also investigated using Fluorescence spectroscopy.

Figure 59 and Figure 60, clearly indicate the decrease in fluorescence intensity for all samples in comparison to free Dox at pH 7.0 and pH 5.5, respectively. Thus, validating the binding of Dox to *PIM1* gene duplex structures. All samples exhibit almost similar changes in Dox fluorescence intensity upon binding to DNA double helix structures.

By taking advantage of decrease in fluorescence intensity, the association constants ($K_a$) of Dox with D1, D2 and D3 were determined via titration experiments [132], [106]. The fluorescence spectra were recorded by monitoring the decrease in the fluorescence intensity as the Dox solution was titrated with DNA-Dox solution. The representative titration experiments and Fraction bound vs Concentration of DNA

(M in strand) obtained from the titration results are shown in Figure 61. The obtained $K_a$ values were $(7.38 \pm 0.08)\times10^6$, $(6.27 \pm 0.06)\times10^6$ and $(6.41 \pm 0.08)\times10^6$ for the binding of Dox to D1, D2 and D3, respectively (Table 9). The calculated $K_a$ values are higher than the $K_a$ value obtained for the DNA duplex structure of *hmga1* gene with Dox ($5.2 \times 10^5$ $M^{-1}$) [136] and Adriamycin interaction with duplex DNA structure of *hmgb1* gene ($2.0 \times 10^5$ $M^{-1}$) [138] reported previously. They are also comparable with $K_a$ values for Dox-DNA (Herring sperm DNA) complexes in phosphate buffered saline (PBS) at pH 7.4 which was calculated as $0.54 \times 10^6$ $M^{-1}$ [139].

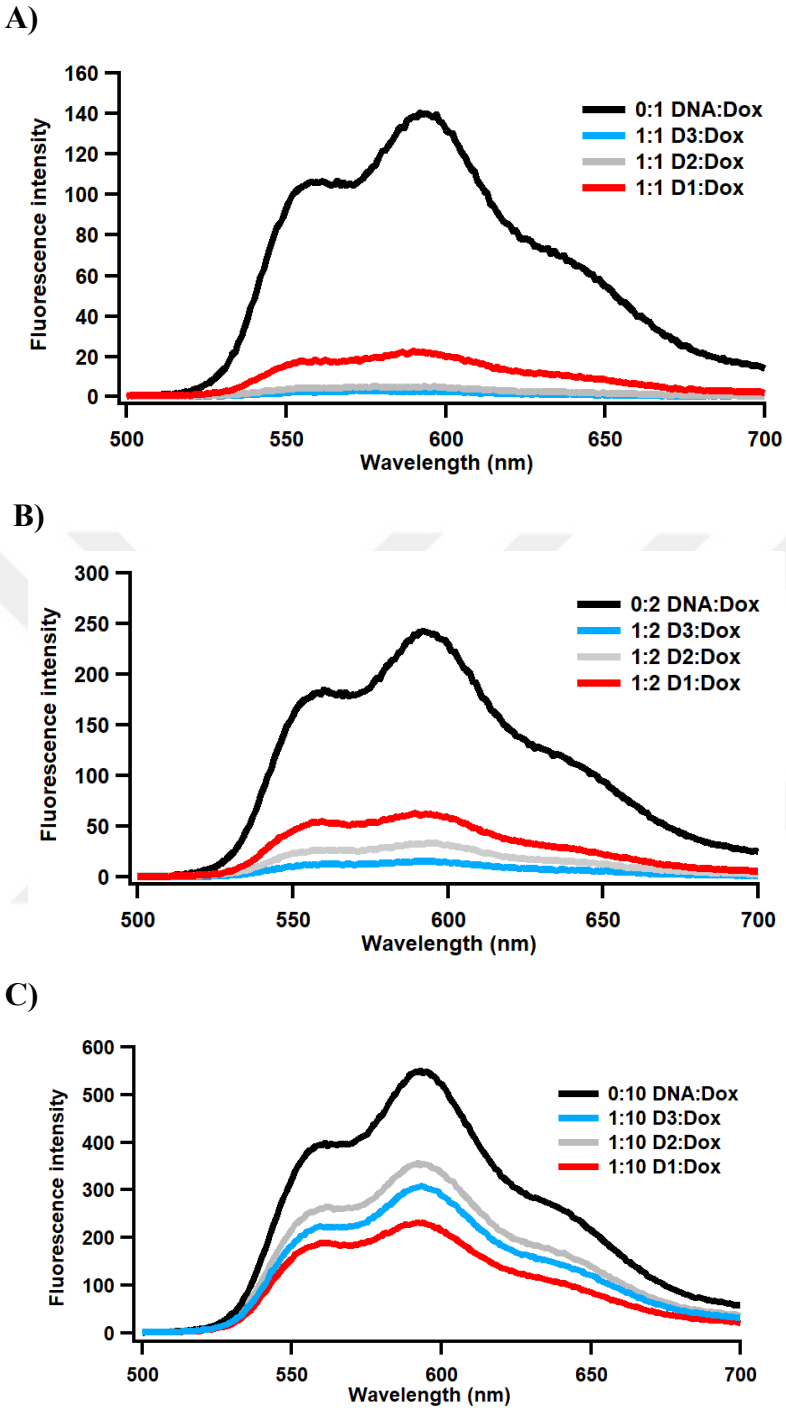


Figure 59. Changes in fluorescence intensity of A) 3.0 µM (1:1) B) 6.0 µM (1:2) C) 30 µM (1:10) free Dox (black line) upon binding to 3.0 µM *PIM1* duplex structures at pH 7.0.

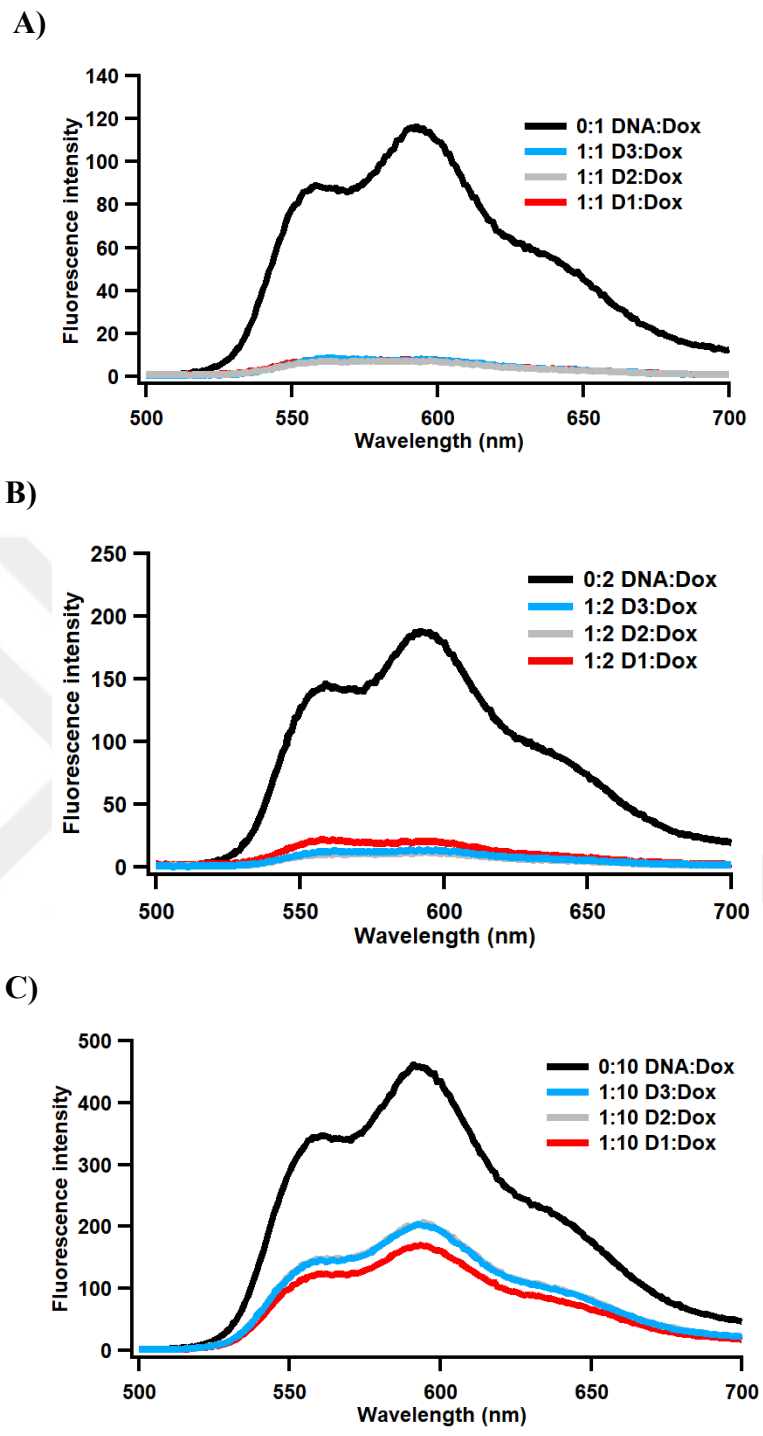


Figure 60. Changes in fluorescence intensity of A) 3.0 µM (1:1) B) 6.0 µM (1:2) C) 30 µM (1:10) free Dox (black line) upon binding to 3.0 µM *PIM1* duplex structures at pH 5.5.

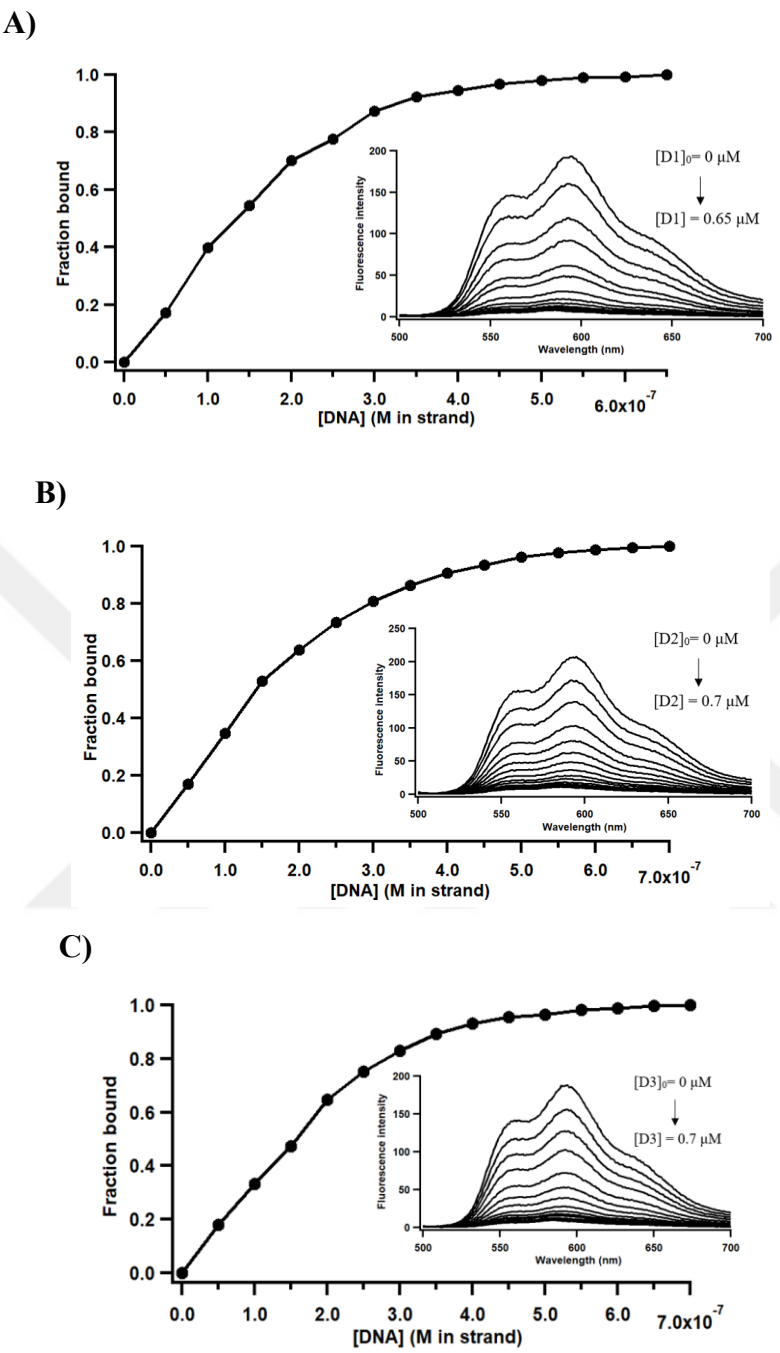


Figure 61. Fluorescence intensity measurements for 1.0 µM solutions of Dox in the presence of increasing concentrations of A) D1 B) D2 C) D3 at pH 7.0 and Fraction bound vs Concentration of DNA (M in strand) obtained from the titration results (1st replicate).

Table 9. Association constants determined by Fluorescence titration experiments of Dox-DNA

| **DNA-Dox** | **1st replicate x-half** | **$K_a$** | **2nd replicate x-half** | **$K_a$** | **$K_a$ Average** |
|---|---|---|---|---|---|
| **D1-Dox** | $1.37\times10^{-7}$ | $7.30\times10^{6}$ | $1.34\times10^{-7}$ | $7.46\times10^{6}$ | $(7.38 \pm 0.08)\times10^{6}$ |
| **D2-Dox** | $1.61\times10^{-7}$ | $6.21\times10^{6}$ | $1.58\times10^{-7}$ | $6.33\times10^{6}$ | $(6.27 \pm 0.06)\times10^{6}$ |
| **D3-Dox** | $1.58\times10^{-7}$ | $6.33\times10^{6}$ | $1.54\times10^{-7}$ | $6.49\times10^{6}$ | $(6.41 \pm 0.08)\times10^{6}$ |

## 3.10 Competition Dialysis

Once the binding of Dox to all PIM 1 secondary structures was established, competition Dialysis experiments were performed in order to reveal the selectivity of Dox towards different nucleic acid structures. To our surprise, the fluorescent titration resulted in similar binding constants for Dox binding to all the secondary structures, and we wanted to verify our results via competition dialysis experiments. Competition dialysis is a commonly used assay for the determination of structure selective ligands [107]. In our study different nucleic acid structures, placed in different dialysis cassettes, were dialyzed against Dox for 48 hours. At the end of the 48 hours long dialysis, the fluorescence intensity in each dialysis cassette was measured. The resulting fluorescence spectra for the 1st and 2nd replicates were shown in Figure 62 and Figure 63, respectively. As can be seen, the highest fluorescence intensity was observed in the cassettes containing I2, I1 and I3; which indicated that these were the structures that had the greatest affinity towards Dox among the other nucleic acid structures. Following that, the Cb/Cf values were calculated for the obtained fluorescence intensities using the calibration curve prepared beforehand (Appendix E, Figure 90) and the results were listed in Table 10. Figure 64 represents the nucleic acids structures vs $C_b/C_f$ values graph. While we

expected the highest affinity toward double stranded structures due to Dox's well known affinity for them [136], the results obtained revealed almost same affinity for all *PIM1* structures (double stranded, i-motif and G4) with the greatest affinity for I2, I1 and I3 having 31.01, 30.40 and 29.75 $C_b/C_f$ values respectively. These results was almost in perfect agreement with the binding constant obtained for G4-Dox, I4-Dox and dsDNA-Dox using the Fluorescence spectroscopy.

On the other hand, as expected Dox did not display any significant affinity towards the other single stranded DNA structure. This is consistent with Dox's reported mechanism of action which is mostly associated with its binding to double-stranded DNA structures with relatively high affinity [140].

It is important to highlight that the binding of Dox to all nine different structures of the *PIM1* gene is nearly identical, suggesting a potential of Dox as a plausible regulator between the different secondary structures. Dox's anti-cancer activity and its binding to double helical structures is a well-known phenomenon. As discussed in 1.5 section, Dox binding ability to different G4 structures was also established previously [86], [88]. However, no studies revealed the binding of Dox to i-motif structures so far. Here, for the first time, our results revealed the Dox's binding ability to all the three plausible structures that can be formed on a single gene, duplex, i-motif and G4 structures on *PIM1* gene. The binding of the Dox to all three structures with relatively same affinity also suggests the plausible modulation of these structures by Dox. However, this also implies that Dox may not be an ideal drug for selectively targeting any specific *PIM1* structure.

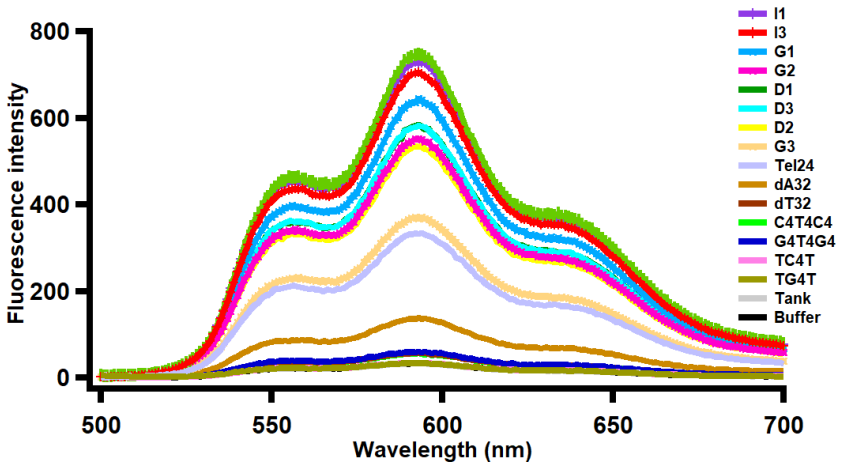


Figure 62. Fluorescence Intensity vs Wavelength (nm) spectra of the samples obtained from the competition dialysis cassettes containing 16 different nucleic acid structures at the end of 48 hours (1st replicate).

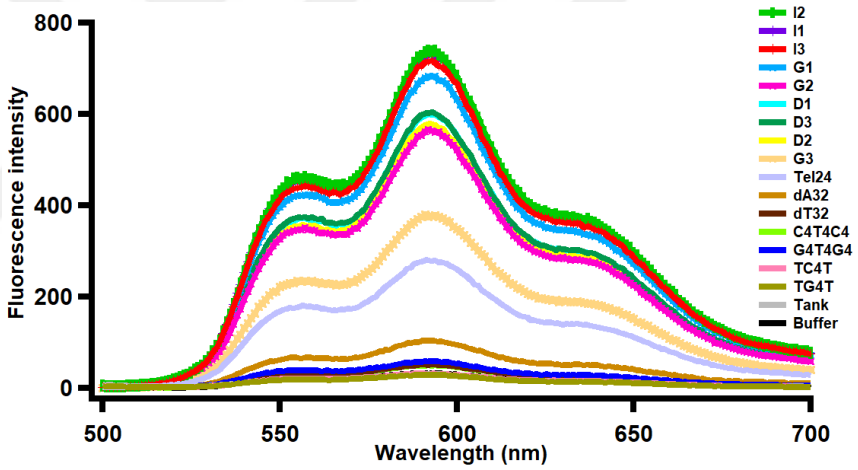


Figure 63. Fluorescence Intensity vs Wavelength (nm) spectra of the samples obtained from the competition dialysis cassettes containing 16 different nucleic acid structures at the end of 48 hours (2nd replicate).

Table 10. Competition Dialysis results of Dox.

| **Nucleic Acid Sequences** | **$C_b/C_f$** | | | |
|---|---|---|---|---|
| | **1st Replicate** | **2nd Replicate** | **Average** | **Standard Deviation** |
| **G1** | 28.58 | 26.16 | 27.37 | 1.71 |
| **G2** | 23.48 | 22.50 | 22.99 | 0.69 |
| **G3** | 15.07 | 14.68 | 14.87 | 0.27 |
| **I1** | 30.60 | 30.20 | 30.40 | 0.28 |
| **I2** | 31.05 | 30.96 | 31.01 | 0.06 |
| **I3** | 30.02 | 29.11 | 29.57 | 0.65 |
| **D1** | 24.93 | 23.86 | 24.40 | 0.76 |
| **D2** | 24.01 | 21.70 | 22.85 | 1.63 |
| **D3** | 25.01 | 23.75 | 24.38 | 0.89 |
| **$Tel_{24}$** | 10.90 | 13.06 | 11.98 | 1.53 |
| **$dA_{32}$** | 3.13 | 4.48 | 3.80 | 0.95 |
| **$dT_{32}$** | 0.81 | 1.04 | 0.93 | 0.17 |
| **$TC_4T$** | -0.08 | 0.01 | -0.04 | 0.07 |
| **$TG_4T$** | -0.17 | 0.02 | -0.08 | 0.14 |
| **$C_4T_4C_4$** | -0.36 | -0.16 | -0.26 | 0.14 |
| **$G_4T_4G_4$** | 1.12 | 1.15 | 1.14 | 0.02 |

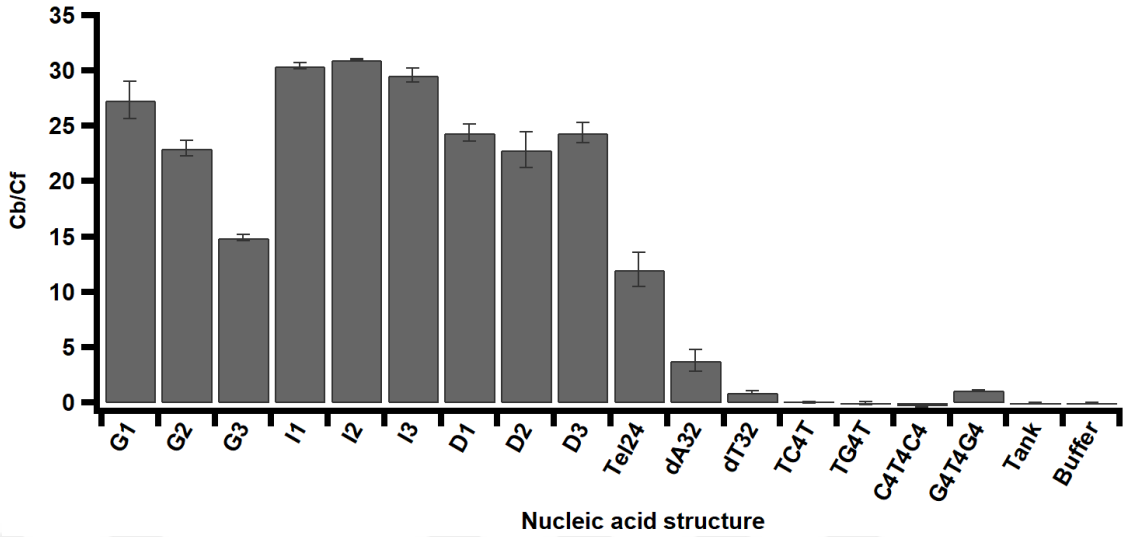


Figure 64. Average $C_b/C_f$ values obtained from the Competition Dialysis experiment.

# CHAPTER 4

# THESIS CONCLUSION

## 4.1 Investigating the Effects of Environmental Conditions on the *PIM1* DNA Structures

Within the scope of this thesis, the *PIM1* secondary structures were characterized at pH 7.0 and 5.5 in the presence of $K^+$ or $Na^+$ ions. Circular Dichroism experiments in K-phosphate buffer for *PIM1*-SLQS02 (G3), *PIM1*-SLQS07 (G2) and *PIM1*-SLQS08 (G1), were in great agreement with the previous study conducted by Tan et al. [99], reporting antiparallel, 3+1 hybrid and both structures for G3, G2 and G1, respectively. The effect of decreasing pH, which was not studied previously, demonstrated a shift for G1 to a completely antiparallel structure while two other sequences stayed intact. According to thermal denaturation experiments the stabilities of these structures were almost similar at pH 7.0. The slightly lower Tm values for G2 and G3 at pH 5.5 indicated a minor destabilization of these two secondary structures. In the next step, we illustrated the effects of buffer changes by using Na-phosphate buffer instead of K-phosphate buffer. The use of $Na^+$ facilitated the prevalence of the hybrid structure for G1. 3+1 hybrid structure of G2 transformed into an antiparallel G-quadruplex structure while no significant change was observed for G3 structure in the presence of $Na^+$. Thermal denaturation analyses in the Na-phosphate buffer revealed lower stability of G4 structures which is consistent with the well-known characteristic of G-quadruplexes [114], [29].

Additionally, the formation of stable and ordered i-motif structures in the complementary C-rich strands of *PIM1* was demonstrated in K-phosphate buffer at pH 5.5, based on Circular Dichroism experiments. Higher Tm values at pH 5.5 along with a good cross-over (at 265 and 295 nm) for Tm profiles at pH 5.5 was also a sign of the presence of stable i-motif structures at acidic pH [117]. The results also prove

the formation of i-motifs at neutral pH while the population of ordered structures are lower compared to the acidic pH.

The results also clearly proved the formation of ordered i-motif structures at pH 5.5 in Na-phosphate buffer. Based on thermal denaturation analyses, the effect of $Na^+$ ions on i-motifs differ from its effects on G-quadruplex structures of *PIM1*, aligning with the belief that salt has moderate impact on the stability of i-motifs in comparison to G-quadruplex structures [120].

Circular Dichroism and thermal denaturation analyses demonstrated the formation of the duplex DNA structure when the two complementary strands coexist in the sample. The results proved presence of i-motif or G-quadruplex structures, with the duplex being the predominant conformation at pH 7.0. However, i-motifs and G-quadruplexes become the prevailing conformations at pH 5.5. Additionally, changing pH to 5.5 leads to a decrease in Tm values for all three samples which reveals higher stabilities at pH 7.0, as we expected.

Both G4 and i-motif conformations can determine binding of various transcription factors to DNA, and they are also potential targets for chemotherapeutic agents against cancer. Considering involvement of these structures in downregulating gene expression, the equilibrium between the dsDNA and four-stranded species in the genome can control genomic events, including telomere regulation, gene expression, and DNA replication. Furthermore, the presence of G4s and i-motifs *in vivo* corroborates the role of four-stranded structures in the regulation of genomic processes [49]. In addition, if the balance between dsDNA and quadruplex species in the genome is not regulated effectively, it will result in genomic and epigenetic instability [19]. Considering the presence of G4s and i-motifs *in vivo* and the involvement of these structures in the regulation of genomic processes, understanding the equilibrium between the dsDNA and four-stranded species and the impact of external conditions on the transition between a duplex and quadruplexes in cellular environments, is important for understanding and elucidating the mechanisms that regulate gene transcriptional activity [141].

On the other hand, there is evidence that i-motif conformation exists *in vivo* at neutral pH even though they are favored energetically at slightly acidic pHs [142]. Thus, characterizing i-motif structures is biologically relevant and warrants further exploration especially for designing pH-responsive i-motif aptamers for efficient therapeutic effect on cancer cells due to the acidic environment of tumors. Moreover, the existence of both G-quadruplexes and i-motifs in a specific gene underscores the importance of examining ligand binding to both structures. The impact of i-motif or G4 structures on regulating gene expression may differ, and the effect of a ligand can vary in terms of stabilizing or destabilizing these structures [94].

Collectively, the confirmation of G4, i-motif and DNA duplex structures in the *PIM1*, along with the influence of pH and ion alterations on these structures, represents an intriguing opportunity. Such insights could guide researchers in designing ligands aimed at downregulating the *PIM1* gene for potential anticancer therapies.

## 4.2 Examining the Interaction Between Doxorubicin and *PIM1* DNA Structures

In the second part of this thesis, the interactions between clinically used anti-cancer drug Dox and different secondary structures of *PIM1* were investigated at pH 7.0 and 5.5, which has not been investigated previously. The hypochromic effect observed in the UV-Vis spectra of Dox in the presence of all structures present, indicating the presence of interactions between the DNA structures and Dox. CD spectroscopy also revealed the formation of DNA-Dox complexes, via the changes in the intensity of the DNA spectra upon Dox binding and some changes in the chirality of Dox upon its binding to *PIM1* secondary structures. Once the binding of Dox to different DNA structures was established, $K_a$ values were determined via fluorometric titration experiments. The determined $K_a$ values implied a strong association between all DNA-Dox complexes. More importantly, the affinity of Dox to G4, i-motif or duplex structures was relatively similar. Competition dialysis assays

were also revealed that the affinity of Dox was almost similar to all different nine secondary structures of *PIM1* gene.

Generally, Doxorubicin interacts with B-DNA by intercalating with its aglycone moieties between DNA base pairs and relaxes the double helix twist [143]. Recent investigations also reveal Dox high affinity towards the G-quadruplex structure of human telomere [85], [86], *VEGF* promoter [87] and *c- MYC* [88] highlighting the importance of targeting G4 structures selectively to provide enhanced treatment strategies for cancer. In this study, our most noteworthy achievement was demonstrating the binding of Dox to the i-motif structure for the first time. Additionally, the results prove that Dox could modulate *PIM1* gene through binding to all secondary structures simultaneously.

The triple-negative breast cancer (TNBC) is a subtype of breast cancer characterized by the absence of targeted therapies and exhibits a poor prognosis. Recently, it was shown that *PIM1* oncogenes were overexpressed in TNBC type breast cancer tumors and *PIM1* genes were adopting unique G-quadruplex-duplex hybrid type secondary structures [99], [103]. Considering that these structures offer promising targets for drug binding aimed at downregulating the *PIM1* gene for anticancer treatment, instead of direct small-molecule binding of oncogenic proteins for inhibition [99], we hypothesized possibility of Dox binding to different *PIM1* secondary structures. In this study, we demonstrated coexistence of G-quadruplex, i-motif and duplex structures in *PIM1* gene and our findings regarding Dox binding to all secondary structures strongly supported our hypothesis.

We are convinced that revealing the interactions between Dox and different secondary structures of *PIM1* gene can shed light on the controversial discussions regarding the action mechanism of the drug and provide solutions to the dose dependent dilemmas. Our findings can contribute to the advances in clinical research by paving the way for improved and promising cancer treatment strategies.

## REFERENCES


[1] Sinden, R. R., Pearson, C., Potaman, V. N., & Ussery, D. W. (2004). DNA structure and function. In CRC Press eBooks, 77–98.

[2] A. Travers and G. Muskhelishvili, (2015) "DNA structure and function," FEBS J, 282 (12), 2279–2295.

[3] Watson J.D., Crick F.H.C. (1953). Molecular structure of nucleic acids - a structure for deoxyribose nucleic acid. Nature, 171, 737–738.

[4] Tateishi-Karimata, H., & Sugimoto, N. (2014). Structure, stability and behaviour of nucleic acids in ionic liquids. Nucleic Acids Research, 42(14), 8831–8844.

[5] Mura, M., Carucci, C., Flaminia Cesare Marincola, Monduzzi, M., Parsons, D. F., & Salis, A. (2023). The melting curves of calf thymus-DNA are buffer specific. Journal of Colloid and Interface Science, 630, 193–201.

[6] Grayling, R. A., Sandman, K., & Reeve, J. N. (1996). DNA Stability and DNA Binding Proteins. Advances in Protein Chemistry, 437–467.

[7] Blake, R. D., & Delcourt, S. G. (1998). Thermal stability of DNA. Nucleic Acids Research, 26(14), 3323–3332.

[8] Schildkraut, C., & Lifson, S. (1965). Dependence of the melting temperature of DNA on salt concentration. Biopolymers, 3(2), 195–208.

[9] Creighton, T. E. (2010); The biophysical chemistry of nucleic acids and proteins. Helvetian Press.

[10] Baker, E. S., & Bowers, M. T. (2007). B-DNA Helix Stability in a Solvent-Free Environment. Journal of the American Society for Mass Spectrometry, 18(7), 1188–1195.

[11] Krall, J. B., Nichols, P. J., Henen, M. A., Vicens, Q., & Vögeli, B. (2023). Structure and Formation of Z-DNA and Z-RNA. Molecules, 28(2), 843.

[12] Sugiyama, H., Kawai, K., Matsunaga, A., Fujimoto, K., Saito, I., Robinson, H., & Andrew H.-J. Wang. (1996). Synthesis, structure and thermodynamic properties of 8-methylguanine-containing oligonucleotides: Z-DNA under physiological salt conditions. Nucleic Acids Research, 24(7), 1272–1278.

[13] Whelan, D. R., Hiscox, T. J., Rood, J. I., Bambery, K. R., McNaughton, D., & Wood, B. R. (2014). Detection of an en masse and reversible B- to A-DNA

conformational transition in prokaryotes in response to desiccation. Journal of the Royal Society Interface, 11(97), 20140454.

[14] Ivanov, V. I., Minchenkova, L. E., Minyat, E. E., Frank-Kamenetskii, M. D., & Schyolkina, A. K. (1974). The B̄ to Ā transition of DNA in solution. Journal of Molecular Biology, 87(4), 817–833.

[15] P1ozza, M. D., Abdullrahman, A., Cardin, C., Gasser, G., & Hall, J. (2022). Three's a crowd – stabilisation, structure, and applications of DNA triplexes. Chemical Science, 13(35), 10193–10215.

[16] Školáková, P., Renčiuk, D., Palacký, J., Krafčík, D., Dvořáková, Z., Kejnovská, I., Bednářová, K., & Vorlíčková, M. (2019). Systematic investigation of sequence requirements for DNA i-motif formation. Nucleic Acids Research, 47(5), 2177–2189.

[17] Franco-Rodríguez, F. C., González-Morales, H., Heredia-Barbero, A., Montoya, L., & Reyes-Medina, Y. (2022). Quiralidad en las ciencias naturales: un acercamiento a distintas escalas. La Granja, 37(1) 8-22.

[18] Bansal, A., Kaushik, S., & Kukreti, S. (2022). Non-canonical DNA structures: Diversity and disease association. Frontiers in Genetics, 13, 1-30.

[19] Maizels, N., & Gray, L. T. (2013). The G4 Genome. PLoS Genetics, 9(4), 1003468.

[20] Spiegel J, Adhikari S, Balasubramanian S (2020) The structure and function of DNA G-Quadruplexes. Trends in Chemistry 2, 123–136.

[21] Teng, F.-Y., Jiang, Z.-Z., Guo, M., Tan, X.-Z., Chen, F., Xi, X.-G., & Xu, Y. (2021). G-quadruplex DNA: a novel target for drug design. Cellular and Molecular Life Sciences, 78(19-20), 6557–6583.

[22] Nishio, M., Tsukakoshi, K., & Ikebukuro, K. (2021). G-quadruplex: flexible conformational changes by cations, pH, crowding and its applications to biosensing. Biosensors and Bioelectronics, 178, 113030.

[23] Siddiqui-Jain A, Grand CL, Bearss DJ, Hurley LH. (2002). Direct evidence for a G-quadruplex in a promoter region and its targeting with a small molecule to repress c-MYC transcription. Proc Natl Acad Sci U S A, 99, 11593-8.

[24] Phan, A. T., Modi, Y. S., & Patel, D. J. (2004). Propeller-type parallel-stranded G-quadruplexes in the human c-myc promoter. Journal of the American Chemical Society, 126(28), 8710–8716.

[25] Brooks, T. A., & Hurley, L. H. (2010). Targeting MYC expression through G-Quadruplexes. Genes & Cancer, 1(6), 641–649.

[26] Gonzalez, V., Guo, K., Hurley, L. H., & Sun, D. (2009). Identification and characterization of nucleolin as a c-myc g-quadruplex-binding protein. Journal of Biological Chemistry, 284(35), 23622–23635.

[27] Hazel, P., Huppert, J., Balasubramanian, S., & Neidle, S. (2004). Loop-length-dependent folding of G-Quadruplexes. Journal of the American Chemical Society, 126(50), 16405–16415.

[28] Hud, N. V., Smith, F. W., Frank, & Feigon, J. (1996). The selectivity for $K^+$ versus $Na^+$ in DNA quadruplexes is dominated by relative free energies of hydration: A thermodynamic analysis by 1H NMR. Biochemistry, 35(48), 15383–15390.

[29] Mergny, J. L., Phan, A.-T., & Lacroix, L. (1998). Following G-quartet formation by UV-spectroscopy. FEBS Letters, 435(1), 74–78.

[30] Hardin, C. C., Watson, T., Corregan, M., & Bailey, C. (1992). Cation-dependent transition between the quadruplex and Watson-Crick hairpin forms of d(CGCG3GCG). Biochemistry, 31(3), 833–841.

[31] Benabou, S., Mazzini, S., Aviñó, A., Eritja, R., & Raimundo Gargallo. (2019). A pH-dependent bolt involving cytosine bases located in the lateral loops of antiparallel G-quadruplex structures within the SMARCA4 gene promotor. Scientific Reports, 9(1).

[32] Yan, Y.-Y., Tan, J.-H., Lu, Y.-J., Yan, S.-C., Wong, K.-Y., Li, D., Huang, Z.-S. (2013). G-Quadruplex conformational change driven by pH variation with potential application as a nanoswitch. Biochimica et Biophysica Acta (BBA) - General Subjects, 1830(10), 4935–4942.

[33] Balasubramanian, S., Hurley, L.H. and Neidle, S. (2011) Targeting G-quadruplexes in gene promoters: A novel anticancer strategy? Nat. Rev. Drug Disc., 10, 261–275.

[34] Zhang, X., Mar, V., Zhou, W., Harrington, L., & Robinson, M. O. (1999). Telomere shortening and apoptosis in telomerase-inhibited human tumor cells. Genes & Development, 13(18), 2388–2399.

[35] Ohnmacht, S. A., Marchetti, C., Gunaratnam, M., Besser, R. J., Haider, S. M., Di Vita, G. Neidle, S. (2015). A G-quadruplex-binding compound showing anti-tumour activity in an in vivo model for pancreatic cancer. Scientific Reports, 5(1).

[36] Dvoráková, Z., Renciuk, D., Kejnovská, I., Školáková, P., Klára Bednárová, Sagi, J., & Vorlícková, M. (2018). i-Motif of cytosine-rich human telomere DNA fragments containing natural base lesions. Nucleic Acids Research, 46(4), 1624–1634.

[37] Takahashi, S., Bhattacharjee, S., Ghosh, S., Sugimoto, N., & Bhowmik, S. (2020). Preferential targeting cancer-related i-motif DNAs by the plant flavonol fisetin for theranostics applications. Scientific Reports, 10(1), 2504.

[38] Gehring K., Leroy J.L., Gueron M. (1993). A tetrameric DNA-structure with protonated cytosine.cytosine Base-Pairs. Nature, 363,561–565.

[39] Mergny, J.-L., Lacroix, L., Han, X., Leroy, J.-L., & Hélène, C. (1995). Intramolecular folding of pyrimidine oligodeoxynucleotides into an i-DNA motif. Journal of the American Chemical Society, 117(35), 8887–8898.

[40] Zhou, J., Wei, C., Jia, G., Wang, X., Feng, Z., & Li, C. (2010). Formation of i-motif structure at neutral and slightly alkaline pH. Mol. BioSyst., 6(3), 580–586.

[41] Li, H., Hai, J., Zhou, J., & Yuan, G. (2016). The formation and characteristics of the i-motif structure within the promoter of the c-myb proto-oncogene. Journal of Photochemistry and Photobiology. B, Biology, 162, 625–632.

[42] Kim, S. E.; Lee, I.-B.; Hyeon, C.; Hong, S.-C. (2014). Destabilization of i-motif by submolar concentrations of a monovalent cation. J. Phys. Chem. B, 118, 4753-4760.

[43] Gao, B., & Hou, X. M. (2021). Opposite effects of potassium ions on the thermal stability of i-Motif DNA in Different Buffer Systems. ACS Omega, 6(13), 8976–8985.

[44] Liu, D., & Balasubramanian, S. (2003). A Proton-Fuelled DNA Nanomachine. Angewandte Chemie International Edition, 42(46), 5734–5736.

[45] Nesterova, I. V., & Nesterov, E. E. (2014). Rational design of highly responsive pH sensors based on DNA i-Motif. Journal of the American Chemical Society, 136(25), 8843–8846.

[46] Li, W., Feng, L., Ren, J., Wu, L., & Qu, X. (2012). Visual detection of glucose using conformational switch of i□Motif DNA and non□crosslinking gold nanoparticles. Chemistry - a European Journal, 18(40), 12637–12642.

[47] Miao, D., Yu, Y., Chen, Y., Liu, Y., & Su, G. (2020). Facile construction of i-Motif DNA-conjugated gold nanostars as Near-Infrared and pH dual-responsive targeted drug delivery systems for combined cancer therapy. Molecular Pharmaceutics, 17(4), 1127–1138.

[48] Devaux, A., Bonnat, L., Lavergne, T., & Defrancq, E. (2020). Access to a stabilized i-motif DNA structure through four successive ligation reactions on a cyclopeptide scaffold. Organic & Biomolecular Chemistry, 18(32), 6394–6406.

[49] Chalikian, T. V., Liu, L., & Macgregor, Jr., R. B. (2020). Duplex-tetraplex equilibria in guanine- and cytosine-rich DNA. Biophysical Chemistry, 267, 106473.

[50] Rachwal, P. A., Brown, T., & Fox, K. R. (2007). Effect of G-Tract Length on the Topology and Stability of Intramolecular DNA Quadruplexes. Biochemistry, 46(11), 3036–3044.

[51] Abou Assi, H., El-Khoury, R., González, C., & Damha, M. J. (2017). 2′-Fluoroarabinonucleic acid modification traps G-quadruplex and i-motif structures in human telomeric DNA. Nucleic Acids Research, 45(20), 11535–11546.

[52] Liu, L., Ma, C., Wells, J. W., & Chalikian, T. V. (2020). Conformational preferences of DNA strands from the promoter region of the c-MYC oncogene. The Journal of Physical Chemistry B, 124(5), 751–762.

[53] Khan, N., Aviñó, A., Tauler, R., González, C., Eritja, R., & Gargallo, R. (2007). Solution equilibria of the i-motif-forming region upstream of the B-cell lymphoma-2 P1 promoter. Biochimie, 89(12), 1562–1572.

[54] Bucek, P., Jaumot, J., Avino, A., Eritja, R., & Gargallo, R. (2009). pH-modulated watson-crick duplex-quadruplex Equilibria of guanine-rich and cytosine-rich DNA sequences 140 base pairs upstream of the c-kit transcription initiation site. Chemistry - a European Journal, 15(46), 12663–12671.

[55] Benabou, S., Ferreira, R., Aviñó, A., González, C., Lyonnais, S., Solà, M.,Gargallo, R. (2014). Solution equilibria of cytosine- and guanine-rich sequences near the promoter region of the n-myc gene that contain stable hairpins within lateral loops. Biochimica et Biophysica Acta (BBA) - General Subjects, 1840(1), 41–52.

[56] Sabale, P. M., Tanpure, A. A., & Srivatsan, S. G. (2018). Probing the competition between duplex and G-quadruplex/i-motif structures using a conformation-sensitive fluorescent nucleoside probe. Organic & Biomolecular Chemistry, 16(22), 4141–4150.

[57] L. B. König, S., Huppert, J. L., K. O. Sigel, R., & Evans, A. C. (2013). Distance-dependent duplex DNA destabilization proximal to G-quadruplex/ i -motif sequences. Nucleic Acids Research, 41(15), 7453–7461.

[58] Lane, A. N., Chaires, J. B., Gray, R. D., & Trent, J. O. (2008). Stability and kinetics of G-quadruplex structures. Nucleic Acids Research, 36(17), 5482–5515.

[59] A. Denny, W. (2001). DNA minor groove alkylating agents. Current Medicinal Chemistry, 8(5), 533–544.

[60] National Cancer Institute. (2021). What is cancer? Retrieved from National Cancer Institute website: https://www.cancer.gov/about-cancer/understanding/what-is-cancer

[61] Ozawa, S., Sugiyama, Y., Mitsuhashi, Y., Kobayashi, T., & Inaba, M. (1988). Cell killing action of cell cycle phase-non-specific antitumor agents is dependent on concentration-time product. Cancer Chemotherapy and Pharmacology, 21(3).

[62] Urruticoechea, A., Alemany, R., Balart, J., Villanueva, A., Vinals, F., & Capella, G. (2010). Recent Advances in Cancer Therapy: An Overview. Current Pharmaceutical Design, 16(1), 3–10.

[63] Bhaduri, S., Ranjan, N., & Arya, D. P. (2018). An overview of recent advances in duplex DNA recognition by small molecules. Beilstein Journal of Organic Chemistry, 14, 1051–1086.

[64] Nakanishi, C., & Seimiya, H. (2020). G-quadruplex in cancer biology and drug discovery. Biochemical and Biophysical Research Communications, 531(1), 45–50.

[65] Wolfe, A. L., Singh, K., Zhong, Y., Drewe, P., Rajasekhar, V. K., Sanghvi, V. R.,Pelletier, J. (2014). RNA G-quadruplexes cause eIF4A-dependent oncogene translation in cancer. Nature, 513(7516), 65–70.

[66] Chen, Y., Qu, K., Zhao, C., Wu, L., Ren, J., Wang, J., & Qu, X. (2012). Insights into the biomedical effects of carboxylated single-wall carbon nanotubes on telomerase and telomeres. Nature Communications, 3(1).

[67] Khan, G. S., Shah, A., Zia-ur-Rehman, & Barker, D. (2012). Chemistry of DNA minor groove binding agents. Journal of Photochemistry and Photobiology B: Biology, 115, 105–118.

[68] Mukherjee, A., & Sasikala, W. D. (2013). Drug–DNA intercalation. dynamics of proteins and nucleic acids, 1–62.

[69] Tomasz, M. (1995). Mitomycin C: small, fast and deadly (but very selective). Chemistry & Biology, 2(9), 575–579.

[70] Barrett, M. P., Gemmell, C. G., & Suckling, C. J. (2013). Minor groove binders as anti-infective agents. Pharmacology & Therapeutics, 139(1), 12–23.

[71] Kopka, M. L., Yoon, C., Goodsell, D., Pjura, P., & Dickerson, R. E. (1985). Binding of an antitumor drug to DNA. Journal of Molecular Biology, 183(4), 553–563.

[72] Rehman, S. U., Sarwar, T., Husain, M. A., Ishqi, H. M., & Tabish, M. (2015). Studying non-covalent drug–DNA interactions. Archives of Biochemistry and Biophysics, 576, 49–60.

[73] Kennard, O. (1993). DNA-drug interactions. Pure and Applied Chemistry, 65(6), 1213–1222.

[74] Minotti, G., Menna, P., Salvatorelli, E., Cairo, G., & Gianni, L. (2004). Anthracyclines: molecular advances and pharmacologic developments in antitumor activity and cardiotoxicity. Pharmacological Reviews, 56(2), 185–229.

[75] Agudelo, D., Bourassa, P., Bérubé, G., & Tajmir-Riahi, H.-A. (2014). Intercalation of antitumor drug doxorubicin and its analogue by DNA duplex: Structural features and biological implications. International Journal of Biological Macromolecules, 66, 144–150.

[76] Kciuk, M., Gielecińska, A., Somdutt Mujwar, Kołat, D., Żaneta Kałuzińska, Celik, I., & Kontek, R. (2023). Doxorubicin—An Agent with Multiple Mechanisms of Anticancer Activity. Cells, 12(4), 659–659.

[77] Sobczuk, P., Czerwińska, M., Kleibert, M., & Cudnoch-Jędrzejewska, A. (2020). Anthracycline-induced cardiotoxicity and renin-angiotensin-aldosterone system—from molecular mechanisms to therapeutic applications. Heart Failure Reviews, 27(1), 295–319.

[78] Mazzini, S., Scaglioni, L., Fabio Animati, & Mondelli, R. (2010). Interaction between double helix DNA fragments and the new antitumor agent sabarubicin, Men10755. Bioorganic & Medicinal Chemistry, 18(4), 1497–1506.

[79] Capranico, G., Zunino, F., Kohn, K. W., & Pommier, Y. (1990). Sequence-selective topoisomerase II inhibition by anthracycline derivatives in SV40 DNA: relationship with DNA binding affinity and cytotoxicity. Biochemistry, 29(2), 562–569.

[80] Joyner, D.E.; Bastar, J.D.; Randall, R.L. Doxorubicin induces cell senescence preferentially over apoptosis in the FU-SY-1 synovial sarcoma cell line. J. Orthop. Res. 2006, 24, 1163–1169.

[81] Zhang, S., Liu, X., Bawa-Khalfe, T., Lu, L.-S., Lyu, Y. L., Liu, L. F., & Yeh, E. T. H. (2012). Identification of the molecular basis of doxorubicin-induced cardiotoxicity. Nature Medicine, 18(11), 1639–1642.

[82] Xu, Y., Liu, Z., Sun, J., Pan, Q., Sun, F., Yan, Z., & Hu, X. (2011). Schisandrin B prevents doxorubicin-induced chronic cardiotoxicity and enhances its anticancer activity in vivo. PLoS ONE, 6(12), 28335.

[83] Khiati, S., Dalla Rosa, I., Sourbier, C., Ma, X., Rao, V. A., Neckers, L. M., Pommier, Y. (2014). Mitochondrial topoisomerase I (Top1mt) is a novel limiting factor of doxorubicin cardiotoxicity. Clinical Cancer Research, 20(18), 4873–4881.

[84] Volkova, M., & Russell, R. (2012). Anthracycline cardiotoxicity: prevalence, pathogenesis and treatment. Current Cardiology Reviews, 7(4), 214–220.

[85] Manet, I., Manoli, F., Zambelli, B., Andreano, G., Masi, A., Cellai, L., Monti, S. (2011). Complexes of the antitumoral drugs Doxorubicin and Sabarubicin with telomeric G-quadruplex in basket conformation: ground and excited state properties. Photochemical & Photobiological Sciences, 10(8), 1326–1337.

[86] Manet, I., Manoli, F., Zambelli, B., Andreano, G., Masi, A., Cellai, L., & Monti, S. (2011). Affinity of the anthracycline antitumor drugs Doxorubicin and Sabarubicin for human telomeric G-quadruplex structures. Physical Chemistry Chemical Physics, 13(2), 540–551.

[87] Bilgen, E., & Persil Çetinkol, Ö. (2020). Doxorubicin exhibits strong and selective association with VEGF Pu22 G-quadruplex. Biochimica et Biophysica Acta. G, General Subjects/Biochimica et Biophysica Acta. General Subjects, 1864(12), 129720–129720.

[88] Shukla, A., Kumari, S., Sankar, M., & Nair, M. S. (2023). Insights into the mechanism of binding of doxorubicin and a chlorin compound with 22-mer c-Myc G quadruplex. Biochimica et Biophysica Acta. G, General Subjects/Biochimica et Biophysica Acta. General Subjects, 1867(12), 130482–130482.

[89] Scaglioni, L., Mondelli, R., Artali, R., Sirtori, F. R., & Mazzini, S. (2016). Nemorubicin and doxorubicin bind the G-quadruplex sequences of the human telomeres and of the c-MYC promoter element Pu22. Biochimica et Biophysica Acta (BBA) - General Subjects, 1860(6), 1129–1138.

[90] Kendrick, S., Kang, H.-J., Alam, M. P., Madathil, M. M., Agrawal, P., Gokhale, V. Hurley, L. H. (2014). The Dynamic character of the BCL2 promoter i-Motif provides a mechanism for modulation of gene expression by compounds that bind selectively to the alternative DNA hairpin structure. Journal of the American Chemical Society, 136(11), 4161–4171.

[91] Xu, C., Zhao, C., Ren, J., & Qu, X. (2011). pH-controlled reversible drug binding and release using a cytosine-rich hairpin DNA. Chemical Communications, 47(28), 8043.

[92] Kim, J. Y., Song, J. B., Jung, H., & Mok, H. (2018). I-motif-coated exosomes as a pH-sensitive carrier for anticancer drugs. Applied Biological Chemistry, 61(6), 599–606.

[93] Liu J, Ma XW, Lei CN, Xue XD, Wei T, Zhao J, Li SY, Liang XJ (2016) A self-assembled DNA nanostructure for targeted and pH triggered drug delivery to combat doxorubicin resistance. Mater Chem B 4(22), 3854–3858.

[94] Abdelhamid, M. A. S., Gates, A. J., & Waller, E. (2018). Destabilization of i-motif DNA at neutral pH by G-Quadruplex ligands. Biochemistry, 58(4), 245–249.

[95] Pagano, A., Iaccarino, N., Abdelhamid, M. A. S., Brancaccio, D., Garzarella, E. U., Di Porzio, A., Novellino, E., Waller, Z. A. E., Pagano, B., Amato, J., and Randazzo, A. (2018) Common G-quadruplex binding agents found to interact with i-motif-forming DNA: unexpected multi-target-directed compounds. Front. Chem. 6, 281.

[96] Amaravadi R, Thompson CB. (2005) The survival kinases Akt and Pim as potential pharmacological targets. J Clin Invest, 115(10), 2618–2624.

[97] Mondello, P., Cuzzocrea, S., & Mian, M. (2014). Pim kinases in hematological malignancies: where are we now and where are we going? Journal of Hematology & Oncology, 7(1), 95.

[98] Zhao, W., Qiu, R., Li, P., & Yang, J. (2017). PIM1: a promising target in patients with triple-negative breast cancer. Medical Oncology, 34(8), 142.

[99] Tan, D. J. Y., Winnerdy, F. R., Lim, K. W., & Phan, A. T. (2020). Coexistence of two quadruplex–duplex hybrids in the PIM1 gene. Nucleic Acids Research, 48(19), 11162–11171.

[100] Brasó-Maristany, F., Filosto, S., Catchpole, S., Marlow, R., Quist, J., Francesch-Domenech, E., Castel, P. (2016). PIM1 kinase regulates cell death, tumor growth and chemotherapy response in triple-negative breast cancer. Nature Medicine, 22(11), 1303–1313.

[101] Keeton, E. K., McEachern, K., Dillman, K., Sangeetha Palakurthi, Cao, Y., Grondine, M., Lyne, P. (2014). AZD1208, a potent and selective pan-Pim kinase inhibitor, demonstrates efficacy in preclinical models of acute myeloid leukemia. Blood, 123(6), 905–913.

[102] Jerusalem, G., Collignon, J., Schroeder, H., & Lousberg, L. (2016). Triple-negative breast cancer: treatment challenges and solutions. Breast Cancer: Targets and Therapy, 8, 93-107.

[103] Horiuchi, D., Camarda, R., Zhou, A. Y., Yau, C., Momcilovic, O., Balakrishnan, S. Goga, A. (2016). PIM1 kinase inhibition as a targeted therapy against triple-negative breast tumors with elevated MYC expression. Nature Medicine, 22(11), 1321–1329.

[104] Pavc, D., Wang, B., Spindler, L., Drevenšek-Olenik, I., Janez Plavec, & Primož Šket. (2020). GC ends control topology of DNA G-quadruplexes and their cation-dependent assembly. Nucleic Acids Research, 48(5), 2749–2761.

[105] Mergny, J., & Lacroix, L. (2009). UV Melting of G□Quadruplexes. Current Protocols in Nucleic Acid Chemistry, 37(1), 17.1.1-17.1.15.

[106] Jarmoskaite, I., AlSadhan, I., Vaidyanathan, P. P., & Herschlag, D. (2020). How to measure and evaluate binding affinities. ELife, 9, 57264.

[107] Ragazzon, P., & Chaires, J. B. (2007). Use of competition dialysis in the discovery of G-quadruplex selective ligands. Methods, 43(4), 313–323.

[108] Ragazzon, P. A., Garbett, N. C., & Chaires, J. B. (2007). Competition dialysis: A method for the study of structural selective nucleic acid binding. Methods, 42(2), 173–182.

[109] Kypr, J., Kejnovská, I., Renčiuk, D., & Vorlíčková, M. (2009). Circular dichroism and conformational polymorphism of DNA. Nucleic Acids Research, 37(6), 1713–1725.

[110] Villar-Guerra, R.; Trent, J.O.; Chaires, J.B. G-Quadruplex secondary structure obtained from Circular Dichroism spectroscopy. Angew. Chem. 57 (2017) 7171–7175.

[111] Lee, J. A., & DeRosa, M. C. (2010). A pH-driven DNA switch based on the A+·G mispair. Chem. Commun., 46(3), 418–420.

[112] Hatzakis, E., Okamoto, K., & Yang, D. (2010). Thermodynamic stability and folding kinetics of the major G quadruplex and its loop isomers formed in the nuclease hypersensitive element in the human c-Myc promoter: effect of loops and Flanking Segments on the Stability of Parallel-Stranded intramolecular G-quadruplexes. Biochemistry, 49(43), 9152–9160.

[113] Wang, Z.-F., Li, M.-H., Hsu, S.-T. D., & Chang, T.-C. (2014). Structural basis of sodium–potassium exchange of a human telomeric DNA quadruplex without topological conversion. Nucleic Acids Research, 42(7), 4723–4733.

[114] Jana, J., & Weisz, K. (2021). Thermodynamic stability of G□quadruplexes: impact of sequence and environment. ChemBioChem, 22(19), 2848–2856.

[115] Rigo, R., Dean, W. L., Gray, R. D., Chaires, J. B., & Sissi, C. (2017). Conformational profiling of a G-rich sequence within the c-KIT promoter. Nucleic Acids Research, 45(22), 13056–13067.

[116] Phan, A. T., & Mergny, J. (2002). Human telomeric DNA: G-quadruplex, i-motif and Watson-Crick double helix. Nucleic Acids Research, 30(21), 4618–4625.

[117] Singh, A., & Kukreti, S. (2018). Homoduplex to i-motif structural switch exhibited by a cytosine rich strand of the MYH7 heavy chain β gene promoter at physiological pH. RSC Advances, 8(60), 34202–34214.

[118] Pataskar, S. S., Dash, D., & Brahmachari, S. K. (2001). Intramolecular i-motif structure at acidic pH for progressive myoclonus epilepsy (EPM1) repeat d(CCCCGCCCCGCG)n. Journal of Biomolecular Structure & Dynamics, 19(2), 307–313.

[119] Chaudhary, S., Kaushik, M., Ahmed, S., & Kukreti, S. (2020). Exploring potential of i-motif DNA formed in the promoter region of GRIN1 gene for nanotechnological applications. Results in Chemistry, 2, 100086.

[120] Kim, S. E., & Hong, S.-C. (2022). Two opposing effects of monovalent cations on the stability of i-motif structure. BioRxiv (Cold Spring Harbor Laboratory), 127(9) 1932–1939.

[121] Li, W., Wu, P., Ohmichi, T., & Sugimoto, N. (2002). Characterization and thermodynamic properties of quadruplex/duplex competition. FEBS Letters, 526(1-3), 77–81.

[122] Serrano-Chacón, I., Mir, B., Escaja, N., & González, C. (2021). Structure of i-Motif/Duplex Junctions at Neutral pH. Journal of the American Chemical Society, 143(33), 12919–12923.

[123] Owczarzy, R., You, Y., Moreira, B. G., Manthey, J. A., Huang, L., Behlke, M. A., & Walder, J. A. (2004). Effects of Sodium Ions on DNA Duplex Oligomers: Improved predictions of melting temperatures. Biochemistry, 43(12), 3537–3554.

[124] Nakano, S., Fujimoto, M., Hara, H., & Sugimoto, N. (1999). Nucleic acid duplex stability: influence of base composition on cation effects. Nucleic Acids Research, 27(14), 2957–2965.

[125] Owczarzy, R., Moreira, B. G., You, Y., Behlke, M. A., & Walder, J. A. (2008). Predicting stability of DNA duplexes in solutions containing magnesium and monovalent cations. Biochemistry, 47(19), 5336–5353.

[126] Cristofari, C., Rigo, R., Greco, M. L., Ghezzo, M., & Sissi, C. (2019). pH-driven conformational switch between non-canonical DNA structures in a C-rich domain of EGFR promoter. Scientific Reports, 9(1), 1210.

[127] Airoldi, M., Barone, G., Gennaro, G., Anna Maria Giuliani, & Giustini, M. (2014). Interaction of doxorubicin with polynucleotides. A Spectroscopic Study. Biochemistry, 53(13), 2197–2207.

[128] Tariq, Z., & Barthwal, R. (2019). Affinity of anticancer drug daunomycin toward tetrahymena telomeric G-quadruplex DNA d-[GGGG(TTGGGG)$_3$]. ACS Omega, 4(4), 6347–6359.

[129] Sirajuddin, M., Ali, S., & Badshah, A. (2013). Drug–DNA interactions and their study by UV–Visible, fluorescence spectroscopies and cyclic voltametry. Journal of Photochemistry and Photobiology B: Biology, 124, 1–19.

[130] Zhang, Y., Chen, J., Ju, H., & Zhou, J. (2019). Thermal denaturation profile: A straightforward signature to characterize parallel G-quadruplexes. Biochimie, 157, 22–25.

[131] Ijäs, H., Shen, B., Heuer-Jungemann, A., Keller, A., Kostiainen, M. A., Liedl, T., Ihalainen, J. A., & Linko, V. (2021). Unraveling the interaction between doxorubicin and DNA origami nanostructures for customizable chemotherapeutic drug release. Nucleic Acids Research, 49, 3048–3062.

[132] Qu, X., & Chaires, J. B. (2000). Analysis of drug-DNA binding data. Methods in Enzymology, 353–369.

[133] Pagano, A., Iaccarino, N., Abdelhamid, M. A. S., Brancaccio, D., Garzarella, E. U., Di Porzio, A. Randazzo, A. (2018). Common G-quadruplex binding agents found to interact with i-motif-forming DNA: unexpected multi-target-directed compounds. Frontiers in Chemistry, 6, 281.

[134] Wang, L., Wu, Y., Chen, T., & Wei, C. (2013). The interactions of phenanthroline compounds with DNAs: Preferential binding to telomeric quadruplex over duplex. International Journal of Biological Macromolecules, 52, 1–8.

[135] Yang, Y., Fu, H., Qian, C., Li, H., & David D.Y. Chen. (2020). Characterization of interaction between Bcl-2 oncogene promoter I-Motif DNA and flavonoids using electrospray ionization mass spectrometry and pressure-assisted capillary electrophoresis frontal analysis. Talanta, 215, 120885–120885.

[136] Akhter, Md. Z., & Rajeswari, M. R. (2014). Interaction of doxorubicin with a regulatory element of hmga1 and its in vitro anti-cancer activity associated

with decreased HMGA1 expression. Journal of Photochemistry and Photobiology. B, Biology, 141, 36–46.

[137] Cera, C., Palù, G., Magno, S. M., & Palumbo, M. (1991). Interaction between second generation anthracyclines and DNA in the nucleosomal structure. Nucleic Acids Research, 19(9), 2309-14.

[138] Lohani, N., & Rajeswari, M. R. (2016). Preferential binding of anticancer drugs to triplex DNA compared to duplex DNA: a spectroscopic and calorimetric study. RSC Advances, 6(46), 39903–39917.

[139] Schneider, Y.-J.., Baurain, R., Zenebergh, A., & Trouet, A. (1979). DNA-binding parameters of daunorubicin and doxorubicin in the conditions used for studying the interaction of anthracycline-DNA complexes with cells in vitro. Cancer Chemotherapy and Pharmacology, 2(1) 7-10.

[140] DuVernay, V. H., Pachter, J. A., & Crooke, S. T. (1979). Deoxyribonucleic acid binding studies on several new anthracycline antitumor antibiotics. Sequence preference and structure-activity relationships of marcellomycin and its analogs as compared to adriamycin. Biochemistry, 18(18), 4024–4030.

[141] Matsumoto, S., Tateishi-Karimata, H., Ohyama, T., & Sugimoto, N. (2021). Effect of DNA modifications on the transition between canonical and non-canonical DNA structures in CpG islands during senescence. RSC Advances, 11(59), 37205–37217.

[142] Luo, X., Zhang, J., Gao, Y., Pan, W., Yang, Y., Li, X., Wang, Y. (2023). Emerging roles of i-motif in gene expression and disease treatment. Frontiers in Pharmacology, 14, 1136251.

[143] Mattioli, R., Ilari, A., Colotti, B., Mosca, L., Fazi, F., & Colotti, G. (2023). Doxorubicin and other anthracyclines in cancers: Activity, chemoresistance and its overcoming. Molecular Aspects of Medicine, 93, 101205–101205.

# APPENDICES

## A. Preparation of Buffer and Stock Solutions

### 100 mM K-phosphate Buffer Preparation

**1.000 M, 0.5000 L $KH_2PO_4$ stock preparation:**

$M = \frac{n}{v}$

$1.000\ M = \frac{n(mol)}{0.5000\ L}$

$n = 0.5000\ mol$, $KH_2PO_4$ Mw:136.09 g/mol and $n\ (mol) = \frac{m(g)}{Mw(mol\ g)}$

$0.5000\ mol = \frac{\frac{m}{136.09g}}{mol}$ so; $m\ (g) = 68.05\ g$

68.05 g $KH_2PO_4$ is dissolved in 500.0 mL Millipore water for preparation of 1.000 M $KH_2PO_4$ solution.

**1.000 M, 0.5000 L $K_2HPO4$ stock preparation:**

$M = \frac{n}{v}$

$1.000\ M = \frac{n(mol)}{0.5000\ L}$

$n = 0.500\ mol$, $KH_2PO_4$ Mw: 174.18 g/mol and $n\ (mol) = \frac{m(g)}{Mw(mol\ g)}$

$0.500\ mol = \frac{\frac{m}{174.18\ g}}{mol}$ so; $m\ (g) = 87.09\ g$

87.09 g $K_2HPO4$ is dissolved in 500.0 mL Millipore water for preparation of 1M $K_2HPO_4$ solution.

For **pH=7** concentrations are arranged by using the following equation:

For $K_2HPO_4$: $1.00\ M \times V_1 = (61.5\times10^{-2})M \times 1.00\ L$ $\quad V_1 = 61.50\ mL$
For $KH_2PO_4$: $1.00\ M \times V_1 = (38.5\times10^{-2})M \times 1.00\ L$ $\quad V_1 = 38.50\ mL$

For **pH=5.5** concentrations are arranged by using the following equation:

For $K_2HPO_4$: $1.00\ M \times V_1 = (8.5\times10^{-2})M \times 1.00\ L$ $\quad V_1 = 8.50\ mL$
For $KH_2PO_4$: $1.00\ M \times V_1 = (91.5\times10^{-2})M \times 1.00\ L$ $\quad V_1 = 91.5\ mL$

The total volume of the above components is equal to 100.0 mL. The buffer solution is completed to 1.00 L with millipore water, and the pH of the solution is adjusted to7.0 and 5.5 with NaOH or HCl solution.

**500.0 mM KCl solution preparation**

$M = \frac{n}{v}$

$0.5000\ M = \frac{n(mol)}{1\ L}$

$n = 0.0500\ mol$, KCl Mw:74.55 g/mol

$0.0500\ mol = \frac{m}{\frac{74.55g}{mol}}$ $m\ (g) = 3.73\ g$

3.73 g KCl is dissolved in 100 mL Millipore water for preparation of 500.0 mM KCl solution.

**100 mM Na-phosphate Buffer Preparation**

**1.000 M, 0.5000 L $NaH_2PO_4$ stock preparation:**

$M = \frac{n}{v}$

$1.000\ M = \frac{n(mol)}{0.5\ L}$

$n = 0.5000\ mol$, $NaH_2PO_4$ Mw:119.98 g/mol and $n\ (mol) = \frac{m(g)}{Mw(mol\ g)}$

$0.5000\ mol = \frac{m}{\frac{119.98g}{mol}}$ so; $m\ (g) = 59.99\ g$

59.99 g $NaH_2PO4$ is dissolved in 500.0 mL Millipore water for preparation of 1M $NaH_2PO_4$ solution.

**1.000 M, 0.5000 L $Na_2HPO_4$ stock preparation:**

$M = \frac{n}{v}$

$1.000\ M = \frac{n(mol)}{0.5000\ L}$

$n = 0.5000\ mol$, $NaH_2PO_4$ Mw: 141.96 g/mol and $n\ (mol) = \frac{m(g)}{Mw(mol\ g)}$

$0.5000\ mol = \frac{m}{\frac{141.96\ g}{mol}}$ so; $m\ (g) = 70.98\ g$

70.98 g $Na_2HPO_4$ is dissolved in 500.0 mL Millipore water for preparation of 1.00M $Na_2HPO_4$ solution.

For **pH=7** concentrations are arranged by using the following equation:

For $Na_2HPO_4$: $1.00\ M \times V_1 = (57.7 \times 10^{-2}) M \times 1.00\ L$ $\quad V_1 = 57.7\ mL$
For $NaH_2PO_4$: $1.00\ M \times V_1 = (42.3 \times 10^{-2}) M \times 1.00\ L$ $\quad V_1 = 42.3\ mL$

The total volume of the above components is equal to 100.0 mL. The buffer solution is completed to 1.000 L with millipore water and the pH of the solution is adjusted to
**7.0** with NaOH or HCl solution.

**500 mM NaCl solution preparation**

$$M = \frac{n}{v}$$

$$0.5000\ M = \frac{n(mol)}{1\ L}$$

$$n = 0.0500\ mol,\ \text{NaCl Mw:58.44 g/mol}$$

$$0.0500\ mol = \frac{\frac{m}{58.44g}}{mol} \qquad m\ (g) = 2.92\ g$$

2.92 g NaCl is dissolved in 100 mL Millipore water for preparation of 500.0 mM NaCl solution.

**Dox sample preparation**

Doxorubicin stock solution was prepared in Millipore water, and the concentration was calculated using UV-Vis spectroscopy ($\varepsilon_{480}$=11500 $M^{-1}$ $cm^{-1}$).

A=ε.b.c

Absorbance= extinction coefficient ×concentration ×pathlength

## B. List of Nucleic Acid Sequences Used in This Study

Table 11. List of nucleic acid sequences used in this study.

| Nucleic Acids | Sequences |
|---|---|
| ***PIM1*-SLQS08 (G1)** | 5'-GC GGGAGGGCGCGCCAGCGGGGTCGGG C-3' |
| ***PIM1*-SLQS07 (G2)** | 5'-GC GGGAGGGCGCGCCAGCGGGGTCGGG-3' |
| ***PIM1*-SLQS02 (G3)** | 5'-GGGAGGGCGCGCCAGCGGGGTCGGG C-3' |
| ***PIM1*-SLQS08-comp (I1)** | 5'-G CCCGACCCCGCTGGCGCGCCCTCCC GC-3' |
| ***PIM1*-SLQS07-comp (I2)** | 5'- CCCGACCCCGCTGGCGCGCCCTCCC GC-3' |
| ***PIM1*-SLQS02-comp (I3)** | 5'-G CCCGACCCCGCTGGCGCGCCCTCCC-3' |
| **$Tel_{24}$** | 5'-TTAGGG TTAGGG TTAGGG TTAGGG-3' |
| **$dA_{32}$** | 5'-AAA AAA AAA AAA AAA AAA AAA AAA AAA AAA AA-3' |
| **$dT_{32}$** | 5'-TTT TTT TTT TTT TTT TTT TTT TTT TTT TTT TT-3' |
| **$TC_4T$** | 5'-TCCCCT -3' |
| **$TG_4T$** | 5'-TGGGGT -3' |
| **$C_4T_4C_4$** | 5'-CCCCTTTTCCCC -3' |
| **$G_4T_4G_4$** | 5'-GGGGTTTTGGGG -3' |

## C. UV-Vis Thermal Denaturation Experiments and Melt Curves

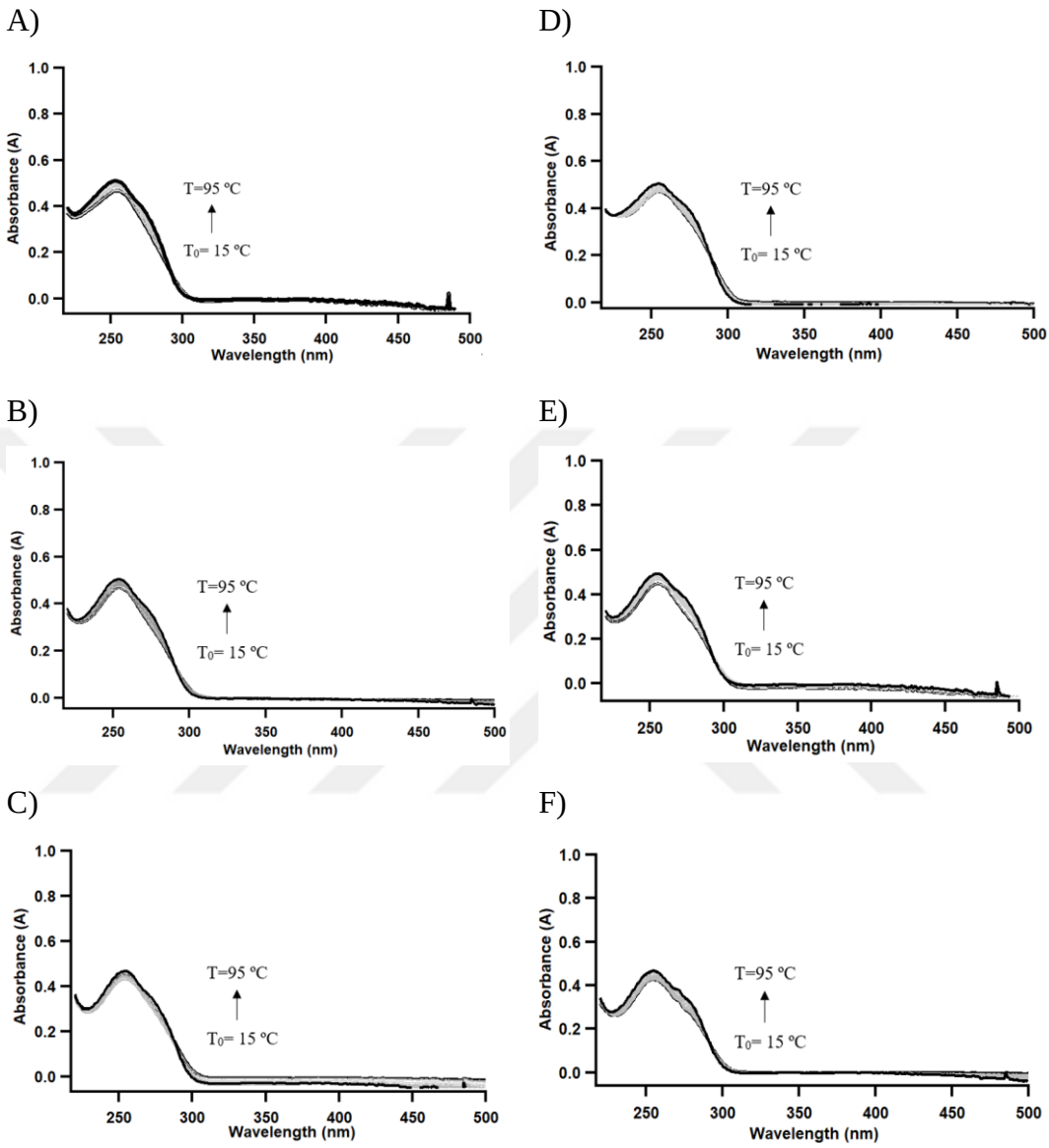


Figure 65. UV-Vis absorption spectra of 3.0 µM A) G1 B) G2 C) G3 in K-phosphate buffer at pH 7.0 and D) G1 E) G2 F) G3 at pH 5.5 obtained during thermal denaturation experiments.

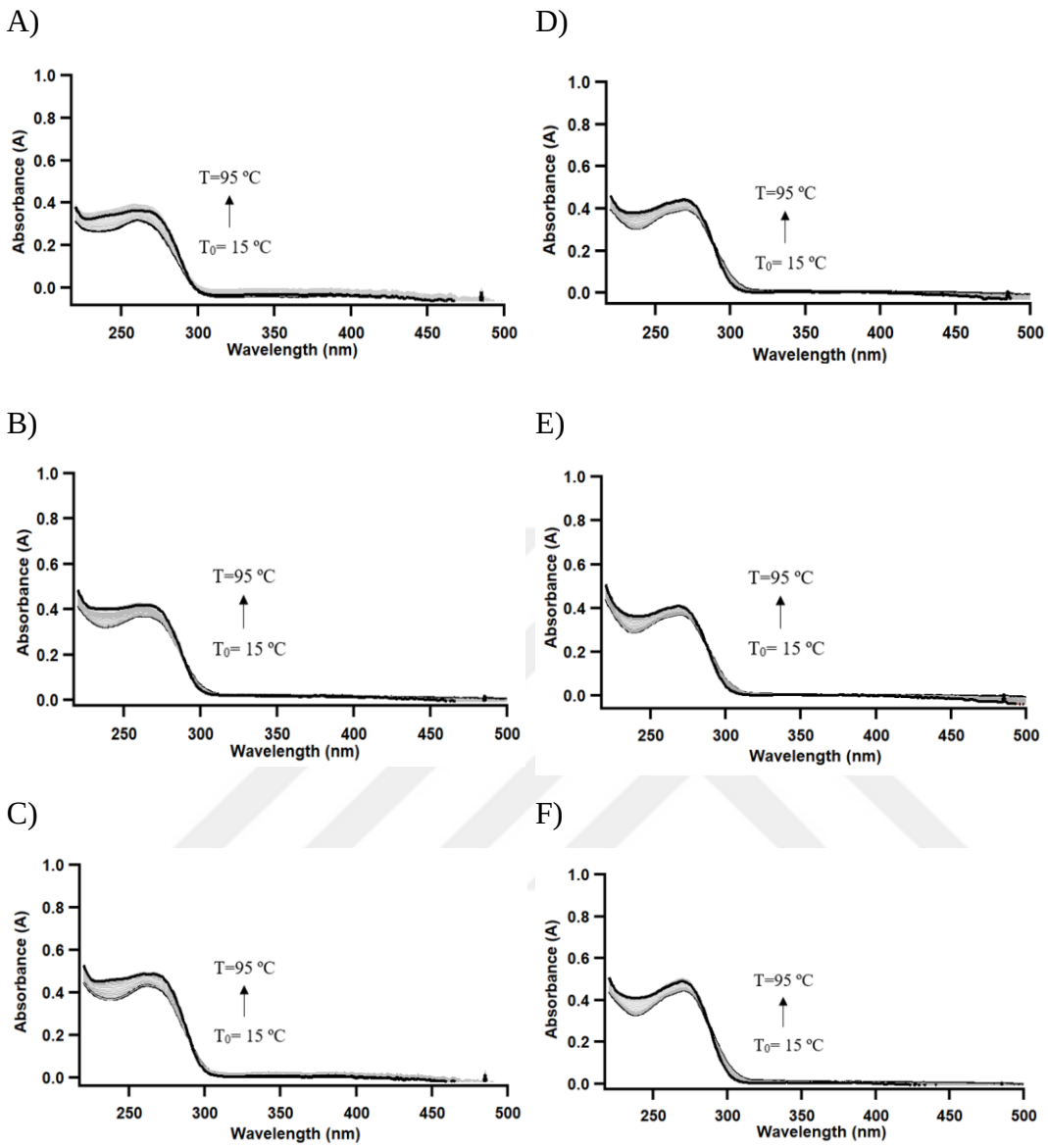


Figure 66. UV-Vis absorption spectra of 3.0 µM A) I1 B) I2 C) I3 in K-phosphate buffer at pH 7.0 and D) I1 E) I2 F) I3 at pH 5.5 obtained during thermal denaturation experiments.

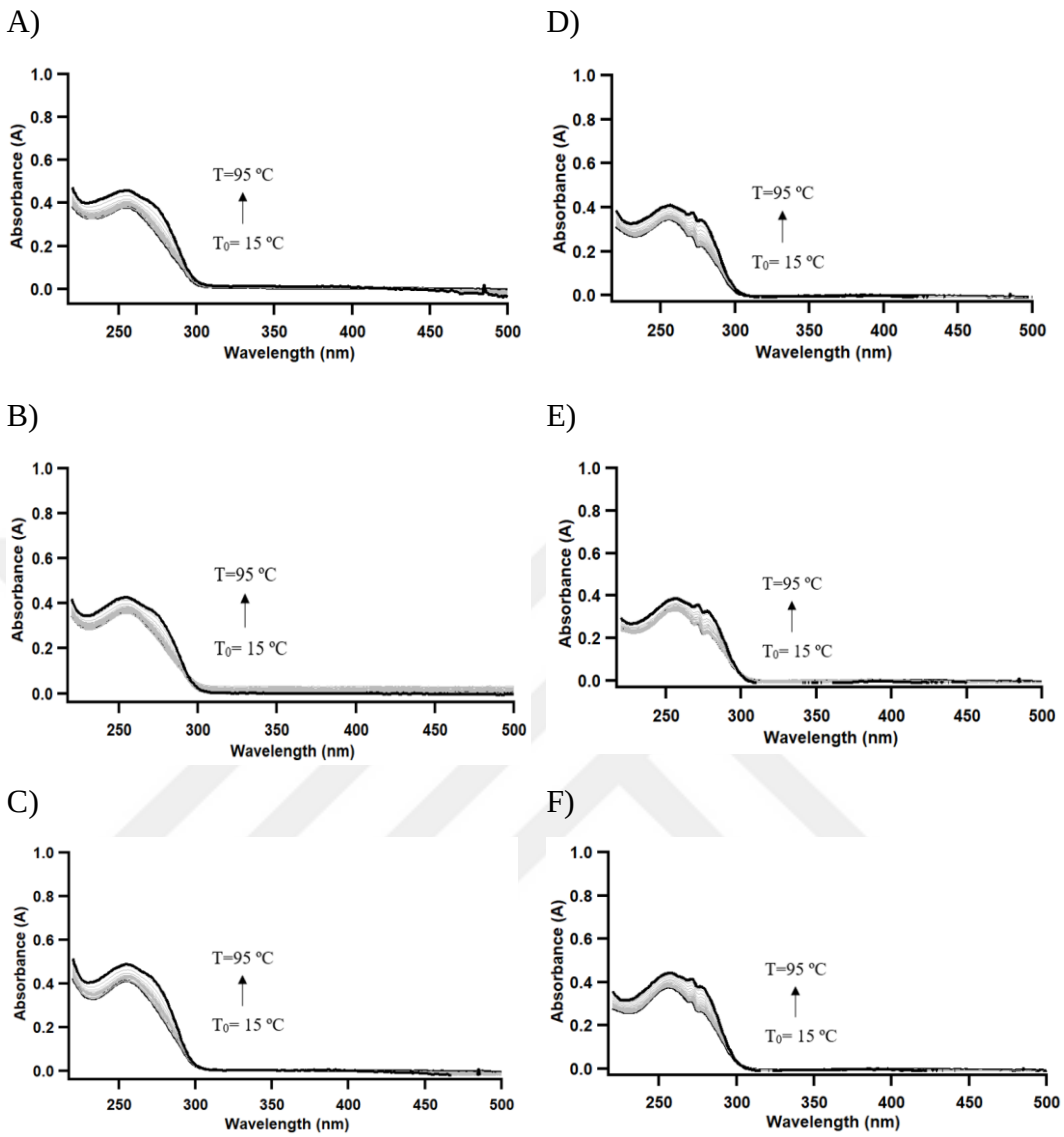


Figure 67. UV-Vis absorption spectra of 3.0 µM A) D1 B) D2 C) D3 in K-phosphate buffer at pH 7.0 and D) D1 E) D2 F) D3 at pH 5.5 obtained during thermal denaturation experiments.

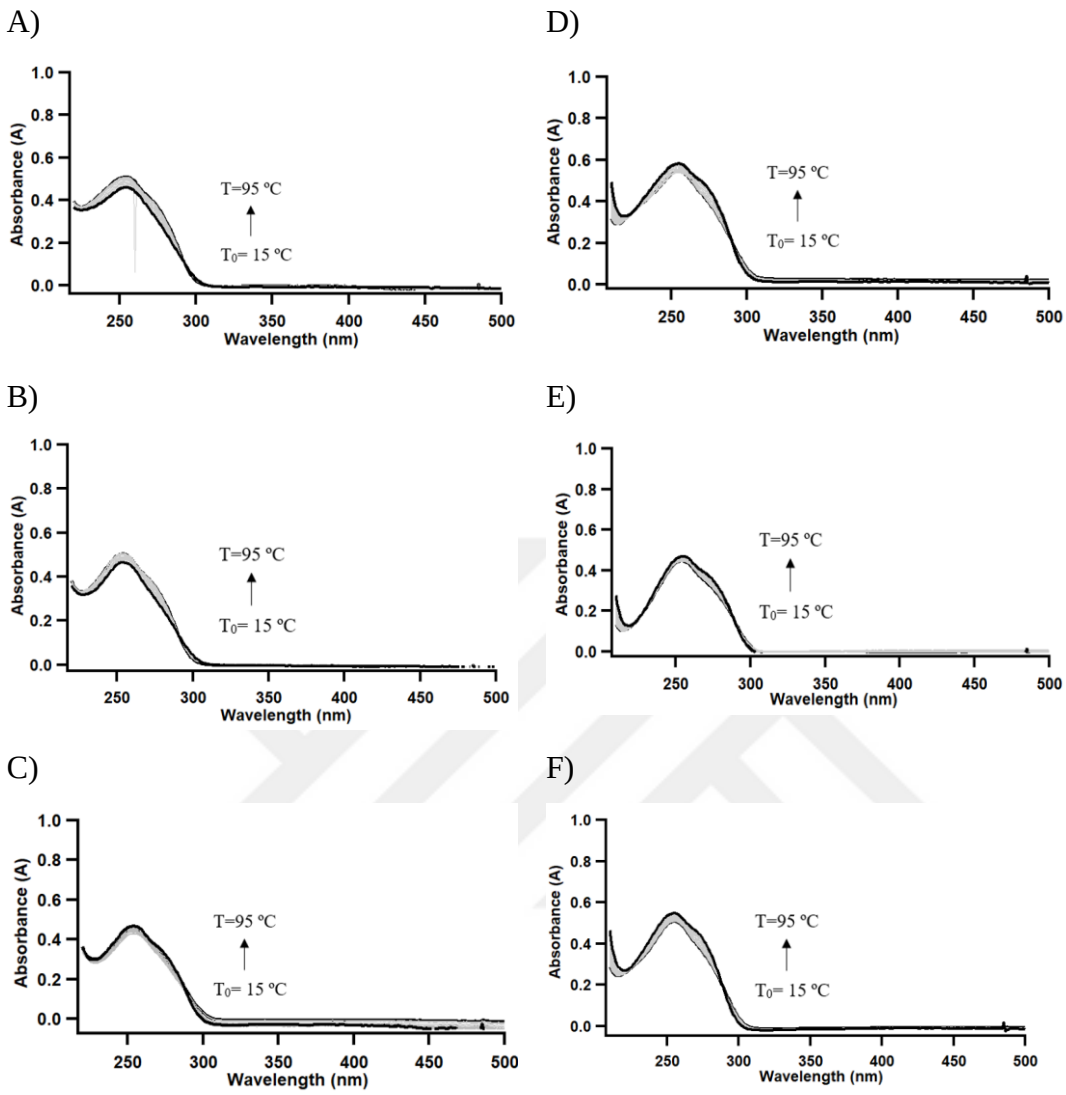


Figure 68. UV-Vis absorption spectra of 3.0 µM A) G1 B) G2 C) G3 in Na-phosphate buffer at pH 7.0 and D) G1 E) G2 F) G3 at pH 5.5 obtained during thermal denaturation experiments

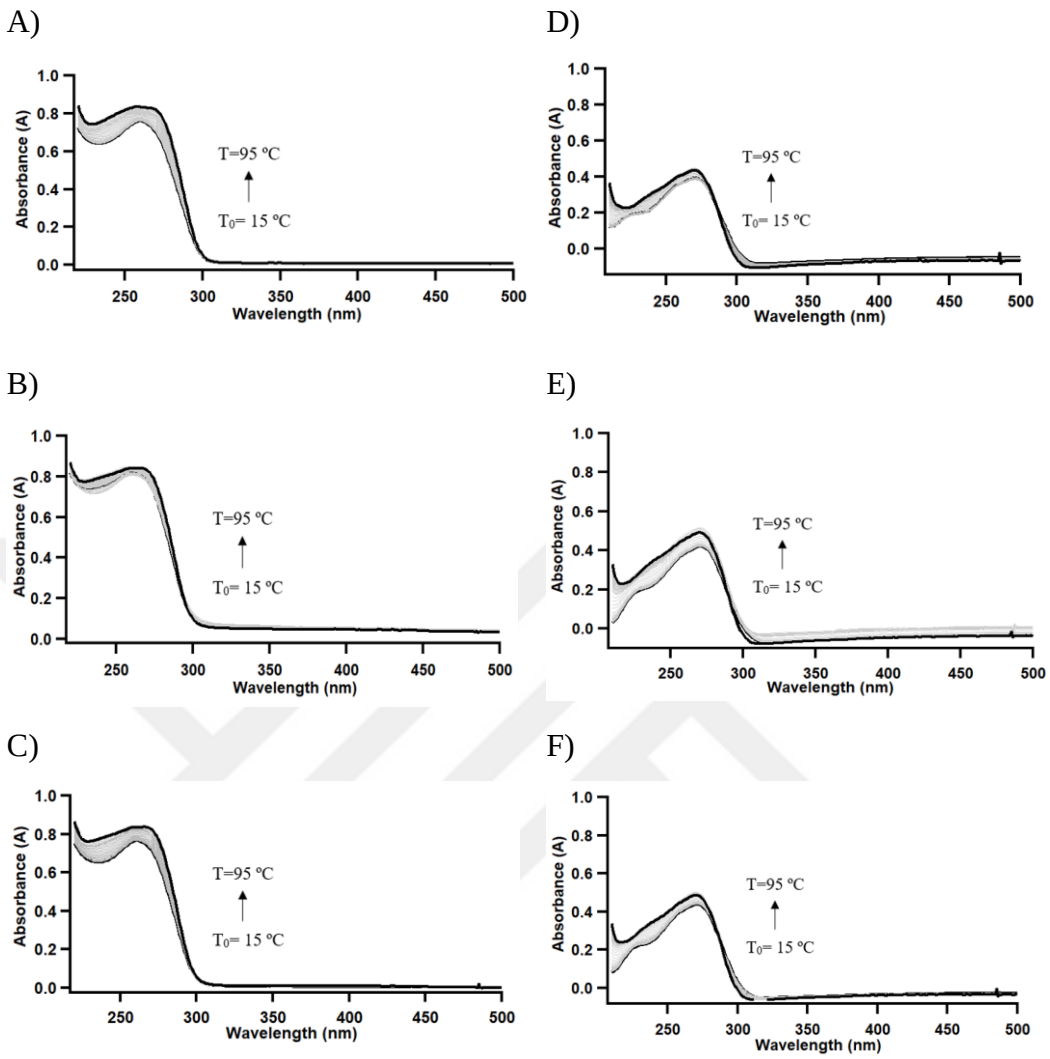


Figure 69. UV-Vis absorption spectra of 3.0 µM A) I1 B) I2 C) I3 in Na-phosphate buffer at pH 7.0 and D) I1 E) I2 F) I3 at pH 5.5 obtained during thermal denaturation experiments.

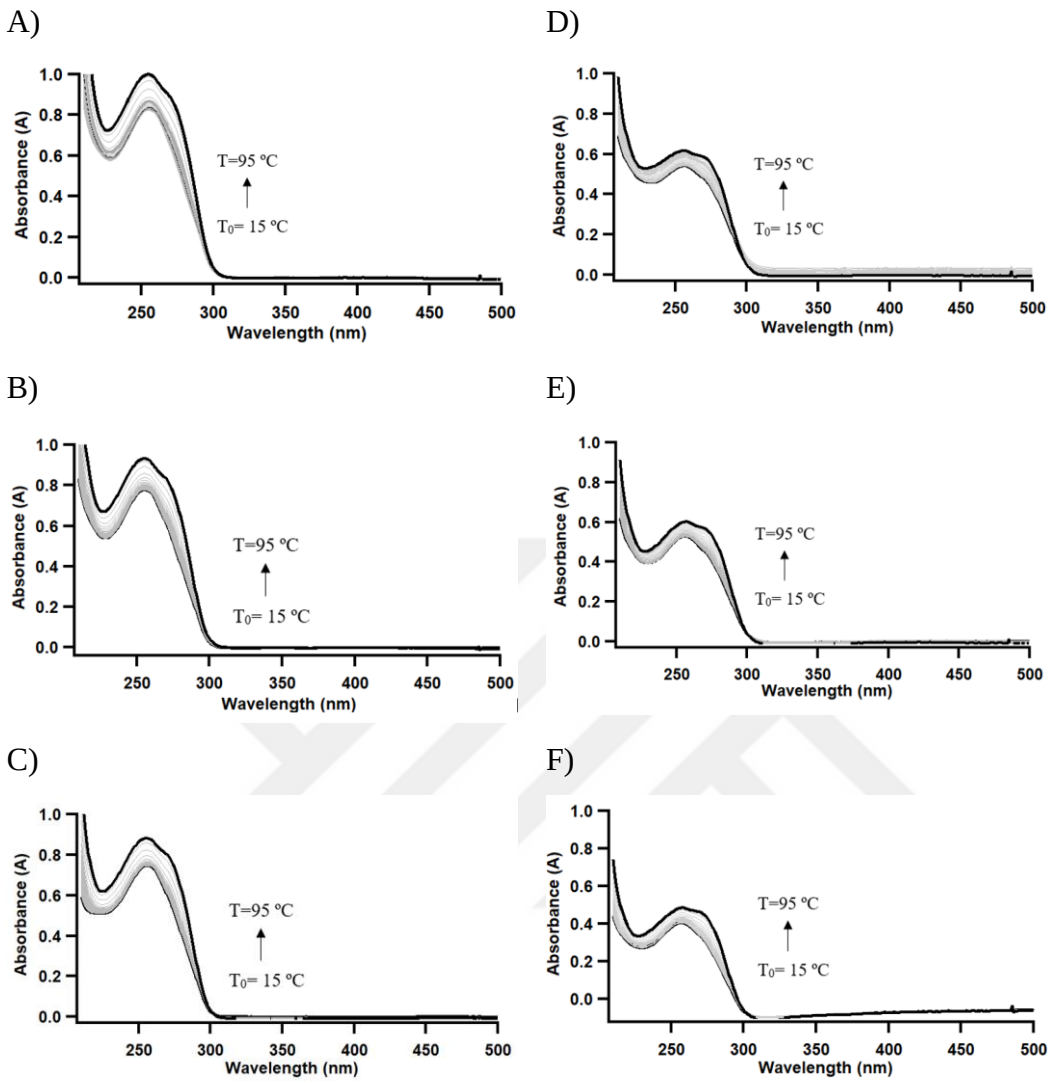


Figure 70. UV-Vis absorption spectra of 3.0 µM A) D1 B) D2 C) D3 in Na-phosphate buffer at pH 7.0 and D) D1 E) D2 F) D3 at pH 5.5 obtained during thermal denaturation experiments.

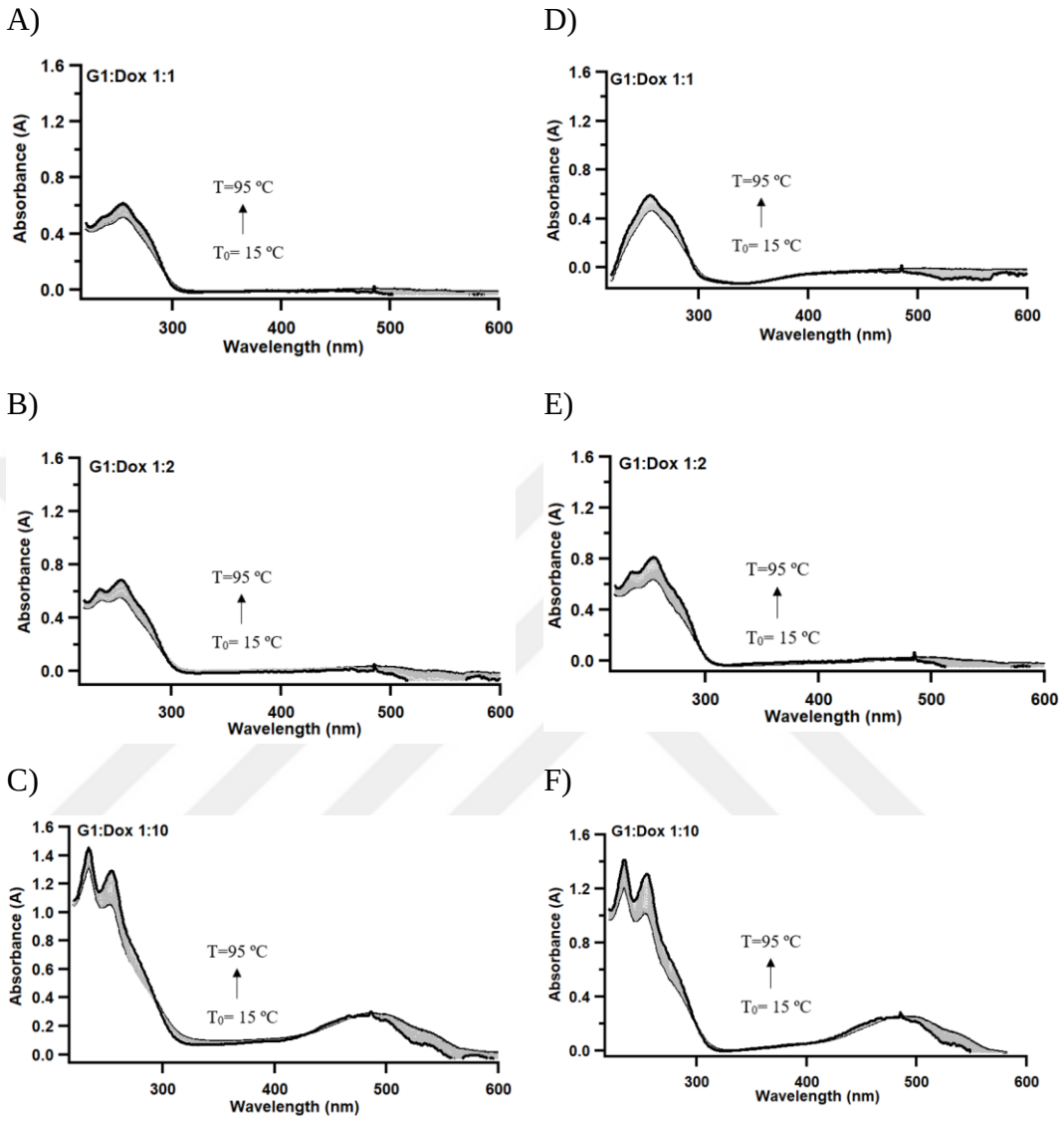


Figure 71. UV-Vis absorption spectra of A) 1:1 B) 1:2 C) 1:10 G1:Dox at pH 7.0 and D) 1:1 E) 1:2 F) 1:10 G2:Dox at pH 5.5 in K-phosphate buffer obtained during thermal denaturation experiments

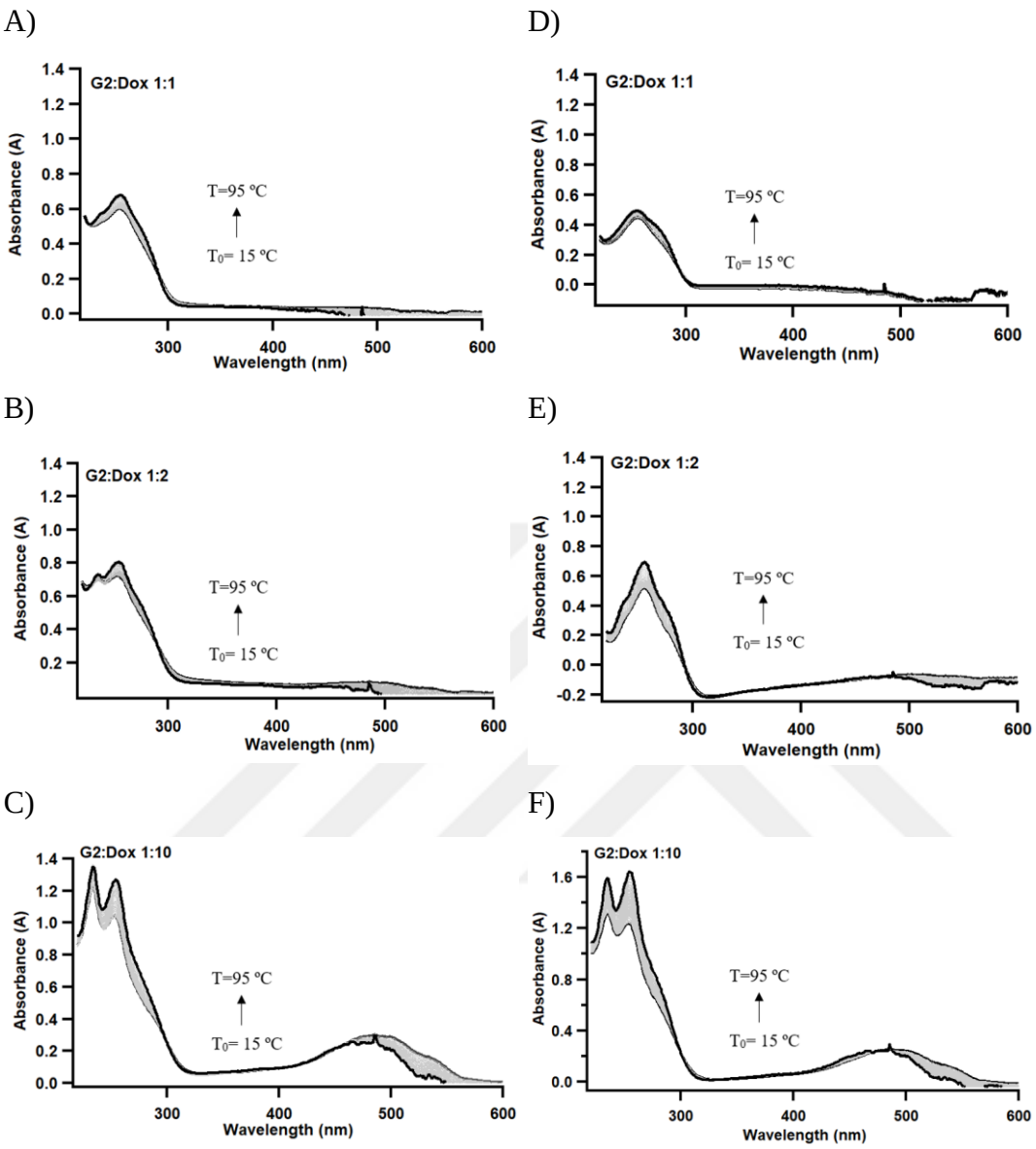


Figure 72. UV-Vis absorption spectra of A) 1:1 B) 1:2 C) 1:10 G2:Dox at pH 7.0 and D) 1:1 E) 1:2 F) 1:10 G2:Dox at pH 5.5 in K-phosphate buffer obtained during thermal denaturation experiments

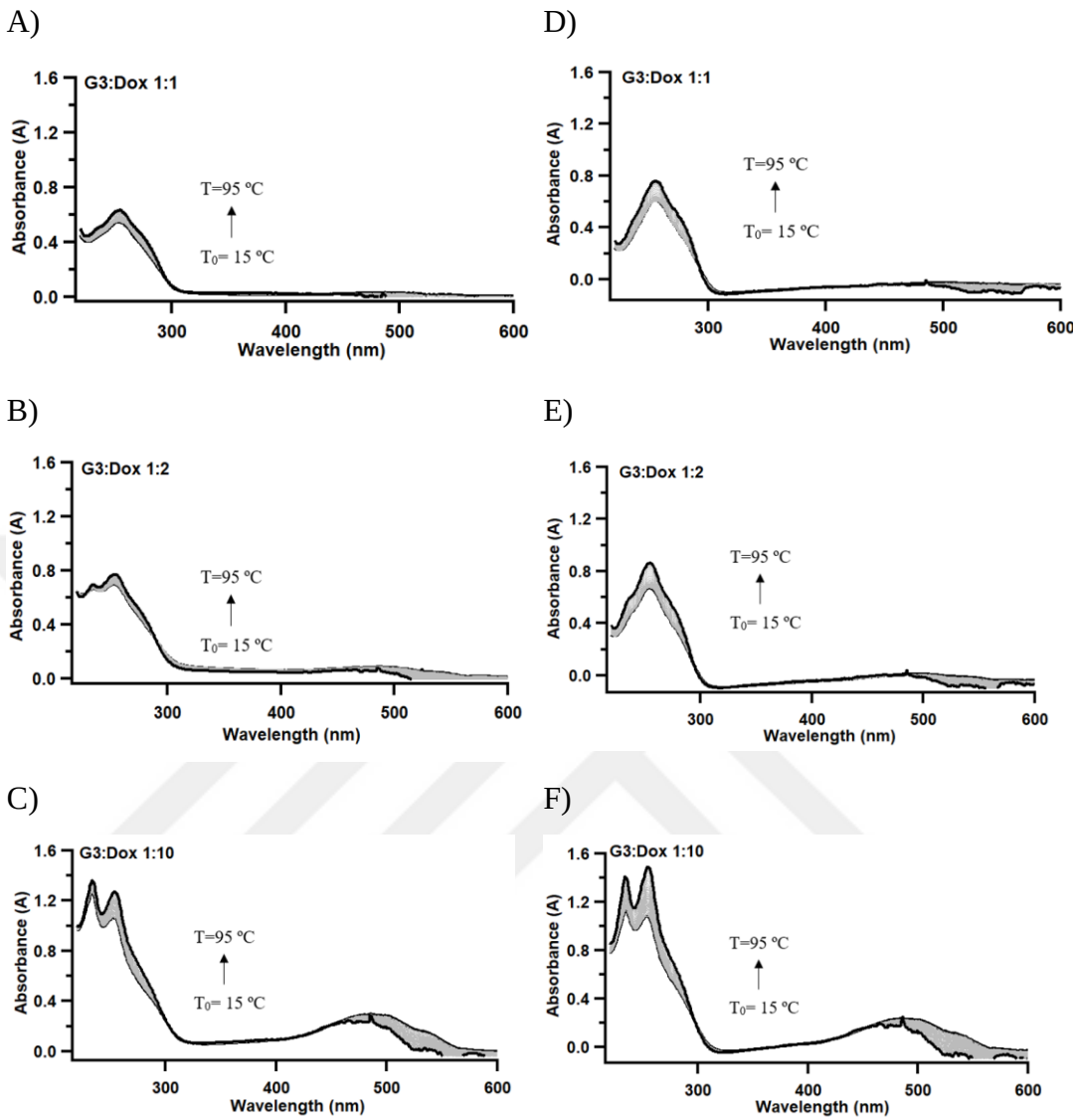


Figure 73. UV-Vis absorption spectra of A) 1:1 B) 1:2 C) 1:10 G3:Dox at pH 7.0 and D) 1:1 E) 1:2 F) 1:10 G3:Dox at pH 5.5 in K-phosphate buffer obtained during thermal denaturation experiments

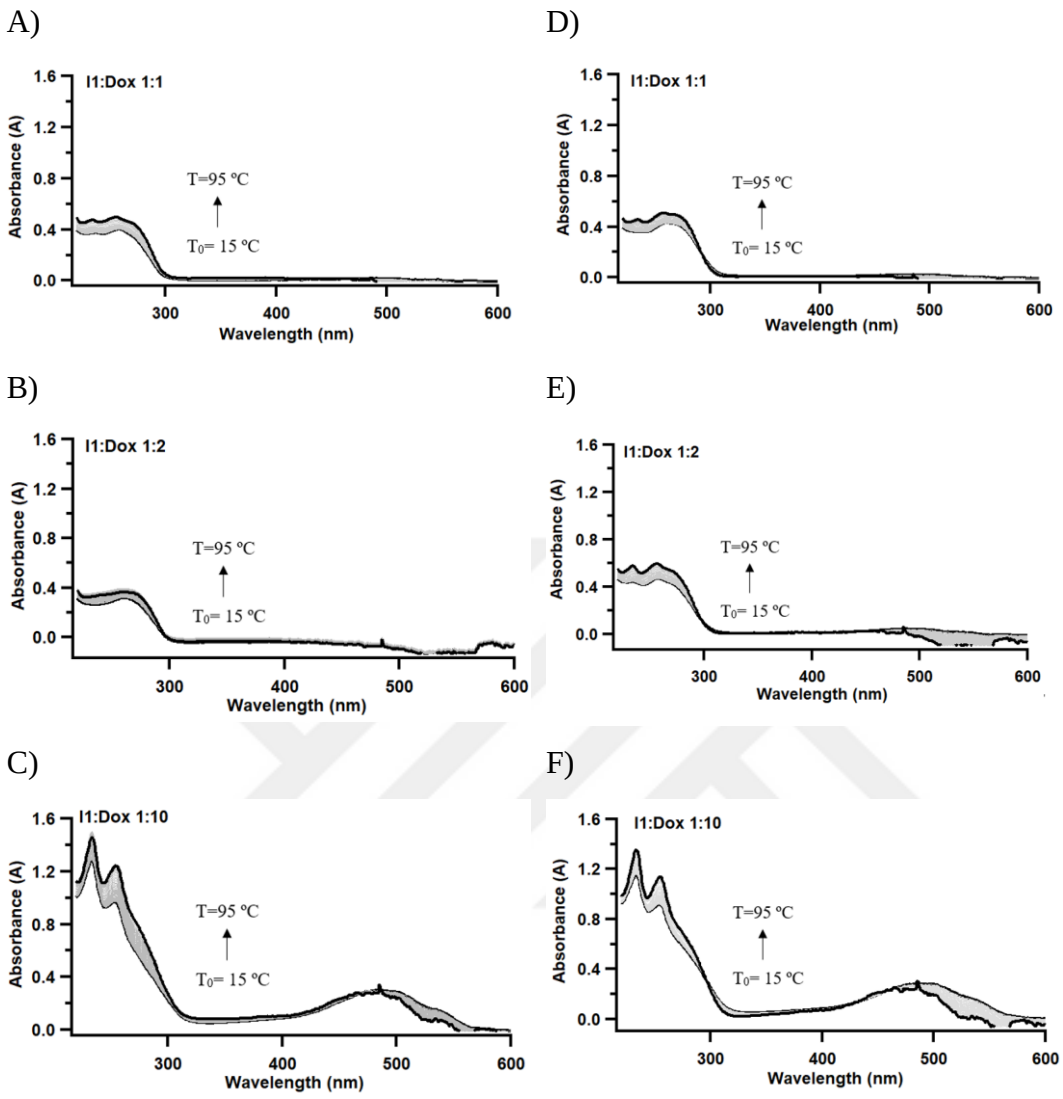


Figure 74. UV-Vis absorption spectra of A) 1:1 B) 1:2 C) 1:10; I1:Dox at pH 7.0 and D) 1:1 E) 1:2 F) 1:10: I1:Dox at pH 5.5 in K-phosphate buffer obtained during thermal denaturation experiments

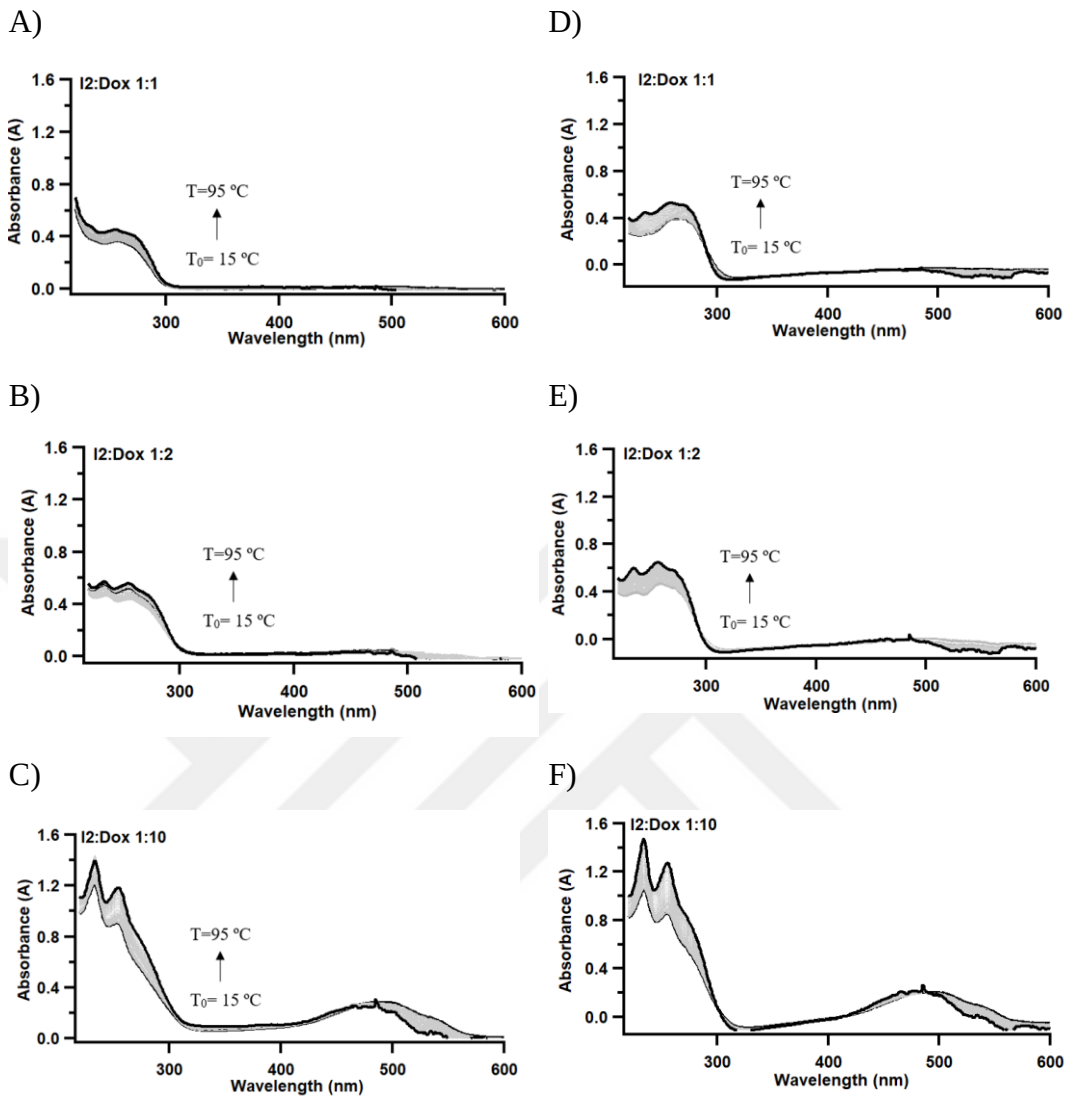


Figure 75. UV-Vis absorption spectra of A) 1:1 B) 1:2 C) 1:10; I2:Dox at pH 7.0 and D) 1:1 E) 1:2 F) 1:10: I2:Dox at pH 5.5 in K-phosphate buffer obtained during thermal denaturation experiments

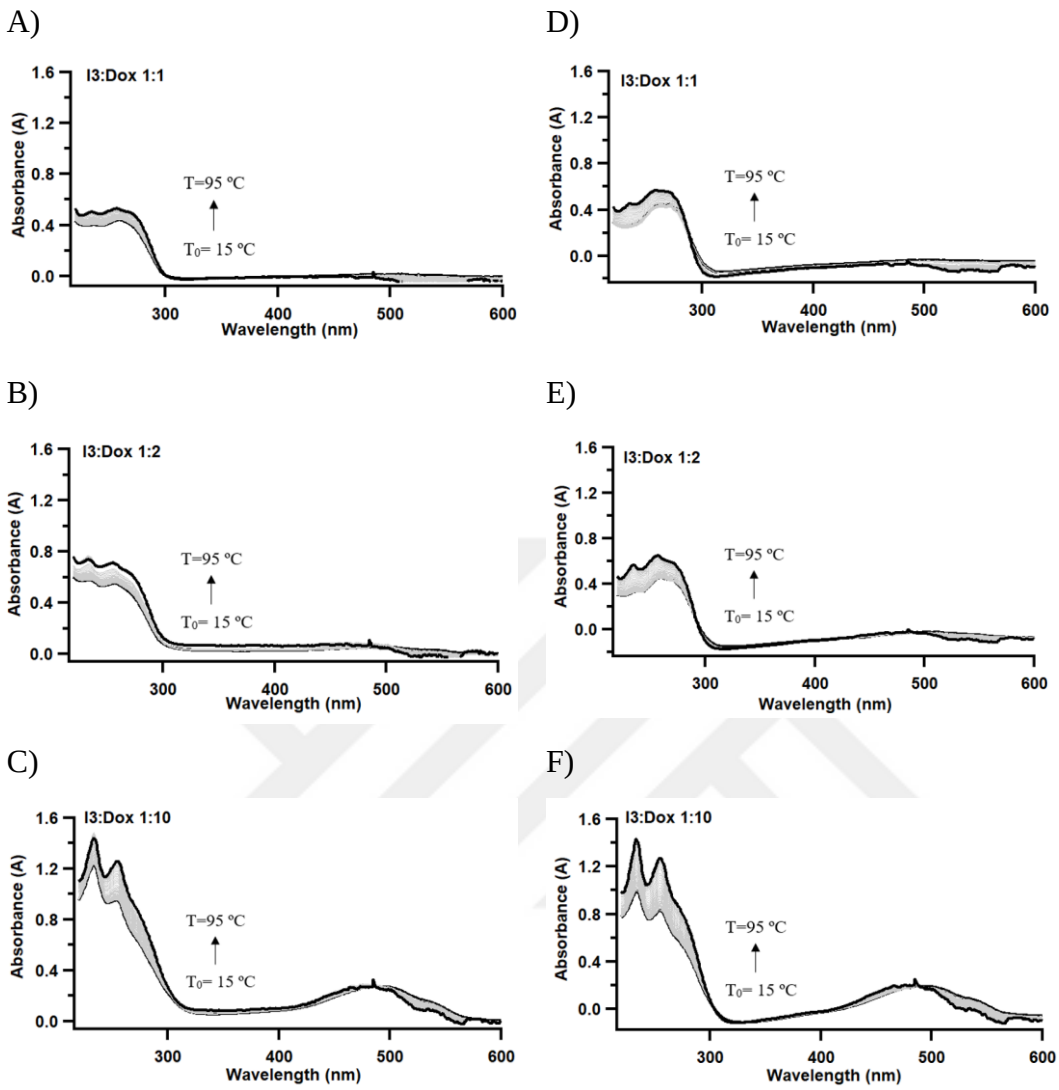


Figure 76. UV-Vis absorption spectra of A) 1:1 B) 1:2 C) 1:10; I3:Dox at pH 7.0 and D) 1:1 E) 1:2 F) 1:10: I3:Dox at pH 5.5 in K-phosphate buffer obtained during thermal denaturation experiments

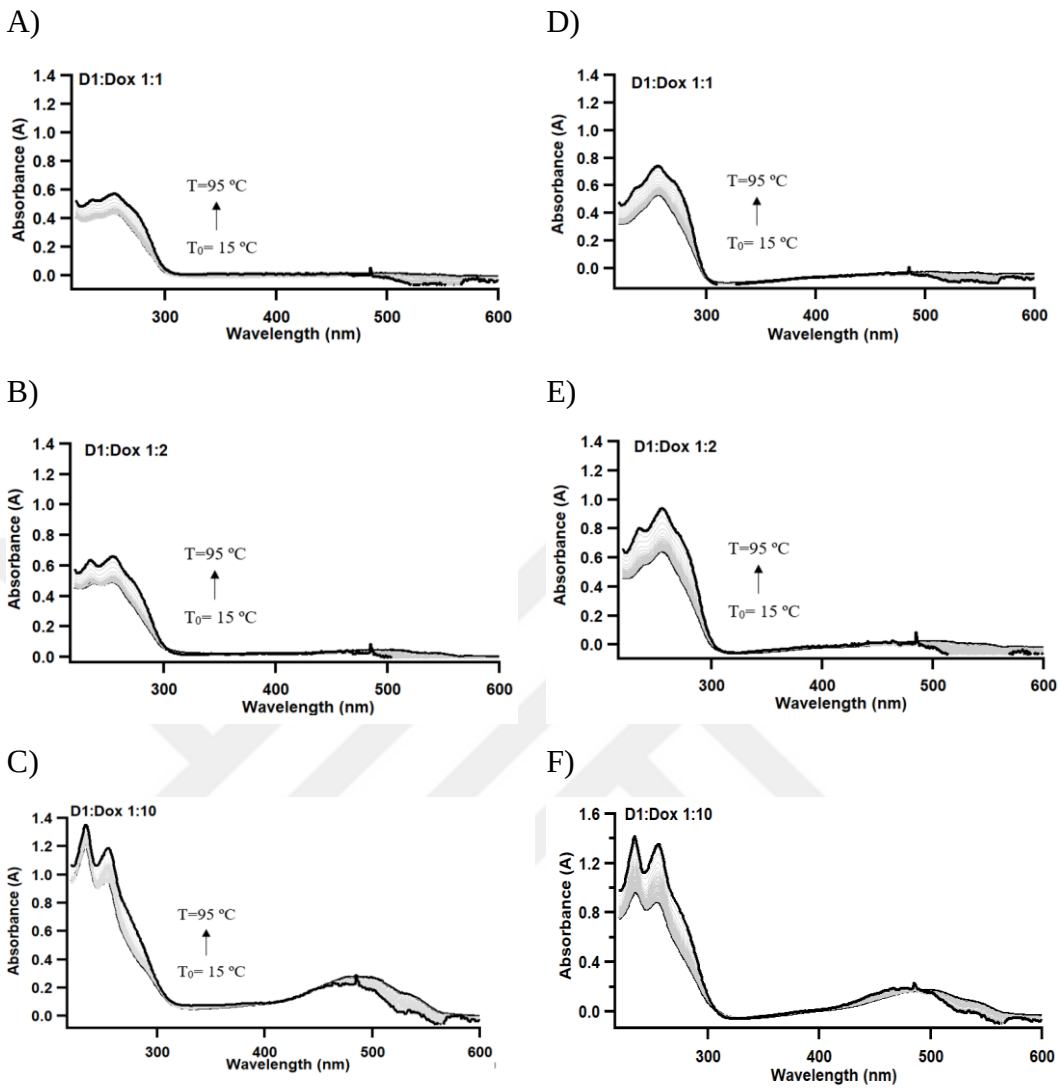


Figure 77. UV-Vis absorption spectra of A) 1:1 B) 1:2 C) 1:10; D1:Dox at pH 7.0 and D) 1:1 E) 1:2 F) 1:10: D1:Dox at pH 5.5 in K-phosphate buffer obtained during thermal denaturation experiments

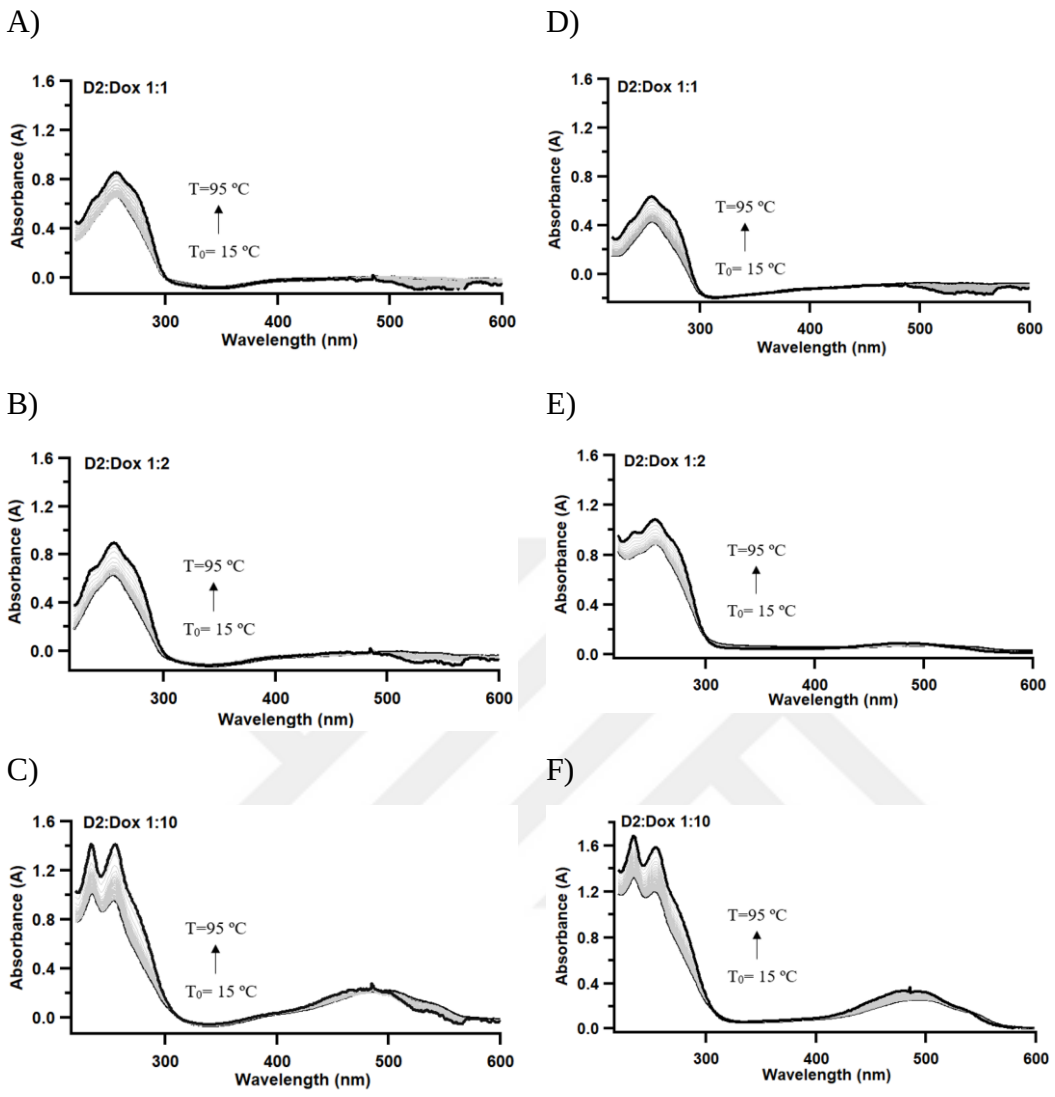


Figure 78. UV-Vis absorption spectra of A) 1:1 B) 1:2 C) 1:10; D2:Dox at pH 7.0 and D) 1:1 E) 1:2 F) 1:10: D2:Dox at pH 5.5 in K-phosphate buffer obtained during thermal denaturation experiments

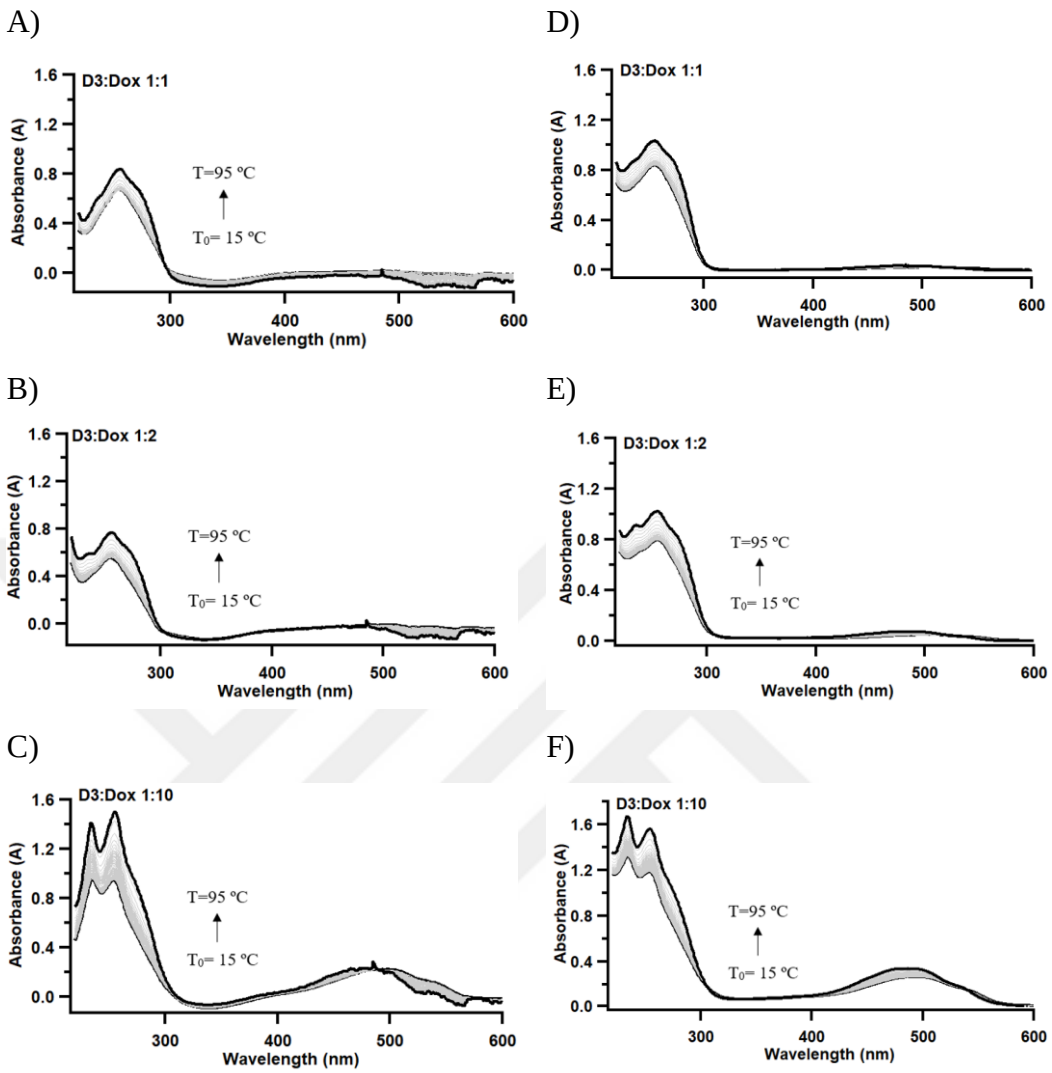


Figure 79. UV-Vis absorption spectra of A) 1:1 B) 1:2 C) 1:10; D3:Dox at pH 7.0 and D) 1:1 E) 1:2 F) 1:10; D3:Dox at pH 5.5 in K-phosphate buffer obtained during thermal denaturation experiments

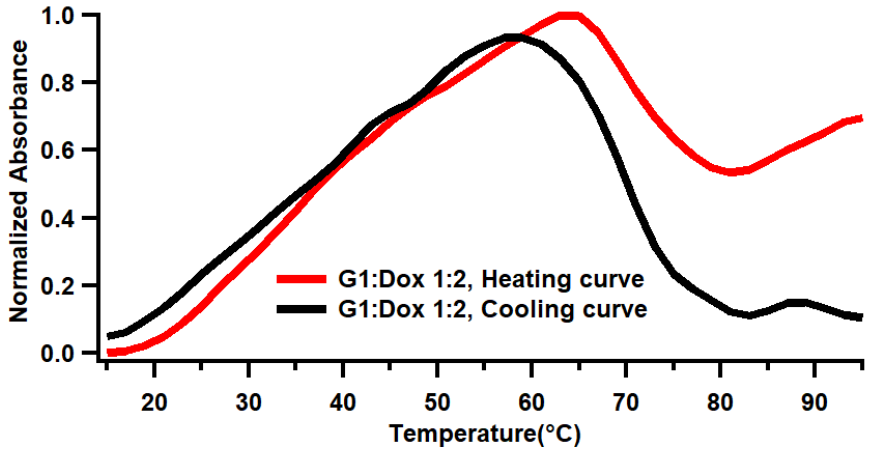


Figure 80. UV-Vis thermal melting profiles of 3.0 µM G1 in K-phosphate buffer at pH 7.0 in the presence of 6.0 µM Dox by monitoring absorbance at 295 nm.

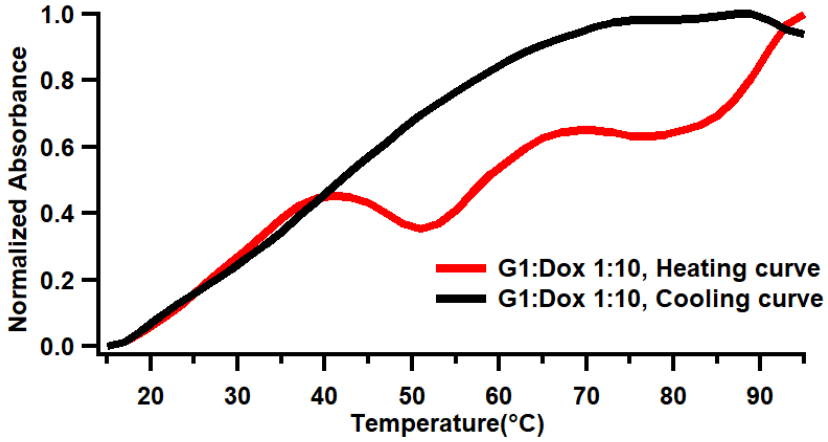


Figure 81. UV-Vis thermal melting profiles of 3.0 µM G1 in K-phosphate buffer at pH 7.0 in the presence of 30 µM Dox by monitoring absorbance at 295 nm.

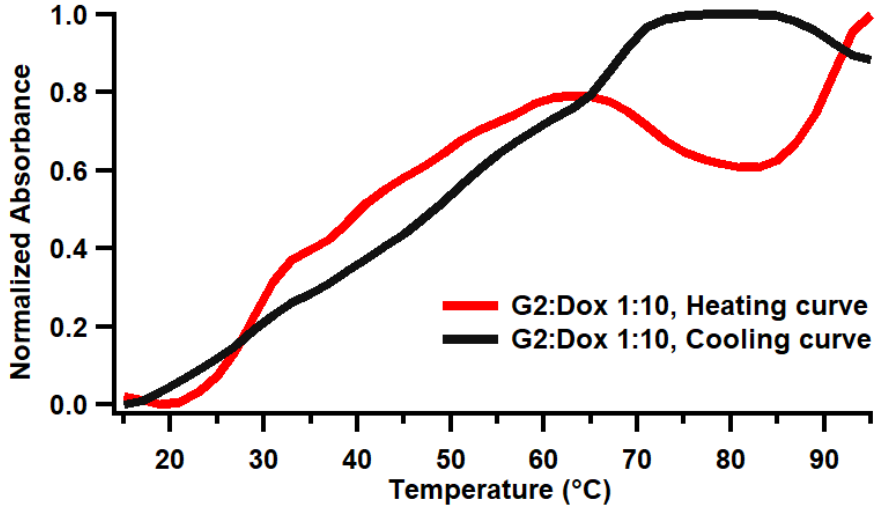


Figure 82. UV-Vis thermal melting profiles of 3.0 µM G2 in K-phosphate buffer at pH 7.0 in the presence of 30 µM Dox by monitoring absorbance at 295 nm.

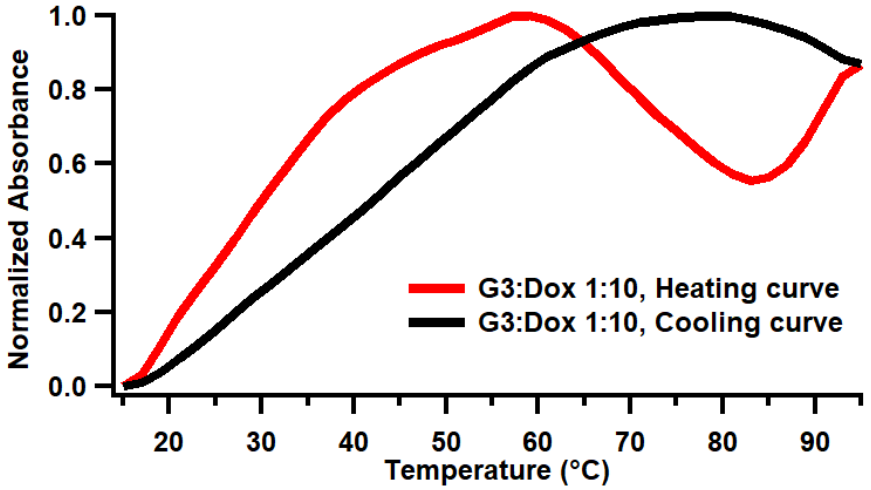


Figure 83. UV-Vis thermal melting profiles of 3.0 µM G3 in K-phosphate buffer at pH 7.0 in the presence of 30 µM Dox by monitoring absorbance at 295 nm.

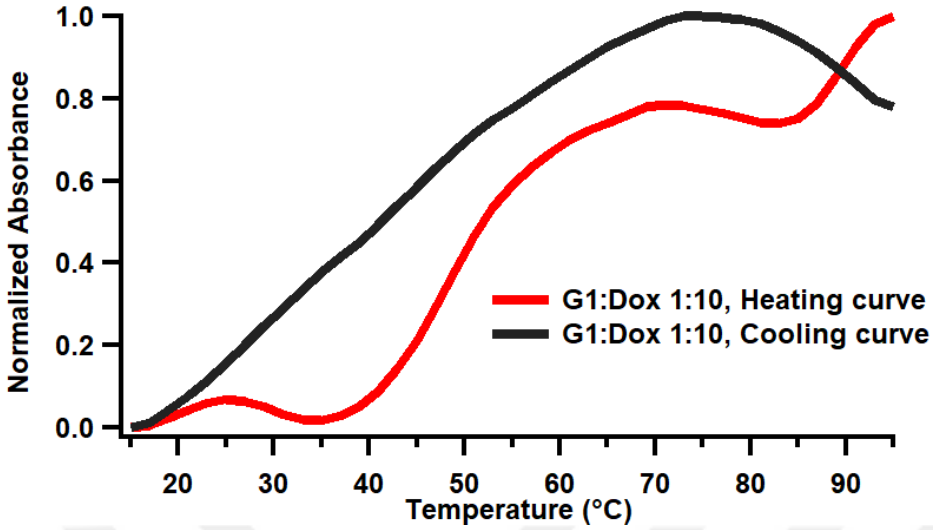


Figure 84. UV-Vis thermal melting profiles of 3.0 µM G1 in K-phosphate buffer at pH 5.5 in the presence of 30 µM Dox by monitoring absorbance at 295 nm.

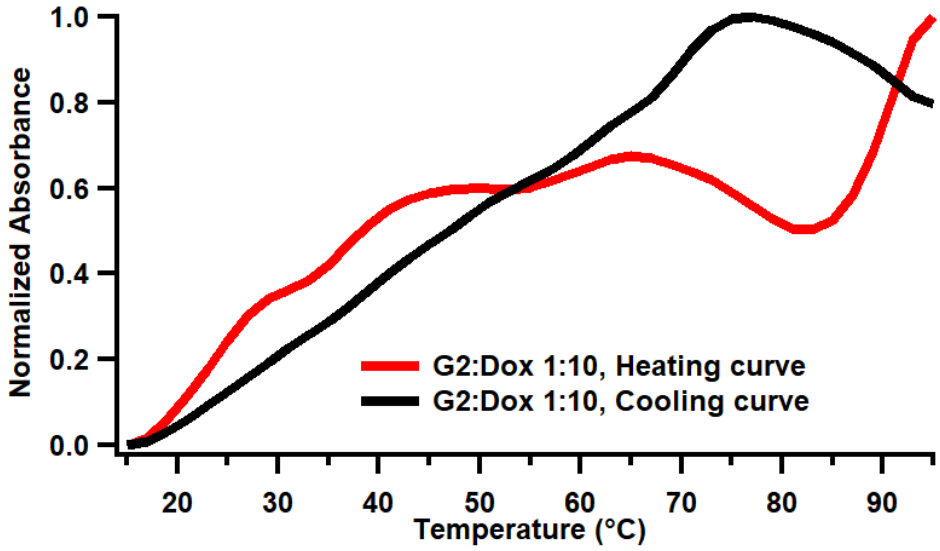


Figure 85. UV-Vis thermal melting profiles of 3.0 µM G2 in K-phosphate buffer at pH 5.5 in the presence of 30 µM Dox by monitoring absorbance at 295 nm.

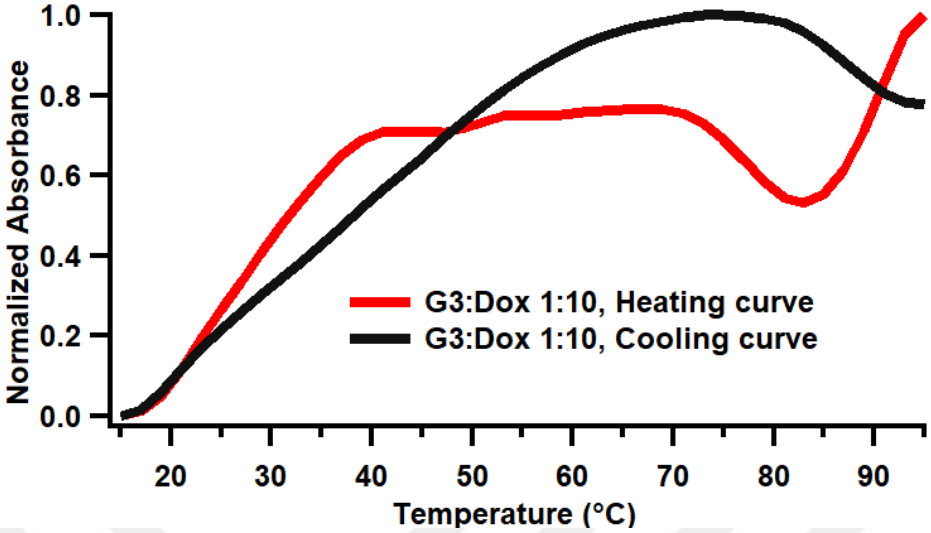


Figure 86. UV-Vis thermal melting profiles of 3.0 µM G3 in K-phosphate buffer at pH 5.5 in the presence of 30 µM Dox by monitoring absorbance at 295 nm.

## D. Association Constant Experiments

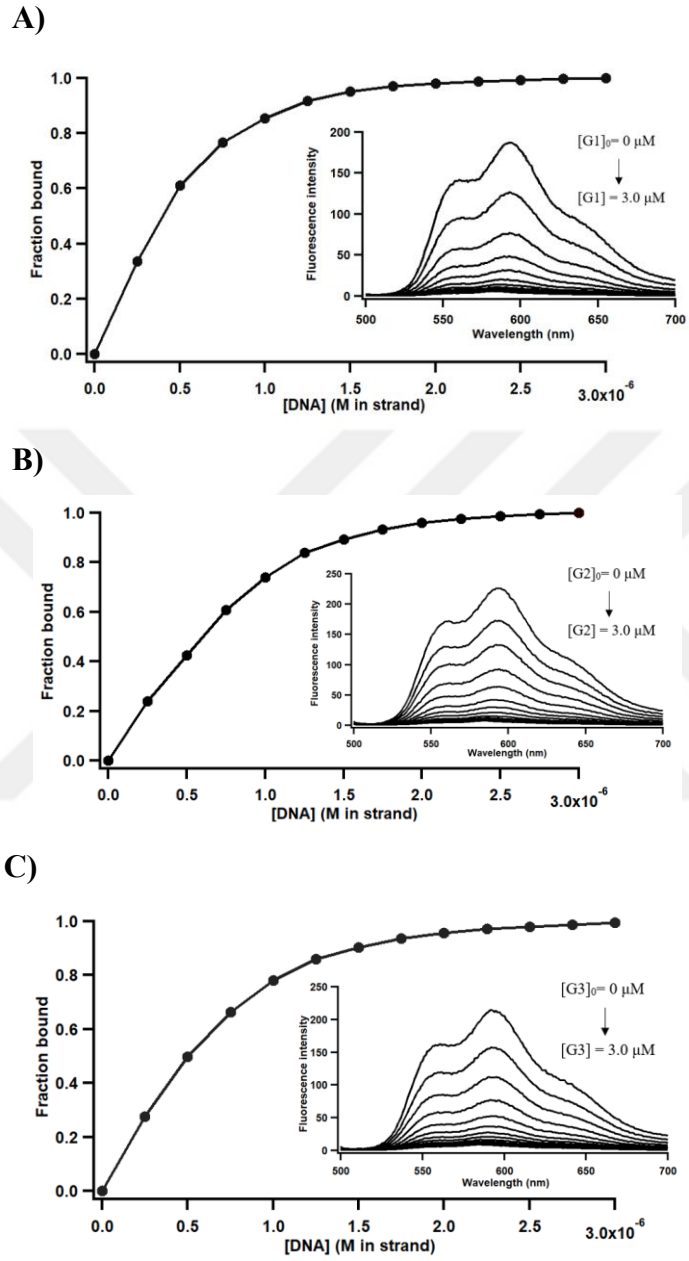


Figure 87. Fluorescence intensity measurements for 1.0 µM solutions of Dox in the presence of increasing concentrations of A) G1 B) G2 C) G3 at pH 7.0 and Fraction bound vs Concentration of DNA (M in strand) obtained from the titration results (2nd replicate)

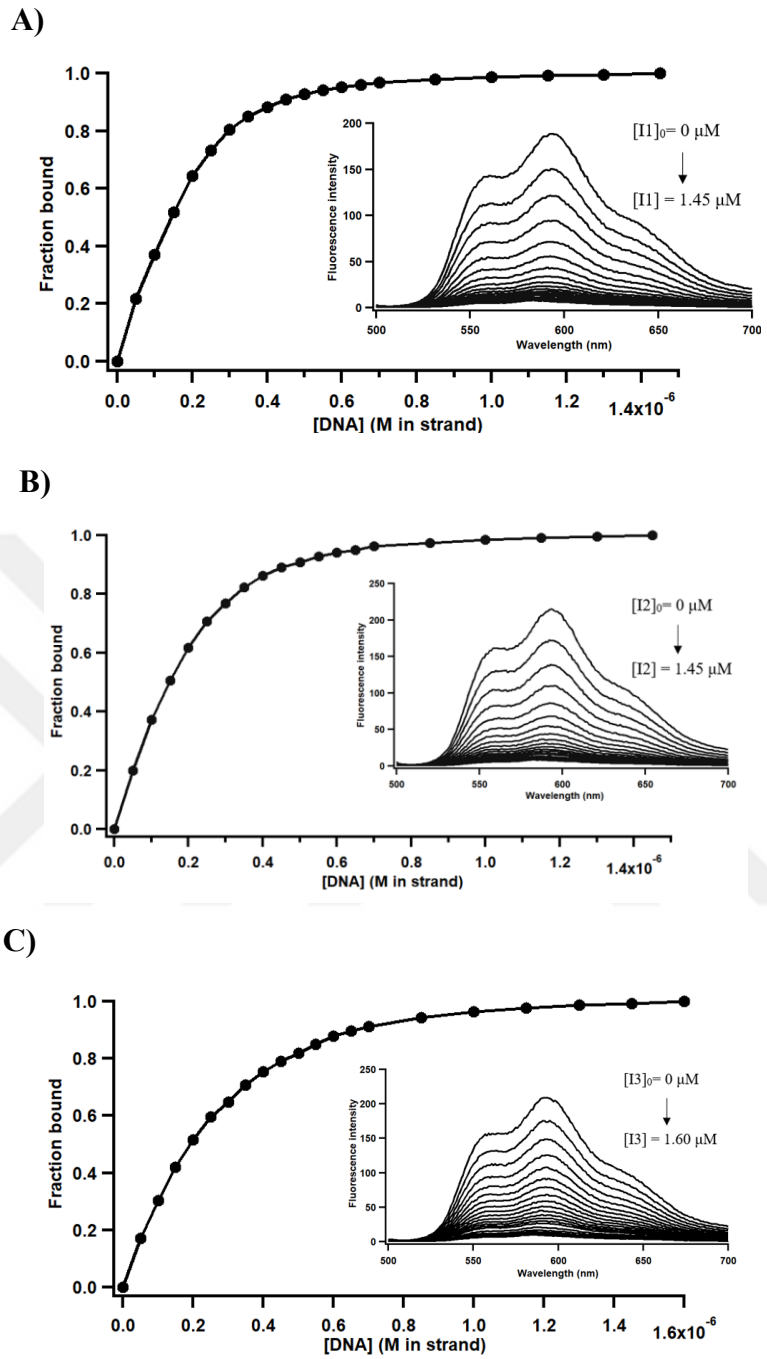


Figure 88. Fluorescence intensity measurements for 1.0 µM solutions of Dox in the presence of increasing concentrations of A) G1 B) G2 C) G3 at pH 7.0 and Fraction bound vs Concentration of DNA (M in strand) obtained from the titration results (2nd replicate)

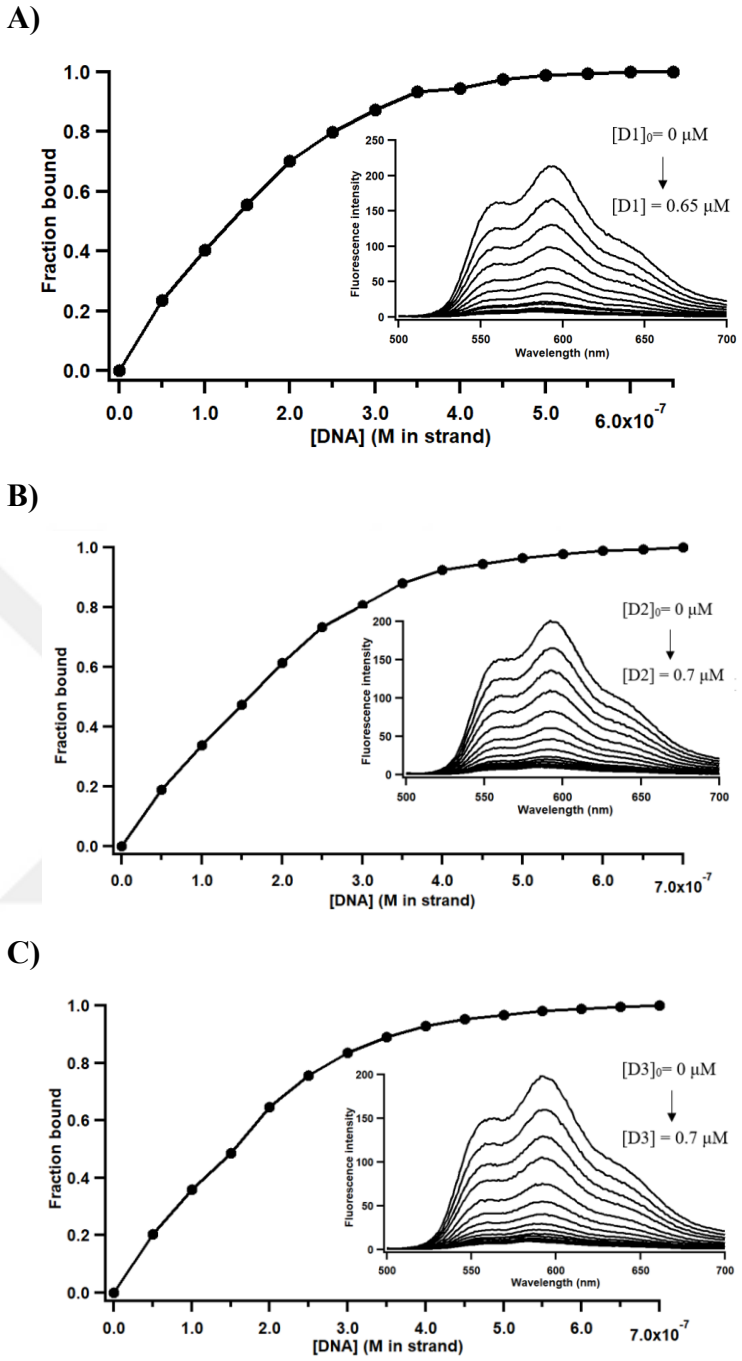


Figure 89. Fluorescence intensity measurements for 1.0 µM solutions of Dox in the presence of increasing concentrations of A) D1 B) D2 C) D3 at pH 7.0 and Fraction bound vs Concentration of DNA (M in strand) obtained from the titration results (2nd replicate)

## E. Competition Dialysis

Table 12. List of nucleic acid structures used in the competition dialysis assay and their extinction coefficient values for concentration adjustments.

| **Nucleic Acids** | **ε ($M^{-1}cm^{-1}$)** | **COMPANY** |
|---|---|---|
| ***PIM1*-SLQS08 (G1)** | 261900 | IDT |
| ***PIM1*-SLQS07 (G2)** | 255800 | IDT |
| ***PIM1*-SLQS02 (G3)** | 245200 | IDT |
| ***PIM1*-SLQS08-comp (I1)** | 228900 | IDT |
| ***PIM1*-SLQS07-comp (I2)** | 218700 | IDT |
| ***PIM1*-SLQS02-comp (I3)** | 212200 | IDT |
| **d[GC$(G)_3$A$(G)_3$CGCG$(C)_2$AGC$(G)_4$TC$(G)_3$C]/ d[CG$(C)_3$T$(C)_3$GCGC$(G)_2$TCG$(C)_4$AG$(C)_3$G] (D1)** | **-** | **-** |
| **d[GC$(G)_3$A$(G)_3$CGCG$(C)_2$AGC$(G)_4$TC$(G)_3$]/ d[CG$(C)_3$T$(C)_3$GCGC$(G)_2$TCG$(C)_4$AG$(C)_3$] (D2)** | **-** | **-** |
| **d[$(G)_3$A$(G)_3$CGCG$(C)_2$AGC$(G)_4$TC$(G)_3$C]/ d[$(C)_3$T$(C)_3$GCGC$(G)_2$TCG$(C)_4$AG$(C)_3$G] (D3)** | **-** | **-** |
| **Tel$_{24}$** | 244300 | IDT |
| **dA$_{32}$** | 387400 | IDT |
| **dT$_{32}$** | 259800 | IDT |
| **TC$_4$T** | 45600 | IDT |
| **TG$_4$T** | 57800 | IDT |
| **C$_4$T$_4$C$_4$** | 90200 | IDT |
| **G$_4$T$_4$G$_4$** | 115200 | IDT |

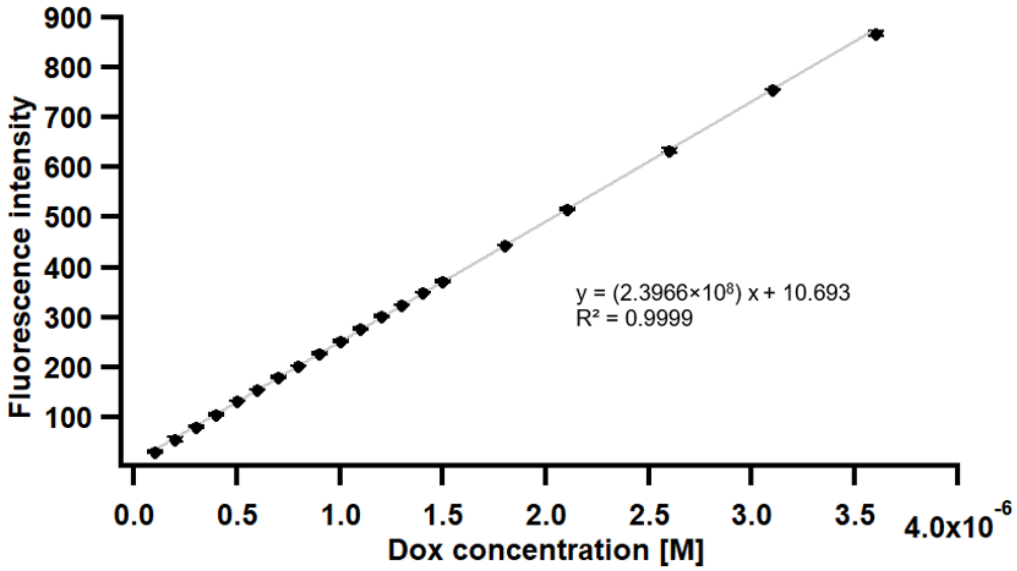


Figure 90. Dox calibration curve constructed for the competition dialysis assay (two replicates).